DALHOUSIE UNIVERSITY

DEPARTMENT OF GEOLOGY

The undersigned hereby certify that they have read and recommended to the Faculty of Graduate Studies for the acceptance a thesis entitled " An evaluation of flexural-slip folding in the Meguma Group, Halifax and Ovens areas, southern Nova Scotia"

by Richard J Horne

in partial fulfillment of the requirements for the degree of Master of Science

Dated 21 Dec '98

Supervisor:

Readers:

DALHOUSIE UNIVERSITY

DATE

AUTHOR: Richard J Horne

TITLE: An evaluation of flexural-slip folding in the Meguma Group, Halifax and Ovens areas, southern Nova Scotia

DEPARTMENT OR SCHOOL: Earth Sciences

DEGREE: M.Sc. CONVOCATION: May YEAR: 1998

Permission is herewith granted to Dalhousie University to circulate and to have copied for non-commercial purposes, at its discretion, the above title upon the request of individuals or institutions.

TABLE OF CONTENTS

List of Figures

List of Tables

Acknowledgements

This thesis was completed with the financial support and commitment of the Nova Scotia Department of Natural Resources, for which I grateful. I know it was to my benefit, and I believe it was to their benefit as well.

Field assistance was provided by Steve Hayson, Lisa MacDonald and Darcy Baker, Katharine Muir and Jim Hunter. A special thanks to Steve Haysom, who was the main "metre-stick" man during measuring of the sections. Now you're an oil man. Oh well.

The vast majority of the drafting was done by the author, however, some drafting was done by the "drafting section" of the Nova Scotia Department of Natural Resources. Reg Morrison took the aerial photographs for the Ovens area.

In addition to my supervisor, I have had many helpful discussions with numerous people regarding the contents of this thesis, in particular Dr. D. Kontak, Dr. J. Waldron, P.K. Smith and Dr. R.A. Jamieson. In addition, I thank all the people on field trips to the Ovens, who always seem to find the obvious which somehow eluded me.

My deepest thanks to my supervisor, Dr. Nicholas Culshaw, who suggested this project to me and has guided and challenged me throughout. Not knowing much about flexural-slip at the time, I was a little apprehensive about what I might be able to do with it. Now it seems that I think it is the answer to everything. Nick, beyond your supervision, thanks for always putting the personal concerns first.

Abstract

An evaluation of flexural-slip folding in the Meguma Group was conducted in the hinge area of the Lawrencetown Anticline (Halifax area) and the Ovens Anticline (Ovens area). Flexural slip in these areas was accommodated on mainly bedding-parallel movement horizons consisting of simple slip surfaces and flexural-slip duplexes. Lateral and frontal ramp movement horizons are locally associated with bedding-parallel movement horizons, forming a linked system accommodating flexural-slip strain. Thrusting locally accompanied flexural-slip. Discordant shear fractures in the Ovens Anticline are kinematically related to flexural slip. Movement horizons are typically coated with slickenfibres and quartz veins commonly occupy flexural-slip structures in the Ovens Anticline, and fluid pressure was likely important during flexural slip. Movement lineations are roughly perpendicular to the fold hinge or systematically form an acute angle with the hinge in the direction of the fold plunge, suggesting flexural slip during non-cylindrical fold growth. Shear sense indicators include slickenfibres, flexural-slip duplex geometry, displaced conjugate veins and thrust geometry, and invariably show a reverse sense which changes systematically across the fold.

The average spacing of bedding-parallel movement horizons ranges from approximately 1-4 metres and spacing is inversely related to limb dip. The flexural-slip amount determined for a section of the Ovens Anticline from displaced discordant veins indicates that flexural-slip accounts for 4°- 8° of limb dip Slip amount is variable, with the largest slip occurring on flexural-slip duplexes and flexural-slip shear strain is uniform across the limb. Spacing and slip amount data suggest that increasing flexural-slip strain during incremental fold growth is accommodated by increased movement on early formed movement horizons and continuous formation of new movement horizons.

Bedding-cleavage relations, the distribution of minor folds and cleavage-parallel strain defined by pressure shadows on arsenopyrite suggest a synfolding origin for cleavage and indicate flexural slip was accompanied by significant layer-parallel shortening in fold hinges, including the flat tops of box folds. Flexural slip is a brittle, post metamorphic deformation which deforms the contact aureole of the ca. 370 Ma South Mountain Batholith. A post metamorphic age is supported by $^{40}Ar/^{39}Ar$ age data which constrain regional metamorphism to ca. 410-385 Ma but synfolding cleavage-parallel strain and the emplacement of (flexural-slip) quartz veins at ca. 375 Ma. A model of folding has been proposed which includes (i) initial box-fold development, (ii) synfolding cleavage development and layer-parallel shortening in the flat segments of box folds with flexural-flow on the limbs under metamorphic conditions and (iii) post metamorphic flexural-slip accompanied by additional cleavage-parallel strain, including layer-parallel shortening in fold hinges.

A synfolding, flexural-slip model is proposed for the auriferous quartz vein array at the Ovens, including synchronous emplacement of bedding-parallel and discordant veins. Most Meguma Gold Districts share general features with the Ovens which are consistent with a flexural-slip model, suggesting a flexural-slip model may be an appropriate and testable model for Meguma gold deposits.

CHAPTER 1 - INTRODUCTION

1.1 INTRODUCTION

It has long been recognized that shortening of multilayered sequences, such as turbidites, is accommodated by chevron- and box-style fold development (Fowler and Winsor, 1996; Ramsay, 1974; Ramsay and Huber, 1987). Experimental studies indicate that such folds initiate by development of conjugate instabilities reflecting the highly anisotropic nature of strongly multilayered sequences, with progressive shortening resulting in development of box folds and chevrons, where folds are characterized by straight limbs throughout the fold history (Fig. 1.1; Biot, 1965; Cobbold et al., 1971; Dubey and Cobbold, 1977; Latham, 1985; Fowler and Winsor, 1996). The degree of anisotropy is controlled by several factors, including viscosity contrast, relative thickness of competent and incompetent layers and length to thickness ratios of competent layers. Folds developed in this manner inherently show no systematic vergence when shortening is perpendicular to layering (Fig. 1.1). Folds developed in multilayered rock sequences are commonly non-cylindrical, and in experimental deformation of multilayers fold amplification occurred by lateral hinge migration (Dubey and Cobbold, 1977).

Straight-limbed folds such as chevrons and box folds typically develop by flexural folding, characterized by reverse, bedding-parallel shear on the limbs (Ramsay, 1974; Ramsay and Huber, 1987). Flexural shear strain can be accommodated by homogeneous strain throughout the sequence, referred to as flexural flow, or inhomogeneous strain focused along discrete movement horizons, referred to as flexural slip (Fig. 1.2). Theoretical studies indicate

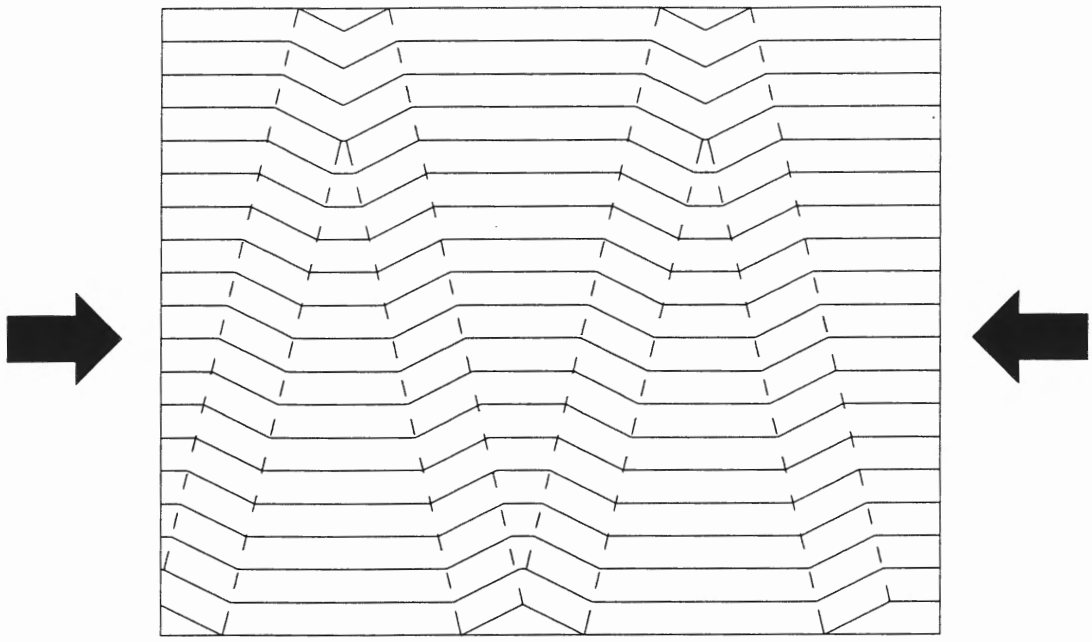

Figure 1.1: Diagram illustrating the development of conjugate kink bands in a highly anisotropic layered sequence when compressed parallel to layering. (After Cobbold et al., 1971).

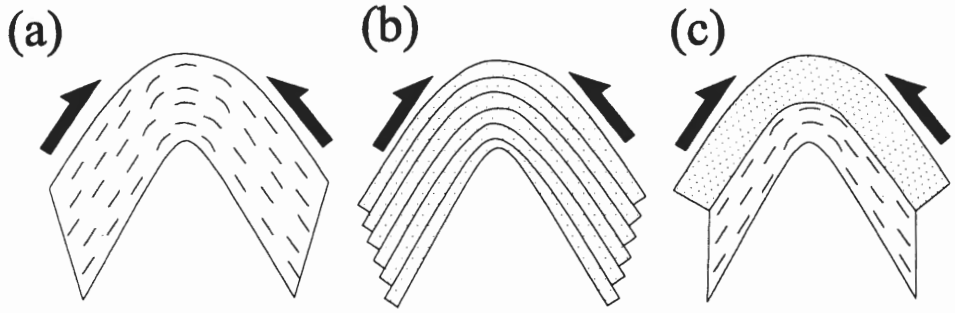

Figure 1.2: Schematic diagram showing the basic models of (a) flexural flow, (b) flexural-slip and (c) combined flexural flow and tangential longitudinal strain. (After Ramsay and Huber, 1987).

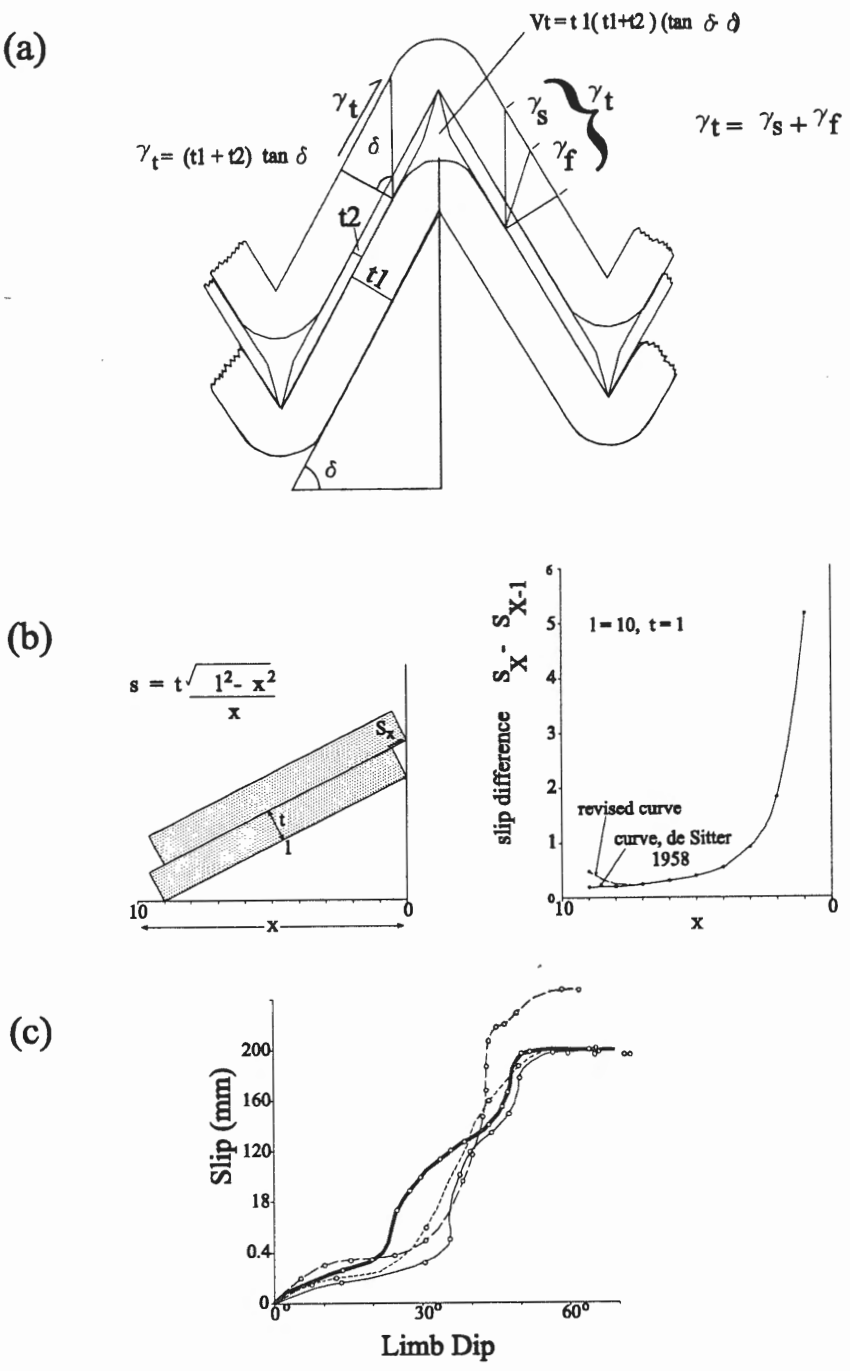

Figure 1.3: (a) Geometric model of chevron folds showing the relationship between flexural shear strain, for competent and incompetent layers of thickness t1 and t2 respectively, and limb dip. γt=total shear strain; γs= flexural-slip strain; γf = flexural-flow strain; Vt = total volume. (After Ramsay, 1974 and Tanner, 1989). (b) Schematic diagram, left, and graph, right, showing the relationship between shortening and slip amount for rotation of planar layers during limb amplification in chevron folds (After Ramsay, 1974). (c) Graph of slip amount against limb dip determined in experimental deformation of multilayers. (After Behzadi and Dubey, 1982).

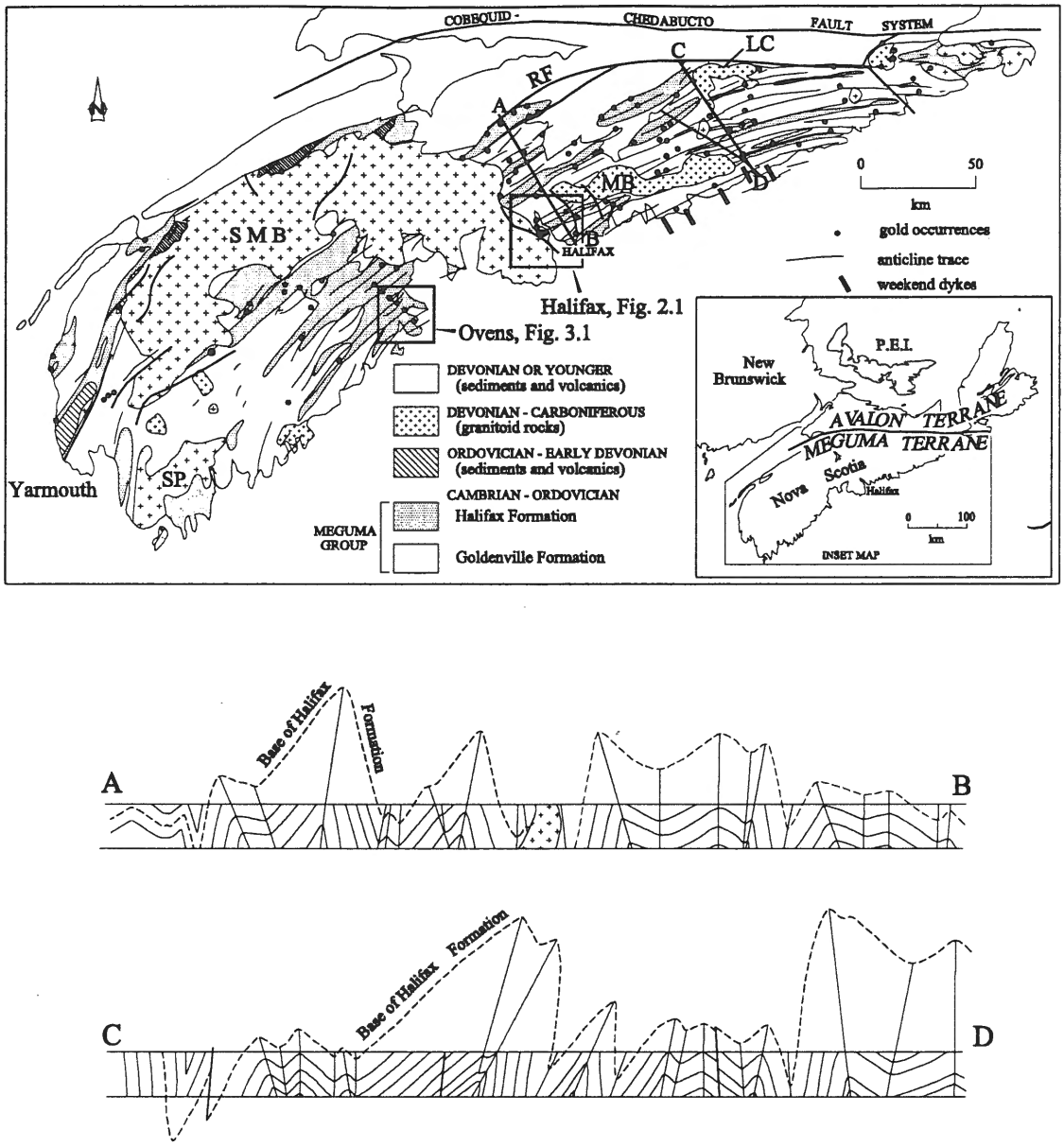

Figure 1.4: Simplified map and cross sections of the Meguma Terrane showing the location of the Halifax and Ovens study areas. Cross sections after Fletcher and Faribault, 1911. SMB South Mountain Batholith; MB = Musquodoboit Batholith; SP = Southern Plutons; RF = Rawdon Fault; LC = Liscomb Complex.

the amount of flexural shear strain and the rate of shear strain are a function of limb dip (Fig. 1.3; Ramsay, 1974, de Sitter, 1958). The rate of shear increases with shortening (increasing limb dip) (Fig. 1.3b) and the shear stress acting along layering decreases, resulting in locking-up of folds at an interlimb angle of about 60° (Ramsay, 1974; de Sitter, 1958). Experimental studies of flexural slip confirm the above (Fig. 1.3c; Behzadi and Dubey, 1980), although some computer modelling suggests that flexural slip continues up to limb dips of 70° (Fowler and Winsor, 1997). Although flexural folding is clearly important in formation of straight limbed folds, studies of natural folds indicate that other mechanisms commonly contribute to the finite fold strain, including layer-parallel shortening, tangential longitudinal strain and homogeneous fold flattening (Boulter, 1979; Keppie, 1976; Yang and Gray, 1994). Unravelling the deformational history of such folds, therefore is generally difficult.

Folds within the turbiditic Meguma Group of Nova Scotia are characterized by straight limbed box fold and chevron profiles (Fig. 1.4) characteristic of layer-parallel shortening of highly anisotropic multilayered sequences, suggesting flexural-folding was important in fold development. Henderson et al. (1986) suggested that flexural flow was the dominant folding mechanism in the Meguma Group and that flexural slip was not significant. However, evidence of flexural slip has been locally documented within the Meguma Group (see section 1.4.2.2) and Dr. N. Culshaw noted evidence of flexural slip in the railway cut in Halifax and at the Ovens. This thesis addresses the mechanics of folding within the Meguma Group. In particular, this study evaluates the flexural-slip mechanism in the Halifax and Ovens areas and addresses the role of flexural slip in the development of these folds, establishing the character, timing, and amount of flexural slip and the role of flexural slip in the localization

and emplacement of auriferous vein arrays around anticlinal hinges.

1.2 THE FLEXURAL-SLIP MECHANISM:

1.2.1 General Statement:

The basic flexural-slip model is commonly envisaged as the slip which occurs between a card deck as it is folded (e.g., Fig. 1.2b). In the simplest scenario the hinge is pinned and movement occurs perpendicular to the hinge with a reverse sense of shear with respect to the fold (Fig. 1.2b). Deformation is a plane strain represented mainly by simple shear on bedding surfaces in the profile plane. Evidence of flexural slip is widely recognized in natural folds (e.g., Tanner, 1989; Ramsay and Huber, 1987; Fowler and Winsor, 1997; Markley and Wojtal, 1996; Chapple and Spang, 1974; Cox et al., 1995). There are few studies, however, which provide detailed assessment of structural features associated with slip or provide quantitative data which would allow for a quantitative model addressing factors controlling flexural slip. This is largely because of the difficulty in recognizing flexural-slip movement horizons in the absence of exposed movement surfaces or markers displaced as a result of flexural slip.

Following is an outline of the major issues related to the flexural-slip mechanism, which provides a framework for the presentation of flexural slip in the Meguma Group given in this thesis. As will be evident, establishing constraints on the shear sense and movement direction on movement horizons is critical to interpreting that these movement horizons result from the flexural-slip mechanism, in contrast to pre- or post-folding displacement.

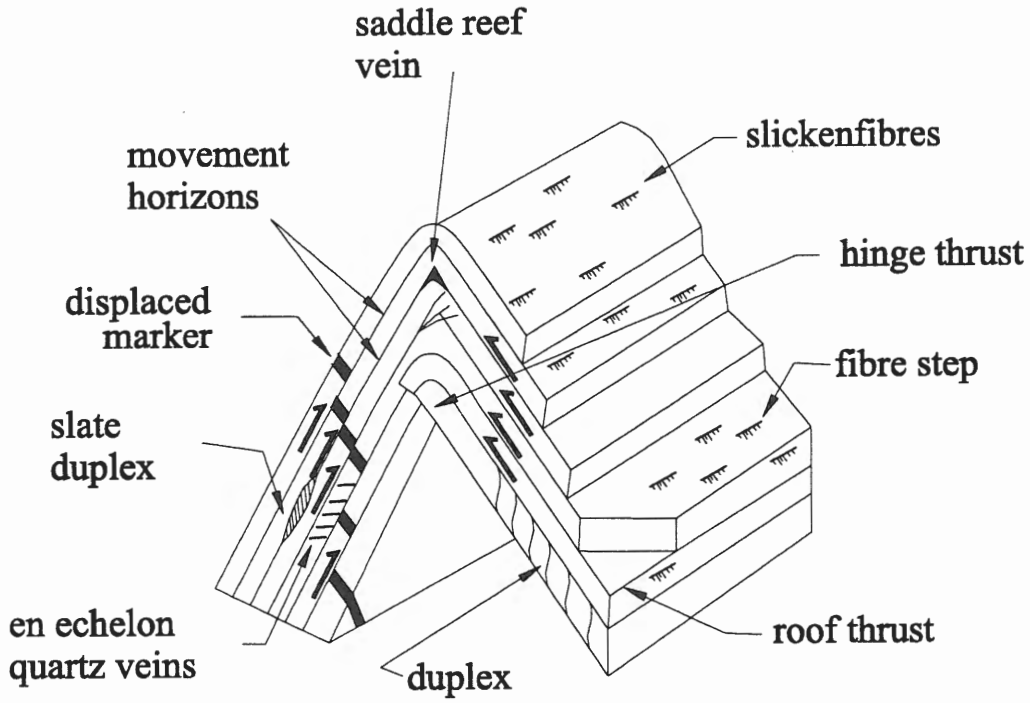

Figure 1.5: Flexural-slip model showing structures resulting from flexural-slip. (After Tanner, 1989)

1.2.2 Identification of movement (horizons) surfaces:

Tanner (1989) introduced the term movement horizon to describe movement surfaces along which flexural slip occurred and the term is adopted herein. Identification of movement horizons along which flexural slip has occurred is fundamental in studies of flexural slip; however identification is a common problem which is limited by the occurrence of displaced markers or exposure of surfaces with evidence of movement. Field studies indicate that flexural slip largely occurs along bedding-parallel surfaces which are characterized by striations and slickenfibres (Tanner, 1989; Ramsay and Huber, 1987; Chapple and Spang, 1974; Markley and Wojtal, 1996; Yang and Gray, 1994; Fowler and Winsor, 1997). In addition to simple slip planes, Tanner (1989; 1992) documented movement horizons defined by thrusts, ramps, imbricate structures and flexural-slip duplexes (Fig. 1.5). Offset discordant sedimentary dykes and quartz veins provide evidence of flexural slip where movement horizon surfaces are not exposed (i.e., Tanner, 1989). Laminated quartz veins, interpreted to reflect accumulation of slickenfibre sheets during progressive flexural slip, have been used to identify movement horizons in some areas (Tanner, 1989; Fowler and Winsor, 1997).

Several studies have demonstrated that flexural slip does not occur at the boundary of each competent-incompetent pair (e.g., Tanner 1989) as suggested in the simplified model of Ramsay (1967; 1974). Also, movement horizons do not necessarily occur at the same stratigraphic horizon across the fold (Markley and Wojtal, 1996; Tanner 1989). Although most studies identified only bedding-parallel movement horizons, Markley and Wojtal (1996) described "oblique ramps", which defined steps between parallel movement horizons.

1.2.3 Movement Direction:

In the simple case of horizontal cylindrical folds, slip occurs perpendicular to the fold axis (Fig. 1.2). However, significant variation in movement direction has been documented between movement horizons and along individual movement horizons (Tanner, 1989; Fowler and Winsor, 1997; Yang and Gray, 1996; Markley and Wojtal, 1996; Price and Cosgrove, 1990; Cosgrove, 1993), although the average slip direction is typically close to perpendicular to the fold hinge. Variation in slip direction may reflect local variation in stress orientation along individual movement horizons during folding (Price and Cosgrove, 1990) or may reflect a change in fold geometry during progressive fold growth (Tanner, 1989; Dubey, 1982).

1.2.4 Shear sense:

Establishing shear sense on movement horizons is critical in relating movement to the flexural-slip mechanism. Flexural slip results in a reverse sense of shear which changes systematically across the fold. Shear sense is not extensively discussed in many previous studies, but has been determined from slickenfibre geometry, offset markers and thrust geometry of flexural-slip duplexes (Tanner, 1989; 1992; Ramsay and Huber, 1987; Price and Cosgrove, 1990).

1.2.5 Quantifying flexural slip:

Flexural shear strain on straight-limbed flexural-slip folds is a function of limb dip (Fig. 1.3a; Ramsay, 1974). Quantifying the amount of flexural slip occurring on movement horizons in natural folds is, however, an outstanding problem and is limited by the lack of

planar strain markers (veins, clastic dykes) which record displacement (Tanner, 1989; Fowler, and Winsor, 1997). Tanner (1989) and Fowler and Winsor (1997) suggested a relationship between the amount of displacement and the thickness of veins occurring along movement horizons, which they have interpreted to result from accumulated slickenfibre growth during progressive flexural slip. However, evaluating the amount of flexural slip, or flexural-slip strain, is tenuous without direct measurement of displacement along movement horizons, by, for example, offset markers. To the author's knowledge there are no studies where flexural slip has been directly quantified.

As discussed by Tanner (1989), the amount of flexural slip in ideal chevron folds could be determined as the difference between the total shear strain and flexural flow shear strain (Fig. 1.3a). However, in order to test this inference we need to know the amount of flexural-flow shear strain, requiring the presence of a marker which records flexural flow. In addition, other fold mechanisms such as tangential longitudinal strain likely account for some of the fold-related strain and all strain markers may be modified by post folding strain.

Tanner (1989) and Fowler and Winsor (1997) suggest that movement horizon spacing decreases sympathetically with increasing limb dip, reflecting increasing shear strain. However, if spacing is to be evaluated with respect to shear strain, the amount of movement along movement horizons and the amount of flexural shear strain is required.

1.2.6 Veins - fluid pressure:

Quartz veins, particularly bedding-parallel veins, are common features of chevron folds and their origin has generated considerable debate (see Fowler, 1996). Many studies

interpret veins as synfolding, reflecting the accumulation of slickenfibre veins during flexural slip (Fowler, 1996; Tanner, 1989; 1990; Cosgrove, 1993; Mawer, 1987; Price and Cosgrove, 1990). Other studies, however, argue a pre-folding origin for these veins (Henderson et al., 1986; Graves and Zentilli, 1982; Fitches et al., 1990; Jessell et al., 1995). This debate clearly extends to the Meguma Group and has consequences for the origin of the numerous gold deposits largely hosted by bedding-parallel veins (see geology of the Meguma Group below).

Price and Cosgrove (1990) and Cosgrove (1993) suggest that, for the development of large-scale flexural-slip folds, high fluid pressure is required during fold initiation to reduce the effective stress normal to bedding (lithostatic load) so that the sequence will deform by buckling rather than shear failure. The cohesion between beds and the coefficient of friction, which limit flexural slip, are substantially reduced as a result of fluid pressure. Cox et al. (1991), Cosgrove (1993) and Price and Cosgrove (1990) discuss the importance of fluid pressure during folding. Clearly, fluid pressure potentially plays a significant role in the development of flexural-slip folds and therefore a discussion of the origin of veins is important. Veins within chevron/box-fold belts are commonly auriferous (e.g., Central Victoria, Australia; Meguma Terrane, Nova Scotia) extending an economic significance to their origin.

1.3 GEOLOGICAL SETTING

The Meguma Terrane is the most outboard terrane of the Appalachians and is separated from the Avalon Terrane to the north by the transcurrent Cobequid-Chedabucto Fault System, which is overlapped by Carboniferous and younger cover rocks (Fig. 1.4). The

Meguma Terrane is dominated by Cambrian-Ordovician metasediments of the Meguma Group and conformably to paraconfomably overlying Ordovician-Early Devonian metasedimentary and metavolcanic rocks. Voluminous, Late Devonian granitic and lesser mafic plutons generally truncate regional fold patterns and related cleavage within the metamorphic rocks.

The Cambrian-Early Devonian metamorphic rocks were deformed and metamorphosed during the Mid-Devonian Acadian Orogeny, constrained to the interval of about 415-385 Ma by $^{40}Ar/^{39}Ar$ dating (Muecke et al. 1988; Keppie and Dallmeyer, 1987; Hicks et al., in press; Kontak et al., 1998), which likely reflects accretion of the Meguma Terrane to Laurentia (Keppie, 1983; Muecke et al., 1988). The spread in metamorphic ages indicated by $^{40}Ar/^{39}Ar$ data has been interpreted to reflect diachronous deformation and development of related cleavage across the terrane (Keppie and Dallmeyer, 1987; Keppie, 1993; Kontak et al., 1998).

NW-transpression during the Acadian deformation resulted in northeast- to north-trending folds in the Meguma Group and overlying units and dextral displacement at the terrane boundary (Keppie, 1993; Fig. 1.4). Continued, post-Acadian transpression of the Meguma Terrane from Late Devonian to Permian time is indicated by: (1) dextral displacement on the Cobequid-Chedabucto Fault System (Mawer and White, 1987; Gibbons et al., 1996); (2) syntectonic strain within the South Mountain Batholith (Horne et al., 1992; Benn et al.,1997); (3) shortening of Meguma Group rocks during the Carboniferous (Culshaw and Liesa, 1997; Horne et al., 1997a); (4) tectono-thermal events recorded by $^{40}Ar/^{39}Ar$ dating (Kontak and Cormier, 1991; Dallmeyer and Keppie, 1987; Keppie and Dallmeyer, 1995;

Muecke et al., 1988) and; (5) shortening of Carboniferous rocks (e.g., Boehner, 1991).

The basement rocks of the Meguma Terrane are not well understood, although these may be represented by gneissic units within the Liscomb Complex and xenoliths within the Weekend Dykes (Clarke et al., 1993; Eberz et al., 1991) (Fig. 1.4). The Liscomb Complex comprises sillimanite grade gneisses and mafic and granitoid intrusions. The gneissic units are interpreted as middle- to lower-crustal material, possibly reflecting deeper levels of the Meguma Terrane which was either tectonically or diapiricly emplaced (Clarke et al., 1993). A Late Devonian age of emplacement for the Liscomb complex to its current crustal position is constrained by $^{40}Ar/^{39}Ar$ ages for the gneissic and intrusive units (Kontak and Reynolds, 1994). Isotopic data suggest the Liscomb gneisses are the probable source rocks for Meguma Terrane granitoids (Clarke et al., 1993). Granulite facies xenoliths entrained within several mantle-derived lamprophyre dykes (Weekend Dykes) have possible Avalon affinity (Eberz et al., 1991), suggesting Avalonian basement underlying the Meguma Terrane. The character of the Liscomb Complex and lamprophyre dykes has lead to the suggestion that gneisses of the Liscomb Complex represent basement to the Meguma Group and that the Meguma Terrane is, or was, underlain by the Avalon Terrane (Clarke et al., 1993). This crustal architecture is consistent with the interpretation of Keppie (1993) that the Meguma Terrane was obducted over the Avalon Terrane, with the Cobequid Chedabucto Fault Zone representing a lateral ramp to the sole thrust beneath the Meguma Terrane.

In summary, the Paleozoic history of the Meguma Terrane includes Middle Devonian terrane accretion and resulting regional deformation and metamorphism, Late Devonian granite emplacement, rapid uplift, and deposition of clastic and marine sediments. Regional

transpression was recorded throughout this period, with the most intense deformation during the Mid-Devonian Acadian Orogeny. Post-Acadian tectonism may have been continuous or episodic. Of particular note is the generation of extensive magma at ca. 370 Ma, coincident with emplacement of the Liscomb Complex and lamprophyre dykes, which implies a significant lower crustal event at this time.

1.4 GEOLOGY OF THE MEGUMA GROUP

1.4.1 Stratigraphy and age:

The Meguma Group has been traditionally divided into the lower metasandstone-dominated Goldenville Formation and overlying slate-dominated Halifax Formations (Fig 1.4; Woodman, 1904; Fletcher and Faribault, 1911; Keppie, 1979). Further stratigraphic subdivision has been documented locally, particularly in the Halifax Formation and the upper part of the Goldenville Formation (Fig. 1.6; O'Brien, 1988; Waldron, 1992; Schenk, 1991; Ryan et al., 1996). The transition between the Goldenville and Halifax Formations is locally gradational and various criteria have been used in defining this boundary, which is often characterized by enrichment in manganese and carbonate. Distinctive rocks in the transition include the Moshers Island and Beaverbank units (Fig. 1.6). For the purposes of this thesis discussion will be primarily limited to the Goldenville and Halifax formations, which define the major stratigraphic-structural units. The two areas studied are located within the lower part of the Halifax Formation, within the Cunard member (Fig. 1.6).

The age of the Meguma Group is not well constrained. Middle Cambrian trilobite fauna have been documented from the upper Goldenville Formation (Tancook Member, Fig.

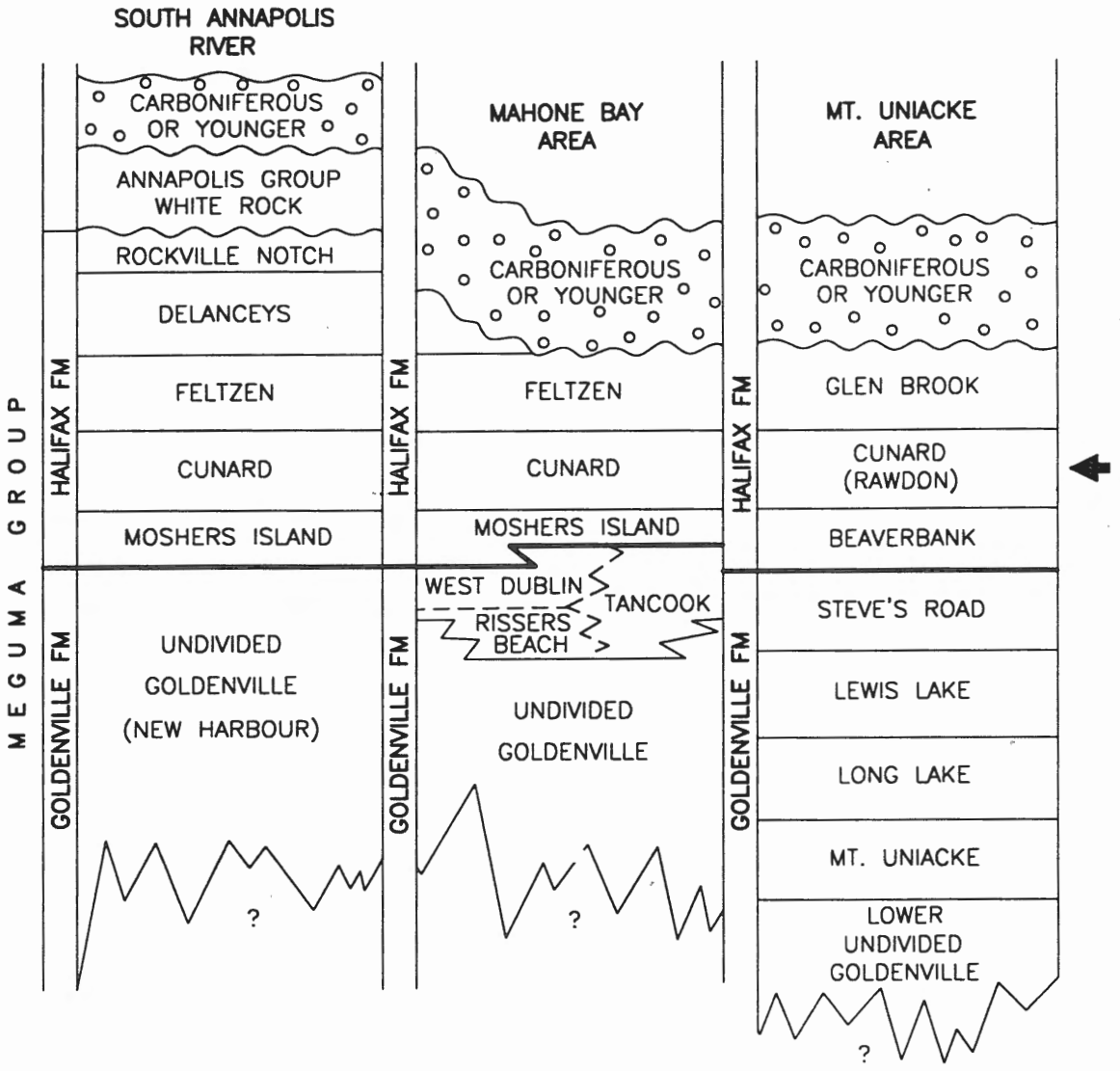

Figure 1.6: Stratigraphic subdivision and of the Meguma Group in the South Annapolis River and Mahone Bay area (Schenk, 1995) and Mount Uniacke area (Ryan et al., 1996). Modified from Schenk (1995).

1.6) (Pratt and Waldron, 1991). Graptolites of Early Ordovician? age occur in the upper part of the Goldenville Formation (Poole, 1971). Detrital zircon from the lower Goldenville (566 ±8 Ma, U-Pb; Krogh and Keppie, 1990) and detrital muscovite (550-600 Ma, $^{40}Ar/^{39}Ar$; Hicks, 1996) help constrain the depositional age of this unit. Early Ordovician (Tremadocian) graptolites occur in the Halifax Formation (Smitheringale, 1960; Crosby, 1962; Cummings, 1985).

1.4.2 Structure and metamorphism:

1.4.2.1 F_1 Folds:

The dominant structures of the Meguma Group are the regional, kilometre-scale folds (Fig. 1.4). Fold axes vary in trend from east-west in the eastern end of the terrane to north-south in the western end, and are generally subhorizontal, with terminations plunging moderately, to locally steeply, in both directions. The non-cylindrical fold style is apparent from the distribution of the Goldenville and Halifax formations (Fig. 1.4). Cross-sections of the Meguma Terrane (Fig. 1.4) indicate that folds consist of tight- to open-chevrons and modified box folds (i.e., with folded flat segments), and no systematic vergence is shown by axial planes. As discussed above, these fold geometries are typical of buckled, anisotropic, multilayered sequences such as turbidites where the location and attitude of axial planes reflects initial instabilities during shortening of the sequence. The modified box folds define a series of regional-scale anticlinoria and synclinoria, which, at the current level of exposure, generally correlate with distribution of the Goldenville and Halifax formations respectively (cross section, Fig 1.4).

Several minor structures are geometrically related to regional folds and are discussed below.

Minor Folds:

Minor decimetre- to centimetre-scale folds are common and show a parasitic relationship to regional folds (Fig. 1.8; Henderson et al., 1986; Horne, 1995; Horne et al., 1997b; 1998). Minor folds include local buckled bedding-parallel quartz veins, rare buckled metasandstone layers and minor folding of layering within slate units.

S_1 cleavage:

Well developed cleavage, including a continuous cleavage in the slates and a variably developed spaced cleavage in the metasandstone, is associated with regional folds and relates minor folds to development of regional-scale folds (Henderson et al.,1986; Horne et al., 1997b). Cleavage has an axial planar relationship to individual folds, with a similar bedding-cleavage angle (β) on both limbs (e.g., O'Brien, 1983; Henderson et al. 1986; Horne et al., 1997b; 1998). However, cleavage patterns across multiple folds, which commonly include conjugate folds with opposing axial planes, have not been documented.

Henderson et al. (1986) proposed that cleavage formed prior to folding. This was based largely on the basis that worm tubes (paleoplumblines) coincide with cleavage regardless of bedding-cleavage angle, and because bedding-plane strain is constant regardless of position on the fold. Treagus (1988), however, argued that the data of Henderson et al. (1986) does not convincingly demonstrate a prefolding origin for cleavage. Volume loss of

up 60% during cleavage formation has been proposed on the basis of geometric strain analysis (Wright and Henderson, 1992) and chemical mass balance analysis (Fueten, 1984), and is supported by a lack of evidence for cleavage-related extension (e.g., Pryer, 1984; Henderson et al., 1986). The interpreted volume loss has been challenged by Erslev and Ward (1994), who used macroprobe analysis to map element distributions which suggest that, although redistribution of elements occurred during cleavage formation, there was no large non-volatile volume loss as a result of cleavage formation. In addition, both hinge-parallel and down-dip extension, defined by pressure shadows on metamorphic porphyroblasts, including sulphides, have been locally documented throughout the Meguma Group (Haysom et al., 1997; Horne et al., 1997b; Graves and Zentilli, 1982; Benn et al., 1997; N. Culshaw, Personal Communication).

Joints and veins:

Joints are abundant in the Meguma Group, particularly within the metasandstone layers of the Goldenville Formation. The most prominent joint set roughly parallels the "ac" plane of folds (Fig. 1.7), and these joints commonly host quartz veins (Henderson, 1983; Henderson et al., 1986; Williams and Hy, 1990; Horne et al., 1997b; O'Brien, 1983).

Several veins sets have been described within the Meguma Group, with most examples from within the numerous gold districts. A varied list of terms have been used for the various veins (e.g., Faribault, 1913; Henderson, 1983; Smith and Kontak, 1988; Williams and Hy, 1990). Several vein sets which are geometrically related to regional folds have been described, including bedding-parallel, saddle reef, en echelon and discordant veins (ac) (Fig. 1.7).

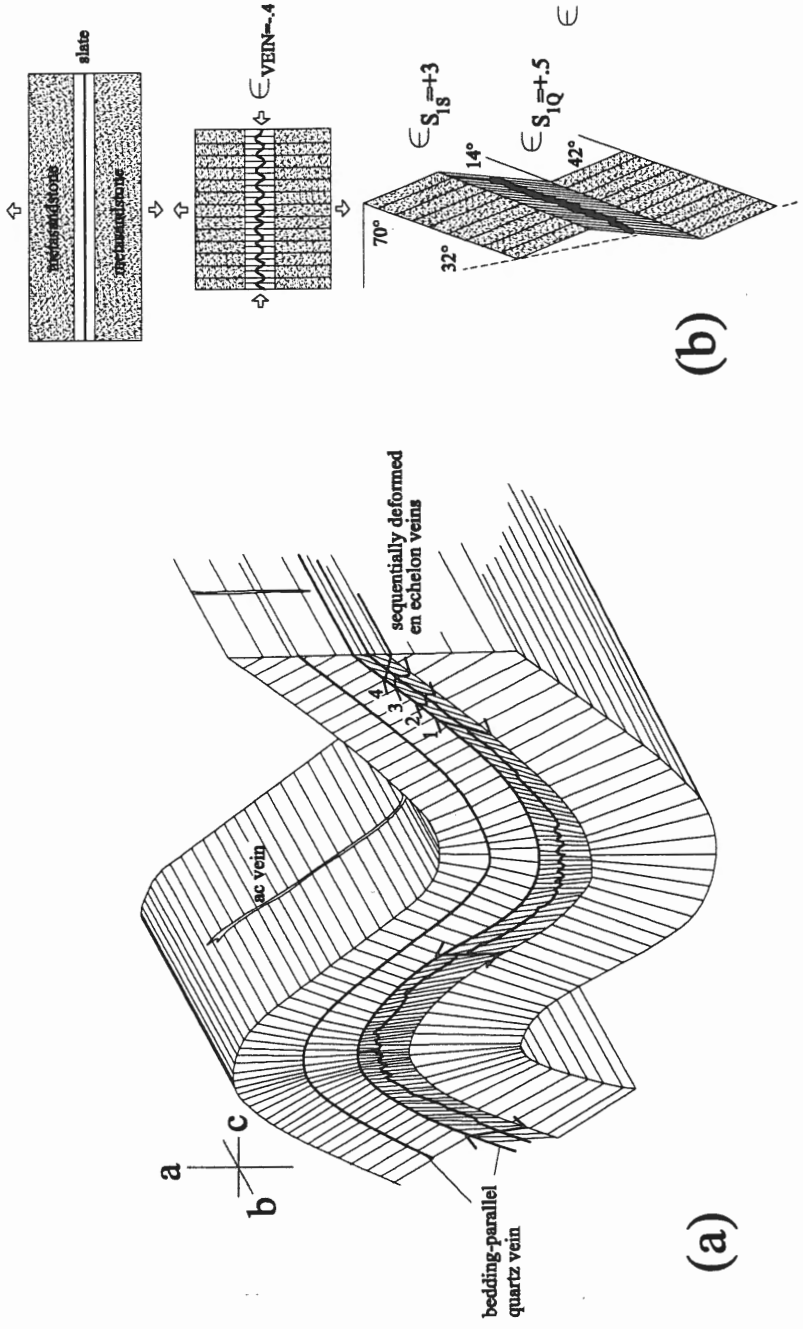

Figure 1.7: (a) Schematic diagram showing the geometry of bedding, cleavage and quartz veins in a Meguma Group fold. (b) Diagram illustrating bedding-cleavage relations resulting from flexural-flow during rotation of bedding, with extension of cleavage in slate (ϵ_{S1S}) and metasandstone (ϵ_{S1Q}) indicated. (After Henderson et al., 1986).

Fold mechanisms:

Few studies have addressed the structural evolution and folding mechanism of the Meguma Group. Henderson et al. (1986) proposed a history of cleavage development and folding for the Meguma Group (Fig. 1.7b) which includes: (1) Formation of bedding-parallel quartz veins by hydraulic fracturing due to fluid over-pressuring resulting from compaction; (2) Homogenous, layer-parallel shortening resulting in cleavage development and buckling of bedding-parallel veins, and; (3) Development of regional folds with limb amplification primarily by flexural flow, with cleavage acting as a passive marker. Differential shear between slate (high shear) and metasandstone (low shear) resulted in strong cleavage refraction. Their measurements of shear strain, using the bedding-cleavage angle, suggested that flexural flow accounts for most of the flexural strain and that flexural slip did not occur. Flexural flow is supported by local en echelon veins, which record progressive and significant shear within slate intervals. These veins are pinned in adjacent metasandstone beds, thus precluding flexural slip across the interval (Fig. 1.7a; Henderson et al., 1986).

In contrast to the proposal of Henderson et al. (1986), several studies have documented evidence of flexural slip within the Meguma Group (Faribault, 1899; 1913; Keppie, 1976; Douglas, 1948; Smith, 1976; O'Brien, 1983). Early workers discuss in detail the flexural slip process in folding of the Meguma Group as evidenced by "striations and slickensides....and....crushed black slates or gouge" (Faribault, 1899) and "drag folding and intense shearing and comminution of some of the beds of slate" (Douglas, 1948) along bedding planes in many of the gold deposits. Faribault and Douglas also recognized that flexural slip was focused within the slate intervals (relatively incompetent beds). Douglas

points out that the amount of flexural slip is a function of rotation of bedding and the thickness of the layers, similar to the model of Ramsay (i.e., Fig. 1.3).

1.4.2.2 Metamorphism:

Metamorphic grade in the Meguma Group ranges from sub-greenschist to amphibolite grade, with regional isograds cutting across the regional structure and stratigraphy (Keppie and Muecke, 1979). A lower limit for the age of regional deformation and metamorphism is constrained by the age of the youngest metamorphosed rocks, the Torbrook Formation. Bouyx et al. (1992) assign a Lochkovian to Lower Emsian age for the Torbrook Formation, which, according to Tucker et al. (1998), spans from 419-394 Ma. Late Devonian granites (ca. 370 Ma, Clarke et al., 1993; Harper, 1988) truncate regional structural trends and metamorphic isograds and contain Meguma Group xenoliths preserving regional deformation and metamorphic fabrics. $^{40}Ar/^{39}Ar$ ages for whole rock samples (Keppie and Dallmeyer 1987; Dallmeyer and Keppie, 1987; Reynolds and Muecke, 1978; Muecke et al., 1988) and muscovite separates of metamorphic origin (Hicks, 1996) constrain a range (ca. 400-385 Ma) for the age of cleavage development, interpreted to reflect either diachronous metamorphism or sampling of different structural levels. Sampling of different structural levels could reflect post-metamorphic flexural-slip folding and thrusting recognized in this study, which would result in a folded regional isotherm reflecting $^{40}Ar/^{39}Ar$ blocking temperatures (Kontak et al., 1998).

1.4.2.3 Post F1 Deformation:

As stated above, there is evidence of post-Acadian, regional, NW-directed transpression of the Meguma Terrane, and this deformation is locally evident within the Meguma Group. Culshaw and Liesa (1997) documented a wide zone of Mid-Carboniferous shear zones and folds overprinting F_1 folds in the Yarmouth area (Fig. 1.4). Carboniferous age deformation of the Meguma Group adjacent to the Rawdon Fault (Fig. 1.4) resulted in the formation of F_2 folds and related crenulation cleavage (Horne et al., 1997a). A crenulation cleavage is locally developed within the Halifax Formation in the central Meguma Terrane area (Horne et al., 1997b; 1998), which may be related to late fold tightening. A crenulation cleavage is locally developed within the Halifax Formation along the eastern shore (O'Brien, 1983; personal observations of the author). Therefore, post-Acadian deformation may be widespread within the Meguma Terrane.

1.4.2.4 Gold deposits:

As stated above, several vein sets are recognized regionally throughout the Meguma Group and these have been used to help interpret the structural evolution of the Meguma Group. Locally, anomalous concentrations of auriferous veins occur, mainly in the culmination of dome structures, which have been referred to as "Gold Districts" (e.g., Malcom, 1929). Several vein sets have been documented within the various gold districts, with variable terminology applied by different workers. There has been considerable debate regarding the origin of the auriferous veins and, although several vein sets occur, bedding-parallel veins have been considered the principal vein set and their origin is generally at the

centre of the debate regarding the origin of the deposits.

Haynes (1986) proposed a syngenetic, exhalative model for vein formation. Graves and Zentilli (1982), Henderson et al. (1986; 1992), and Henderson and Henderson (1986) proposed that bedding-parallel veins formed by hydraulic fracturing prior to regional folding. A variety of syn-folding models have been proposed by Faribault (1899; 1913), Douglas (1948), Mawer (1987) and Keppie (1976). Faribault (1899; 1913) and Douglas (1948) proposed a direct relationship between bedding-parallel veins and flexural slip and a saddle reef (flexural-slip) model was proposed by Keppie (1976). Kontak et al. (1990a) and Williams and Hy (1990) suggest that regional shear zones were important in gold mineralization.

1.5 OBJECTIVES

The general aim of this thesis is to document the character of flexural slip within the Meguma Group and to evaluate the importance and timing of flexural slip with respect to regional fold development. In addition, the origin of vein arrays defining Meguma Gold Districts will be addressed with respect to the flexural-slip mechanism. Assessment will include:

1 - Establishing and qualifying flexural-slip features;

2 - Quantifying flexural slip, including spacing of movement horizons and slip amount;

3 - Evaluating the age of flexural slip and related strain with respect to regional folding;

4 - Evaluating the role of flexural slip in the localization of Au-quartz veins at the Ovens and discussing the potential role of fluid pressure to the flexural-slip mechanism.

The results of this study will be discussed in terms of regional folding and gold deposit formation within the Meguma Group, and therefore will add to our knowledge of the deformational and metallogenetic history of the Meguma Group. In addition, these results will add to the general knowledge of folding and related strain history of folded multilayered sequences. In particular, quantitative evaluations of slip amount provide a basis on which to evaluate current hypotheses on flexural-slip folding.

1.6 TERMINOLOGY

Following is an explanation for structural terms as they are applied in this thesis.

1.6.1 General fold-related terms:

(See figure 1.8 for illustration of the features defined below.)

Bedding-cleavage intersection lineation: The line defined by the intersection of cleavage and bedding. The bedding-cleavage intersection is parallel to the fold hinge where cleavage is axial planar to the fold.

Fold hinge: A line connecting the points of maximum curvature of the fold

Hinge Zone: Curved section of fold between planar limbs.

Axial plane: A plane which bisects the limbs of the fold. For parallel chevrons, such as the folds in this thesis, this definition is similar to a plane including hinge lines.

Interlimb angle: Dihedral angle between planar segments of limbs.

Principal axis: The principal axes of the fold are, by convention: a axis is normal to the axial plane, the b axis parallels the fold hinge and the c axis is perpendicular to the hinge and contained within the axial plane.

Profile (ac) plane: Plane which is perpendicular to the fold hinge. Contains the a and c fold axes.

ac joint: Joint which parallels the ac plane.

Plunge: Angle between the fold hinge and the horizontal measured within a vertical plane containing the fold hinge.

1.6.2 *Stereonet terms:*

Pole: Line perpendicular to a plane; i.e., pole to bedding.

π-girdle: Great circle defined by poles to bedding in a fold.

Eigenvectors: Results of a method of evaluating the clustering of stereonet data, defined as three principal directions (vectors), where the minimum vector (1) is normal to the best-fitting girdle through the data and the maximum vector (3) is the direction that best fits the maximum clustering.

1.6.3 *Orientation Data*

Strike: Azimuth of structural contour, or intersection of plane with the horizontal.

Dip: Inclination of planar surface.

Dip azimuth: Azimuth of the dip projected into the horizontal.

Trend: Azimuth, projected into the horizontal, and dip, within a vertical plane, of a lineation.

Rake: Acute angle between the horizontal and a lineation within a plane.

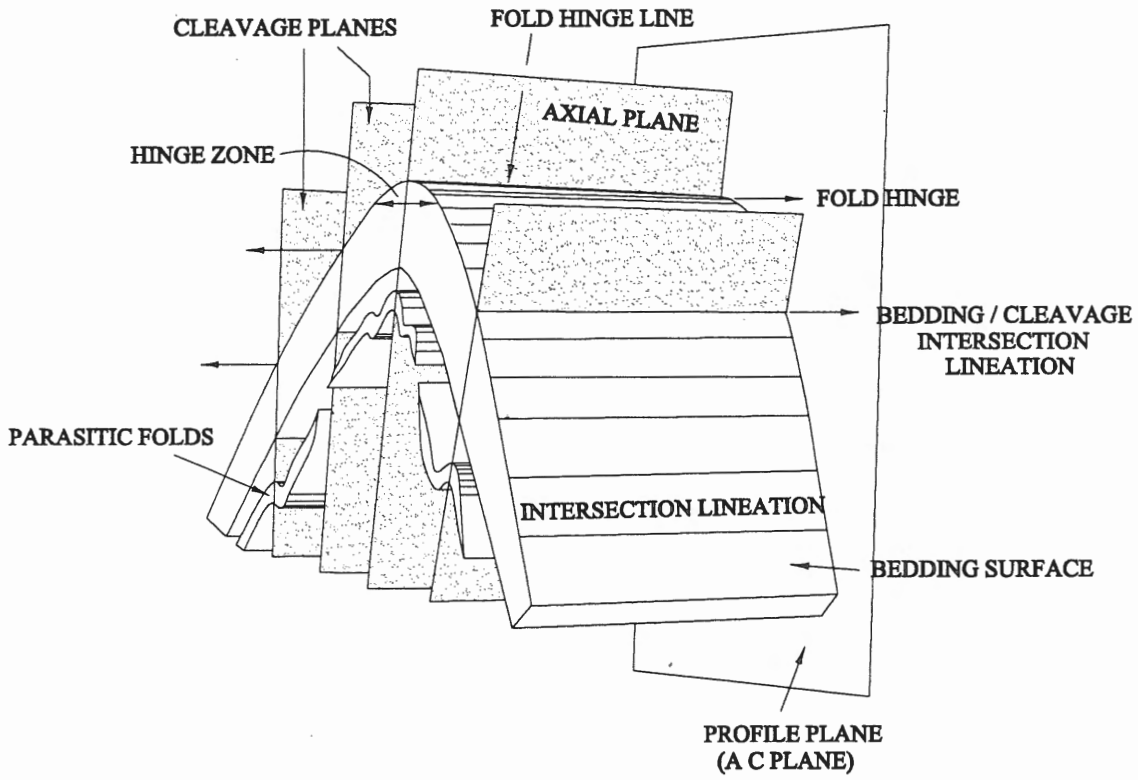

Figure 1.8: Schematic diagram showing the structural features of a fold. (After Boulter, 1989).

CHAPTER 2

HALIFAX STUDY AREA

2.1 Introduction:

The Halifax area is underlain primarily by the Meguma Group, with granitoids of the South Mountain Batholith (SMB) and Musquodoboit Batholith exposed in the southwest and northeast respectively (Fig. 2.1). A contact aureole adjacent to the SMB is represented by abundant cordierite porphyroblasts and partial annealing of cleavage, and extends within the study area of the railway tracks section investigated in this study (Figs. 2.1, 2.2). The map pattern of the Meguma Group in the Halifax area reflects regional folding, with the overall southwest-plunging character of folds illustrated by the distribution of the Halifax Formation between the Cow Bay and Dartmouth synclines (Fig. 2.1). This plunge is supported by bedding-cleavage intersection lineation data in the railway section (Figs. 2.2, 2.3). A cross section through the Meguma Group in the area (Fig. 2.1) indicates a fold profile typical of the Meguma Group (compare with Fig. 1.4), defined by regional, kilometre-scale, modified box folds and chevrons. The railway tracks study area straddles the Lawrencetown Anticline, which represents a minor, chevron-shaped anticline within the core of a broad synclinorium, herein referred to as the Point Pleasant synclinorium (Fig. 2.1). The cross section indicates that, although the railway tracks study area occurs within exposed Halifax Formation, the Goldenville Formation is close to surface within the hinge area of the Lawrencetown Anticline (Fig. 2.1).

The railway tracks study area consists of a nearly continuously exposed section of

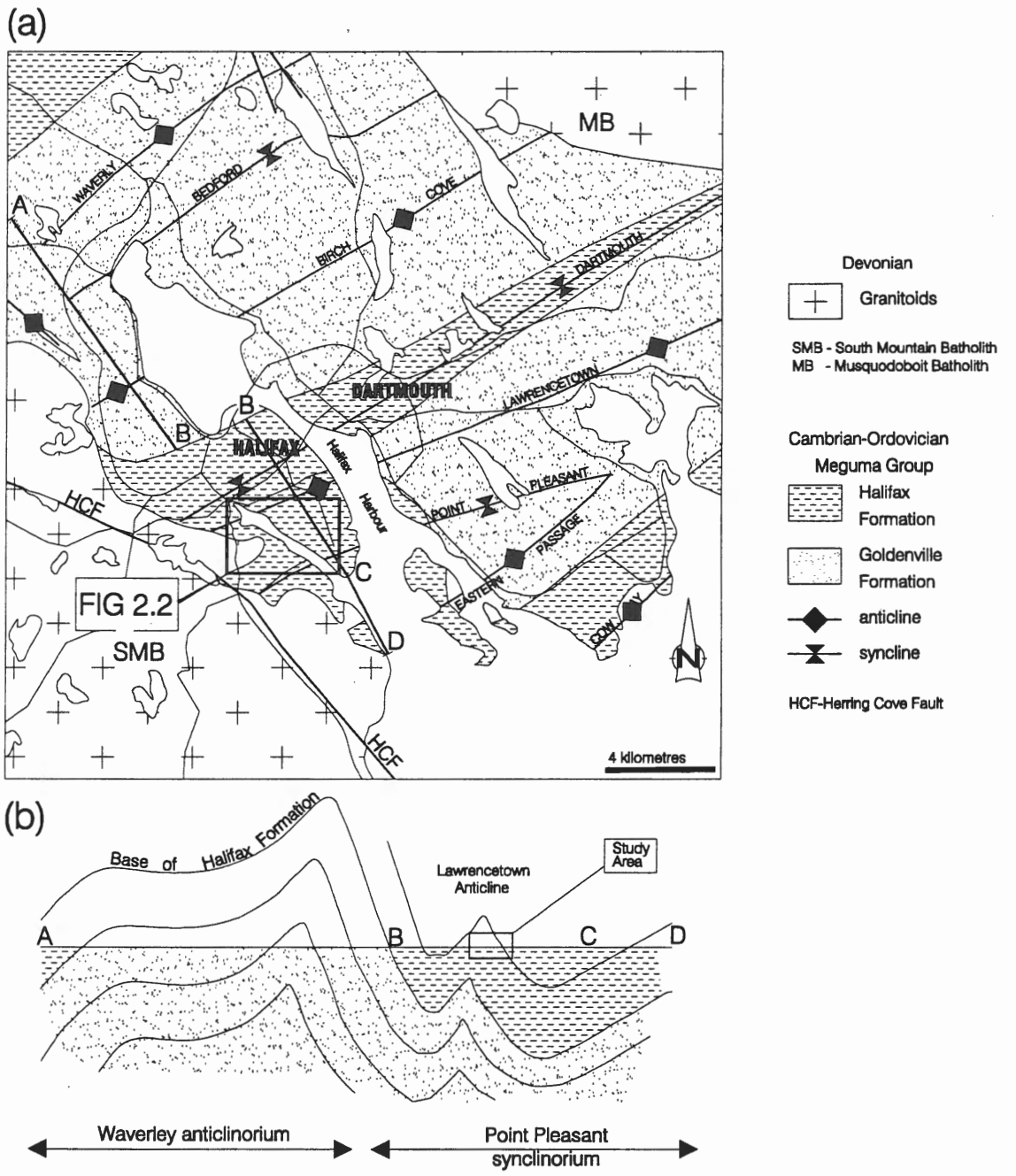

Figure 2.1: Simplified geology map (a) and cross-section (b) of the Halifax area showing the location of the Halifax (railway tracks) study area (Fig. 2.2). Modified after Faribault (1908).

the Meguma Group along the C.N. railway tracks along the northern side of Northwest Arm (Fig. 2.2), and provides an excellent setting to address the structure of the Meguma Group. Most of this section is approximately perpendicular to the fold hinge (Fig. 2.2), providing a profile section through the fold, which allows for evaluation of the typical bedding-parallel structures related to flexural slip. In addition, the southern part of the section trends approximately parallel to strike, permitting assessment of the nature of flexural-slip structures along strike. Together, the profile and strike-parallel sections provide a third dimension to the general model presented for flexural-slip in previous studies of fold profiles (e.g., Tanner, 1989).

Flexural slip is evident throughout the railway section by movement horizons, which show movement indicators and sense of shear consistent with flexural slip. In an attempt to best evaluate flexural slip in the area three principal methods were utilized.

(1) Construction of detailed stratigraphic and structural logs for several profile sections. These allow for evaluation of the character and spacing of strike-parallel structures, including bedding-parallel and frontal ramp movement horizons.

(2) Detailed mapping of strike-parallel sections, including construction of stratigraphic and structural logs and detailed mapping of flexural-slip structures using photomosaics. These allow for along-strike evaluation of flexural-slip features.

(3) General evaluation of stratigraphy and structure throughout the entire section, including recording orientation data for flexural-slip structures. This allows for stratigraphic subdivision within the section and evaluation of the importance of flexural slip throughout the area.

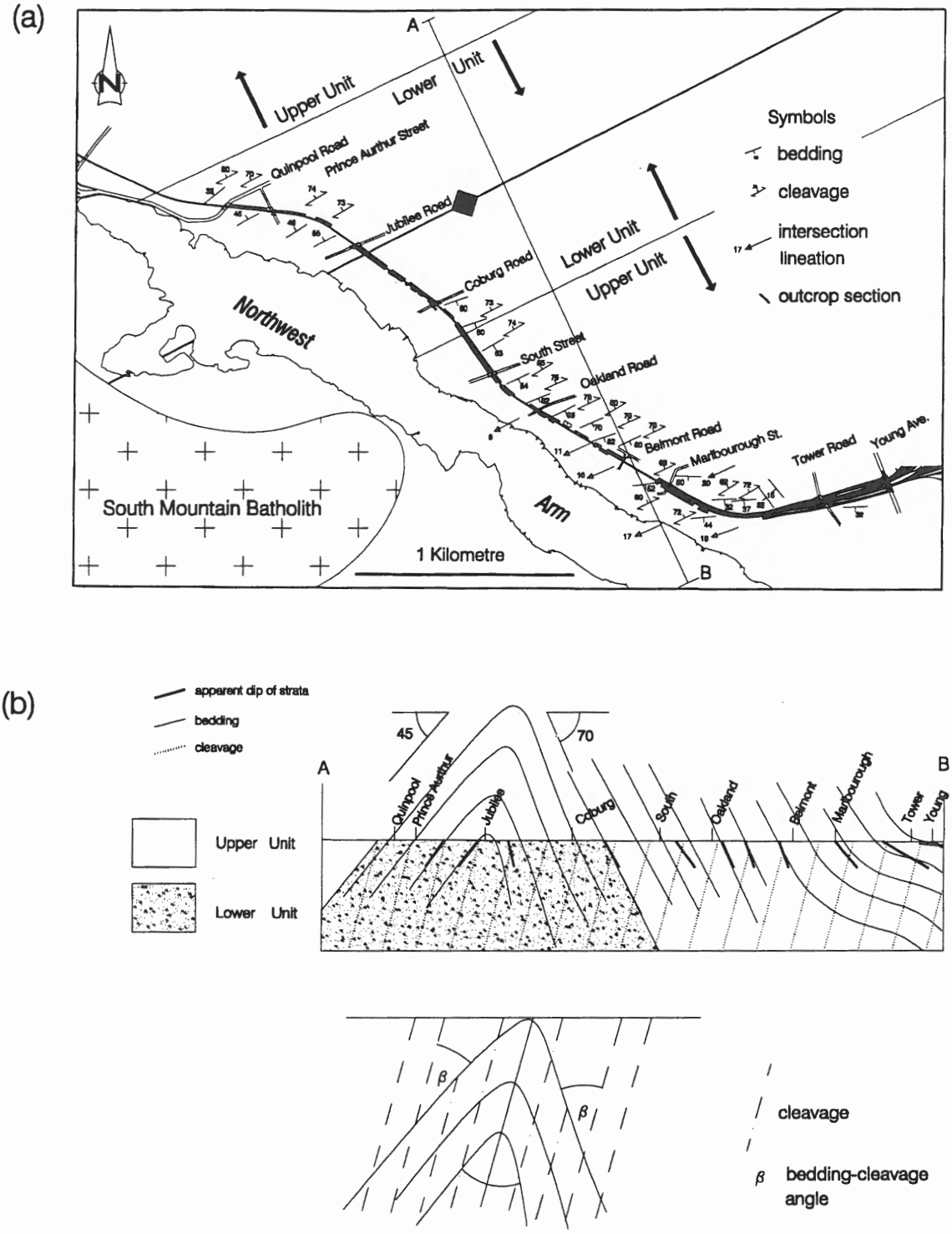

Figure 2.2: (a) Detailed geology map of the railway section study area. (b) Cross section (A-B in (a)) through the study area. Note that cleavage is axial planar to the fold, resulting in a similar bedding-cleavage angle on both limbs.

2.1 Geology of the railway section

2.1.1 Stratigraphy:

Faribault (1908) included the railway section within the Halifax Formation (Fig. 2.1). Mapping during this study indicates stratigraphic variation within the area which may warrant further subdivision within this formation (Fig. 2.2). The area of the hinge zone is characterized by black slate with a high proportion of thick metasandstone beds, as indicated in measured sections for this area (logs A-E, Fig. 2.4, in pocket at back), and is herein referred to as the *lower unit*. In contrast, the stratigraphically higher part of the section, exposed on the south limb, is characterized by mainly black, sulphide-rich slate with thin (<10 cm) interbedded metasandstone (logs F-H, Fig. 2.4, in pocket at back), herein referred to as the *upper unit*. The upper, slate-dominated unit is typical of the regionally extensive Cunard member of the Halifax Formation (personal observation), which is recognized throughout the Meguma Group (e.g., O'Brien, 1988; Waldron, 1992; Schenk, 1991; Horne et al., 1997b; 1998). The high proportion of thick metasandstone beds within the lower unit, exposed within the hinge area of the anticline, is interpreted to reflect proximity of the underlying Goldenville Formation in the area (see cross-section, Fig. 2.1). Manganese concretions are common within metasandstone beds of the lower unit, consistent with stratigraphy of the Meguma Group near the boundary of the Halifax and Goldenville formations (e.g., O'Brien, 1988; Waldron, 1992).

2.1.2 Structure:

The Lawrencetown Anticline in the area defines a kilometre-scale, slightly inclined

chevron fold with an interlimb angle of approximately 65-70° (Fig. 2.2). A minor fold occurs on the south limb, near the southern part of the studied section (Fig. 2.2). The hinge zone of the Lawrencetown Anticline, exposed a few metres south of Jubilee Road, is defined by a rounded hinge which is a few tens of metres wide (Fig. 2.5). Minor folds of thin metasandstone occur in the hinge (Fig. 2.5), but are absent on the limbs.

Stereoplots of structural data for the area illustrate systematic trends, with all data clearly related to the fold geometry (Fig. 2.3). The pole of the π girdle, which represents the fold hinge, trends 246/10 (vector 1, Fig. 2.3a), parallel to the average of the bedding-cleavage intersection lineation data, which trends 245/10 (vector 3, Fig 2.3b). A finely spaced, continuous cleavage is well developed within slate intervals throughout the section, although partially annealed due to contact metamorphism related to the SMB. Cleavage is generally not apparent within the metasandstone intervals. Cleavage within the slate intervals dips uniformly to the northwest across the fold (Fig. 2.3c), maintaining an axial planar relationship to the fold, and the angle between bedding and cleavage (β) is similar on both limbs (Fig. 2.2b).

Joints are ubiquitous throughout the section. They are closely spaced, typically less than 2 metres apart, and are more common and better developed within metasandstone beds than slate beds. The average of the poles to discordant joints trends 249/1 (vector 3, Fig. 2.3d). This is roughly parallel to the bedding-cleavage intersection lineation data and the pole to the π girdle, suggesting these fractures are ac joints (i.e., parallel to the profile plane of the fold). Quartz veins are common within joints and a few laminated, bedding-parallel veins occur within the section (Fig. 2.4, in pocket at back).

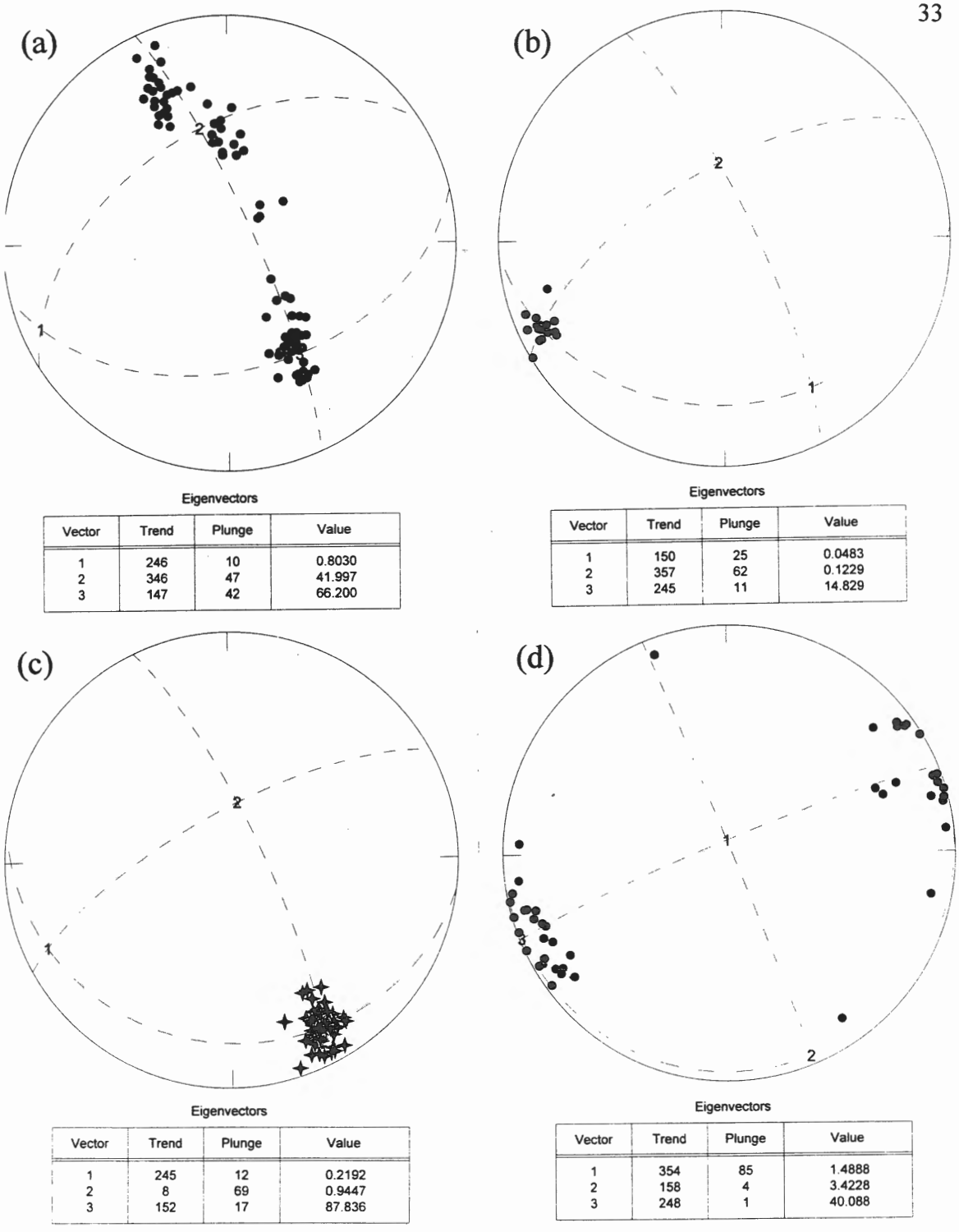

Eigenvectors

Vector	Trend	Plunge	Value
1	246	10	0.8030
2	346	47	41.997
3	147	42	66.200

Eigenvectors

Vector	Trend	Plunge	Value
1	150	25	0.0483
2	357	62	0.1229
3	245	11	14.829

Eigenvectors

Vector	Trend	Plunge	Value
1	245	12	0.2192
2	8	69	0.9447
3	152	17	87.836

Eigenvectors

Vector	Trend	Plunge	Value
1	354	85	1.4888
2	158	4	3.4228
3	248	1	40.088

Figure 2.3: Equal area lower hemisphere stereoplots of (a) poles to bedding, (b) bedding-cleavage intersection lineations, (c) poles to cleavage and (d) poles to joints, for the Lawrencetown Anticline in the railway section. Eigenvector data: vector 3 is the direction of the best fitting maximum cluster; vector 1 is the pole to the best fitting plane (girdle) through the data.

Figure 2.5: Photograph of the hinge zone of the Lawrencetown Anticline exposed in the railway tracks near Jubilee Road. Note minor folding of thin layers in the hinge zone (indicated by arrows). View looking northeast. Metal box at left approximately 1 metre wide.

2.2 FLEXURAL SLIP:

2.2.1 General Statement:

As stated above, features related to flexural-slip folding have been recognized within the railway section. Establishing that structures are related to flexural slip follows the guidelines outlined in Chapter 1. This chapter presents data on the character, density, shear sense and movement direction of flexural-slip structures within the area.

Three common sets of movement horizons related to flexural-slip folding have been distinguished on the basis of their geometric relationship to bedding and the fold geometry. These include bedding-parallel, lateral ramp and frontal ramp movement horizons, and are illustrated in Fig 2.6. As will be shown, these structures are all genetically related, with lateral ramp and frontal ramp movement horizons related to bedding-parallel movement horizons in the same way as similar structures are to thrust faults in thrust systems. In addition, a set of movement horizons which have a conjugate relationship with bedding-parallel movement horizons are locally developed.

2.2.2 Bedding-parallel movement horizons:

Bedding-parallel movement horizons are abundant, and defined by bedding-parallel fractures characterized by striations or sheets of quartz slickenfibres (Fig. 2.7). Identification of bedding-parallel movement horizons is limited to exposed surfaces where movement indicators are present. Discordant markers which would indicate displacement are not present and laminated bedding-parallel veins, used by Tanner (1989) and Fowler and Winsor (1997) to identify movement horizons, are rare. Observations on well exposed movement horizons

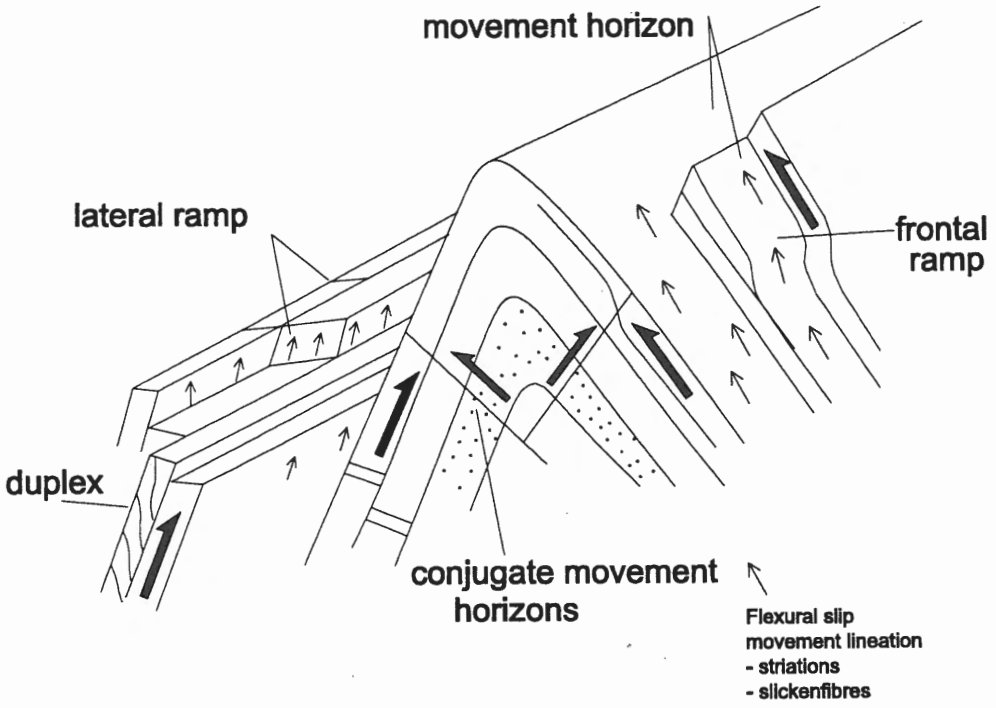

Figure 2.6: Schematic diagram of the Lawrencetown Anticline within the railway tracks study area showing the relationship of flexural-slip related structures to the fold.

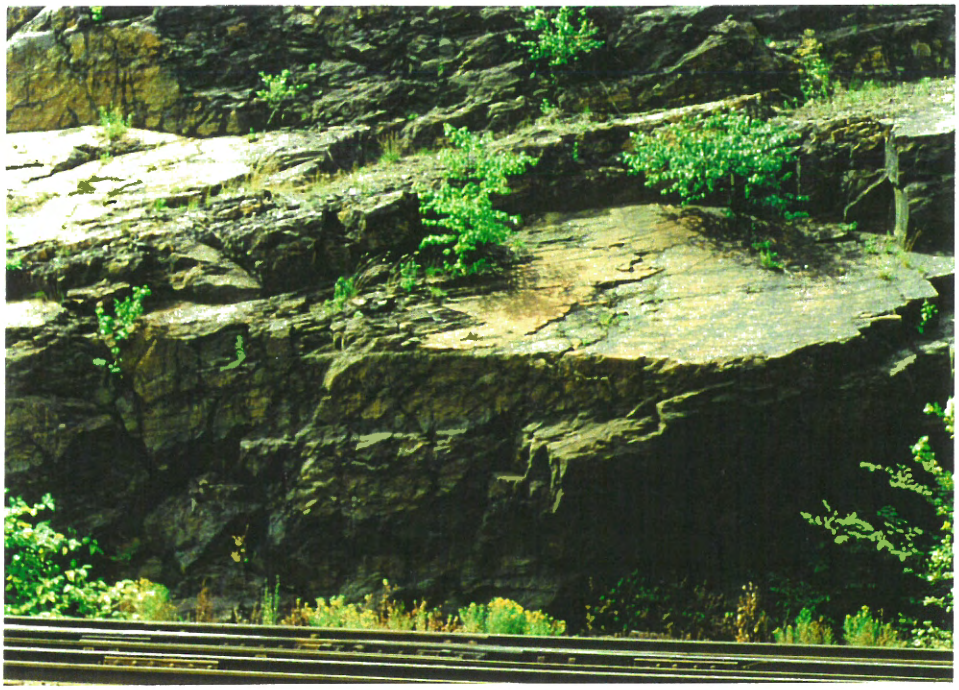

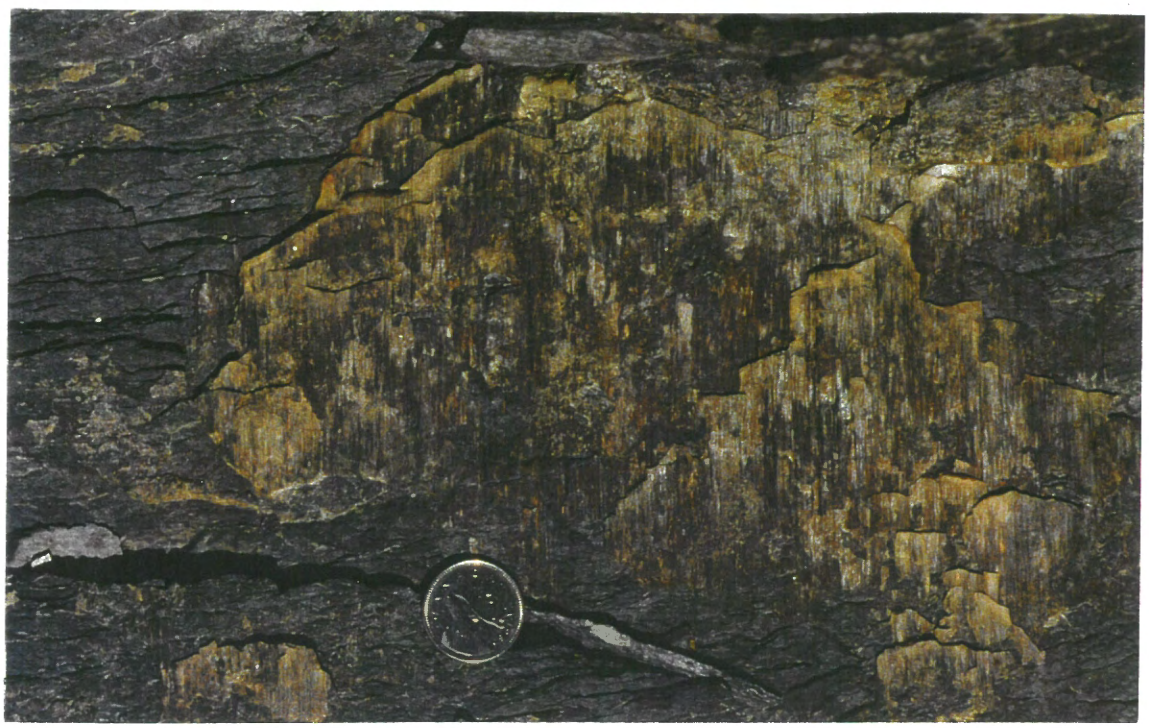

Figure 2.7: (a) Photograph of typical movement horizon in the railway section, consisting of a single movement surface. (b) Photograph of bedding-parallel movement horizon coated with quartz slickenfibres. Long axis of photograph trends roughly parallel to strike and dips toward the bottom of photo. Geometry of slickenfibres clearly indicate movement of the upper block toward the top of the page, consistent with flexural slip. Coin diameter 2.3 cm.

indicate that the occurrence and abundance of slickenlines and slickenfibres varies along movement horizon surfaces. Within a particular movement horizon slickenlines or slickenfibres may vary from abundant (e.g., continuous slickenfibre sheet) in one area to hardly any indication of movement in other areas. This is of concern as there are many bedding-parallel fractures within the section where poor exposure of the surface limits evaluation of the presence of slickenlines or slickenfibres and therefore these could not be classified as movement horizons.

The majority of bedding-parallel movement horizons within the studied section consist of simple slip surfaces (e.g., Fig. 2.7), with minimal deformation of the foot wall or hanging wall. Locally, movement horizons are defined by zones of brecciation and, rarely, domino structures are developed in the footwall of movement horizons (Fig. 2.8). Domino structures are bounded by shear fractures with the sense of shear indicated by offset of bedding laminations (Fig. 2.8). The shear fractures are commonly coated with quartz slickenfibres, which show a sense of shear similar to offset of bedding. Minor extensional veins locally developed within the domino structures (Fig. 2.8) are consistent with bedding-parallel shear indicated by dominoes.

The continuity of bedding-parallel movement horizons is not easy to assess, and assessment is certainly not possible at the scale of the fold. Except within the hinge zone, matching of a particular movement horizon across the fold is not possible. Indeed, the monotony of stratigraphy will not permit correlation of individual beds across the folds, restricting correlation of movement horizons based on stratigraphic position. Profile sections, which represent the majority of the exposure studied, reveal only a small segment (few

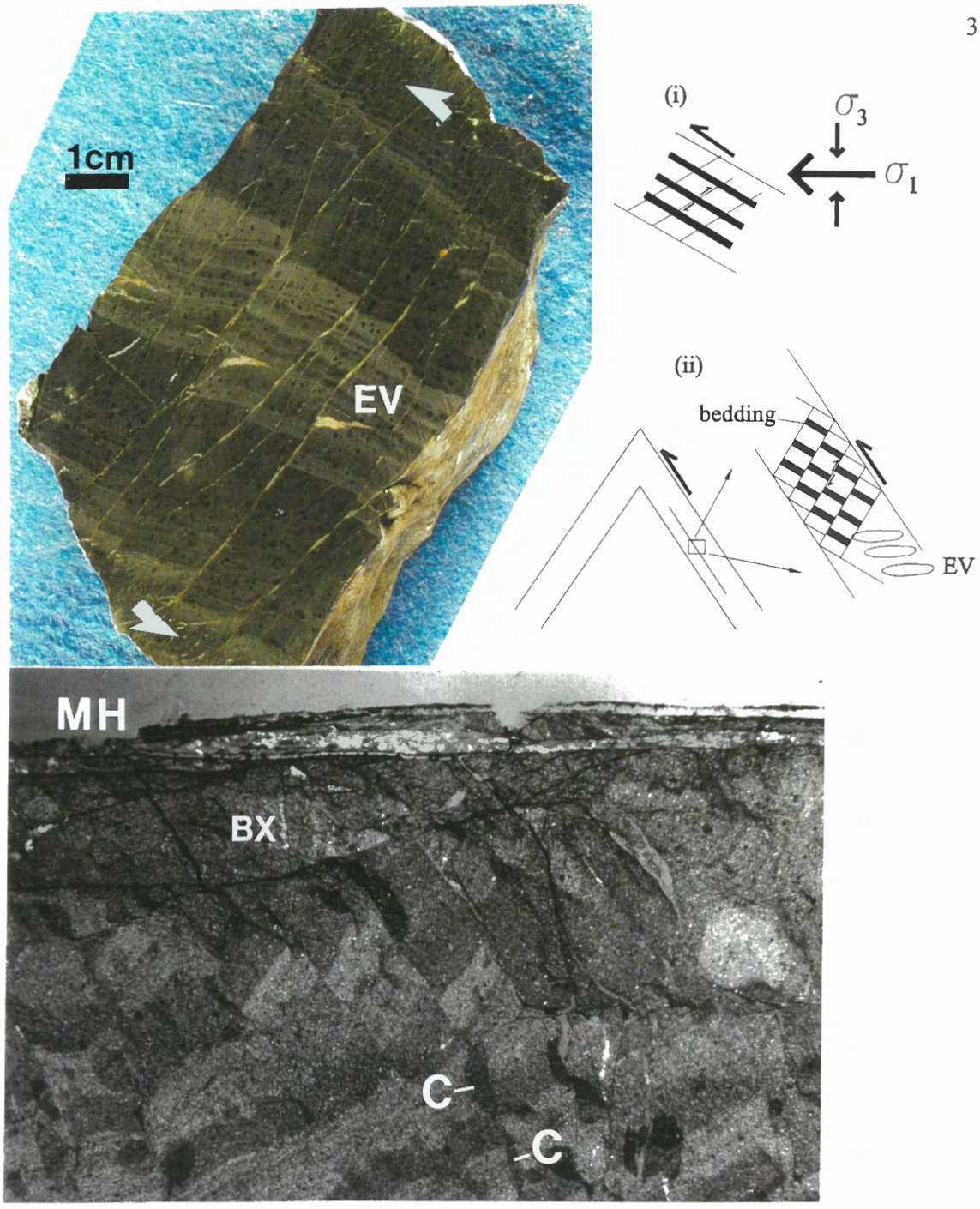

Figure 2.8: (a) Photograph of slab cut through a flexural-slip domino structure defined by offset of sedimentary layering. Slab cut perpendicular to movement horizon and parallel to movement lineations (profile view). Shear sense indicated. Note quartz veins along shear fractures between domino structures and minor extensional veins (EV), which are consistent with fold-related strain. Inset figure shows relation between fold-related stress and initial domino formation (i) and schematic diagram of domino showing relationship to the fold (ii). (b) Photomicrograph of domino structure showing displacement of cordierite porphyroblast (C) by shear fracture and local breccia (BX) development adjacent movement horizon.

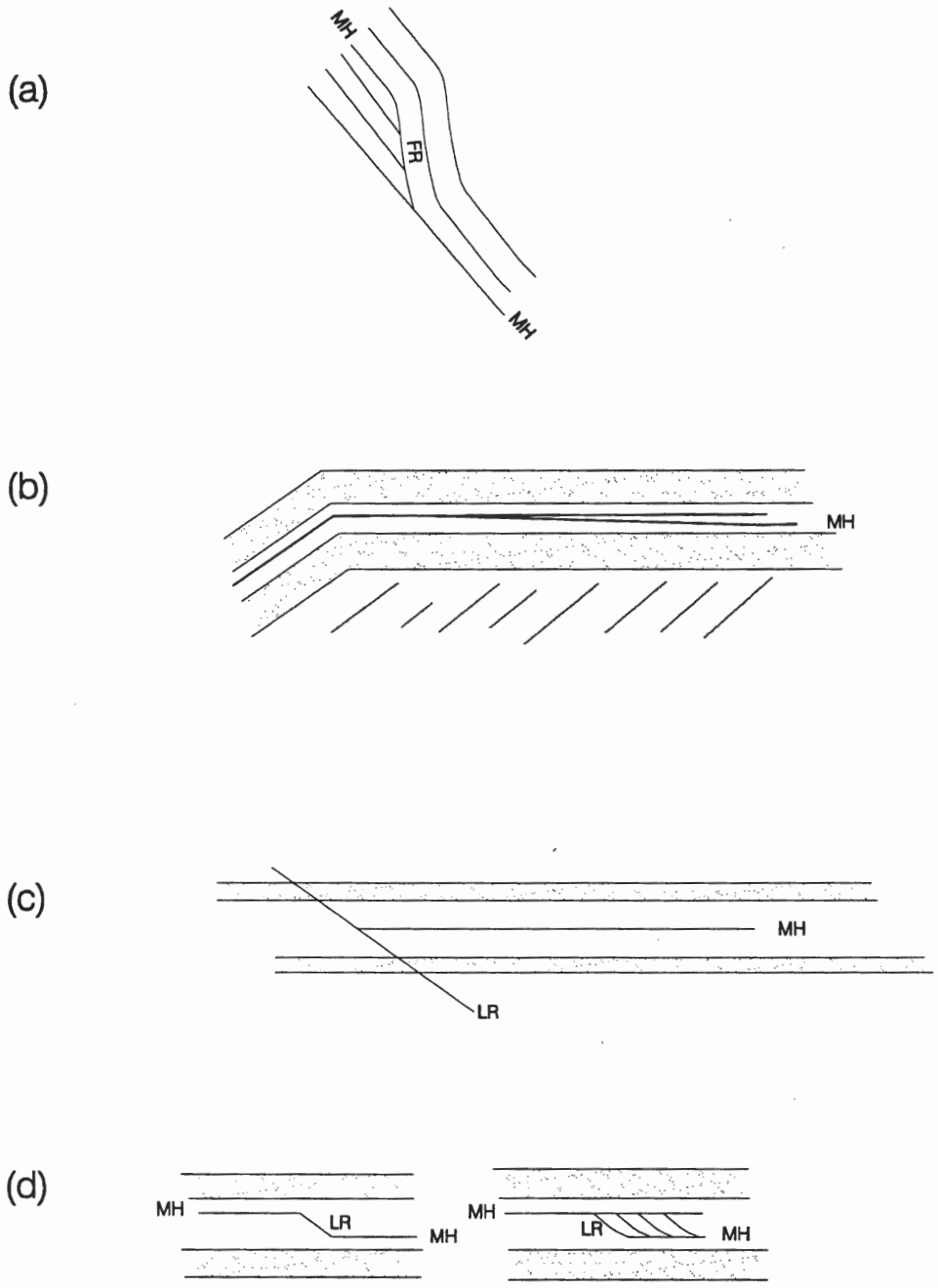

Figure 2.9: Schematic diagrams showing the relationship of various flexural-slip movement horizons. MH = bedding-parallel movement horizon; FR = frontal ramp movement horizon; LR = lateral ramp movement horizon. (a) profile view, (b-d) down dip view.

metres) of the possible down-dip continuity of bedding parallel movement horizons along fold limbs which are typically kilometres in length. In profile sections most movement horizons are continuous and remain at the same stratigraphic location over the few metres of exposure (Fig. 2.7a). Locally, some movement horizons are transferred onto frontal ramp movement horizons (Fig. 2.9a).

Strike-parallel exposures in the southern part of the section allow for evaluation of the continuity of movement horizons for several hundreds of metres of strike length. Photomosaics and sketches of exposures of sections in this area indicate considerable continuity for many bedding-parallel movement horizons, with several prominent ones continuous at the same stratigraphic horizon for hundreds of metres along strike (Fig. 2.10, in pocket at back). Less well developed bedding-parallel movement horizons are discontinuous and either die out along strike or are transferred to lateral ramps along strike (Fig 2.9b, c). In some cases bedding-parallel movement horizons are transferred to a different stratigraphic level along a single or series of lateral ramp movement horizons (Fig. 2.9d). Considering the scale of the folds, these observations indicate that bedding-parallel movement horizons can not be considered continuous in the sense of a simplified flexural-slip model.

Movement Direction and sense of shear :

Stereoplots of movement lineations for several intervals of the railway tracks section are shown in Fig. 2.11(in pocket at back). These data illustrate considerable variation in the trend of movement lineations between bedding-parallel movement horizons for some intervals (e.g., b and c). However, the average trend for each interval, represented by the eigenvector

of greatest clustering (V3), is similar and roughly perpendicular to the fold hinge, consistent with a flexural-slip origin. The variation in movement lineation trends for all movement horizons in any particular interval is comparable for the variation found for the trend of several movement lineations determined along a single, well-exposed movement horizon in the Tower Road area (Fig. 2.12). Variation in movement direction is common on slip surfaces and may reflect irregularity of the movement horizon surface (noted on this surface) or variation in movement direction may occur during the movement history.

For intervals a-e (Fig. 2.11), where there are significant amounts of movement lineation data, the average trend for movement lineation data does not, however, fall along the π-girdle, but is systematically slightly oblique to the fold hinge such that the acute angle between the fold hinge and the average trend is in the direction of plunge of the fold (Fig. 2.11, in pocket at back). Indeed, nearly all movement lineations occur on the plunge side of the π-girdle. The average movement lineation is, however, nearly parallel to the dip azimuth (DA) of bedding (Fig. 2.11, in pocket at back). This indicates that slip did not occur perpendicular to the fold hinge (which plunges slightly to the southwest), as in the simple flexural-slip model, but occured up dip of bedding. Note that these relationships occur on both limbs, precluding a prefolding origin for the movement lineations. This movement direction is consistent with either folding of an inclined surface or flexural slip during formation of non-cylindrical folds (Fig. 2.13). Regardless, the movement lineation data suggests that movement postdates the inclination of the fold hinge.

Shear sense indicators on bedding-parallel movement horizons include slickenfibres and domino structures. Slickenfibres are the most abundant shear sense indicator, occurring

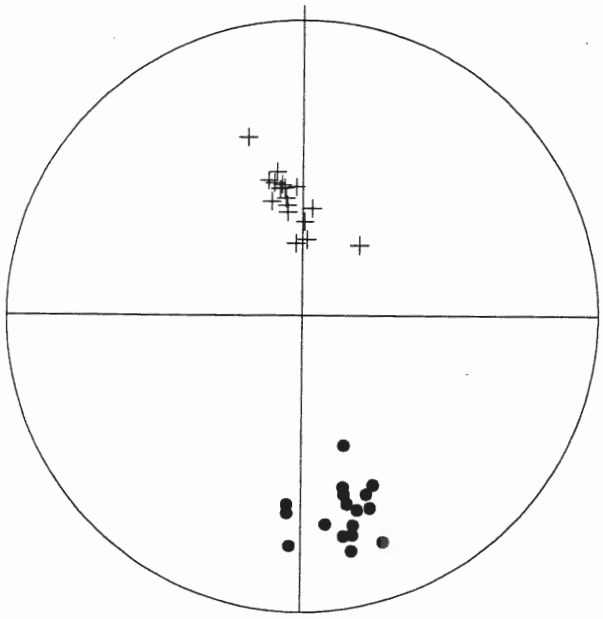

+ pole to movement horizon

• movement lineation

Figure 2.12: Stereonet of movement horizon data for a single movement horizon exposed along the railway tracks section at Tower Road (see Fig. 2.2), showing the variation in the attitude of movement horizons and trend of movement lineations on a single movement horizon.

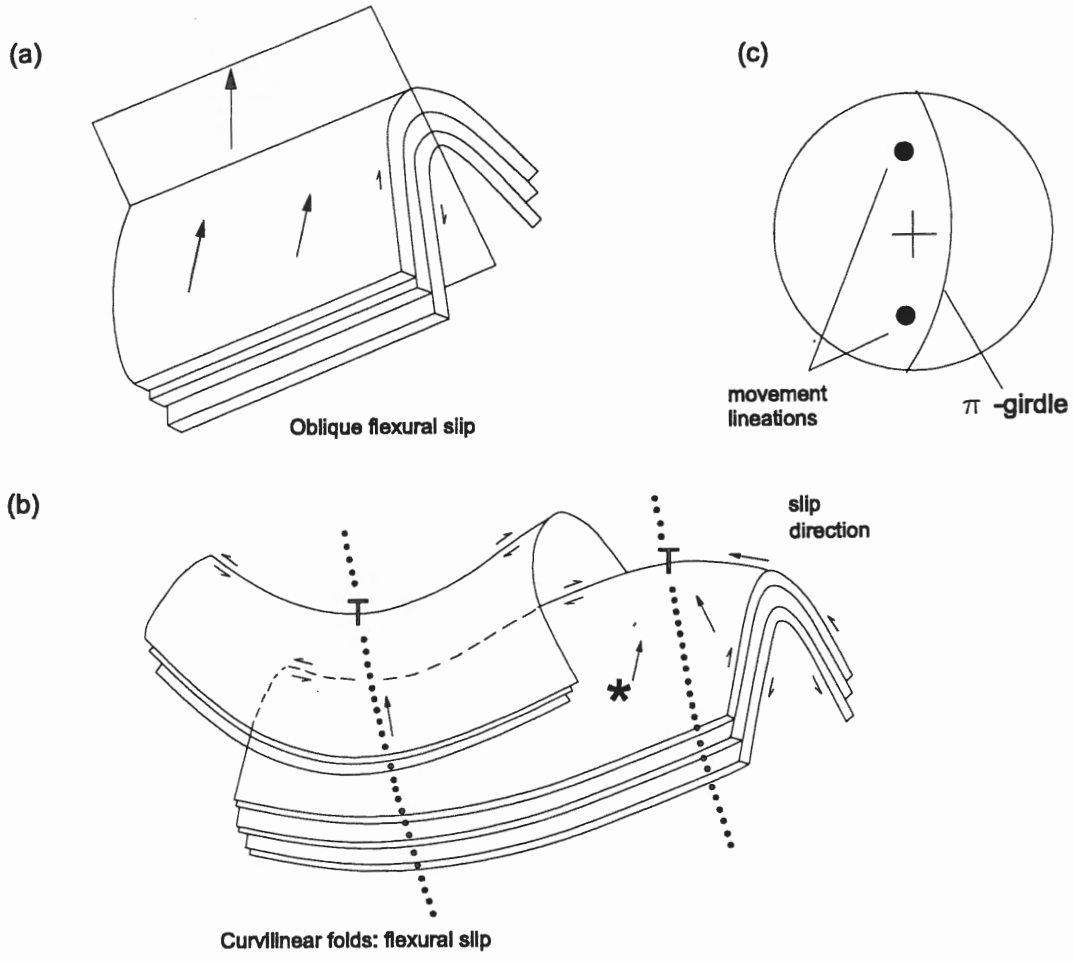

Figure 2.13: Diagrams illustrating slip direction related to flexural slip for (a) an inclined fold and, (b) a non-cylindrical fold. (c) Stereoplot illustrates the position of lineations relative to the π-girdle for the inclined fold in (a) and the area of the non-cylindrical fold indicated by * in (b). (a and b after Tanner, 1989).

on most movement horizons, and as discussed above, are common shear sense indicators in studies of flexural slip. Slickenfibre geometry is interpreted to reflect growth during shear, with the face of the slickenfibre pointing in the direction of movement of the opposite block (Fig. 2.14a; Durney and Ramsay,1973; Ramsay and Huber, 1983). Slickenfibre geometry can generally be determined in the field (e.g., Fig. 2.7b) thus providing an easy method of establishing shear sense. Where slickenfibres are not well developed and their geometry is unclear, shear sense can be evaluated by the "roughness-smoothness" effect of slickenfibre development; the surface will have a rough feel in the direction opposite to the steps.

Durney and Ramsay (1973) attribute the formation of slickenfibres to irregularities along the movement surface, with slickenfibres reflecting differential displacement across the fault at a small angle to the fault plane (Fig. 2.14a). Slickenfibres within the railway study area support this interpretation, with thick (up to 15 mm) slickenfibre sheets developed within concavities on irregular movement surfaces. In thin section, the relationship of slickenfibre sheets and movement surface is clear, with individual quartz fibres originating along the lee side of irregularities on the movement surface (Fig. 2.15a-c). Locally, wall rock inclusions near the base of slickenfibres parallel the slickenfibre-wall rock boundary, supporting the interpretation that slickenfibres track displacement across the fault plane (Fig. 2.15b). This feature also suggests that the surface irregularity may, in part, result from extensional fractures formed oblique to the movement horizon during shear along the movement horizon, as suggested by Ramsay and Huber (1983) (Fig. 2.14b) and Fowler (1996), for flexural-slip veins in Central Victoria, Australia. The formation of irregularities from extensional fractures

is consistent with the geometry of slickenfibre surfaces (e.g., Figs. 2.15b, c) and with fold-related stress (Fig. 2.15a). Slickenfibres locally truncate cordierite porphyroblasts (Fig. 2.15a), indicating at least a component of flexural slip postdates granite intrusion. This is supported by strain shadows around porphyroblasts (Fig. 2.15a) which are consistent with fold-related strain during flexural slip (inset, Fig. 2.15a). Shear sense for all slickenfibres on bedding-parallel movement horizons indicates reverse movement, consistent with a flexural-slip origin.

The shear sense of domino structures is clearly indicated by the rotation of sedimentary laminations within the dominoes (Fig. 2.8) and indicates a reverse sense of shear, consistent with flexural slip. This sense of rotation of domino structures is confirmed by slickenfibre geometry and by the relative offset of cordierite porphyroblasts displaced by the shear fractures (Fig. 2.8).

Spacing

Spacing of bedding-parallel movement horizons was determined for several measured intervals across the fold, where stratigraphy and the location of movement horizons were determined. The locations of movement horizons are shown in stratigraphic log drawings (Fig. 2.4, in pocket at back) and spacing data is given in Appendix 1. The location of "bedding-parallel fractures" not classified as movement horizons due to a lack of confirmed movement lineations, and discordant movement horizons interpreted to represent "frontal ramps" (see below) are also indicated on these logs.

(a)

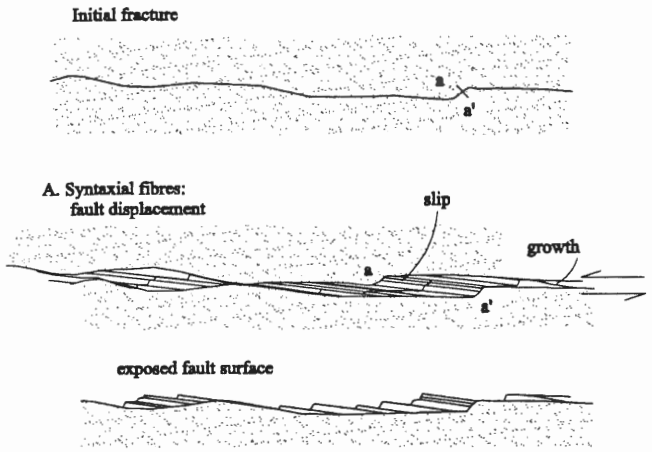

(b)

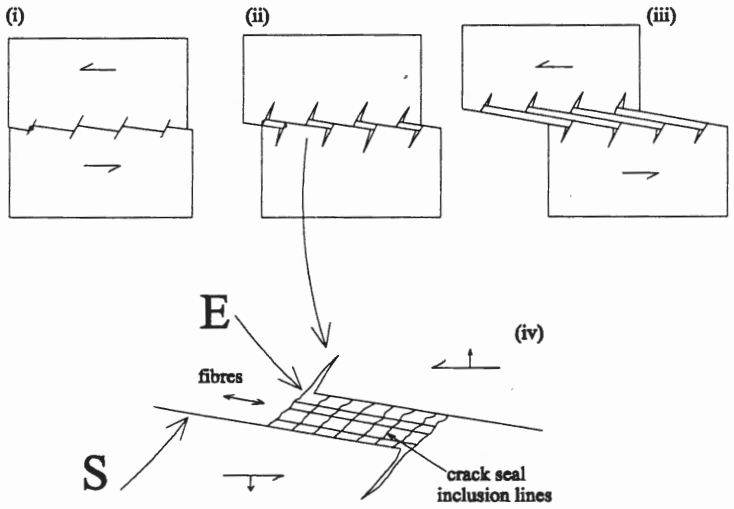

Figure 2.14: (a) Diagram showing the development of slickenfibres by syntaxial or antitaxial fibre growth within dilatancy formed by displacement along an irregular surface (After Durney and Ramsay, 1973). (b) Schematic diagram showing the sequential development of slickenfibres along movement surface consisting of shear (S) and extensional (E) sectors (i-iii). iv illustrates the character of crack seal inclusion bands in slickenfibres, which parallel extension sectors. (After Ramsay and Huber, 1983).

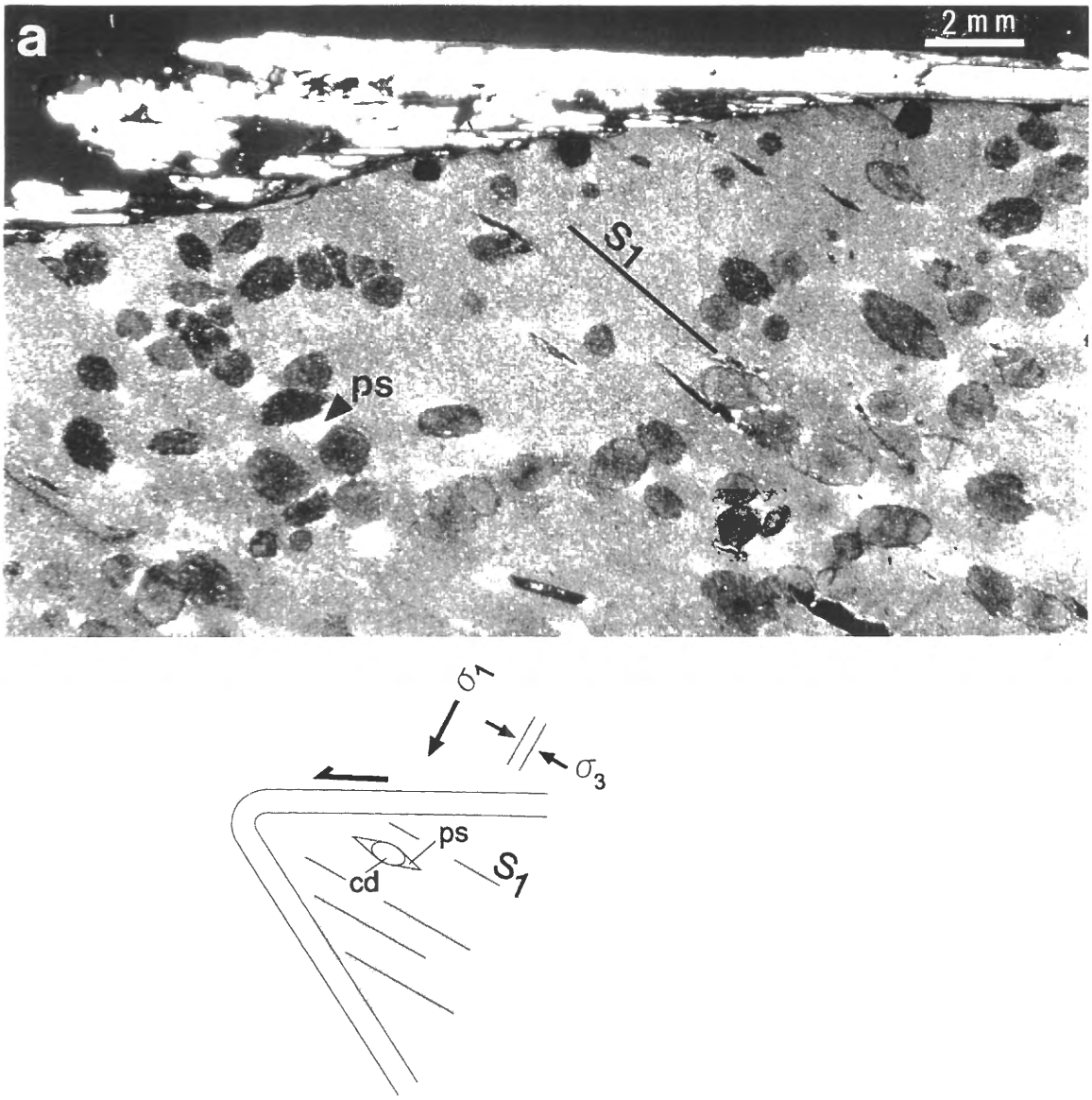

Figure 2.15: (a-c) Microphotographs of quartz slickenfibres on bedding-parallel movement horizons. Slickenfibres are at a small angle to movement horizon and developed on the lee side of irregularities on movement horizons. Step-like wall rock boundary in b and c may represent shear and extensional fractures as shown in Fig. 2.14b. Inclusions parallel to the extensional sectors in (b) (arrows) track slickenfibre growth and confirm a shear origin. Note also the inclusion bands formed at the boundary between different slickenfibres, which extend from the shear sectors of the steps in (b) and (c), and pressure shadows around cordierite porphyroblasts in (a) which define a lineation within the cleavage plane (S_1). Inset figure in (a) illustrates how the pressure shadows and extensional sectors of movement horizons are consistent with fold-related strain. All sections cut perpendicular to bedding and parallel to slickenfibres.

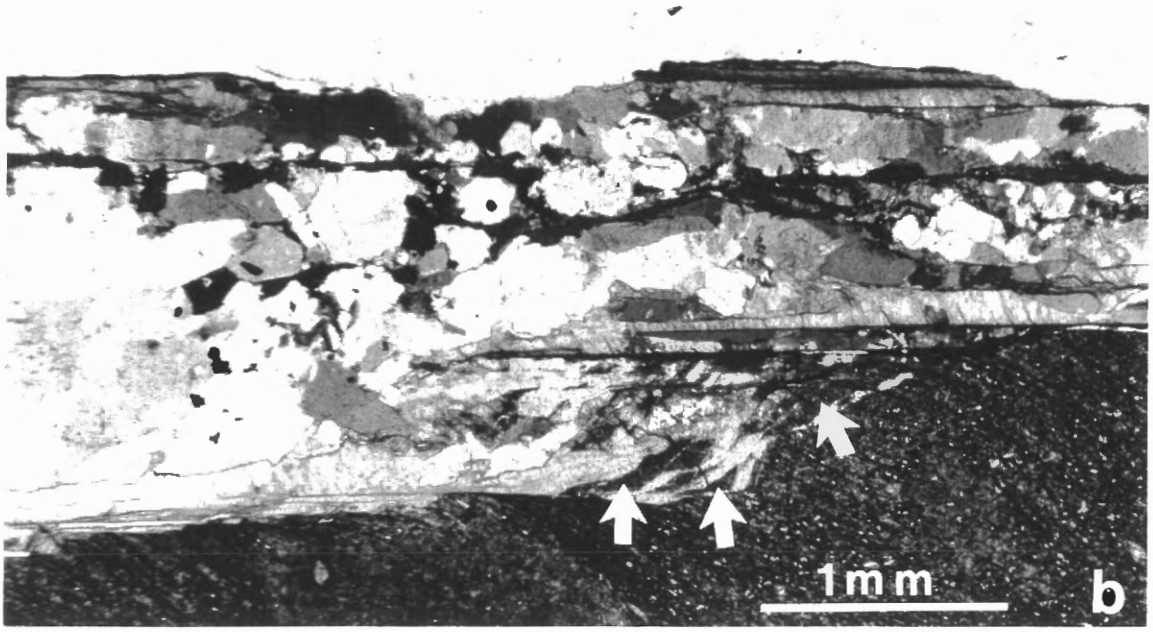

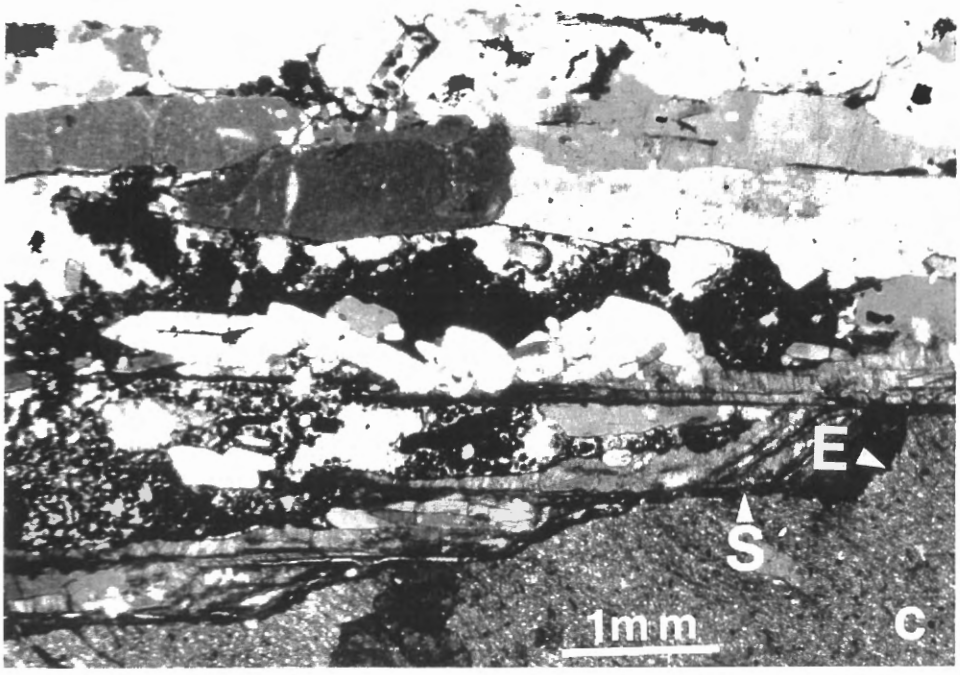

Figure 2.15 continued.

Bedding-parallel movement horizons invariably occur within slate intervals and commonly occur close to metasandstone layers (Fig. 2.4, in pocket at back). The movement horizons "apparently" within metasandstone layers in these logs occur within thin slate "seams" which are too thin to be represented on the logs. Common relationships include the occurrence of movement horizons on either side of metasandstone layers and the common occurrence of movement horizons in groups.

The mean spacing of bedding-parallel movement horizons for each measured interval is indicated at the bottom of each log. The significance of the spacing data must be considered in light of the fact that bedding-parallel movement horizons are discontinuous both along strike and down dip. Clearly, if bedding-parallel movement horizons are discontinuous, then spacing for any stratigraphic interval will vary for different exposures. In addition, there remains uncertainty of the status of poorly exposed bedding-parallel fractures without any evidence of movement, which may, however represent bedding-parallel movement horizons. A discussion of the spacing, including the effects of limb dip and lithology, is more fully presented in chapter 4.

2.2.3 Frontal ramp movement horizons

Frontal ramp movement horizons consist of strike-parallel movement surfaces which dip more steeply than bedding-parallel movement horizons (Fig. 2.11, in pocket at back). Locally, these structures are seen to form ramps linking closely spaced (< 1 metre) bedding-parallel movement horizons (Fig. 2.9; 2.10). However, the majority of these structures were

simply identified on the basis of their discordant relationship to bedding and their extent and relationship to other structures is largely unknown due to limited exposure. Many of these structures are parallel to cleavage (compare poles to cleavage, Fig. 2.3c) and poles to frontal ramps for intervals b and c (Fig. 2.11, in pocket at back). Frontal ramp surfaces are characterized by striations and slickenfibres, similar to bedding-parallel movement horizons, which trend parallel to those on bedding-parallel movement horizons (Fig. 2.11, in pocket at back). Slickenfibre geometry invariably indicates a reverse sense of movement. These relationships support a general interpretation that strike-parallel movement horizons which dip more steeply than bedding represent frontal ramp structures associated with bedding-parallel movement horizons. A lack of strike-parallel discordant movement horizons which dip less steeply than bedding also supports a ramp origin for these structures. Common development of these structures along, or parallel to, cleavage suggests the development of ramps was influenced by cleavage.

2.2.4 Lateral ramp movement horizons

Lateral ramp movement horizons, herein referred to as lateral ramps, consist of a well developed set of moderately dipping discordant movement horizons which are oblique to bedding and trend at a high angle to the fold hinge (Figs. 2.6; 2.10 and 2.11 in pocket at back; 2.16). All lateral ramps recognized dip in the same direction, toward the southwest (Fig. 2.11, in pocket at back). No conjugate set of lateral ramps (i.e., northeast dipping) occurs. Lateral ramps are characterized by quartz slickenfibres, similar to those on bedding-parallel movement horizons and frontal ramps. The trend of slickenfibres on lateral ramps is parallel

Figure 2.16: Photograph of well developed, regularly spaced lateral ramp movement horizons, indicated by arrows, exposed along the railway tracks west of Tower Road (see Fig. 2.2 for location). BS = bedding surface, which strikes roughly parallel to the photograph and dips out of the photograph.

to movement direction indicators on bedding-parallel movement horizons. The intersection of lateral ramps and bedding-parallel movement horizons is parallel to the movement direction lineations on both structures (Figs. 2.10 and 2.11, in pocket at back). Slickenfibre sheets on lateral ramps are commonly continuous with those on bedding-parallel movement horizons (Fig. 2.11) and the sense of shear indicated by slickenfibres is reverse, similar to that for movement horizons. These relationships indicate a genetic relationship between lateral ramps and bedding-parallel movement horizons. As a consequence of the relationship between lateral ramps and movement horizons there is no apparent offset of sedimentary layering resulting from movement on lateral ramps (Fig. 2.10, in pocket at back).

Lateral ramps were only recognized in the eastern, strike-parallel, part of the railway section (Fig. 2.2) which may simply reflect the fact that the intersection of lateral ramps in profile sections is parallel to bedding. Where recognized, lateral ramps form a well-developed, regularly spaced set of movement horizons which are developed at several scales. A well developed, systematic set of thoroughgoing lateral ramps spaced several metres apart transect the strike-parallel section at the east end of the study area (Fig. 2.10, in pocket at back). Regular spaced (metre spacing) lateral ramps are locally developed in an oblique section of the railway section (Fig. 2.16). Locally, small-scale lateral ramps linking movement horizons separated by only a few centimetres occur (Fig 2.9).

2.2.5 Conjugate movement horizons:

A set of shear fractures which have a conjugate relationship (mirror image) to bedding-parallel movement horizons were locally recognized near South Street (Fig. 2.2).

These structures strike parallel to bedding and dip in an opposite direction (Figs. 2.10e, f in pocket at back; 2.17) and their surface is striated or coated with quartz slickenfibres which trend opposite to movement lineations on bedding-parallel movement horizons (Fig. 2.10e, f). Slickenfibres indicate a reverse sense of shear. Although movement lineations suggest movement along these surfaces, there is little apparent offset indicated at the intersection of bedding-parallel and conjugate shear movement horizons (Fig. 2.17).

The conjugate nature of these shear fractures, indicated by the shear sense, is not strictly consistent with the formation of conjugate fractures, as the inferred maximum principal stress bisects the obtuse angle between fractures (Fig. 2.17). However, it is interesting to note that there is a geometric relationship between the stress orientations inferred from shear sense and fold geometry such that, the maximum principal stress ($\sigma 1$) is subparallel to the a axis of the fold, the intermediate principal stress ($\sigma 2$) is subparallel to the b-axis (fold hinge) and the minimum stress axis ($\sigma 3$) is subparallel to the a-axis (Fig. 2.17). The inferred stress orientations are consistent with fold development. The development of conjugate shear fractures in addition to bedding-parallel flexural-slip movement horizons may reflect shortening after locking of the fold prevented further folding by flexural-slip alone.

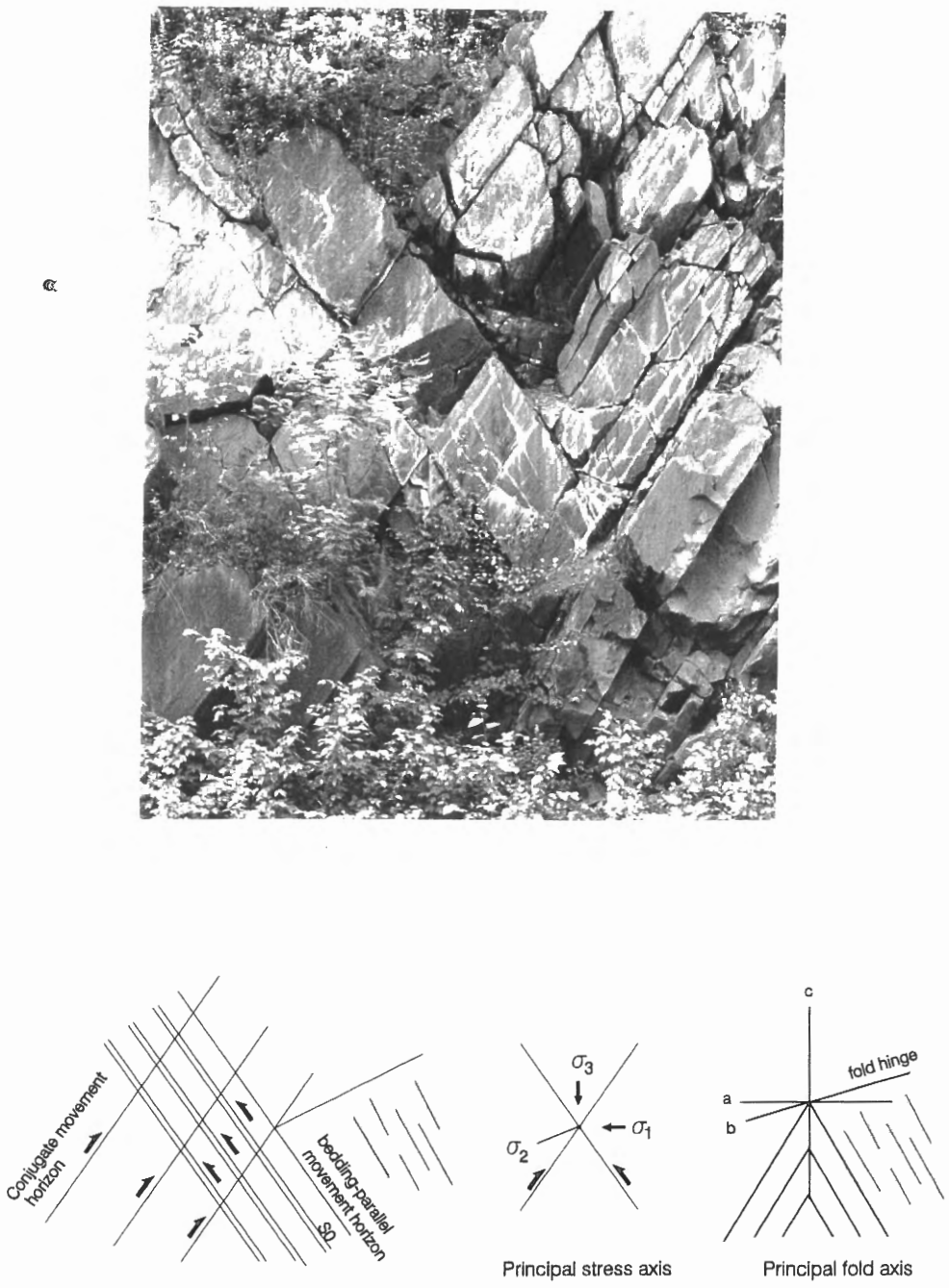

Figure 2.17: Photograph and sketch of conjugate movement horizons and bedding-parallel movement horizons from near the South Street bridge (see Fig. 2.2). Profile view looking northeast. Sketches of bedding-parallel and conjugate movement horizons illustrate sense of shear, interpreted principal stress orientations and principal fold axis. S0 = bedding; MH = bedding-parallel movement horizon; CMH = conjugate movement horizon.

2.3 DISCUSSION:

2.3.1 General flexural-slip model

Investigations in the railway section have demonstrated the occurrence of abundant structures related to flexural-slip folding. All these structures show a systematic relationship to fold geometry. Movement lineations on bedding-parallel movement horizons show subtle, but consistent, deflection from perpendicular to the fold hinge, commensurate with the fold plunge, which is attributable to up-dip flexural slip on the limbs of a plunging fold. Shear sense is invariably reverse and changes across the fold. These observations support the interpretation that these structures are related to flexural slip and can not be explained by folding of movement horizons developed prior to folding.

2.3.2 Family of flexural-slip structures; A 3D model of flexural slip:

Classic models of flexural slip (e.g., Tanner, 1989) have typically considered a simplified two dimensional model, with movement occurring along simple bedding-parallel surfaces and duplex structures. Is has been recognized that the amount of slip on a movement horizon may vary within the profile plane, especially as the hinge area is approached (Ramsay, 1967; Tanner, 1989), however along-strike variation in slip has not been considered.

This study has identified several movement horizons sets, including bedding-parallel, frontal ramps and lateral ramps, which are geometrically and kinematically related so as to form a linked system of movement horizons which accommodated flexural slip during folding. In addition, it has been shown that movement horizons may be discontinuous along strike as well as down dip, implying variation in the amount of displacement along movement horizons.

These features suggest a three dimensional model for flexural slip (e.g., Fig. 2.6) may more appropriately represent the flexural-slip mechanism and that the distribution of flexural-slip strain may vary throughout the fold.

The strike-parallel section, at the eastern end of the study area, provides the best assessment of movement horizon continuity, where it is apparent that there are several regularly spaced movement horizons which are continuous over the distance of the exposure and therefore define major structures (Fig. 2.10, in pocket at back). Between these continuous structures movement horizons are typically discontinuous and define relatively minor structures. The degree of development of the various movement horizons likely reflects the amount of displacement which has occurred, with the continuous movement horizons representing horizons of significant movement. This interpretation would imply that flexural-slip strain is largely accommodated by the continuous movement horizons, where strain is likely homogenous and consistent with a simplified flexural-slip model. Between the continuous movement horizons flexural-slip strain is minor and generally inhomogeneous, as shown by discontinuity of movement horizons. That the continuous movement horizons account for the bulk of the flexural-slip strain suggests they likely represent early-formed structures. The continuous movement horizons likely evolved from less regular, discontinuous movement horizons, and therefore the latter may providing insight into the initial development of movement horizons.

A three dimensional model for flexural-slip structures accommodates the observations of discontinuous and discordant movement horizons. These observations are important as they influence quantitative evaluation and history of development of flexural-slip movement

horizons. Firstly, the discontinuous nature of flexural-slip structures indicates that spacing of movement horizons will vary between different profile sections. The interpretation that there is progressive development of movement horizons, with the continuous movement horizons forming early, does not support a simple model where flexural-slip strain is evenly distributed on movement horizons (e.g., Ramsay, 1974).

Local variation in the distribution of flexural-slip strain is implied from this discussion, however strain is likely homogeneous at the scale of the folds. This is supported by similar spacing data for bedding-parallel movement horizons in the various measured sections (Fig. 2.4, in pocket at back).

2.3.3 Age of Flexural Slip:

Several features constrain the relative and absolute age of flexural-slip within the area. Structures related to flexural slip are brittle in character, defined by brecciation, polishing and striations. Flexural-slip structures truncate and deform cleavage, which in the area has been partially annealed as a result of contact metamorphism, suggesting a post-granite age for flexural slip. This is supported by truncation and offset of cordierite porphyroblasts within the contact aureole of the South Mountain Batholith by flexural slip movement horizons (Figs. 2.8, 2.15), indicating at least a component of post-granite flexural-slip. The development of strain shadows around cordierite porphyroblasts is consistent with folding-related strain (Fig. 2.15a) and indicates that significant cleavage-parallel strain between flexural-slip movement horizons accompanied flexural-slip folding.

CHAPTER 3 - OVENS STUDY AREA

3.1 INTRODUCTION

The Ovens study area is located along the south coast of Nova Scotia, southwest of Lunenburg (Fig. 3.1). It occurs within the largest exposed area of Halifax Formation within the Meguma Terrane (Fig. 1.4), indicating a relatively high structural level of exposure. O'Brien (1988) proposed a revised stratigraphy of the Meguma Group within the area, including introduction of the Green Bay Formation between the Goldenville and Halifax Formations and subdivision of the Halifax and Goldenville formations at the member level. The study area lies within the Cunard member of the Halifax Formation (Fig. 1.6) of O'Brien (1988), although cross-sections through the Ovens area suggest exposure in the hinge zone is approaching the underlying Green Bay Formation (Fig. 3.1).

Regional folds in the area are characterized by modified box folds and chevrons (Fig. 3.1), consistent with Meguma folds elsewhere (compare with Fig. 1.4). The Ovens area occurs within the regional chlorite isograd (greenschist facies) and illite-muscovite crystallinity studies indicate borderline anchizone to epizone (diagenetic to greenschist facies) metamorphism in the Ovens area (Hicks, 1996). The closest exposed intrusion is the South Mountain Batholith, outcropping approximately 25 km to the north (Fig. 1.4).

Investigations in the Ovens area focused on the well-exposed hinge zone of the Ovens Anticline in the areas of Cunard Cove and Rose Bay (Fig. 3.1). This area hosts abundant auriferous veins and constitutes one of the numerous gold districts within the Meguma Group.

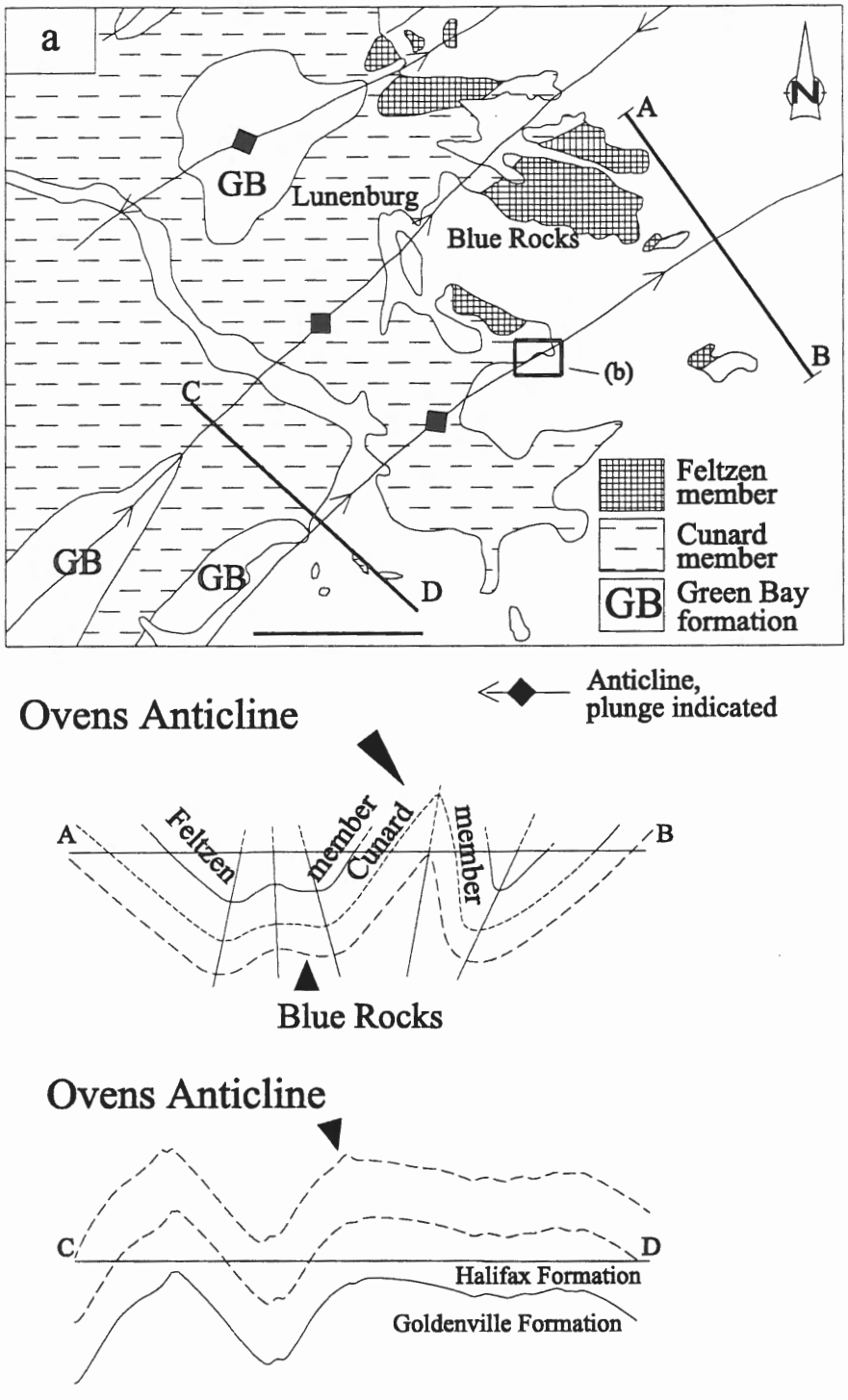

Figure 3.1: Simplified geology map of the Lunenburg area showing the location of the Ovens study area. Map and section A-B after O'Brien (1988), section C-D after Faribault (1929).

Gold production was primarily from placer deposits in the beach sands, which are reported to have yielded approximately 2500 ounces of gold over a brief period during 1861-62 (Faribault, 1934; Messervey, 1929). Auriferous veins were also mined (eg., Fig. 3.2), although with only limited success (Messervey, 1929; Young, 1961).

The earliest documented mapping of the area was by Faribault (1929; 1934), who published a geological map which defines the Ovens Anticline and shows the location of mined auriferous "leads" and the occurrence of placer deposits (Fig. 3.2). Sedimentology studies of the Ovens area were conducted by D'Orsay (1980) and Hall (1981). O'Brien (1988) conducted regional (1:50 000 scale) mapping throughout the area. The structure, veining and gold mineralization have been addressed by Graves (1976), Graves and Zentilli (1982), O'Brien (1988) and Henderson et al. (1992). The results of these studies are discussed in relevant sections below.

Evidence of flexural slip was noted in the area by Dr. N. Culshaw (personal communication), who recognized systematic offset of discordant veins along bedding-parallel movement horizons. Continuous outcrop of the Meguma Group along the coastline in this area provides excellent exposure, including the hinge zone of the Ovens Anticline, for studying structures related to flexural slip. As in the railway section, various methods were employed to evaluate flexural slip in the Ovens area. General mapping of the area was undertaken, and two areas, Cunard Cove and Rose Bay (Fig. 3.2), were selected for detailed evaluation.

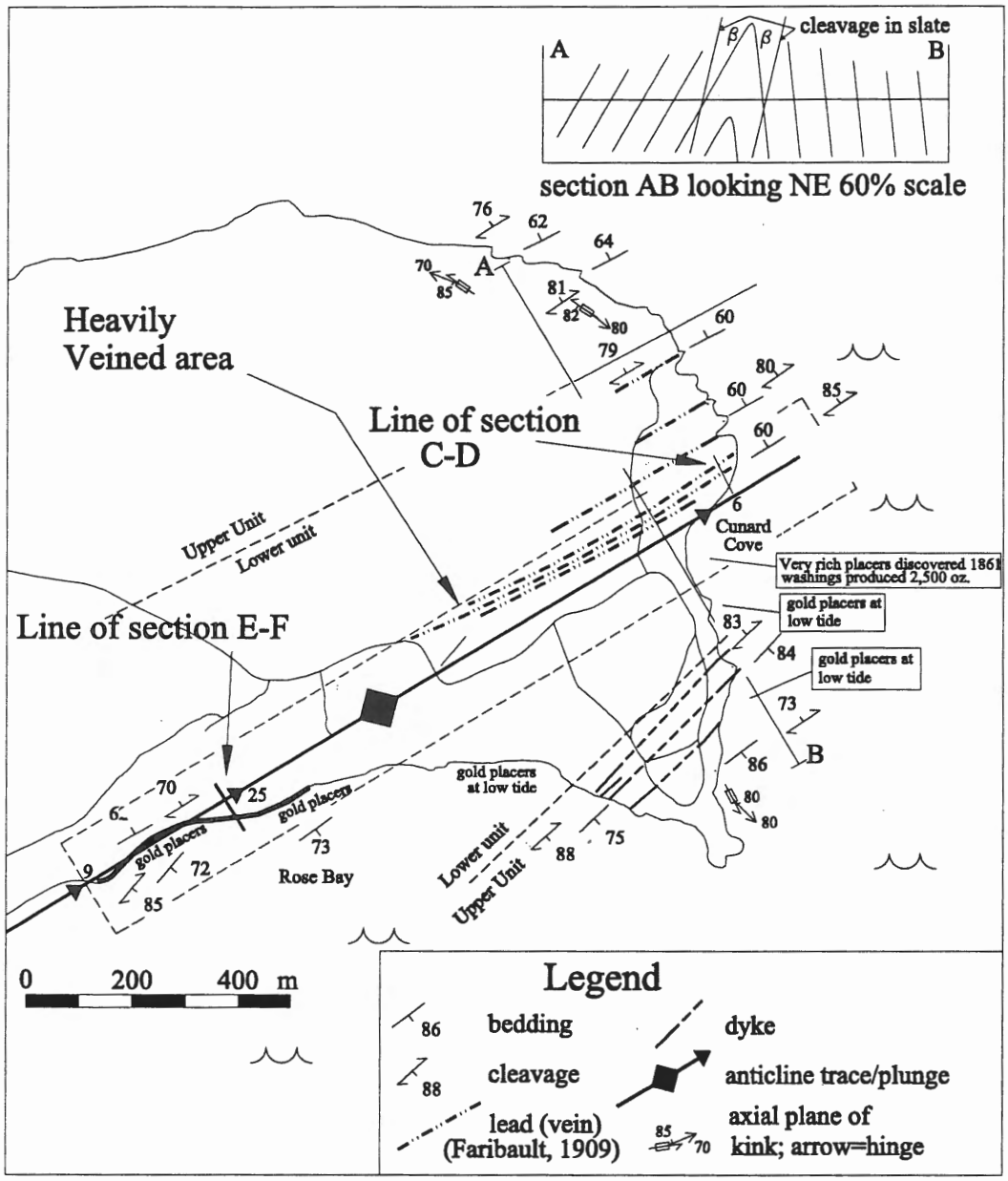

Figure 3.2: Simplified geology map of the Ovens area showing the location of the Cunard Cove and Rose Bay sections. Stratigraphic subdivisions of upper and lower units discussed in text. Veins, placers, and dykes after Faribault (1934).

3.2 GEOLOGY OF THE OVENS AREA

The Cunard member in the Ovens area is characterized by interbedded black slate and metasandstone (O'Brien, 1988; D'Orsay, 1980; Hall, 1980). Mapping during this study suggests that local stratigraphic subdivision can be made on the basis of the percentage and thickness of metasandstone beds, which is similar to stratigraphic subdivision made in the railway tracks area. The upper part of the stratigraphy (upper unit), exposed away from the hinge zone (Fig. 3.2), is typical of the Cunard member described elsewhere in the Meguma Group (e.g., O'Brien, 1988; Waldron, 1992; Schenk, 1991; Horne et al., 1997b), comprising mainly slate with thin (generally <15 cm) interbedded metasandstone beds (Fig. 3.3). The stratigraphic lower part of the section (lower unit), exposed in the hinge zone, is characterized by abundant thick (~0.5-1 m) metasandstone beds, comprising approximately 25 % of the stratigraphy (Figs. 3.4; 3.5). This unit is exposed in both the Cunard Cove and Rose Bay areas (Fig. 3.2). As in the railway section, the higher abundance of metasandstone in the lower unit is interpreted to reflect proximity to the underlying Green Bay Formation in the hinge zone, as was noted above.

The fold structure at the Ovens is well exposed, and defines a classic chevron structure with a tight (interlimb angle of 35-45°), angular hinge and straight limbs (Figs. 3.2; see also Figs. 3.6c, 3.20). The axial plane dips steeply (~77°) to the northwest and the hinge plunges moderately (6-25°) to the northeast (Fig. 3.2). A well developed continuous cleavage occurs within slate intervals whereas a poorly developed spaced cleavage is variably developed in the metasandstone. Slaty cleavage is roughly axial planar, defining a slightly divergent fan, and the bedding-cleavage angle is similar on both limbs (Fig. 3.2).

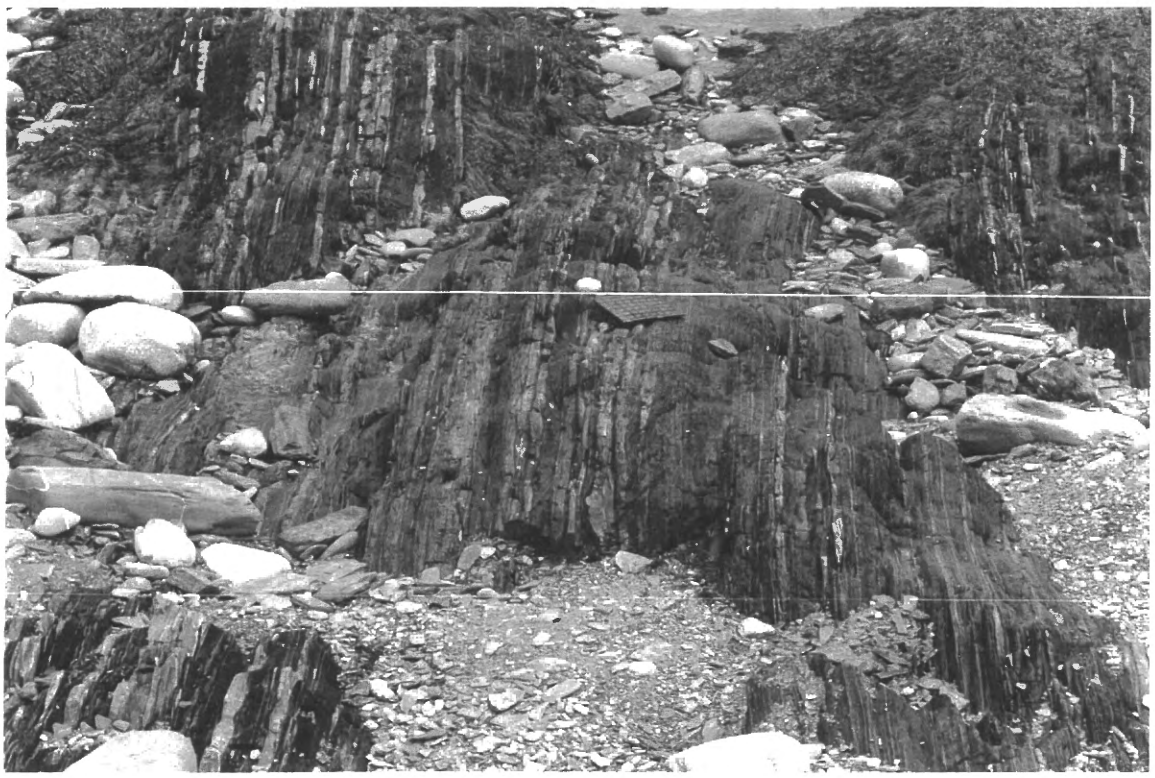

Figure 3.3: Photograph of a typical outcrop of the upper unit in the Ovens area, consisting of mainly black slate with abundant thin metasandstone beds (light coloured layers).

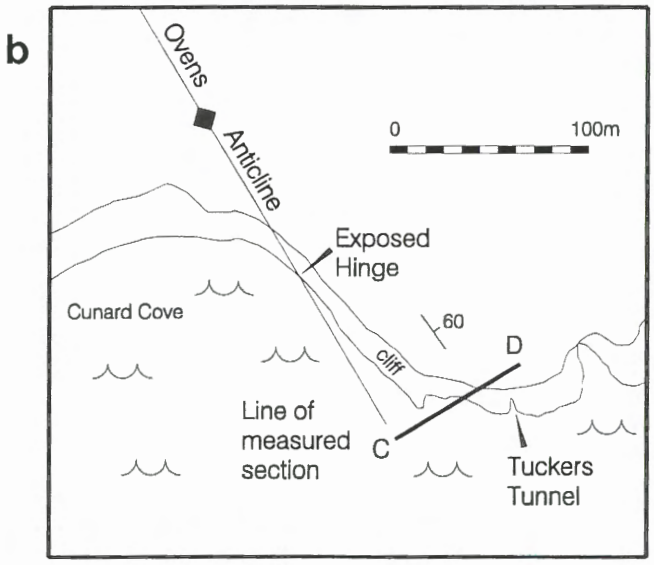

Figure 3.4: (a) Photograph of measured Section C-D, Cunard Cove, indicated on map in (b). Note stratigraphy, consisting of metasandstone (light coloured beds) and slate. Flexural-slip movement horizons are locally apparent by offset discordant quartz veins, indicated by arrows. (b) Simplified map of the Cunard Cove area showing the location of the exposed hinge and measured section C-D.

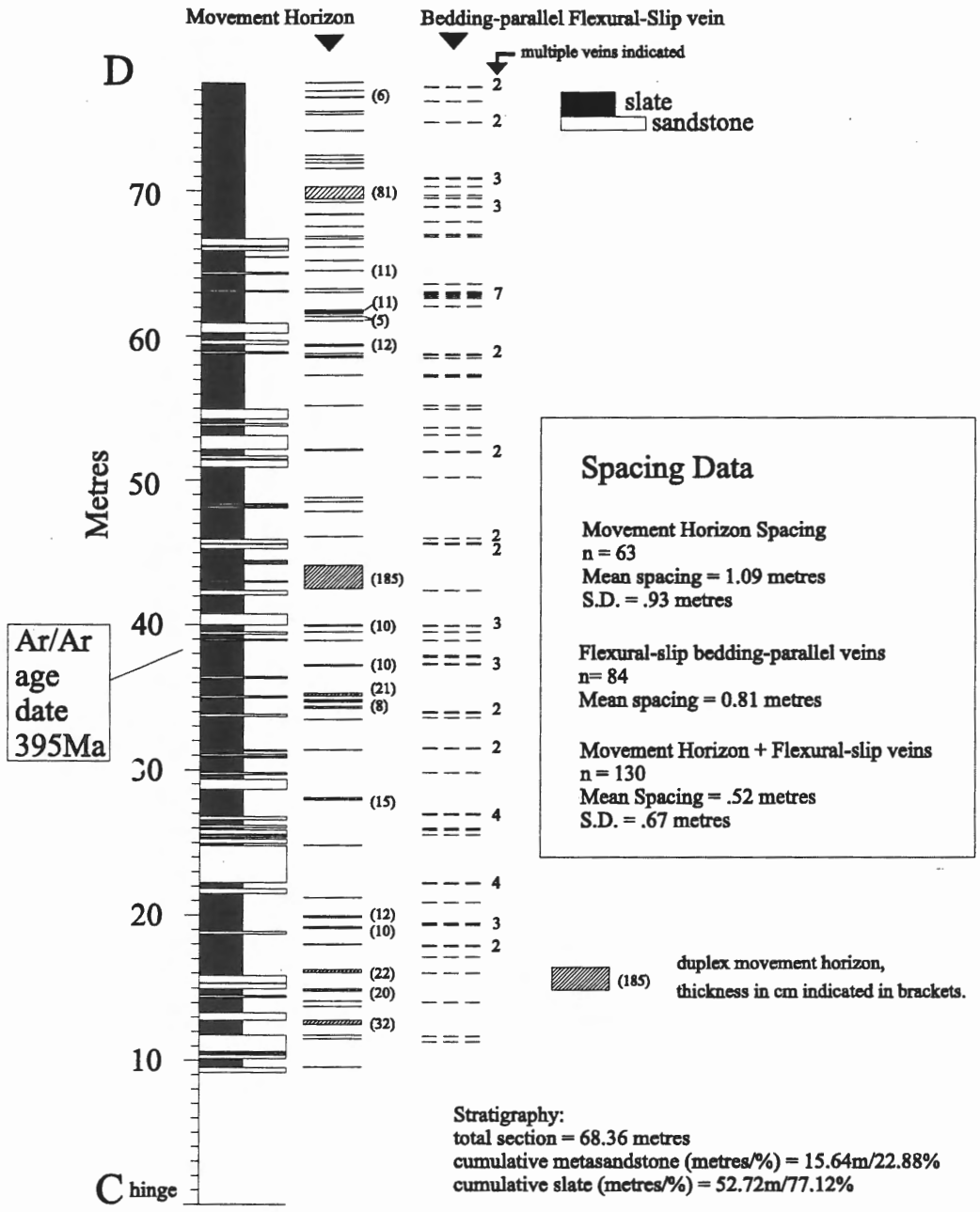

Figure 3.5: Stratigraphic log of the north limb of the Ovens Anticline in Cunard Cove (Section C-D, Fig. 3.4) showing the location of flexural-slip movement horizons and flexural-slip bedding-parallel veins. See Appendix 1 for flexural-slip movement horizon and bedding-parallel vein spacing data.

Several "accommodation structures" (Ramsay, 1974) typical of chevron fold development are present in the hinge zone, including hinge thrusts, bulbous hinge forms and saddle-reef veins. Numerous features related to flexural-slip folding are present and are discussed in detail below.

The hinge zone of the Ovens Anticline has a high concentration of auriferous quartz veins, which were the focus of past mining activity and presumably the source of placer deposits in the near shore. Several vein sets have been distinguished on the basis of their geometric relationship to the fold, relationship to other structures and relative age. Vein types, relationships between veins, and the nature of veins with respect to the structural evolution of the Ovens Anticline are discussed in detail below.

Several nearly concordant dykes of granodiorite to quartz monzodiorite composition (normative mineralogy; Hall, 1980) are exposed on the south limb of the fold (Fig. 3.2). Hall suggested that these dykes have a chemical affinity with the "southern plutons" in the Shelburne area (Fig. 1.4). The absolute age of the dykes is unknown; however xenoliths of cleaved slate indicate a post-deformational age (Hall, 1980). Kink folds are common throughout the area (Fig. 3.2), which is typical of the Halifax Formation elsewhere in the Meguma Group (Fyson, 1966).

3.3 CUNARD COVE

3.3.1 Introduction:

Investigations in the Cunard Cove area focused on a continuous coastal exposure of the north limb of the Ovens Anticline. Observations were made within the exposed hinge zone and a detailed structural and stratigraphic log, similar to those produced in the railway section, was constructed for a 77 metre section on the north limb adjacent to the hinge (Section Line C-D, Fig. 3.4; 3.5). This log provides a profile of the fold limb, including qualitative and quantitative descriptions of movement horizons, movement direction and sense of shear. All flexural-slip data given below are from this measured section. A set of discordant veins offset during flexural slip transect the entire measured section and allow for the determination of the amount of (post discordant vein) offset along flexural-slip movement horizons. Measurements of structural data and relationships between structural features and veins were recorded for quantitative and qualitative evaluation. Photographs and sketches were utilized to record the character and relationship of stratigraphy, structure and veins in the area.

3.3.1.1 *Geology of the Hinge Zone:*

The hinge zone of the Ovens Anticline exposed in Cunard Cove (Fig. 3.4) is a narrow (approximately 2 metres) rounded fold defined by sedimentary layering (Fig. 3.6a). Metasandstone beds maintain thickness across the fold whereas slate intervals are thickened (Fig. 3.6a). Slaty cleavage defines a distinctive, divergent pattern within the hinge zone. A similar cleavage pattern occurs around small-scale folds defined by buckled bedding-parallel

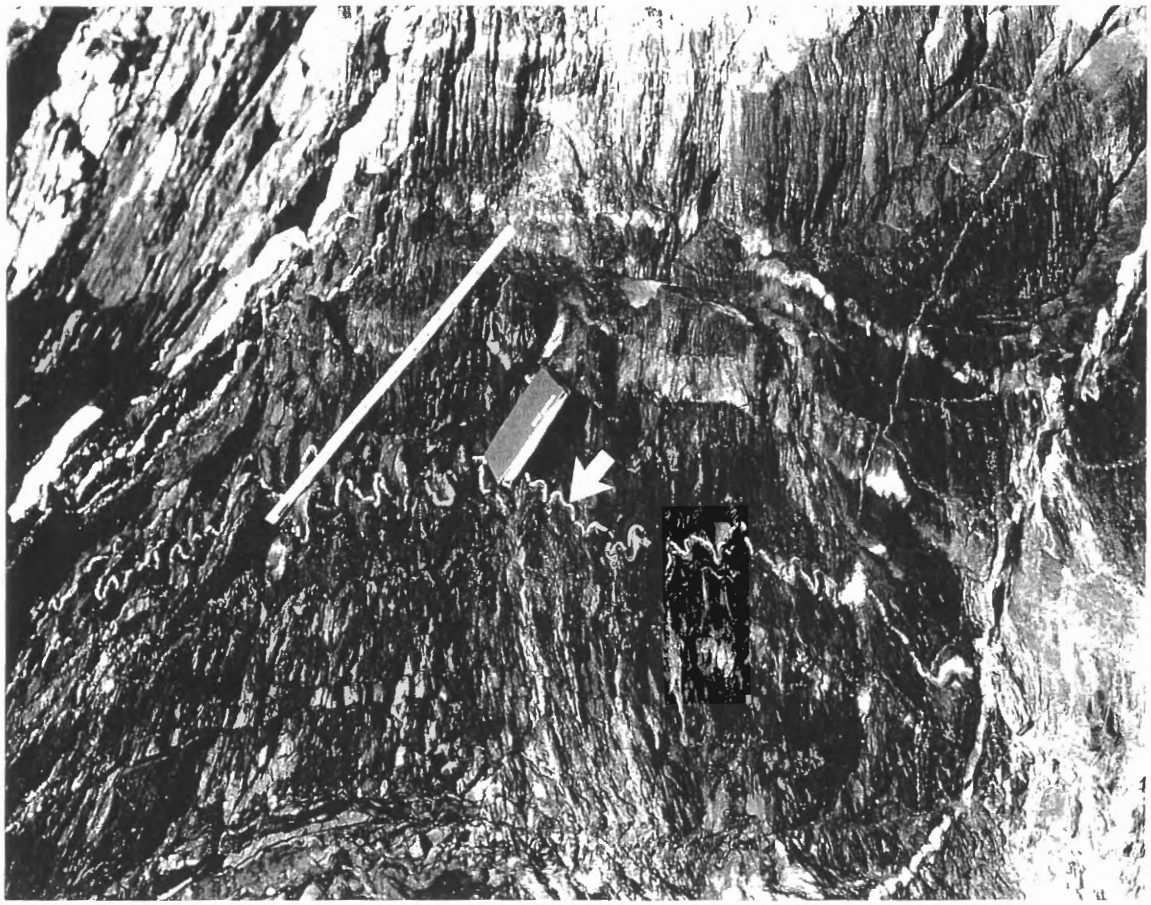

Figure 3.6a: Photograph of the hinge zone of the Ovens Anticline in Cunard Cove. Note the divergent cleavage pattern and buckled bedding-parallel vein (indicated by arrow). View looking southwest.

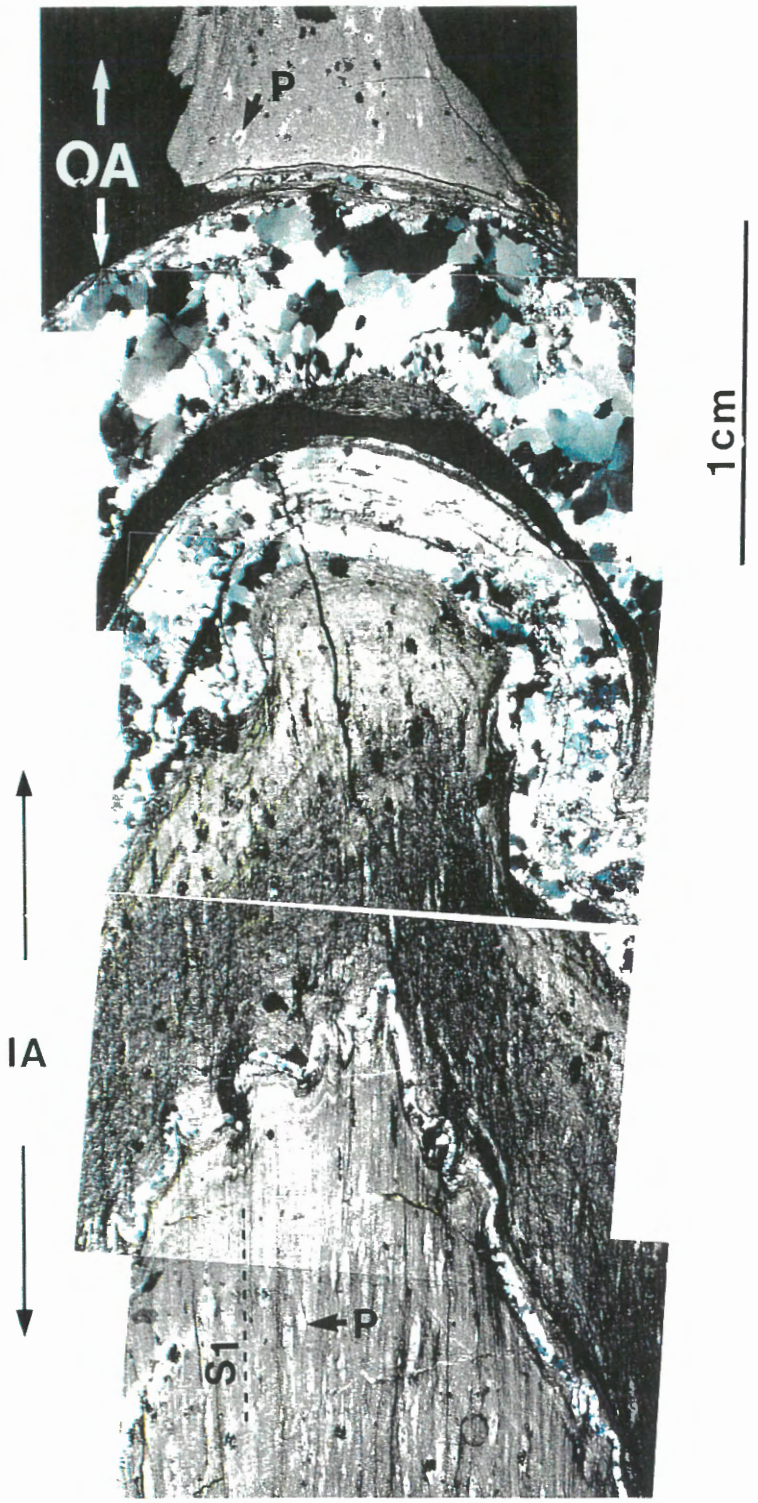

Figure 3.6b: Photomicrograph of buckled bedding-parallel vein from the hinge zone in Cunard Cove. Note in particular the variation in strain within the slate host, where there is intense cleavage (S_1) development and commensurate deformation of porphyroblasts (P) in the inner arc (IA) of the vein, and no cleavage or deformation of porphyroblasts in the outer arc (OA). This is consistent with inverse tangential longitudinal strain within the slate (see text).

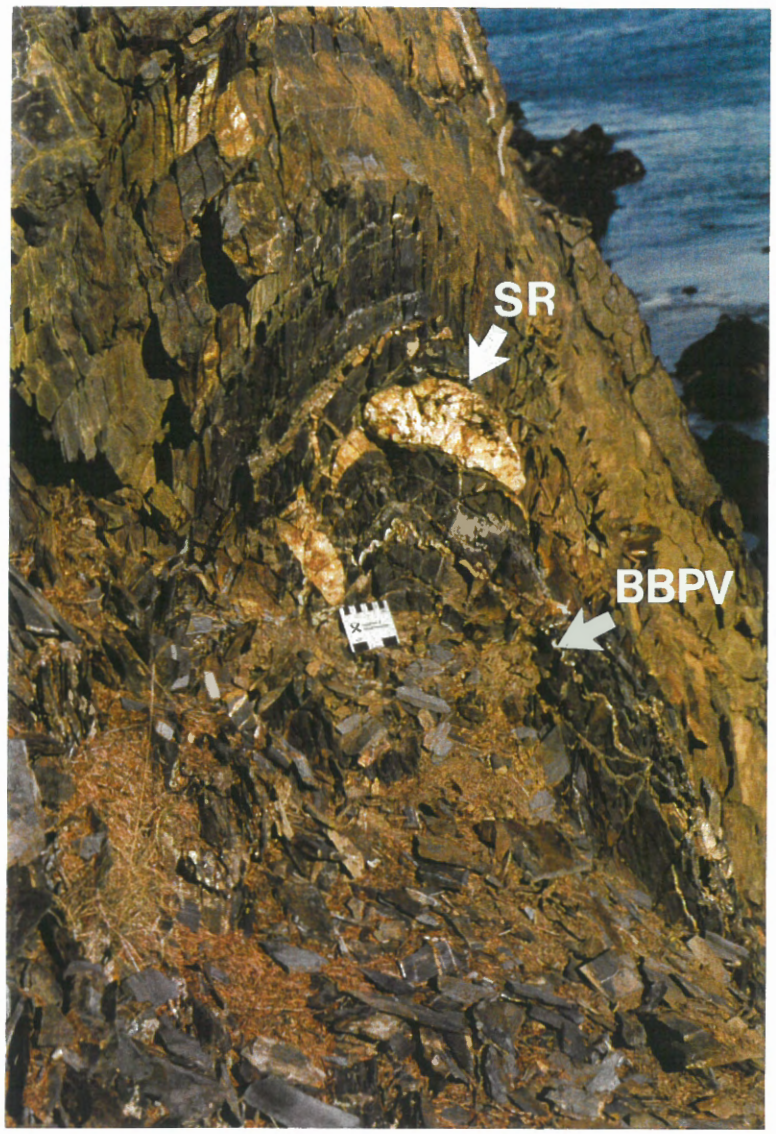

Figure 3.6c: Photograph of the hinge zone of the Ovens Anticline, Cunard Cove, showing a small saddle-reef vein (SR) above a buckled bedding-parallel vein (BBPV). Small intervals on the top of scale are 1 centimetre. View looking northeast.

veins within the hinge zone, where cleavage in the slate is intensely developed within the inner arc of the folded vein and poorly developed in the outer arc (Fig. 3.6b). This cleavage pattern reflects deformation by tangential longitudinal strain in the competent metasandstone beds and quartz veins and "inverse tangential longitudinal strain" in the incompetent slate beds (Ramsay and Huber, 1987; page 448), where layer parallel stretching in the outer arc of the competent layers extends into the inner arc of the slate bed. This cleavage pattern is also interpreted to indicate there was only minor or no homogeneous shortening prior to folding (Ramsay and Huber, 1987, Fig. 21.26). A small saddle reef vein is exposed within the hinge in the cliff section, occurring about twenty centimetres above a buckled bedding-parallel vein (Fig.3.6c).

3.3.1.2 *Geology of the North Limb (Section C-D):*

The north limb of the fold, section C-D, dips uniformly at 60-62° to the northwest (Figs. 3.2, 3.4) and consists of a conformable sequence of interbedded metasandstone and slate (Figs. 3.4, 3.5). No sedimentary or structural discontinuities cut stratigraphy in the section and bedding is planar throughout the section, with no minor-scale folds noted (Fig. 3.4). Axial planar cleavage (S_1) within the slate intervals dips uniformly to the north, and is roughly axial planar to the fold (Figs. 3.2, 3.7). In thin section, S_1 cleavage in slate is defined by a fine continuous cleavage (Fig. 3.8a). Locally, in silty slate, a layer parallel alignment of muscovite occurs and S_1 cleavage is a fine crenulation cleavage (e.g., see Fig. 3.24). Cleavage within the metasandstone beds is indistinct and difficult to distinguish in the field. In thin section, there is commonly no apparent cleavage developed within the metasandstone beds, although a layer-parallel alignment of muscovite, similar to silty slate beds, occurs (Fig. 3.8b).

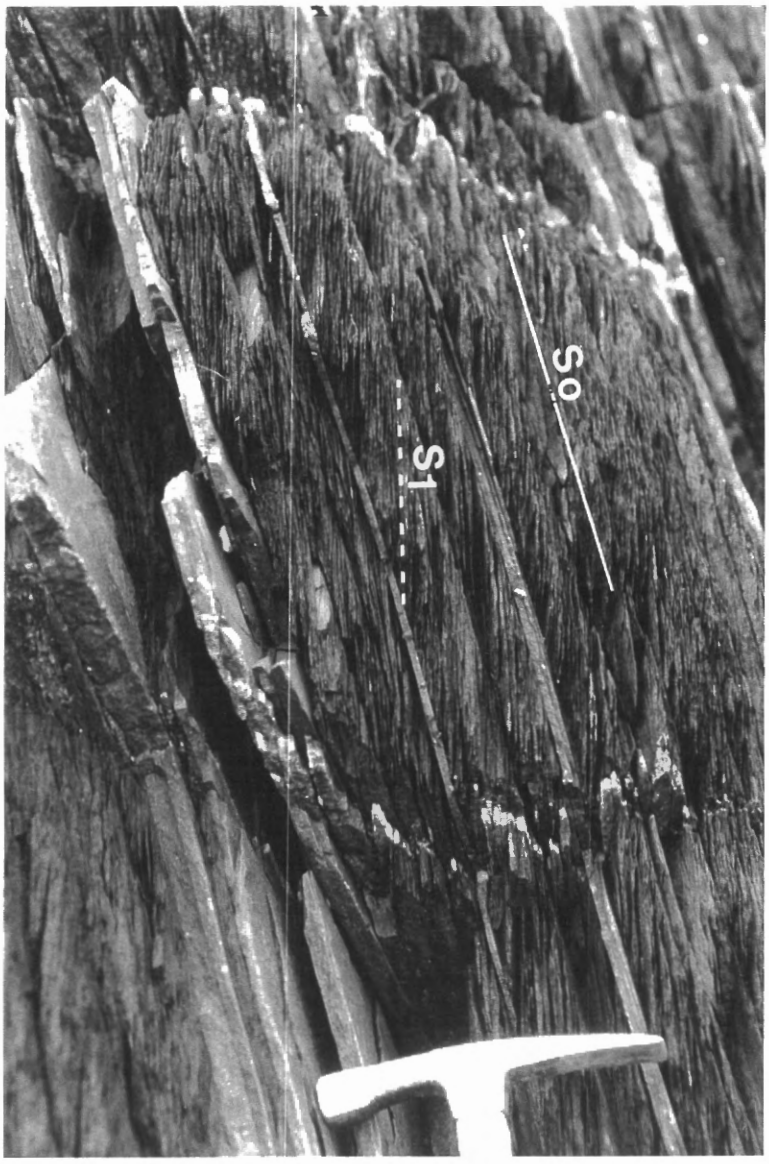

Figure 3.7: Photograph of bedding-cleavage relationships on the north limb of the Ovens Anticline in Cunard Cove (section C-D). View looking to the southwest. Hammer for scale. S_0 = bedding; S_1 = cleavage.

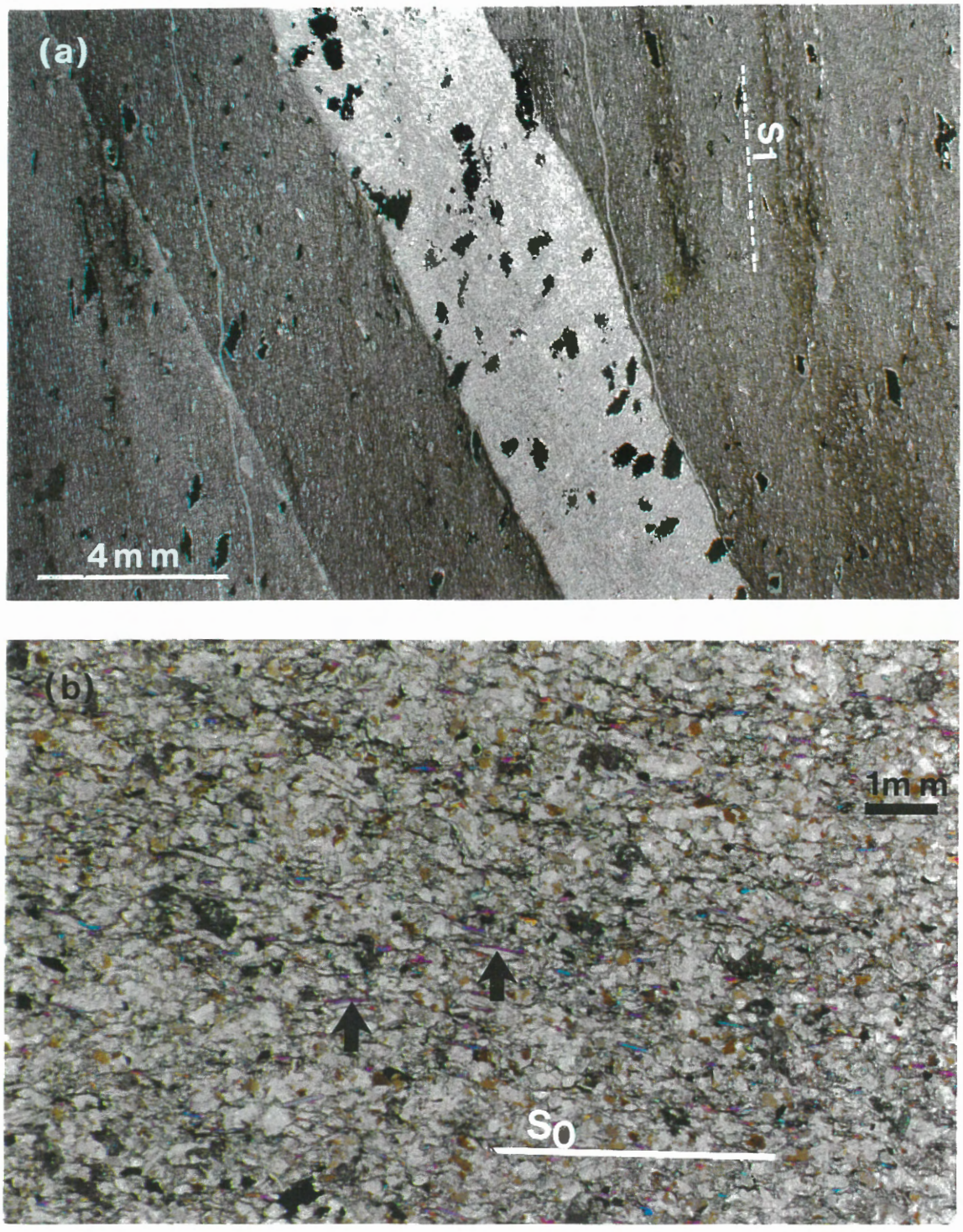

Figure 3.8: Photomicrographs from the north limb of the Ovens Anticline, Cunard Cove; (a) Slate and thin metasandstone bed showing fine continuous cleavage in the slate; (b) Metasandstone with no evidence of cleavage, but with a well defined layer-parallel foliation defined by (detrital?) muscovite (indicated by arrow). S_0 = bedding, S_1 = cleavage. Both under partial crossed polars and represent profile sections looking southwest.

A down-dip stretching lineation within the cleavage plane is apparent in the slate, defined by deformed porphyroblasts (Fig. 3.6b) and local quartz±muscovite±chlorite pressure shadows around arsenopyrite within metasandstone layers.

Quartz veins, including bedding-parallel and discordant types, are abundant within the measured section and are discussed in detail below. Coarse disseminated arsenopyrite is locally abundant, typically concentrated within specific, generally thin, metasandstone layers.

3.3.2 FLEXURAL SLIP

Flexural slip was investigated within the measured section (C-D). Following is a discussion of the structure and spacing of flexural-slip movement horizons and the amount of flexural-slip displacement for two intervals of the section.

3.3.2.1 Flexural-slip structures:

Flexural-slip structures in Section C-D are characterized by regularly spaced, bedding-parallel movement horizons. All movement horizons in Section C-D were identified by offset discordant veins (e.g., Figs. 3.4, 3.9a), without which the presence of many of these movement horizons would be unknown. All movement horizon surfaces are characterized by movement indicators, including slickensides, striations and slickenfibres (Fig. 3.9b). Slickenfibres consist mainly of quartz, although calcite and sulphide (pyrite) slickenfibres occur locally. As discussed below, the movement direction and sense of shear established for all movement horizons is consistent with the interpretation that they resulted from flexural slip.

The majority of movement horizons are single movement planes without any marginal

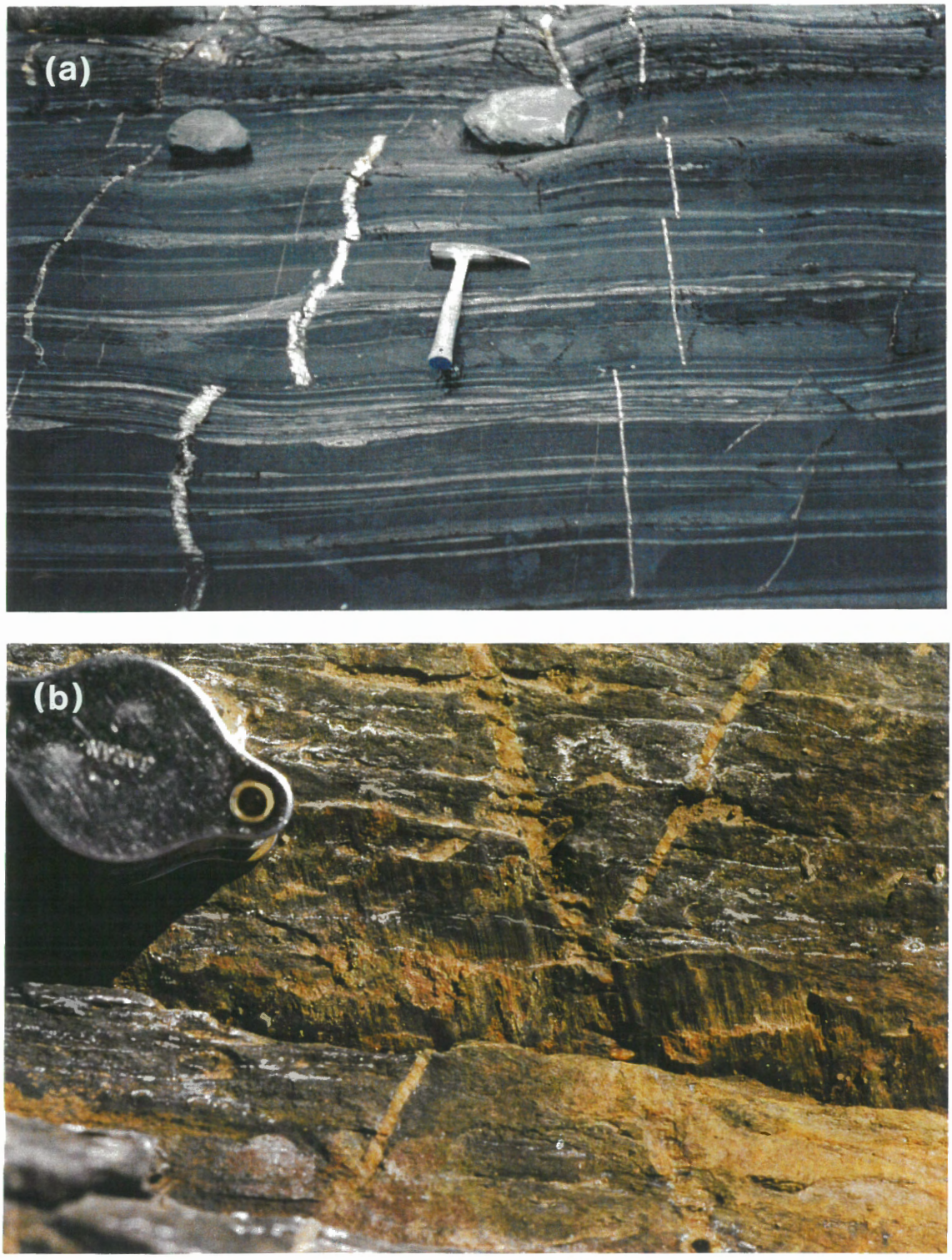

Figure 3.9: (a) Photograph showing strike separation (plan view) of discordant veins across flexural-slip movement horizons. (b) Photograph of striations on flexural-slip movement horizon offsetting thin discordant veins.

deformation. These movement horizons, therefore, can only be recognized by displaced discordant veins (e.g., Fig. 3.9a) or the local exposure of a striated movement surface (Fig. 3.9b). Quartz veins ("flexural-slip" bedding-parallel veins, see below) varying from 1 mm to 8 cm in thickness are common along movement horizons (Fig. 3.5 and see section 3.5), with striations typically occurring on the vein margins.

Flexural-slip duplexes (Tanner, 1992) mark several bedding-parallel movement horizons and include common "slate duplexes" (Figs. 3.10a, b) and less common imbricated metasandstone layers (Fig. 3.11). The slate duplexes are characterized in the field by zones of rotated slaty cleavage, fault boundaries and abundant striated ramps. The internal structure of slate duplexes is not apparent in the field. However, cut slabs reveal typical duplex geometry, defined by imbrication of sedimentary layering and discordant quartz veins (Fig. 3.10b). Duplex boundaries (floor and roof thrusts) are bedding-parallel and are marked by movement horizons with slickenfibres, striations and veins. Ramps, which invariably have a geometry consistent with reverse movement (Fig. 3.10b), link floor and roof thrusts and are also characterized by movement indicators. The trend of lineations on ramps parallels those on the roof and floor thrusts. Duplex zones range in thickness from 5 cm to 185 cm (Fig. 3.5) and most duplexes are continuous over the entire profile exposure (approximately 10-20 metres; Fig. 3.10a). Where duplex zones terminate, movement is transferred to the higher structural level (roof thrust) on the leading thrust (e.g., Tanner, 1992), which then defines a simple movement horizon. This is consistent with formation of duplexes from simple movement horizons during flexural slip. Movement may also be transferred from floor to roof thrusts along ramps within the duplex. Cataclastic zones are developed along the floor

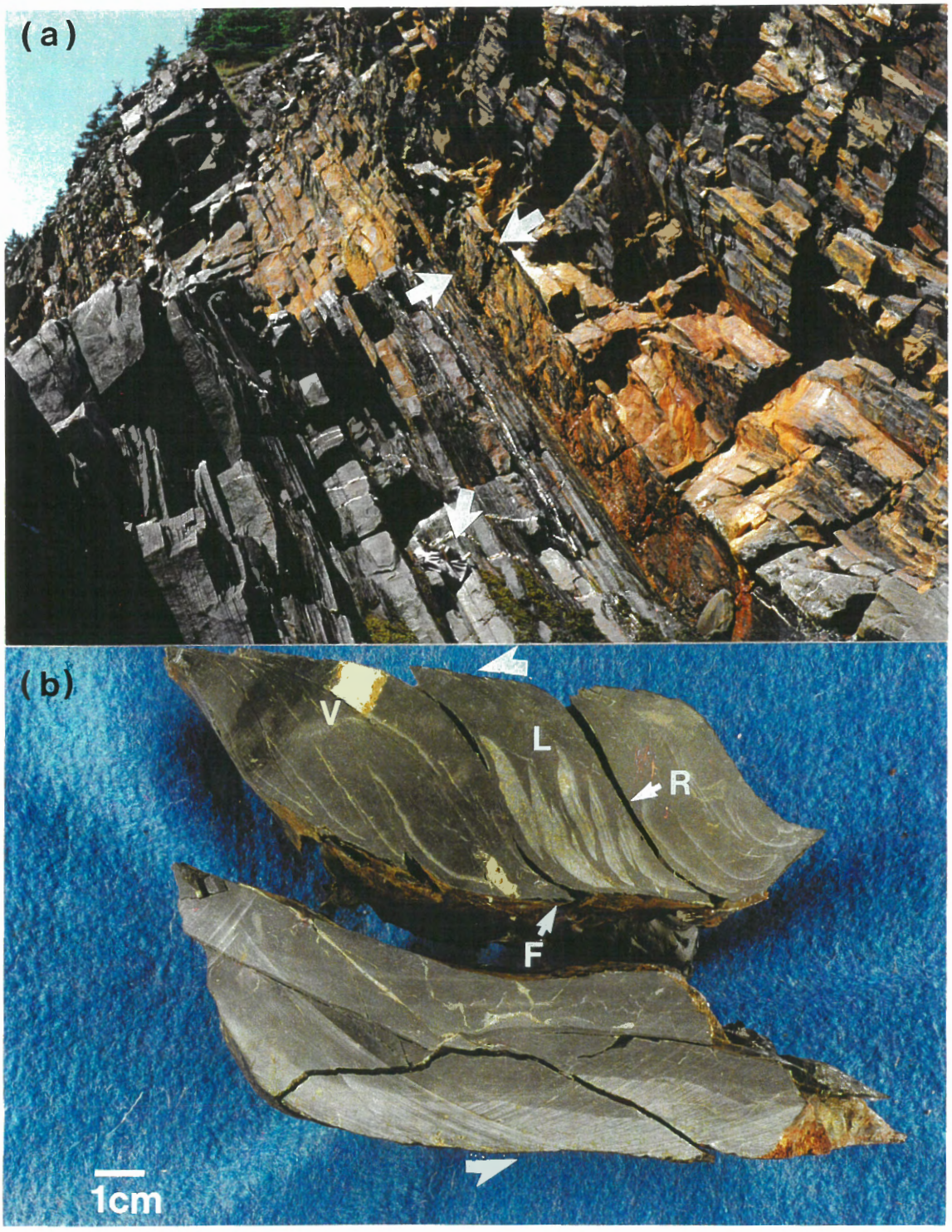

Figure 3.10: (a) Photograph of flexural-slip duplex (between arrows) in section C-D, Cunard Cove, illustrating continuity of these structures; backpack (arrow) for scale. (b) Cut slab of a segment of a flexural-slip duplex showing internal geometry, including flats (F), ramps (R), and imbrication of sedimentary layering (L) and discordant veins (V). Cut perpendicular to bedding and parallel to movement lineations.

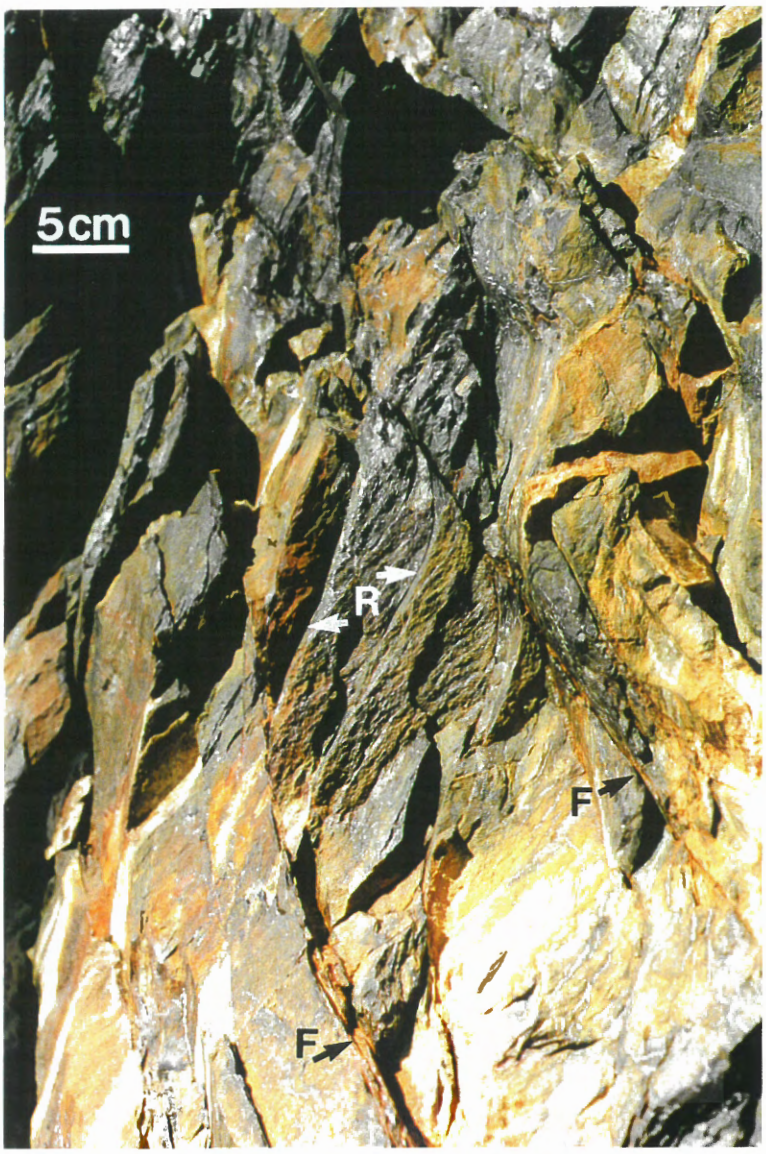

Figure 3.11: Photograph of flexural-slip duplex, defined by bedding-parallel flats (F) and sigmoidal ramps (R), developed within metasandstone bed.

or roof thrusts of some duplex zones. Flexural-slip duplexes occur throughout Section C-D (Fig. 3.5) and mark horizons with the largest amount of calculated offset (see below), suggesting that they developed along early-formed movement horizons only after significant displacement. Quartz veins occur along flat and ramp structures of some flexural-slip duplexes.

3.3.2.2 Movement Horizon Spacing:

The distribution and abundance of movement horizons within Section C-D is shown in Fig. 3.5. The average movement horizon spacing for the section is 1.09m (Fig. 3.5; Appendix 1), similar to that determined for stratigraphically similar sections in the railway exposure (i.e., Lower unit; Fig. 2.4, in pocket at back). Movement horizons occur throughout the section and flexural-slip duplexes are intermixed with simple movement horizon planes. Movement horizons are restricted to slate intervals, and commonly occur close to metasandstone beds (Fig. 3.5).

As indicated above, Fowler and Winsor (1997) and Tanner (1989) identified movement horizons by the presence of bedding-parallel quartz veins, the microstructure of which they interpreted to result from flexural slip. Many movement horizons in the studied section host bedding-parallel quartz veins, with veining interpreted to have occurred during flexural-slip folding (see flexural-slip bedding-parallel veins below). Numerous similar bedding-parallel veins which do not occur along defined movement horizons occur within the section, and indeed these may represent movement horizons formed prior to emplacement of discordant veins. If these veins were included in the total, a mean spacing of 0.52 metres

between movement horizons would be indicated (Fig. 3.5).

3.3.2.3 Movement Direction and Sense of Shear:

Movement direction:

Movement lineations are present on most bedding-parallel movement horizons within Section C-D, although it was often necessary to search along movement horizons to find well defined lineations. Movement lineations from this section display considerable variation in trend (Fig. 3.12). Some lineations trend roughly perpendicular to the fold hinge. However, many lineations trend obliquely to the fold hinge (Fig. 3.12a). Oblique lineations trend in a direction between the perpendicular to the hinge and the trend of the hinge (Fig. 3.12a), as did lineations in the Halifax area. However, unlike the Halifax area, the oblique lineations do not coincide with the dip azimuth (DA) direction for bedding. Two lineations, including one oblique and another perpendicular to the hinge, were noted on some movement horizons. Movement lineations occur on all observed thrust surfaces of flexural-slip duplexes.

Sense of shear:

Sense of shear on movement horizons in the Cunard Cove section is provided by offset discordant quartz veins, slickenfibre geometry and duplex geometry. Tanner (1989) cautions against using offset markers to determine movement sense, as the apparent displacement is controlled by the attitude of the displaced marker, the direction of movement and the plane in which the offset is viewed. At the Ovens, however, discordant veins form a conjugate set (see vein section below), allowing an unambiguous shear sense to be determined from displaced veins (Fig. 3.13). Using displaced veins to determine shear sense is particularly useful as all movement horizons were defined by offset of these discordant veins. A reverse

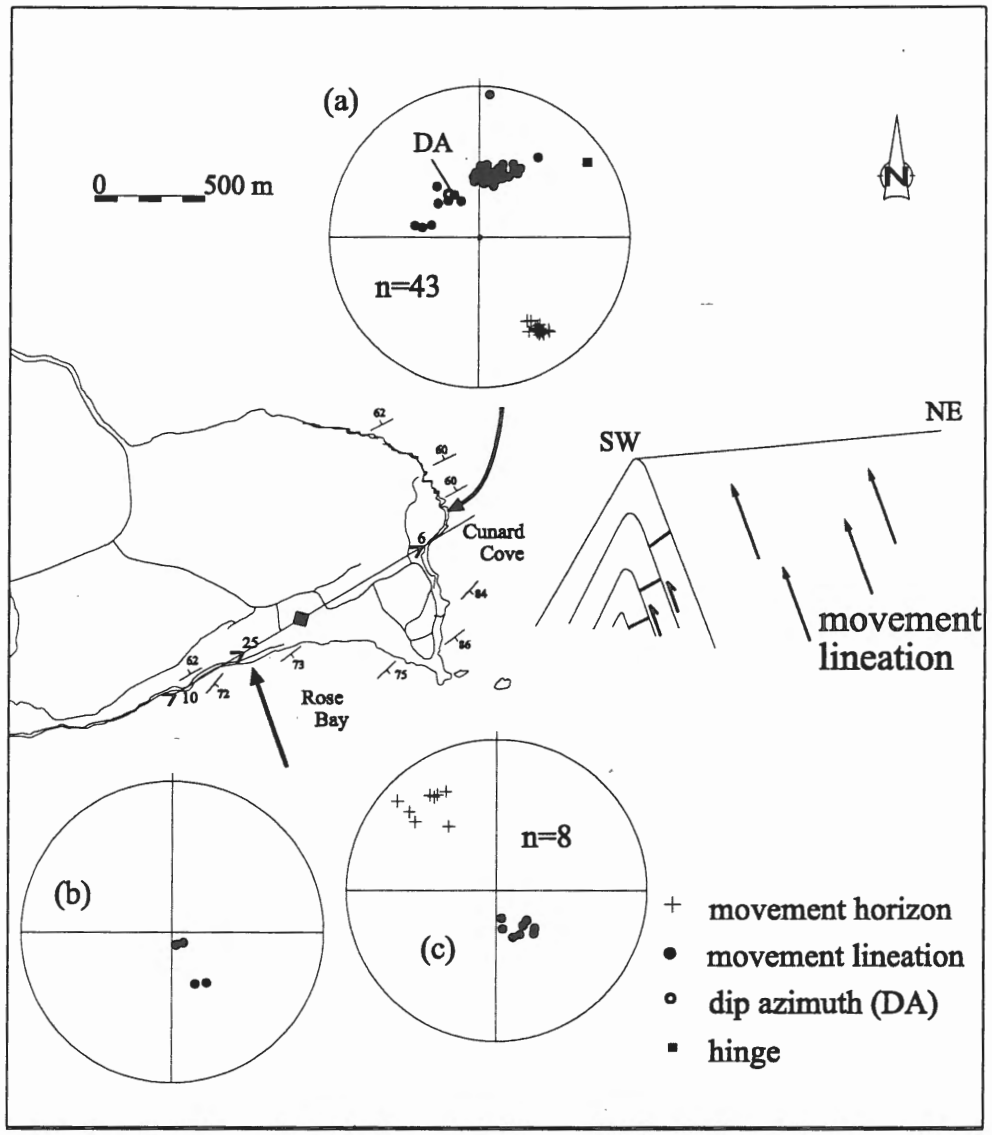

Figure 3.12: Stereoplots of (a) poles to flexural-slip movement horizons and lineations for Cunard Cove (section C-D), (b) movement direction lineations for flexural-slip movement horizons in Zone A, Rose Bay and, (c) poles to thrusts and movement lineations on thrusts from Zone B, Rose Bay.

sense of shear is indicated by displaced discordant veins in all instances where matching of veins across movement horizons could be established. A reverse shear sense is supported by slickenfibres, which occur on many movement horizons, including ramps within duplexes, and by the geometry of flexural-slip duplexes (e.g., Fig. 3.10b).

3.3.2.4 Quantifying Flexural Slip (Flexural-slip strain)

As discussed by Tanner (1989) quantifying slip amount resulting from flexural slip is generally difficult and requires unique circumstances where movement horizons are recognized, movement direction can be established, the shear sense can be determined and the slip amount measured. Tanner (1989) locally documented displaced quartz veins along flexural slip movement horizons in Wales; however he was unable to determine the movement lineation and therefore could not determine the shear sense or slip amount. These problems, related to establishing the slip amount along flexural-slip movement horizons, are very common and, as far as the author is aware, there are no documented studies which have quantified displacement resulting from flexural slip.

Displacement of discordant veins along flexural-slip movement horizons throughout Section C-D provides a unique situation where the slip amount can be determined. As discussed above, the conjugate character of the displaced veins provides an unambiguous shear sense, which invariably is consistent with flexural slip. The flexural-slip movement vector could be determined for each movement horizon in two intervals of the section, where confident matching of displaced veins could be made. This information allows for calculation of the slip amount by the method shown in Fig. 3.14. The importance of matching displaced

veins across movement horizons is obvious and particular caution was taken when doing this. Down-dip and strike parallel variation was noted in the thickness and attitude of the displaced (conjugate) veins, which commonly taper and bifurcate. Therefore, matching of several veins across movement horizons was generally established to ensure data was from corresponding veins (e.g., Fig. 3.9a). Offset veins could not be confidently matched across movement horizons in the interval of Section C-D between ~39 - 57 metres and calculation of offset was not determined (Fig. 3.15).

The method for determining the slip amount along movement horizons indicated by offset discordant veins is illustrated in Fig. 3.14. The details of how each of the variables required to calculate the offset were determined and the calculated values for each movement horizon are discussed in Appendix 2. The slip amounts were determined for two intervals of the measured section (C-D) and the results are shown graphically for each movement horizon in Fig. 3.15. The slip amount for each interval is presented for the total cumulative offset amount measured for each movement horizon (x_t) and the corrected offset amount (x_C) (Fig. 3.15), the latter representing projection of the total offset on to the profile plane of the fold. The method of calculating the corrected offset amounts is discussed in Appendix 2.

The calculated slip records only slip occurring after emplacement of the offset conjugate veins and therefore slip predating discordant veins is unrecorded. The discordant veins are relatively late in the fold history, as they have experienced limited, but significant, shortening, and thus some early slip may be unaccounted for. However, discordant veins are coeval with flexural-slip veins interpreted to have formed during flexural slip (see section 3.5)

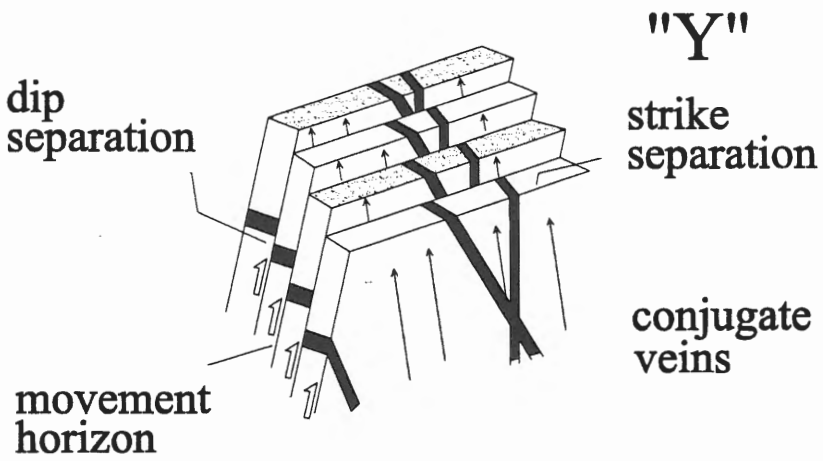

Figure 3.13: Schematic diagram of offset discordant veins showing strike separation and dip separation. Note variation in strike separation reflecting opposite dip of conjugate veins.

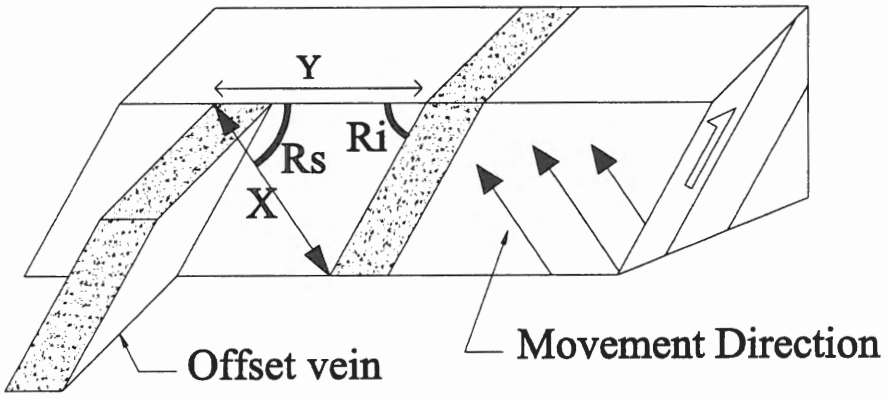

$$X = \frac{Y \sin Ri}{\cos(Rs-(90-Ri))}$$

Figure 3.14: Schematic diagram showing the method used to determine the amount of flexural-slip offset (X) recorded by displaced discordant veins.

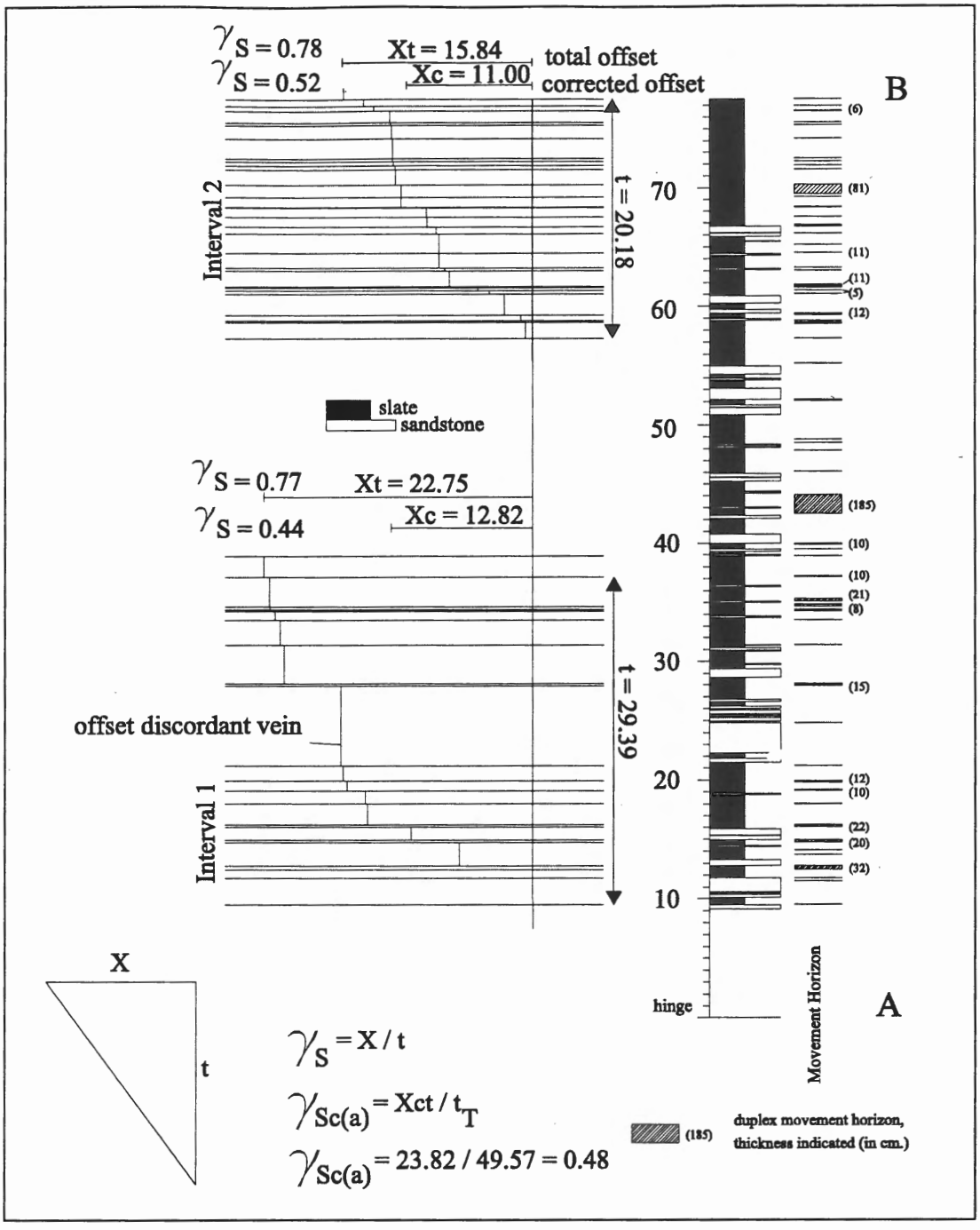

Figure 3.15: Diagram showing a graphic representation of the total and corrected flexural-slip offset and associated shear strain for two intervals of Section C-D, Cunard Cove. The average shear strain is determined from the combined offset and thickness for the two intervals. See text and Appendix 2. γ_S = flexural slip shear strain; $\gamma_{Sc(a)}$ = average corrected flexural-slip shear strain for the two intervals; tT= total thickness of both intervals; X_{CT} = total corrected offset for both intervals.

and therefore probably record most of the flexural slip. As discussed above, unrecorded flexural slip may be indicated by bedding-parallel flexural-slip quartz veins which predate (are cut by) discordant veins and along which the occurrence of flexural slip was not established. Displaced quartz veins may not evaluate all of the flexural slip; however, they do give a minimum estimate of flexural slip during late fold growth.

The slip amount recorded is a measure of the flexural-slip strain (γ_S), which is a ratio of the slip amount to the thickness of the interval. Values of γ_S are similar for both intervals (Fig. 3.15), suggesting uniform flexural slip at this scale. The average flexural-slip shear strain for the two intervals, based on the corrected offset amounts, is equal to the ratio of the combined slip amount to the combined thickness of the two intervals (X_{cT}/t_T), and is equal to 0.48 (Fig 3.15). The increment of folding attributed to flexural slip is related to the flexural-slip shear strain, and varies as a function of the initial limb dip. It has been argued here that flexural-slip represents a late folding event, although other mechanisms may have caused late fold tightening. Assuming that flexural slip accounts for the last increment of folding and that shear strain is related to limb dip, the average corrected flexural-slip shear strain determined would reflect an 8.8° increment of angular shear strain (Appendix 2, Fig. A2.2). Flexural slip, therefore, would account for 8.8° of the 60° of limb dip for the north limb of the Ovens Anticline in Cunard Cove. The Ovens Anticline is inclined, and has an interlimb angle of ~40°, and therefore the limb dip with respect to the axial plane is ~70°. If flexural slip accounts for the last increment of folding with respect to this limb dip, the average corrected flexural-slip shear strain accounts for an increment of angular shear strain, or limb rotation, of only 3.8° (Appendix 2).

The amount of slip varies between movement horizons (Fig. 3.15; Table A2-1, Appendix 2), and may reflect variation in stratigraphy and spacing, although this is not quantifiable for a single section. The largest offset occurs along flexural-slip duplex movement

	Movement Horizons	Duplexes
number	34	13
sum offset	11.36 metres	27.2 metres
mean offset	0.33 metres	2.09 metres
median offset	0.17 metres	1.38 metres

Table 3.1: *Table of statistical data of flexural-slip offset amount on flexural-slip movement horizons and flexural-slip duplexes in section C-D, Cunard Cove. Data represents offset amounts for both intervals where offset was determined (Fig. 3.15).*(See Appendix 3).

horizons (Fig. 3.15; Table 3.1) and there is a positive correlation between the amount of offset and duplex thickness (Fig. 3.16). This suggests that flexural-slip duplexes develop from simple movement horizons only after significant displacement has occurred.

Although displacement amount is highly variable between movement horizons, the shear strain is similar for both of the intervals where offset was determined and flexural-slip duplexes (horizons of significant displacement) are regularly distributed throughout the section (Fig. 3.15). This suggests that the calculated flexural-slip shear strain for the two intervals is representative for the north limb of the Ovens Anticline in the Cunard Cove area. The mean and median offset amount on simple movement horizons and duplexes show a

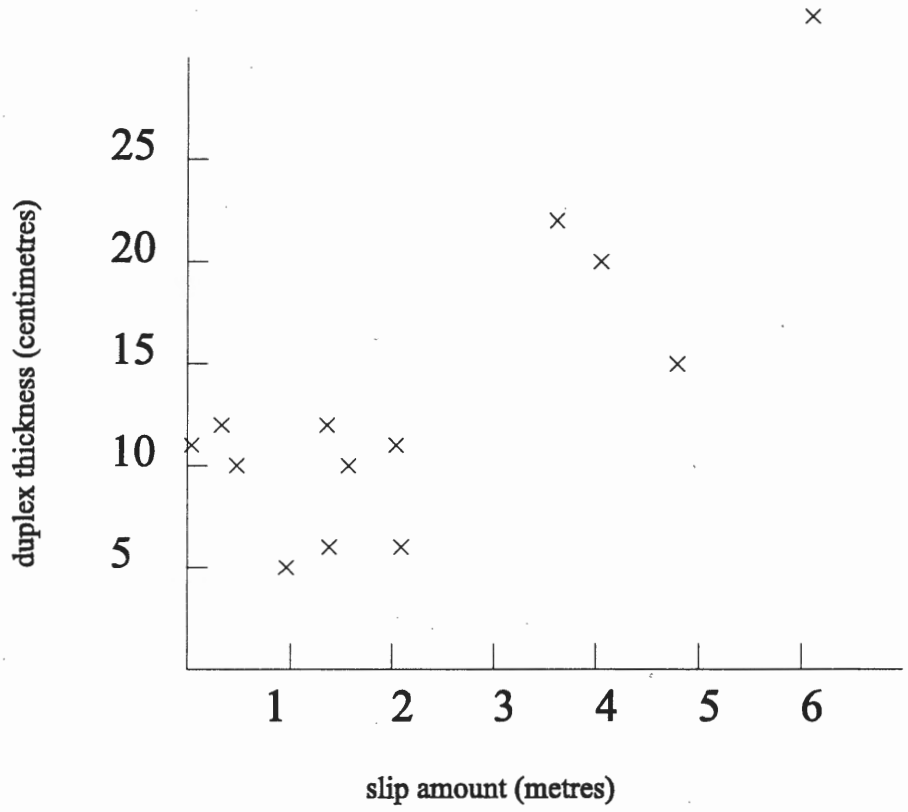

Figure 3.16: Graph of duplex thickness against slip amount for flexural-slip duplexes, Section C-D, Cunard Cove. (See Appendix 3).

bimodal population (Table 3.1) indicating that most of the strain is taken up on the duplexes, with only minor strain accounted for by simple movement horizons distributed between flexural-slip duplexes. This is similar to the Halifax area, where continuous movement horizons formed early and accommodated most of the slip, with discontinuous movement horizons between the continuous movement horizons accommodating minor slip.

3.4 ROSE BAY

3.4.1 Introduction:

The Rose Bay section consists of continuous outcrop along a portion of Rose Bay which is strike-parallel or oblique to the fold hinge, and which includes exposure of the hinge zone in two areas (Fig. 3.17). Assessment of this area was achieved by detailed mapping of continuous exposure along the coast. Data are presented mainly as sketches and photographs, including a detailed, scaled cross-section of the mapped area.

Detailed mapping of the Rose Bay section revealed a complex structural character resulting from fold development. Two structurally distinct zones are recognized in the Rose Bay section, and are obvious in a constructed cross-section through the area (Fig. 3.18). Structural 'Zone A' is represented by the hinge zone of the Ovens Anticline and is structurally similar to the Cunard Cove section, characterized by a tight chevron structure (Figs. 3.17b, 3.18, 3.19, 3.20). Structural "Zone B" occurs on the south limb on the Ovens Anticline and is characterized by several outcrop-scale thrusts (Figs. 3.17b, 3.18). Stratigraphy in the Rose Bay section is similar to the lower, slate-metasandstone unit in Cunard Cove, consistent with along-strike projection (Fig. 3.2). Details of the structure of each zone follow.

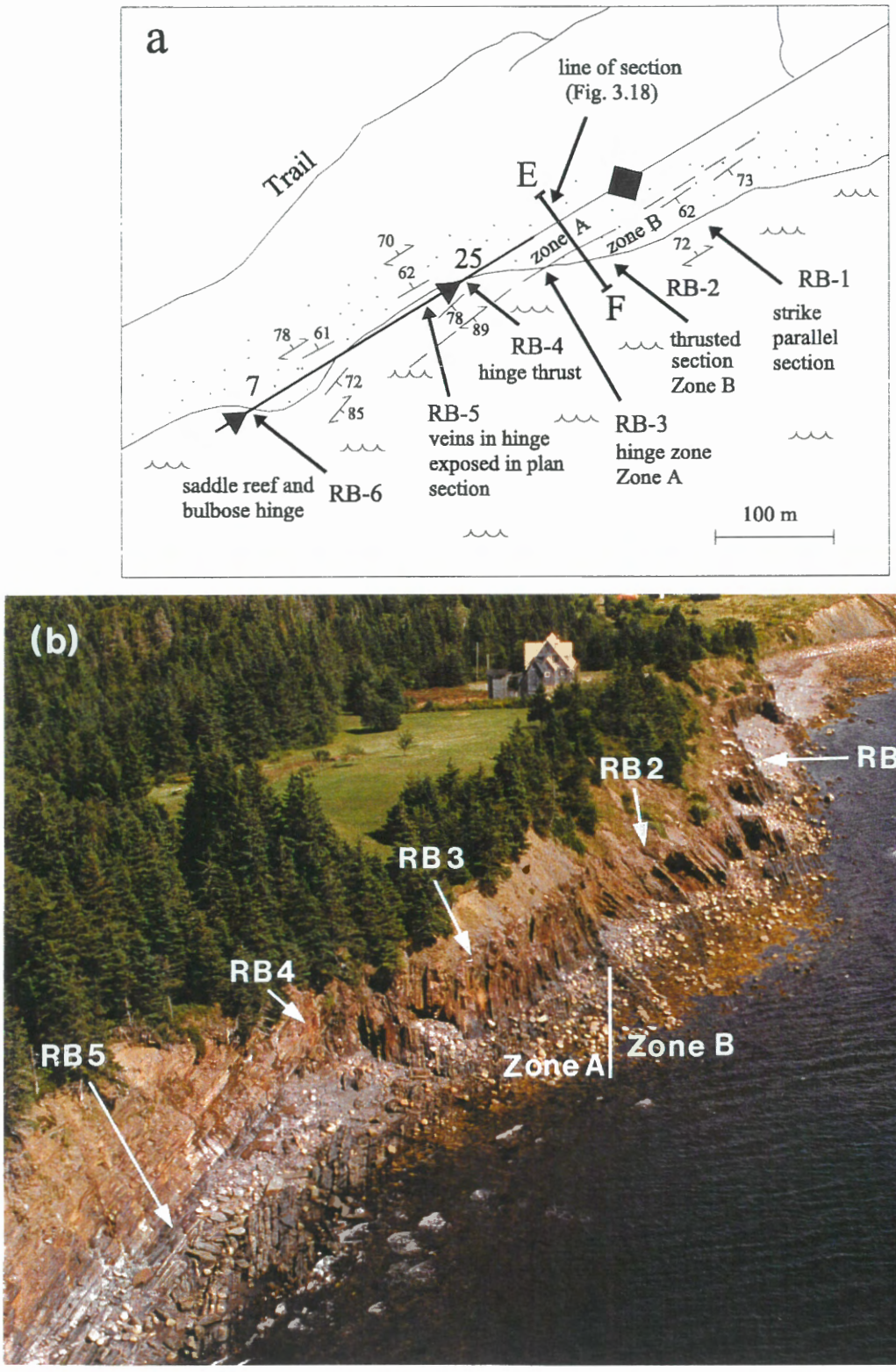

Figure 3.17: Simplified geology map (a) and photograph (b) of the Rose Bay study area, showing the location of various areas (RB-1 ... RB-6) referred to in the text and structural Zones A and B. Photograph looking toward the northeast.

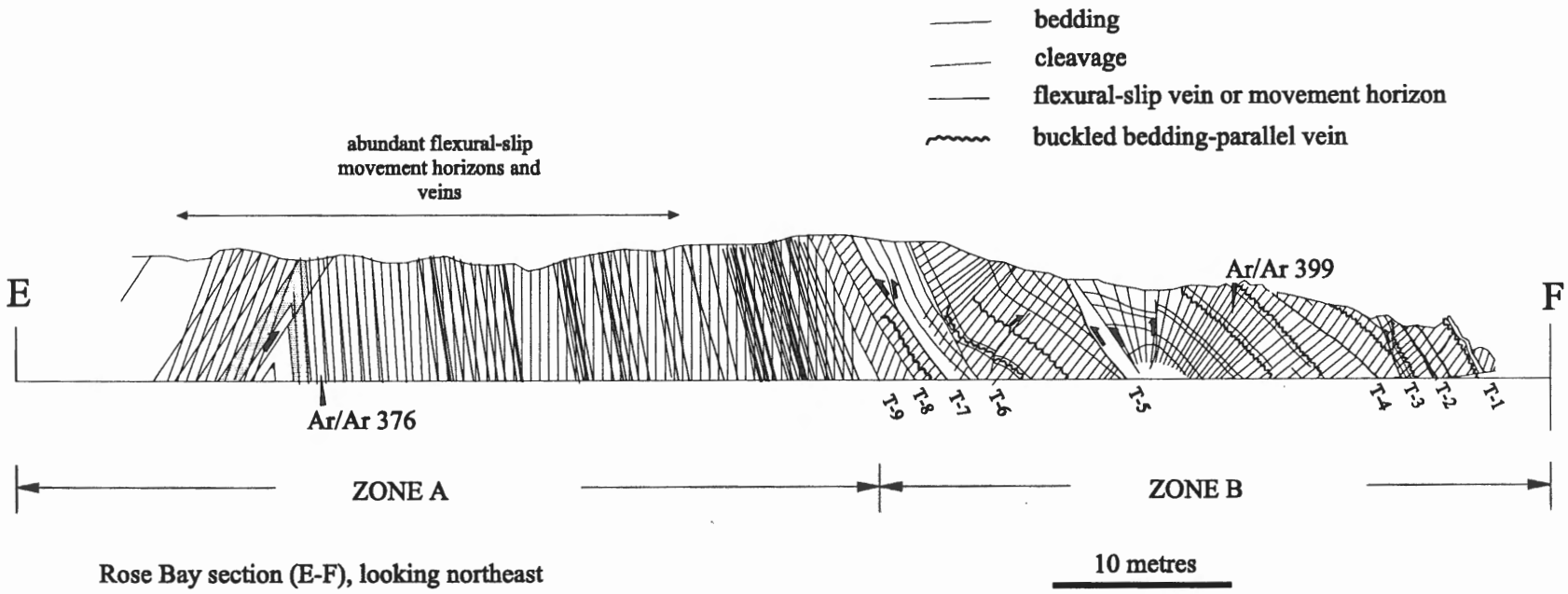

Figure 3.18: Cross section of the Ovens Anticline in the Rose Bay area showing the contrasting structural character of Zones A and B. A more detailed cross section is found in a pocket in the back. See Figure 3.17a for location of section line.

3.4.2 ZONE A

3.4.2.1 General Statement:

Zone A represents the hinge zone and adjacent limbs of the Ovens Anticline and is structurally similar to the Cunard Cove Section. The fold hinge is exposed in the western part of the section (locations RB-4 and RB-6, Fig.3.17a, b), and is characterized by an angular, chevron form (Figs. 3.19 and 3.20). The axial plane dips steeply to the northwest, plunges moderately (7-25°) to the northeast and the fold has an interlimb angle of 41-46°. Pyrite and arsenopyrite are locally abundant within Zone A. Pyrite occur as thin discordant veins, some offset by flexural-slip movement horizons, and along movement horizons. Locally there is significant massive and disseminated pyrite within slate intervals where movement horizons and flexural-slip bedding-parallel veins occur. Arsenopyrite occurs as fine- to coarse-disseminations, particularly within thin metasandstone beds. The concentration and grain size of arsenopyrite displays an apparent relationship to the grainsize of the host, suggesting porosity was important in controlling sulphide deposition. This is most apparent in graded beds, where the amount and coarseness of sulphide decreases in the direction of fining. Discordant quartz veins are abundant, equal in concentration to the Cunard Cove area.

3.4.2.2 *Geology of the Hinge Zone:*

The fold hinge of the Ovens Anticline in the Rose Bay area is angular and extremely narrow (Figs. 3.17b, 3.20, 3.21). Accommodation structures reflecting chevron fold development, discussed above, include saddle-reef veins, bulbous hinge forms and limb thrusts

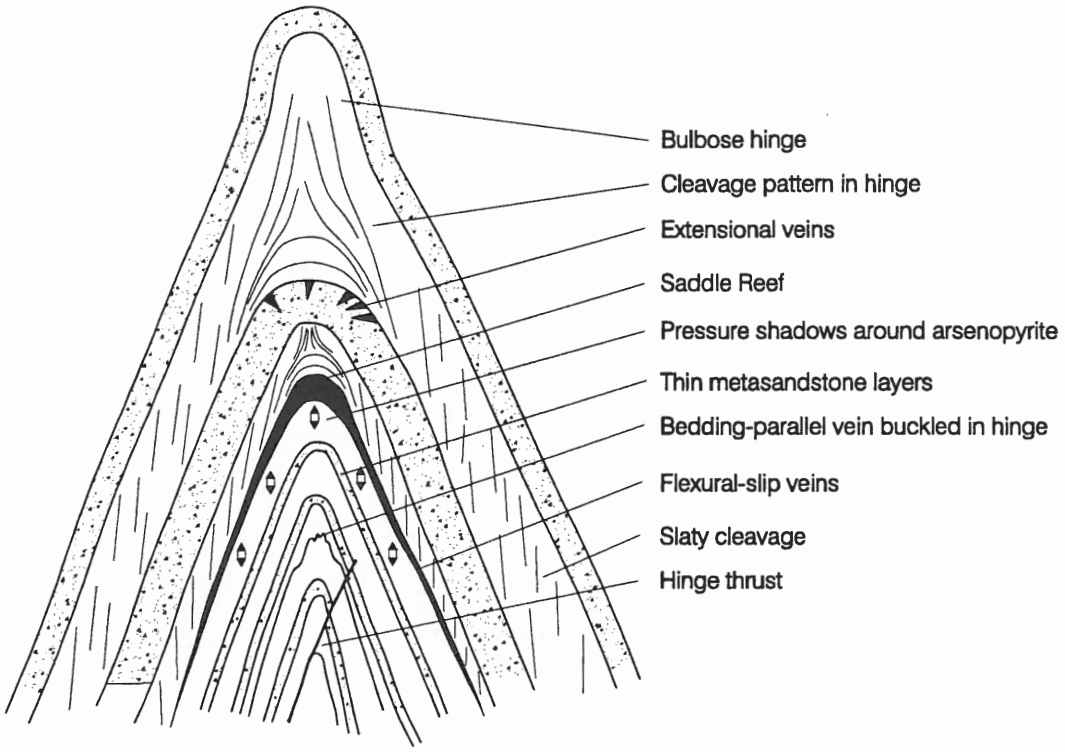

Figure 3.19: Composite sketch of the hinge area of the Ovens Anticline in the Rose Bay area, including structures exposed in location RB-3 to RB-6 (Fig. 3.17). Not to scale.

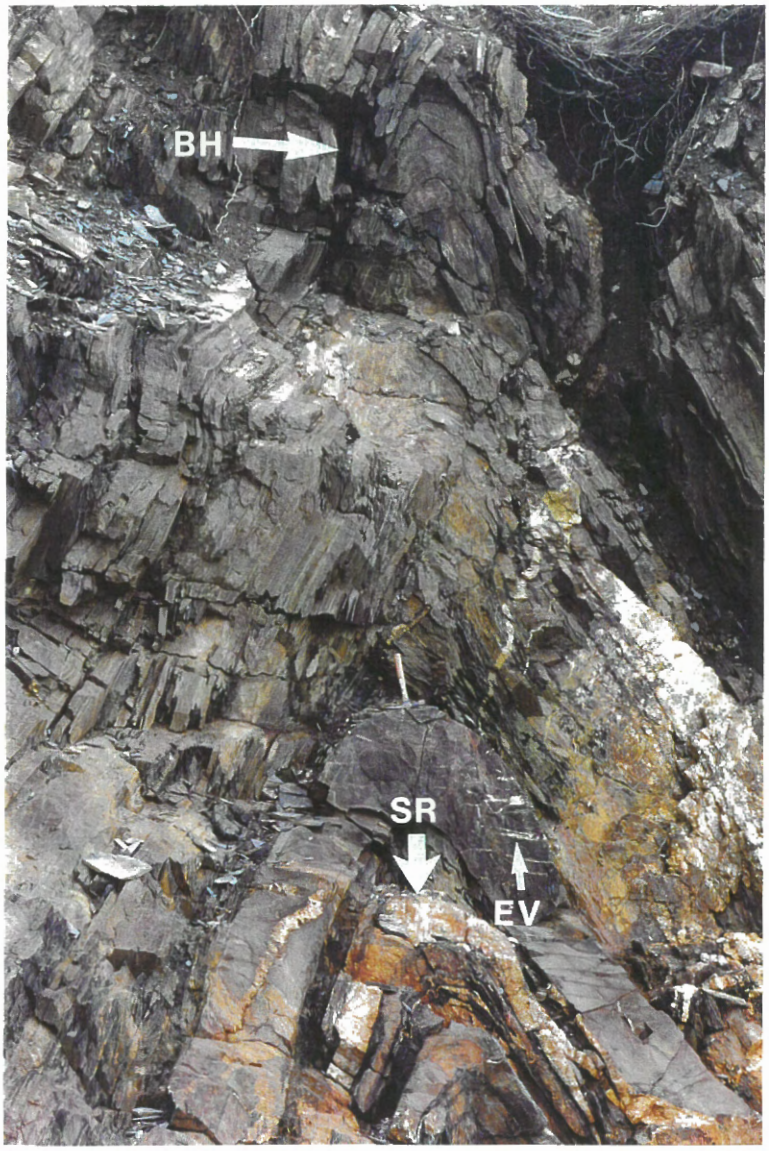

Figure 3.20: Photograph of the hinge of the Ovens Anticline at location RB-6 (Fig. 3.17), Rose Bay. Note the angular, chevron profile, saddle reef vein (SR), bulbous hinge form (BH) and extensional veins (EV) in the outer arc of a metasandstone layer, which maintains constant thickness and is deformed by tangential longitudinal strain. In contrast slate layers are thickened in the hinge zone. Profile view looking northeast.

Figure 3.21: Photograph of the fold hinge at location RB-4 (Fig. 3.17) showing the location of a hinge thrust (HT) on the north limb. Note also sharp hinge exposed below the hinge thrust defined by thin metasandstone layers (light colour), which are not buckled within the hinge zone or on the limbs. Location of Figure 3.22 indicated by arrow.

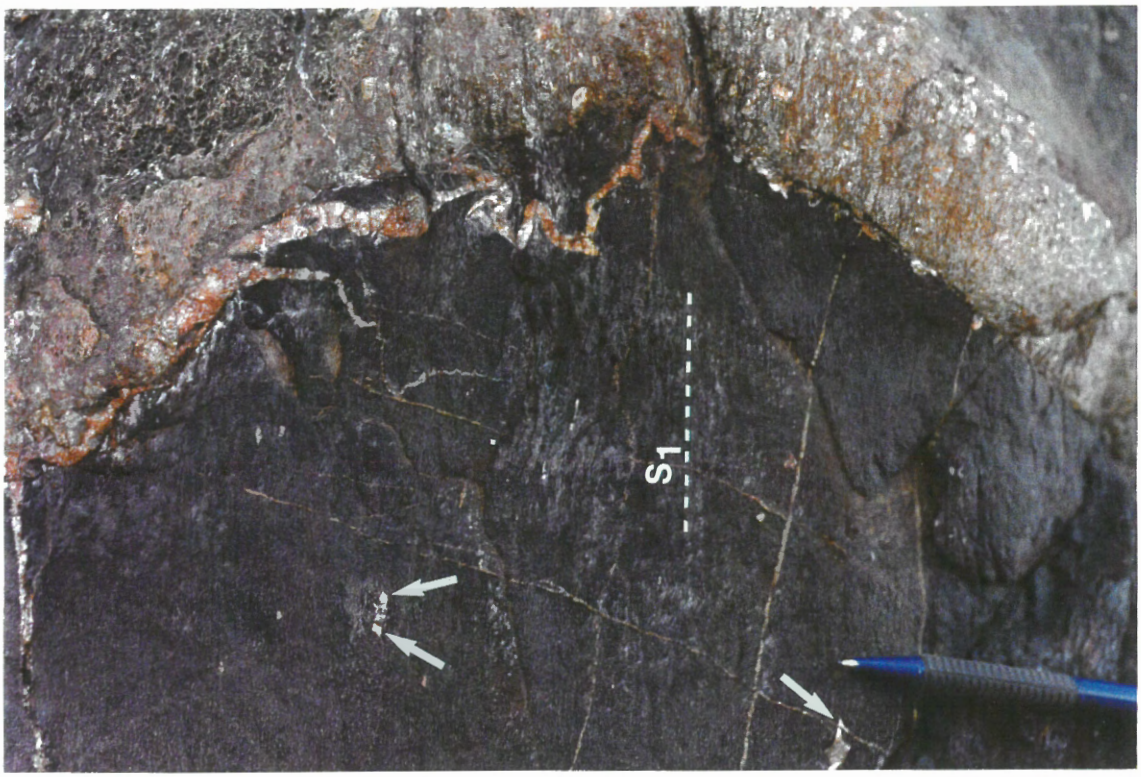

Figure 3.22: Photograph of the fold hinge at location RB-4 (see Figure 3.21 for location) showing well developed quartz±chlorite±muscovite pressure shadows (indicated by arrows) developed around arsenopyrite crystals. Pressure shadows define a pronounced down-dip lineation within the cleavage plane, indicating significant extension parallel the axial plane and perpendicular the fold hinge. S_1 = cleavage. Pen for scale.

(Figs. 3.19, 3.20, 3.21). Metasandstone beds maintain constant thickness through the fold hinge and locally have extensional veins in their outer arc (Figs. 3.19, 3.20), consistent with deformation by tangential longitudinal strain. Slate beds show thickening in the hinge region (Fig. 3.20) and the cleavage pattern within slate intervals at the hinge is similar to the Cunard Cove section, characterized by an overall downward divergent fan about the fold hinge (Fig. 3.19), indicating inverse tangential longitudinal strain within the slates. Cleavage is sub-parallel to bedding in the inner arc of the fold, adjacent to competent metasandstone bed, and intensely developed and axial planar in the outer arc. A similar cleavage pattern is defined around buckled bedding-parallel quartz veins which drape over the hinge at location RB-4 (Fig. 17b), similar to those in Cunard Cove (i.e., Fig. 3.6b).

Quartz ± muscovite pressure shadows around arsenopyrite porphyroblasts at the hinge define a well developed down-dip lineation within the cleavage plane (Fig. 3.22), indicating considerable extension parallel to cleavage and perpendicular to the fold hinge. This strain postdates the formation of arsenopyrite. Although local buckling of bedding-parallel veins occurs within the immediate hinge zone, there is no buckling of thin metasandstone layers, even where they occur within thick slate layers (eg. Fig 3.20, 3.21).

3.4.2.3 *Geology of the Limbs:*

Layering on the fold limbs within Zone A is planar, with no minor folding of thin metasandstone beds or bedding-parallel quartz veins noted (Figs. 3.21; 3.23). Stratigraphy (lower unit) is conformable and no stratigraphic or structural discontinuities occur on the limbs within Zone A (Figs. 3.21; 3.23). Cleavage is similar to that in the Cunard Cove area, with a fine continuous cleavage in the slate intervals (Fig. 3.24). In the metasandstone layers,

Figure 3.23: Photograph of the south limb of the Ovens Anticline, Zone A, Rose Bay. View looking northeast. Note stratigraphy of the lower unit, consisting of slate and metasandstone, and planar character of layering.

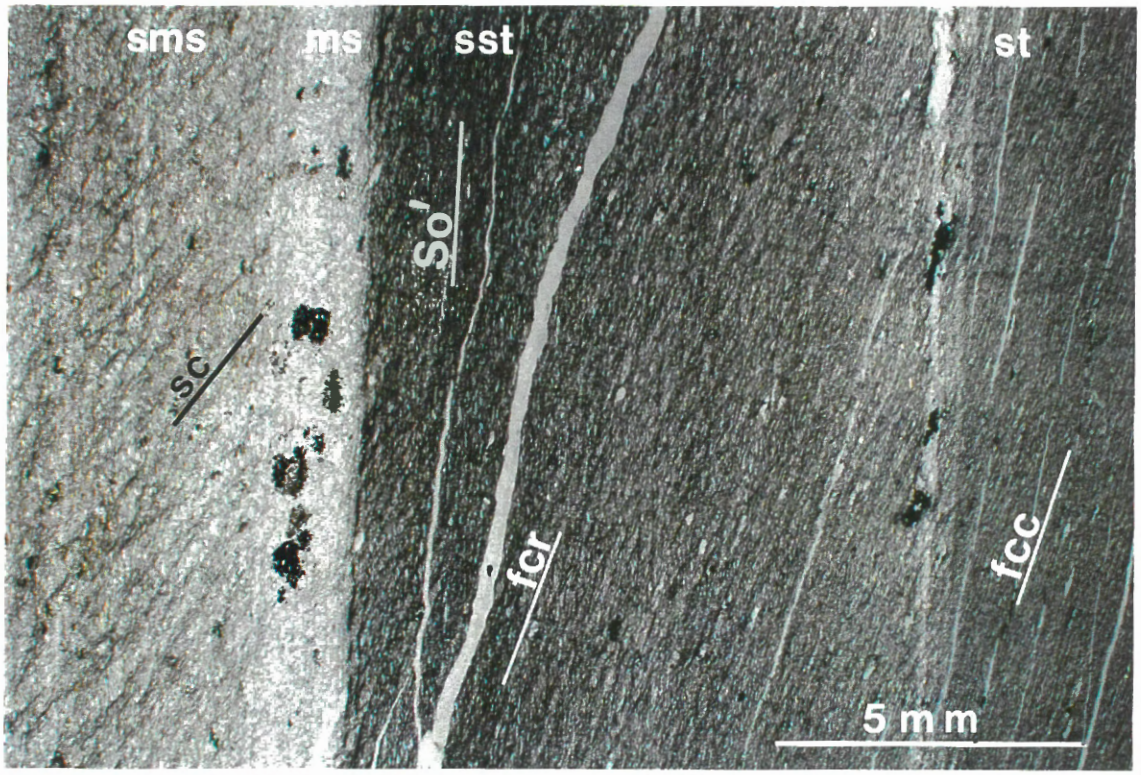

Figure 3.24: Photomicrograph of metasandstone and slate from the south limb of the Ovens Anticline, Zone A, Rose Bay (location RB-3, Fig. 3.17). Cleavage is a spaced cleavage (sc) in the silty metasandstone (sms), a fine crenulation (of So') cleavage (fcr) in silty slate (sst) and a fine continuous cleavage (fcc) in the slate (st). So' is a layer-parallel foliation defined mainly by elongate mica. There is no apparent cleavage developed in the metasandstone (ms) interval. Profile view with section cut perpendicular to cleavage and bedding.

cleavage is poorly developed and spaced or entirely lacking (Fig. 3.25). Figure 3.24 illustrates lithologic influence on the type of cleavage developed and the bedding-cleavage angle. A layer-parallel foliation occurs within the silty sandstone and silty slate units, with S_1 defining a crenulation cleavage in the silty slate (Fig. 3.24). A well developed continuous cleavage in the slate intervals is axial planar to the fold, with a similar, small, bedding-cleavage angle on both limbs (Fig. 3.18, in pocket).

Quartz-muscovite pressure shadows are well developed on coarse arsenopyrite crystals (Fig. 3.25). Fibre growth in pressure shadows is face-controlled and suture lines between differently oriented fibre groups, which record the progressive displacement history (Ramsay and Huber, 1983), are generally difficult to distinguish; in many instances fibres do not occur on adjacent faces. Where suture lines occur, they parallel a spaced cleavage (in the metasandstone host) in both profile sections and strike parallel sections cut perpendicular to bedding (Fig. 3.25a, b), consistent with down-dip extension within the cleavage plane (Fig. 3.25c). This interpretation is supported by quartz-filled extensional fractures within the arsenopyrite (Figs. 3.25a, b). The suture lines are not well defined and it is unclear if the strain is coaxial or non-coaxial.

3.3.2.4 Flexural slip:

Bedding-parallel flexural-slip movement horizons, defined by offset of discordant veins, are abundant on the south limb of Zone A (Fig. 3.18, in pocket). The majority of movement horizons consist of thin slip surfaces, with only a few flexural-slip duplexes observed. Quartz veins ("flexural-slip bedding-parallel veins", see below) occur along most of the movement horizons in this section. As in the Cunard Cove Section, movement horizons

are concordant to bedding, confined to slate intervals and laterally continuous. Several well developed movement horizons are traceable along the same stratigraphic horizon on the north limb along the strike-parallel exposure between location RB-4 and RB-6, a distance of approximately 200 metres (Fig. 17a). Movement direction data on movement horizon surfaces in this section are rare, mainly due to poor exposure of movement planes. Limited data (Fig. 3.12b) indicate movement roughly perpendicular to the hinge. Flexural-slip movement horizons and flexural-slip bedding-parallel veins in a section of the south limb in area RB-3 (Fig. 17a) have an average spacing of 0.46 metres (Fig. 3.18 in pocket). This spacing is comparable to the spacing of movement horizons and flexural-slip veins for the Cunard Cove Section (0.52 m, Fig. 3.5).

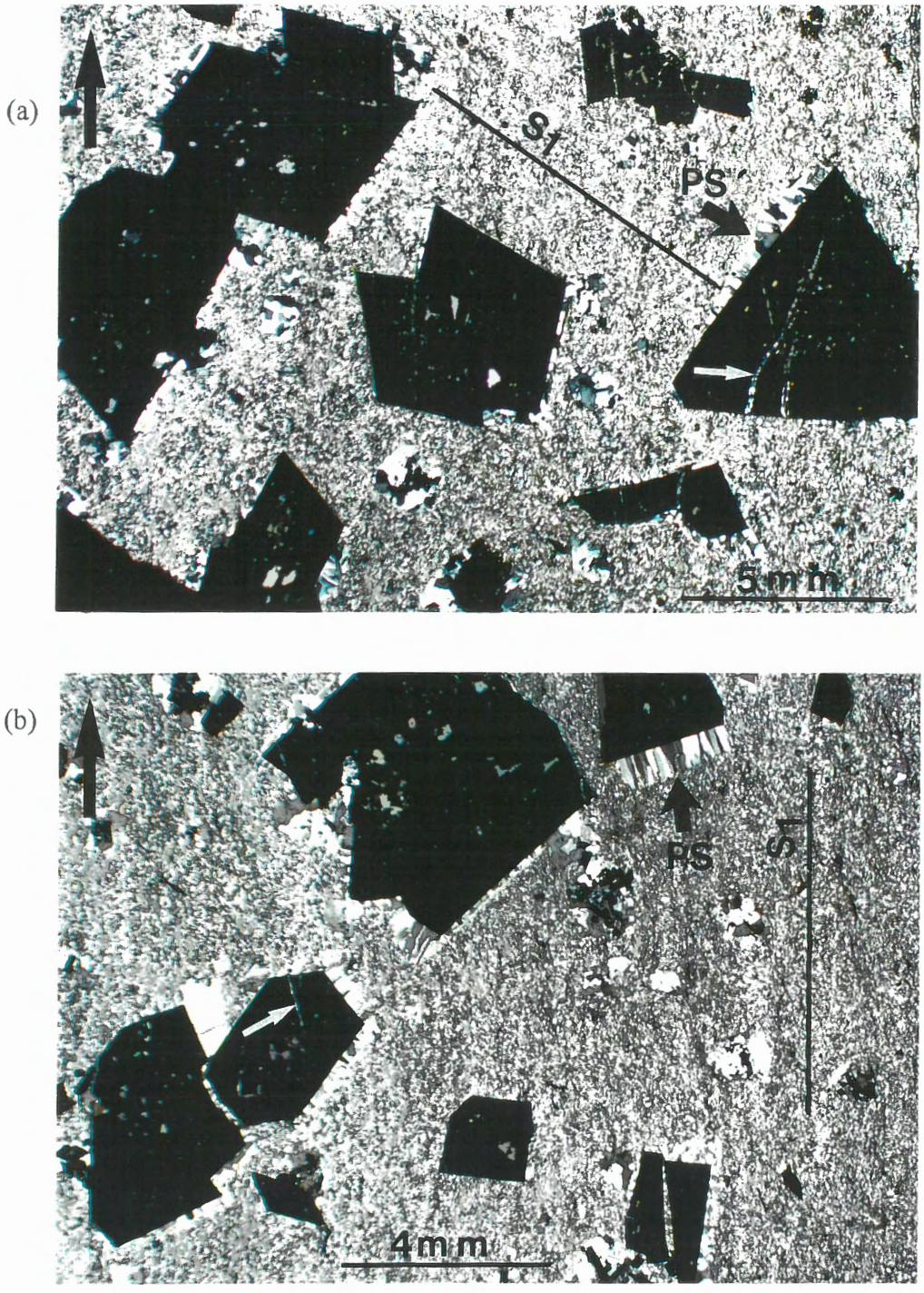

Figure 3.25: Photomicrographs showing face controlled quartz-muscovite pressure shadows (PS) on arsenopyrite (opaque) and extensional fractures in arsenopyrite (white arrows) from the north limb of the Ovens Anticline in Rose Bay; (a) represents a profile section and (b) is cut parallel to strike and perpendicular to bedding (see (c) for location). Vertical arrows in top left of photos match arrows in (c). S_1 = cleavage.

(c)

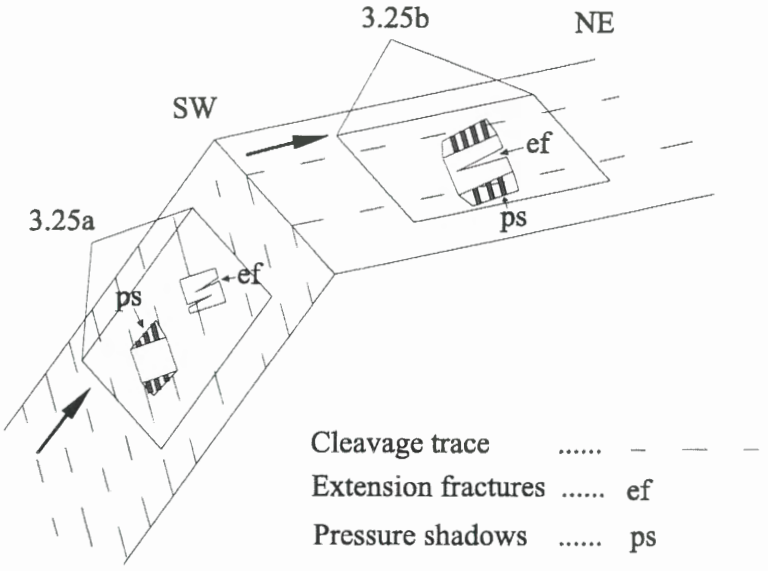

(d)

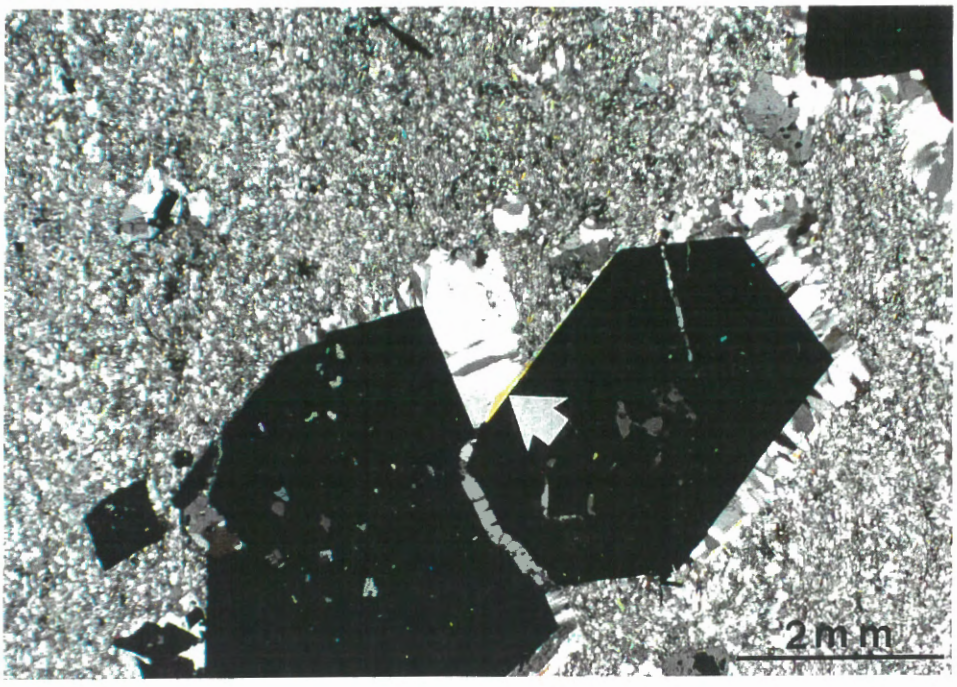

Fig. 3.25 continued: (c) Sketch showing the relationship of (a) and (b) to the fold and schematic representation of general relationship of pressure shadows and extensional fractures to the fold. (d) Close up of a portion of (a) showing coarse muscovite (arrow) within pressure shadow.

3.4.3 ZONE B

3.4.3.1 General Statement:

Zone B occurs south of Zone A on the south limb and is characterized by several outcrop-scale, strike-parallel thrusts, with nine thrusts identified in the exposed section (Figs. 3.18, in pocket at back; 3.26). The thrusts are defined by discordant movement horizons and/or a marked contrast in internal structure between thrust sheets, which is most apparent in the variation in bedding-cleavage angle (Fig. 3.18, in pocket at back). Whereas cleavage is axial planar to the Ovens Anticline in Zone A, cleavage dips in Zone B shows no relationship to the main fold and the bedding-cleavage angle varies between thrust sheets.

3.3.3.2 Thrusts

Thrust planes are marked by single movement surfaces and duplex zones, similar to those along major flexural-slip movement horizons in Cunard Cove. All thrust surfaces exhibit striations and (or) slickenfibres which trend down dip (Fig. 3.12c), and quartz veins are common. Some thrusts have ramp and flat geometry (e.g., Thrust 6) whereas others are bedding-parallel flats. The thrust sheets are characterized by fault-related folding (see below) and back thrusts. These structures are consistent with the ramp and flat geometry exhibited by the overall thrust system.

3.4.3.2.1 Movement direction and shear sense:

Movement direction indicators (striations, slickenfibres) trend perpendicular to the

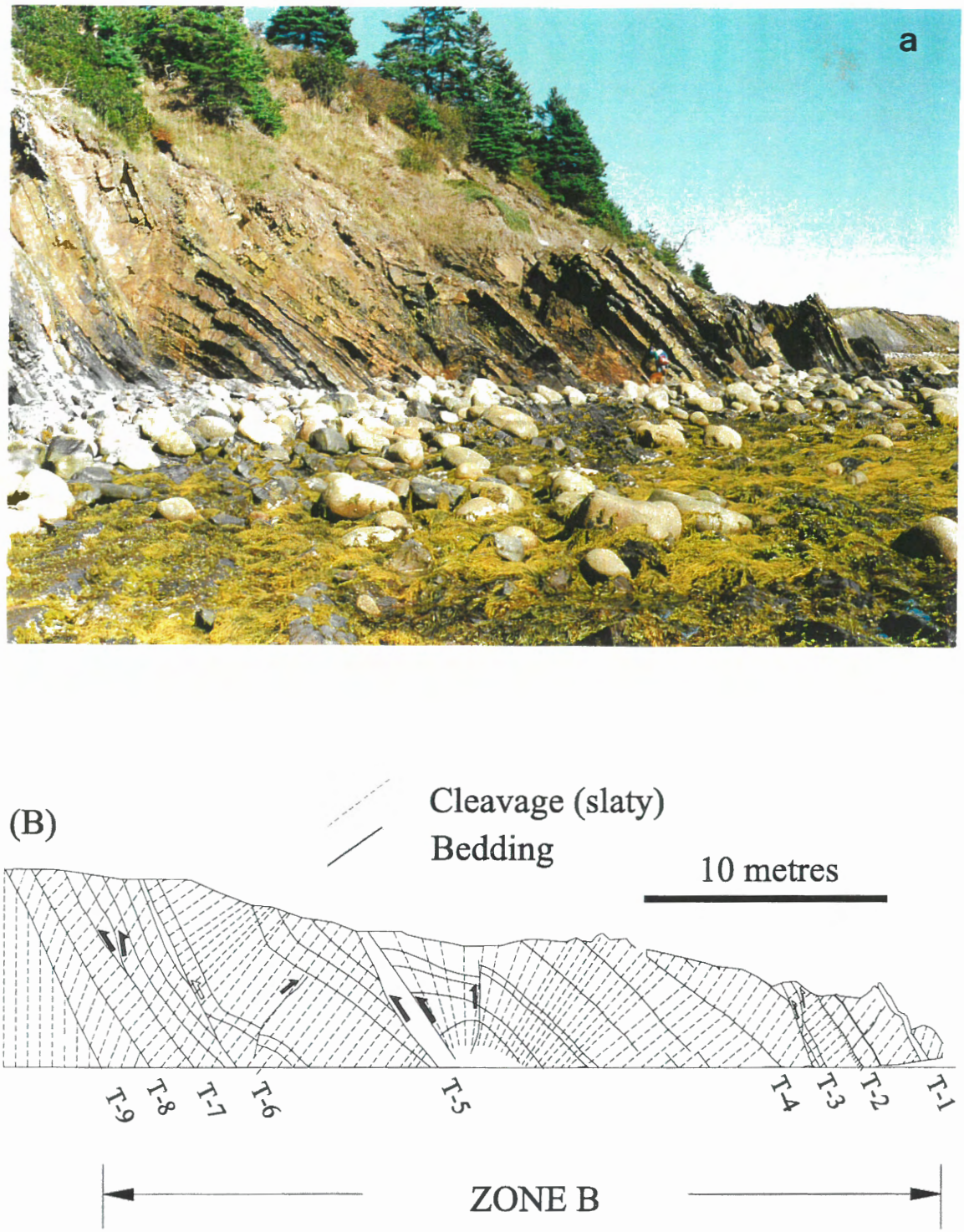

Figure 3.26: Photograph (a) and sketch (b) of Zone B, Rose Bay, showing the character and structure of the thrusts. Thrusts numbered T1 .. T9. Note in particular the variation in cleavage between thrust sheets. A more detailed version of (b) is presented in Fig 3.18 (in pocket at back) and the detail of individual thrusts are presented in Figures 3.27, 3.28, 3.29.

fold hinge (Fig. 3.12c). Shear sense is indicated by offset of stratigraphy and buckled bedding-parallel veins (eg. T-3, Fig. 3.27), offset of discordant veins, slickenfibre geometry and thrust geometry (Figs. 3.18, 3.27-29). These structures all indicate reverse movement, consistent with thrusting occurring during flexural-slip folding. A lack of distinct stratigraphic markers does not generally allow for the amount of displacement along thrusts to be evaluated. Displacement of a distinctive buckled bedding-parallel vein-slate interval across T-3 (Fig 3.27) indicates approximately 1.2 metres of reverse displacement. Approximately 2 metres of displacement is indicated along T- 7 by offset of layering and bedding-parallel thrust surfaces (Fig. 3.29).

3.4.3.2.2 Internal structure of thrust sheets:

As stated above, the internal structure of the thrust sheets differs from the hinge area (i.e., Cunard Cove and Zone A) of the Ovens Anticline and variation exists between thrust sheets. The internal structure of the thrust sheets is described below and will be used to interpret the history and relationship of folding and thrusting in the area.

Cleavage and minor folds: The cross-section of Zone B (Figs. 3.18, in pocket at back; 3.26) illustrates variation in the internal structure of the various thrust sheets, particularly in bedding-cleavage angle. The internal structure of each thrust sheet, however, is consistent, and structural elements within thrust sheets are related. Cleavage within the thrust sheets is typically at a high angle to bedding and the bedding-cleavage angle remains constant throughout each sheet. Small-scale buckling of thin metasandstone beds, and mullion

structures formed in the moderately thick beds, are common within the thrust sheets (Figs. 3.29, 3.30). Thin (typically 1-2 mm) buckled bedding-parallel quartz veins are folded sympathetically with thin metasandstone beds (Figs 3.18 in pocket at back, 3.27-3.29; see also Fig. 3.34). Slaty cleavage is axial planar to small-scale buckled folds and mullions within the thrust sheets, and the asymmetry of buckle folds is sympathetic to bedding-cleavage angles, therefore relating cleavage development and buckling. The cleavage pattern around buckled metasandstone beds (Fig. 3.30) and bedding-parallel quartz veins defines a similar, divergent pattern as developed around thick metasandstone beds and folded bedding-parallel veins in the hinge zone of the Ovens Anticline (see above) As discussed above, this reflects inverse tangential longitudinal strain in the slate layers and suggests there was only minor or no homogeneous shortening (cleavage formation) prior to development of these minor folds.

Fault-related folds: Several fault-related folds occur within the thrust sheets. Because only a limited part of the thrust structures are exposed the nature and interpretation of fold formation is uncertain. However, a major fold in the hanging wall of thrust 5 resembles a fault propagation fold (Fig. 3.28) and a fold in the hanging wall of thrust 6 resembles a ramp anticline (Fig. 3.29). That these folds are fault-related is supported by the fact that bedding-cleavage angles and the symmetry of minor folds remains constant within the thrust sheets and are folded by these folds (e.g. Figs. 3.28, 3.29).

Bedding-parallel veins: Thin, buckled bedding-parallel quartz veins are common within the thrust sheets (Figs. 3.18 in pocket in back, 3.27, 3,28, 3.29; see also Fig. 3.34). This is in

sharp contrast to Zone A and the Cunard Cove area where buckled veins are absent from the limbs and only locally occur within the hinge. "Flexural-slip" veins (see veins below) occur along the thrusts, but are rare within the thrust sheets.

Flexural slip: Evidence of flexural slip is scarce within thrust sheets, with only a few minor bedding-parallel movement horizons noted (Fig. 3.18, in pocket at back). Note that the discordant vein set which is offset by flexural slip in the hinge zone cut the thrust sheets so that any flexural slip present would have been easily recognized.

Discordant Veins: The discordant vein set identified within Zone A and the Cunard Cove Section are abundant within the thrust sheets and are offset by the thrusts, indicating that thrusting postdates emplacement of these veins, consistent with thrusting during flexural-slip folding.

Discussion of internal structure: The internal structure of the thrust sheets is markedly different from the hinge area of the Ovens Anticline, represented by structural Zone A of Rose Bay and the north limb in the Cunard Cove area. Bedding-cleavage angles and symmetry of related minor folding show no relationship to the Ovens Anticline and are consistent with shortening when bedding was subhorizontal. Consistent bedding-cleavage angles throughout fault-related folds indicate that cleavage is not related to these folds and imply that cleavage-related shortening predates thrusting. Any apparent cleavage fans about these folds (i.e., Fig. 3.28) reflect thrust-related folding. In contrast to the hinge area, evidence of flexural slip

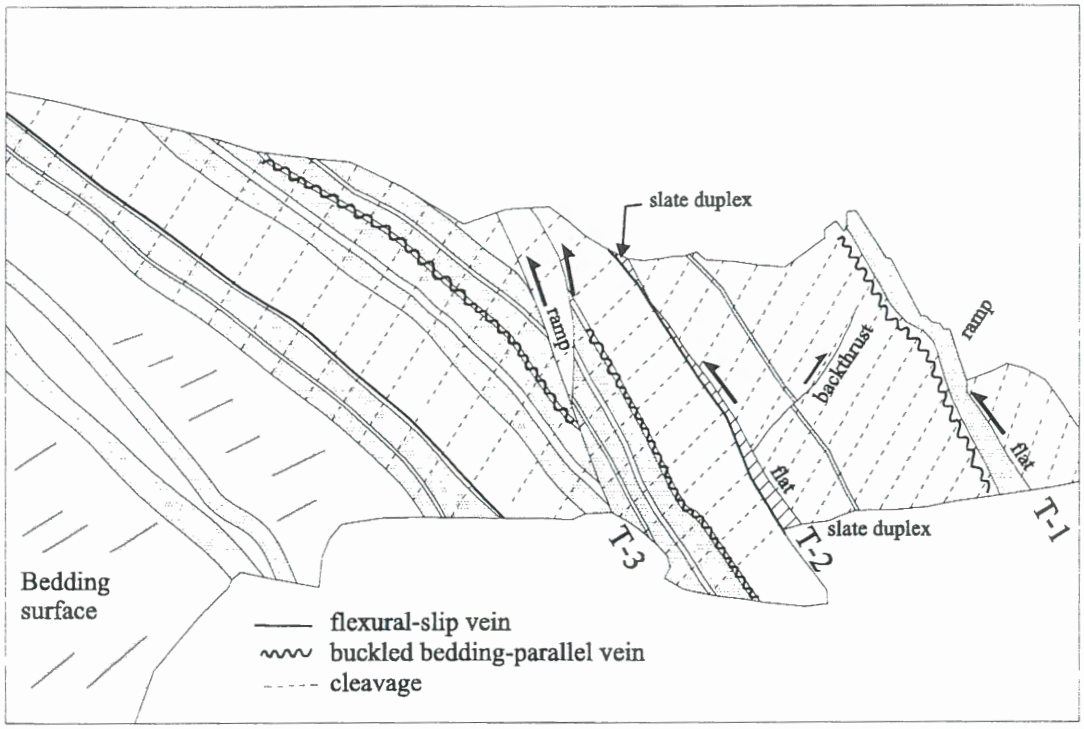

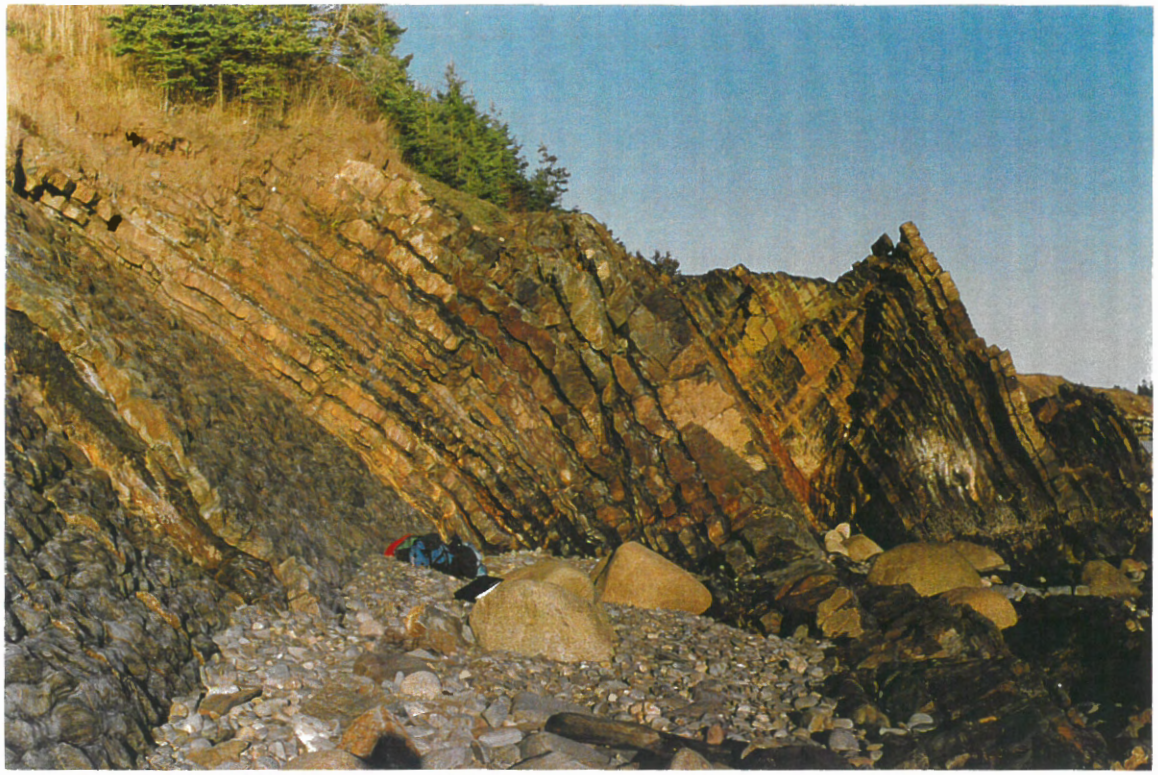

Figure 3.27: Line drawing and photograph of thrusts 1-3 of Zone B, Rose Bay, showing the structural detail of thrusts and thrust sheets. See Fig 3.26 for location. Knapsack and binder for scale.

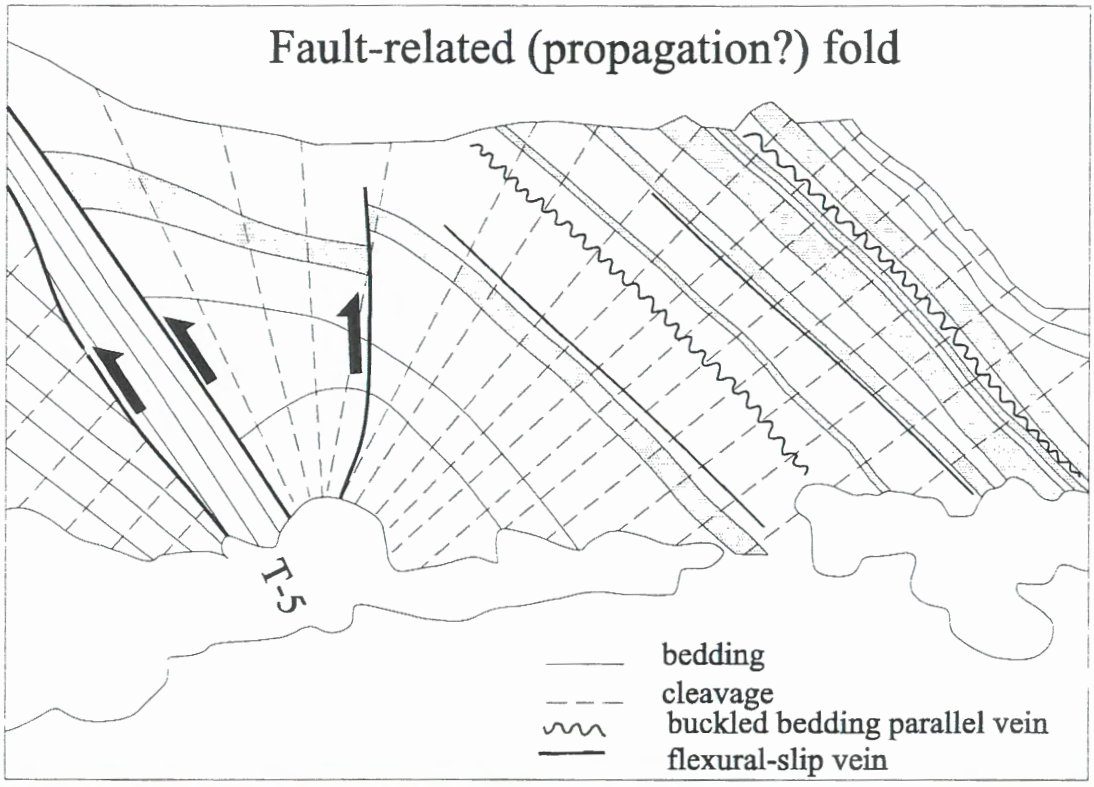

Figure 3.28: Line drawing and photograph of Thrust 5, Zone B, Rose Bay, showing structural detail of thrust and internal detail of hanging wall thrust sheet. See Fig 3.26 for location. Human and canine for scale.

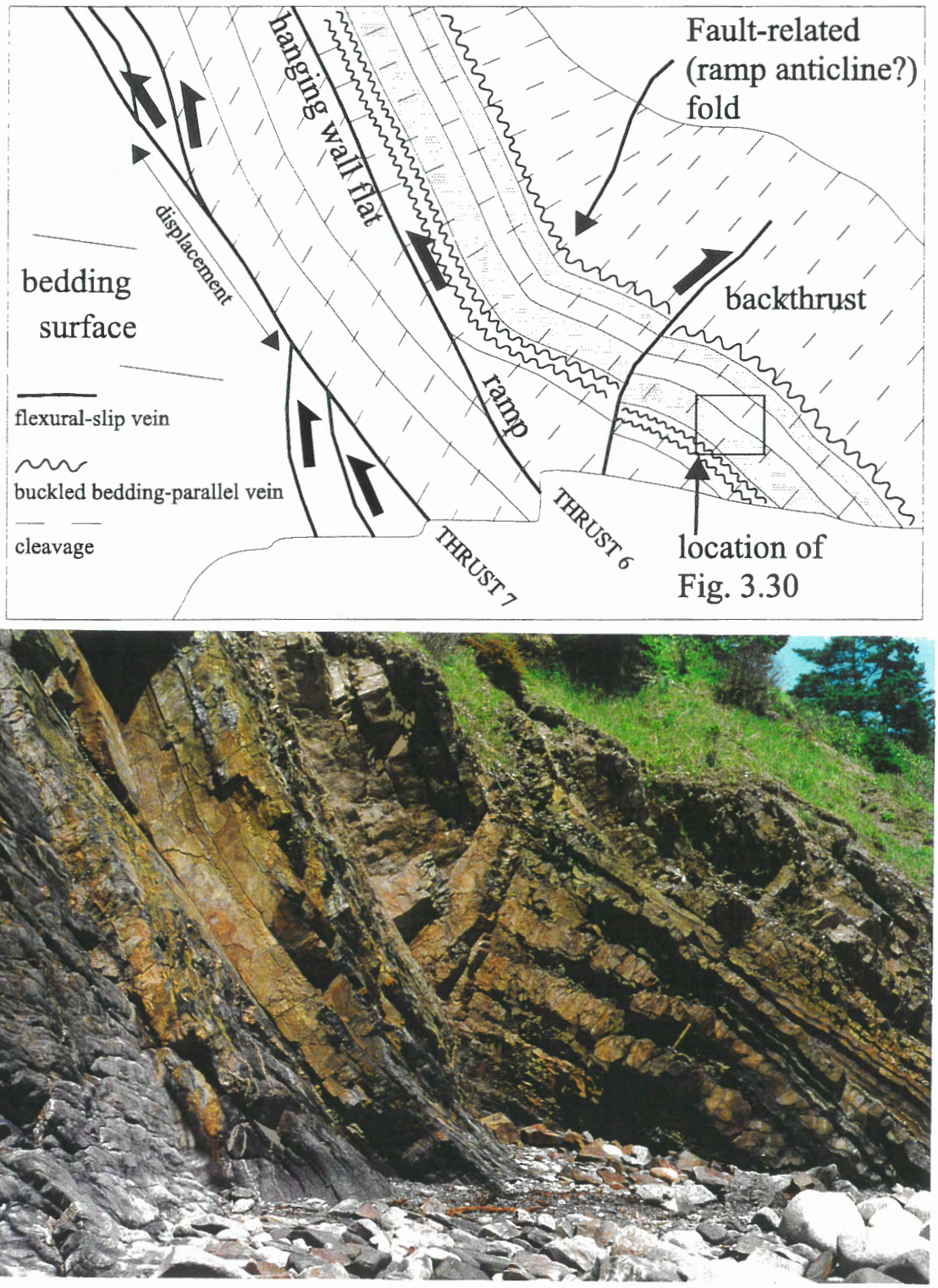

Figure 3.29: Line drawing and photograph of thrusts 6 and 7, Zone B, Rose Bay, showing structural detail of thrusts and internal structure of thrust sheets. See Fig. 3.27 for location. Hammer below backthrust for scale. Note mullion structures in metasandstone beds.

Figure 3.30: Photographs of metasandstone - slate intervals from thrust sheet above Thrust 6 (Fig. 3.29) showing (a) close-up of mullion structures (M) in metasandstone and (b) a divergent cleavage pattern (dashed lines) around mullions in slate.

within the thrust sheets, such as flexural-slip bedding-parallel veins, is uncommon. Buckled bedding-parallel veins, which are absent on the limbs in the hinge area, are common within the thrust sheets. These features indicate that the thrust sheets of Zone B represent segments of the fold deformed at low limb dips which were emplaced onto the steep south limb of the Ovens Anticline with no significant internal strain related to development of the main fold structure. Further discussion of the implications of these thrusts is given below.

3.4.4 $^{40}Ar/^{39}Ar$ DATING

Recent $^{40}Ar/^{39}Ar$ dating of slate samples has been conducted in the Ovens section. Whole rock ages of ca 399 Ma for a sample from the fault-related fold in the hanging wall of thrust 5, Zone B (see Fig 3.18, in pocket at back) and ca 395Ma for a sample adjacent a flexural-slip vein in Section C-D, Cunard Cove (see Fig 3.5) (Kontak et al., 1998) have been obtained. A muscovite (hand picked) age of ca 376 Ma was obtained from Zone A of Rose Bay, (Hicks, 1996; location of sample indicated in Fig. 3.18 in pocket at back) who interpreted the muscovite to represent cleavage parallel, metamorphic muscovite and suggested that the young age reflected late deformation related to flexural-slip folding. However, reexamination of the dated sample indicates the presence of coarse muscovite within pressure shadows around arsenopyrite, noted above (e.g., Fig. 3.25d); Hicks et al. (in press) consider this to represent the dated muscovite. The older ages are similar to the age constraints on regional metamorphism (see chapter 1) whereas the younger date constrains a much younger age for the strain recorded by pressure shadows around arsenopyrite. The implications of these ages are addressed further below.

3.5 VEINS

3.4.1 General Statement:

As mentioned in Chapter 1, quartz veins, particularly bedding-parallel veins, are common in chevron folds where flexural slip occurred, and fluid pressure related to veining may be important in the flexural-slip process. Also, the structure, character and relationship between vein sets provide useful information on the deformational history.

There is a high concentration of quartz veins within the hinge zone of the Ovens Anticline. The zone of "anomalous concentration" of veins is restricted to within approximately 50 metres either side of the hinge and is exposed over a strike length of approximately 1500 metres, thus defining a narrow, linear zone coinciding with the fold hinge (Fig. 3.2). The veined zone presumably extends into Rose and Lunenburg Bays, and therefore 1500 metres is a minimum strike length. The following is a discussion of vein sets at the Ovens which is aimed at evaluating the relationship of veining to folding.

3.5.2 Previous work:

Buckled bedding-parallel veins have been referred to and illustrated in discussions of gold mineralization at the Ovens (Douglas, 1948; Graves, 1976; Graves and Zentilli, 1982; Henderson et at. 1992). Graves and Zentilli (1982) discussed buckled bedding-parallel veins draping over the hinge of the Ovens Anticline at Cunard Cove, which they considered as pre-folding in origin, with vein folds being parasitic to the main fold. A similar interpretation was proposed for these veins by Henderson et al. (1992), with buckling of veins accounting for approximately 60% shortening. Henderson et al. (1992) also referred to younger veins, with one vein occurring in "a dilational jog where a high angle reverse fault (hinge thrust?) steps

across the crest of the anticline". O'Brien (1988) described a complex, synfolding vein array from the Mahone Bay area, based largely on observations from the Ovens and Cross Island areas.

There have been numerous other studies on the emplacement of auriferous quartz veins in gold deposits of the Meguma Group and these will addressed below as they relate to the interpretation of veining at the Ovens presented here.

3.5.3 Vein Sets, this study:

Four systematic vein sets have been identified in the Ovens study area on the basis of their relationship to the fold and fold-related structures (Fig. 3.31). Each vein set provides significant information regarding fold development. As will be demonstrated, much of the veining can be related to the flexural-slip process.

3.5.3.1 *Buckled bedding-parallel veins:*

Buckled bedding-parallel veins are thin (typically in the range of 2 mm to 2 cm thick) and are tightly buckled into close to ptygmatic folds (Figs. 3.6b, 3.32). These veins are commonly laminated, characterized by vein-parallel inclusions of wall rock material (Fig. 3.6b). Buckled bedding-parallel veins were observed in two environments; (1) draped over the fold hinge and; (2) within the thrust sheets of Zone B of the Rose Bay section (Fig. 3.31). No buckled bedding-parallel veins were observed on the steep fold limbs in Cunard Cove or Zone A of the Rose Bay area.

Buckled veins within the hinge area of the Ovens Anticline were observed in the

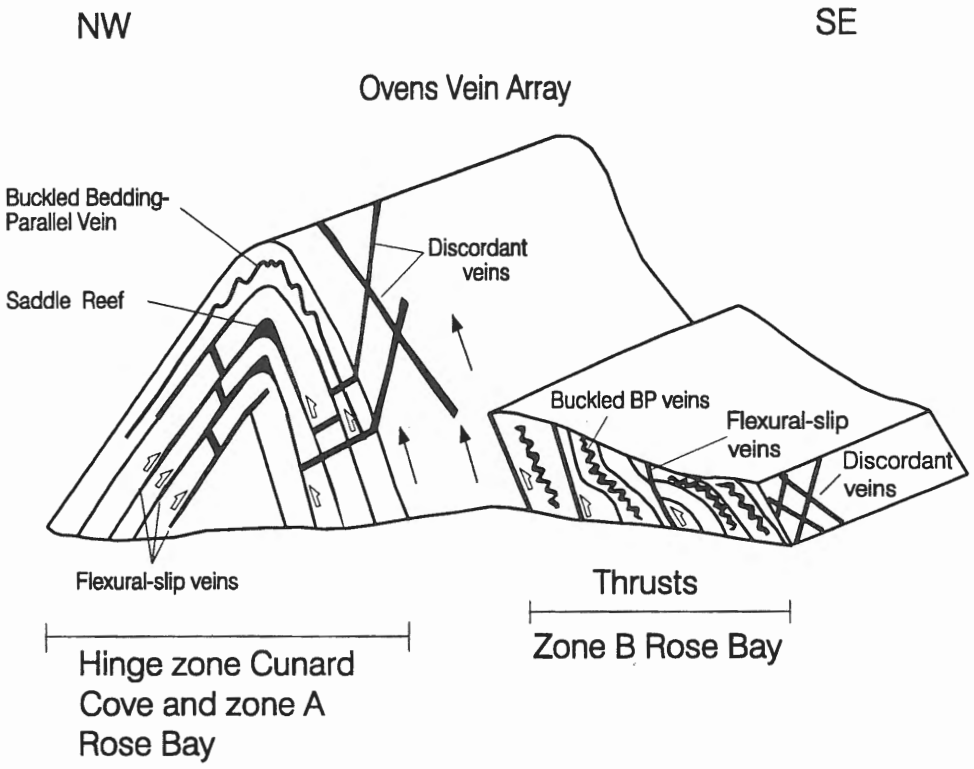

Figure 3.31: Schematic diagram of the Ovens Anticline in the study area showing the principal vein sets identified in this study.

Cunard Cove Section (Figs. 3.6c, 3.32) and Zone A of the Rose Bay section (Fig. 3.33). In both areas these buckled veins occur together with saddle-reef veins and non-buckled "flexural-slip veins" which also drape over the hinge (e.g., Figs. 3.6c, 3.33). Buckled bedding-parallel veins are tightly buckled in the hinge zone, however, where traceable down the limbs the degree of buckling decreases and they become planar on the straight limbs (Fig. 3.6c, 3.33). Slaty cleavage is axial planar to the vein folds, regardless of bedding-cleavage angle, and fold symmetry of veins is parasitic to the main fold (Fig. 3.33). In thin section the veins display significant intra crystalline strain, characterized by subgrains and undulose extinction (Fig. 3.6b).

Buckled bedding-parallel veins within the thrust sheets of Zone B in Rose Bay consist of thin (mm-scale), continuous veins within slate intervals and typically extend the length (in profile sections) of the exposed layers (Figs. 3.18 in pocket at back, 3.34). Folds occur at various scales, including the minor folds defined by buckled metasandstone layers and smaller-scale folds which are parasitic to the minor folds (Fig. 3.34). Slaty cleavage is axial planar to buckled veins, although the bedding-cleavage angle varies between thrust sheets.

As discussed above, the strain pattern around folded veins (i.e., Fig 3.6b), both in the hinge of the Ovens Anticline and in the thrust sheets, defines the same divergent pattern as occurs around the main fold. This strain pattern is also defined by variation in element distribution around buckled bedding-parallel veins in the Meguma Group (Erslev and Ward, 1994) including enrichment of SiO_2 in the inner arc of host slate (adjacent to the outer arc of the vein) and depletion in the highly cleaved outer arc of the slate. Sympathetic enrichment and depletion of other elements is consistent with intense dissolution during cleavage

Figure 3.32: (a) Photograph of buckled bedding-parallel vein (arrow) in the hinge of the Ovens Anticline, Cunard Cove. Profile view looking southwest. Metre stick for scale.

Figure 3.33: Photograph of the fold hinge at location RB-5 (Fig. 3.17) showing the trace of several bedding-parallel veins draped over the hinge in plan section. View looking northeast, roughly down plunge. Some veins are tightly folded in the hinge region whereas others are not. All veins are planar and have features typical of flexural-slip veins on the limbs.

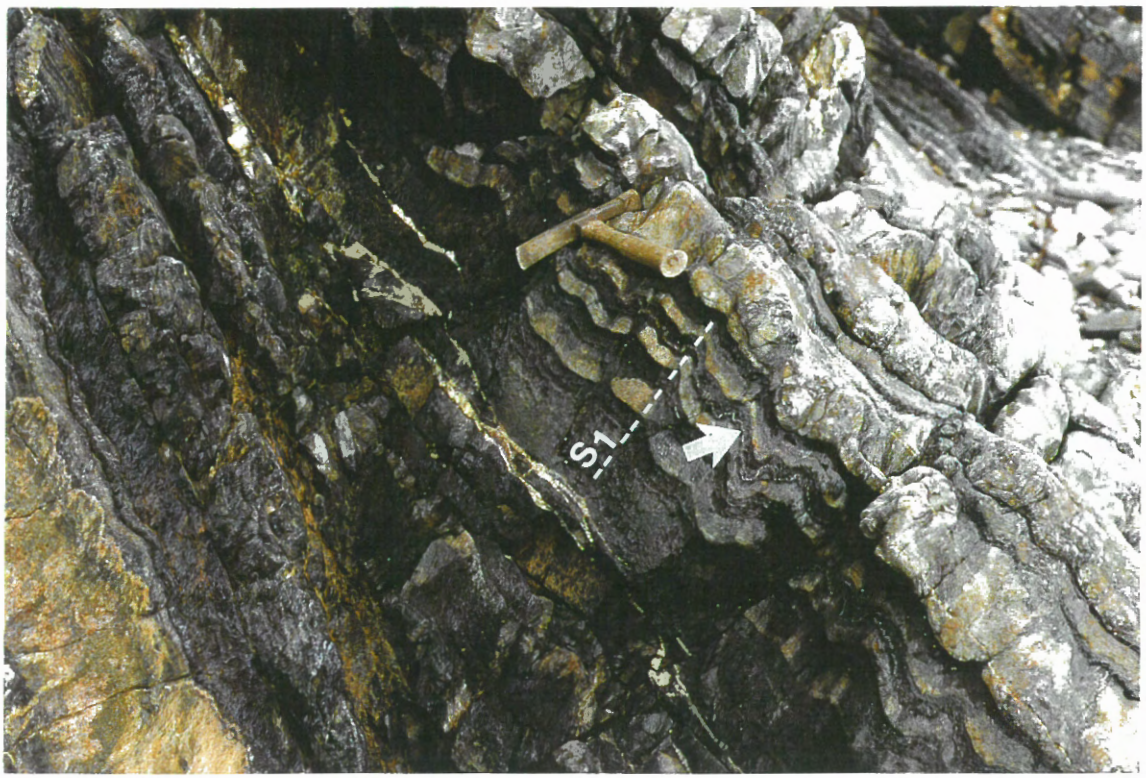

Figure 3.34: Photograph of Thrust 8, Zone B of Rose Bay, showing tightly buckled, thin bedding-parallel vein (indicated by arrow) in hanging wall thrust sheet. Vein is folded at several scales and folding of quartz vein is sympathetic to buckled metasandstone layers. Cleavage (S_1) is axial planar to folds. Hammer for scale.

development in the outer arc and deposition of material (SiO_2) in the inner arc, where strain is low. The low strain in the inner arc is related to inverse tangential longitudinal strain adjacent to the folded vein. As stated above, this strain pattern indicates there was only minor to no homogeneous layer-parallel shortening (cleavage formation) prior to folding of the veins.

Buckled bedding-parallel veins are locally truncated by a set of discordant veins (see below) and these veins have been offset along the thrusts in Zone B of Rose Bay. Gold was noted within a buckled bedding-parallel vein exposed in Cunard Cove.

3.5.3.2 *Flexural-slip Bedding-Parallel Veins and Saddle Reef Veins*

As suggested by their name, flexural-slip bedding-parallel veins (flexural-slip veins) occur along flexural-slip movement horizons (Fig. 3.35), including flexural-slip duplexes, along which they are interpreted to have been emplaced. Flexural-slip veins are planar and characterized by a laminated texture, interpreted as wall rock inclusion bands by Baker (1996). Flexural-slip veins are typically continuous along movement horizons, although they commonly display a pinch and swell geometry, which is evident along strike (Fig. 3.35) and down dip (Fig. 3.36). It is not uncommon for flexural-slip veins to pinch out completely along a movement horizon for several metres. However, a vein generally can be found laterally along the same movement horizon. Locally, flexural-slip bedding-parallel veins have vuggy segments or contain brecciated and rotated slate fragments (Fig. 3.36), indicating post-cleavage vein emplacement. Some veins are clearly composite, including laminated-textured and massive quartz segments. Sulphide, particularly arsenopyrite, and coarse scheelite locally

occur as accessory phases in flexural-slip veins. Locally, flexural-slip veins define the down-dip extension of saddle reef veins. At the western most end of Rose Bay (location RB-6; Fig. 3.17) a classic saddle reef vein is exposed (Fig. 3.20), with a flexural-slip vein traceable down the north limb from the saddle reef. The down-limb extension consists of a typical, laminated, flexural-slip vein occurring along a flexural-slip movement horizon defined by offset discordant veins. Flexural-slip veins are commonly striated along their margins (Fig. 3.37) and the striations are consistent with the orientation of flexural-slip lineations in the area.

The relationship between flexural slip veins and discordant veins (discussed below), the offset of which defines flexural-slip movement horizons, is complex. For example, in Figure 3.35 flexural-slip veins occurring along movement horizons clearly truncate the discordant veins which have been displaced, supporting the interpretation that flexural-slip veins were emplaced along flexural-slip structures. These same flexural-slip veins, however, are truncated by a later discordant vein (Fig. 3.35). Locally, discordant veins show apparent offset across movement horizons. However, the discordant vein maintains continuity along the movement horizon and postdates (truncates) the flexural-slip vein (vein d, Fig. 3.38a and veins d1 and d2, Fig. 3.38b), whereas other discordant veins are clearly offset and truncated by the same flexural-slip vein (veins a,b,c Fig. 3.38a and veins a and b Fig. 3.38b). Other veins truncate the flexural-slip veins and show no displacement (vein c, Fig. 3.38b). These relationships imply a complex and synchronous history of vein emplacement and flexural slip. The continuity of discordant veins along flexural-slip movement horizons (veins d, d1,d2, Fig 3.38a, b) is confusing and could suggest that the offset of discordant veins is more apparent than real, with veins occupying different fractures on either side of the movement horizon.

However, as generally is the case, the offset veins define distinct sets, offset of which is most reasonably explained by displacement along flexural-slip movement horizons. The local continuity of discordant veins along movement horizons is interpreted to indicate either post flexural-slip veining along offset fractures or emplacement of the discordant vein during flexural slip. Either interpretation is consistent with synchronous emplacement of discordant veins and flexural slip.

The existence of flexural-slip veins along movement horizons is no assurance of a flexural-slip origin and these veins could be the loci of later movement during flexural slip (e.g., Yang and Gray, 1994). However, the mutual cross-cutting relationship with late discordant veins, the local continuity with saddle-reef veins (which by definition result from late flexural slip; Ramsay, 1974), the association with slickenfibres, and inclusions of rotated cleaved slate fragments within the veins, support late emplacement of these veins. Therefore, their coincidence with flexural-slip structures provides strong support for a flexural-slip origin. In addition to flexural-slip veins which occur along defined movement horizons, there are numerous similar veins where evidence of displacement (offset) is lacking. However, based on similar characteristics, these veins have been grouped with flexural-slip veins (Fig. 3.5). As discussed above, Tanner (1989) and Fowler and Winsor (1997) have defined movement horizons solely on the occurrence of bedding-parallel veins. Interpreting laminated veins to represent movement horizons is supported here by the presence of veins along many defined movement horizons. The presence of veins along movement horizons may reflect the need for high fluid pressure for initiation and development of flexural slip.

Flexural-slip veins are abundant in the immediate area of the fold hinge. The measured

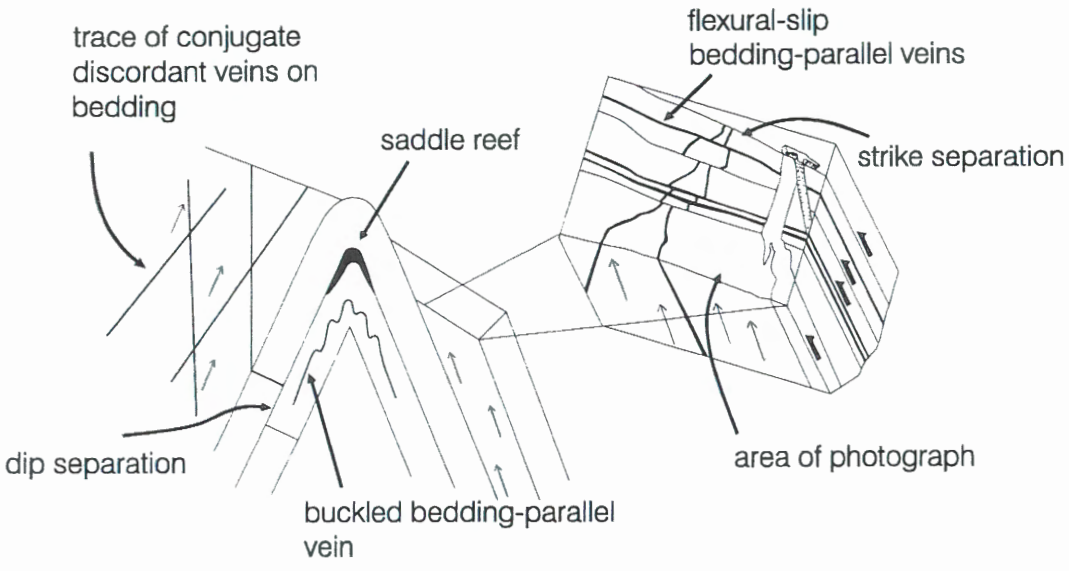

Figure 3.35: Photograph and sketch of flexural-slip bedding-parallel veins along movement horizons defined by offset discordant veins. The flexural-slip veins truncate and thus postdate, the offset veins. However, these same flexural-slip veins are cut by the wide discordant vein at right (under hammer). This indicates synchronous emplacement of bedding-parallel flexural-slip and discordant veins.

Figure 3.36: Photograph of flexural-slip veins exposed in Zone A, Rose Bay (location RB-3, Fig. 3.17). Profile view looking northeast. Note laminated texture of vein on the right, the general pinch and swell character and the inclusions of slate fragments in both veins. Paper clip for scale is 3 cm. long.

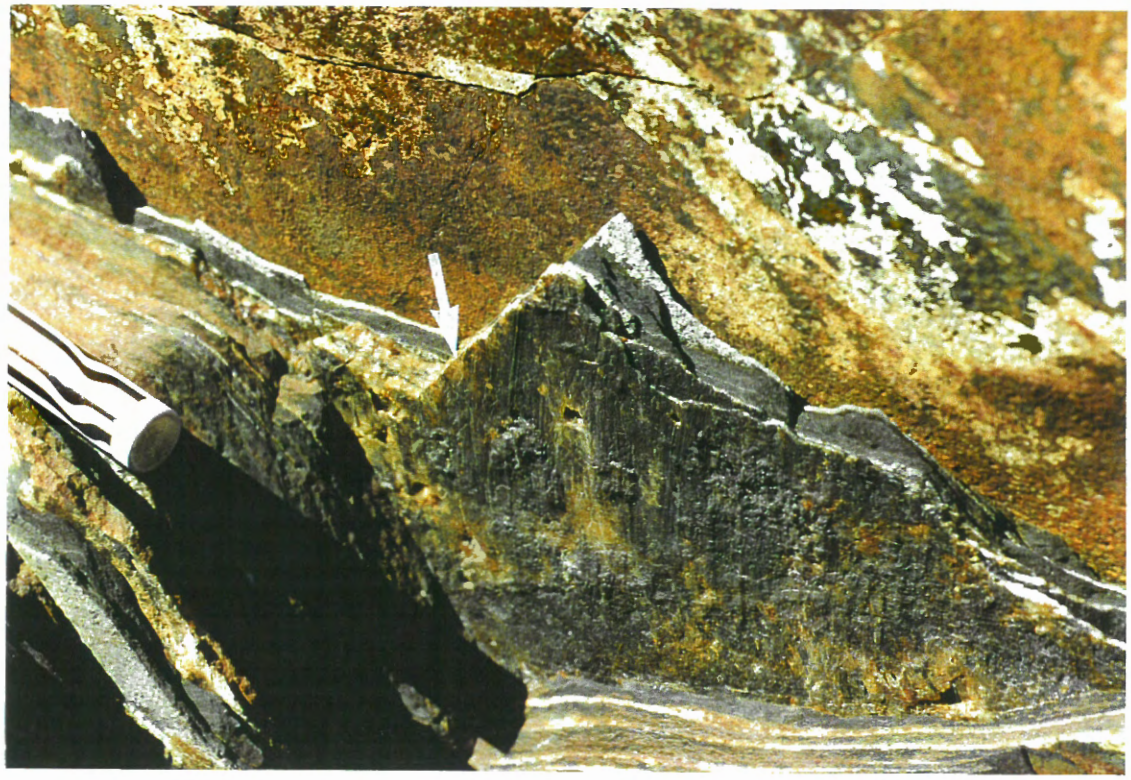

Figure 3.37: Photograph of flexural-slip vein (indicated by arrow) from Cunard Cove (section C-D), showing well-developed striations on the lower margin of vein. Felt marker at left for scale is 1.5 cm. wide.

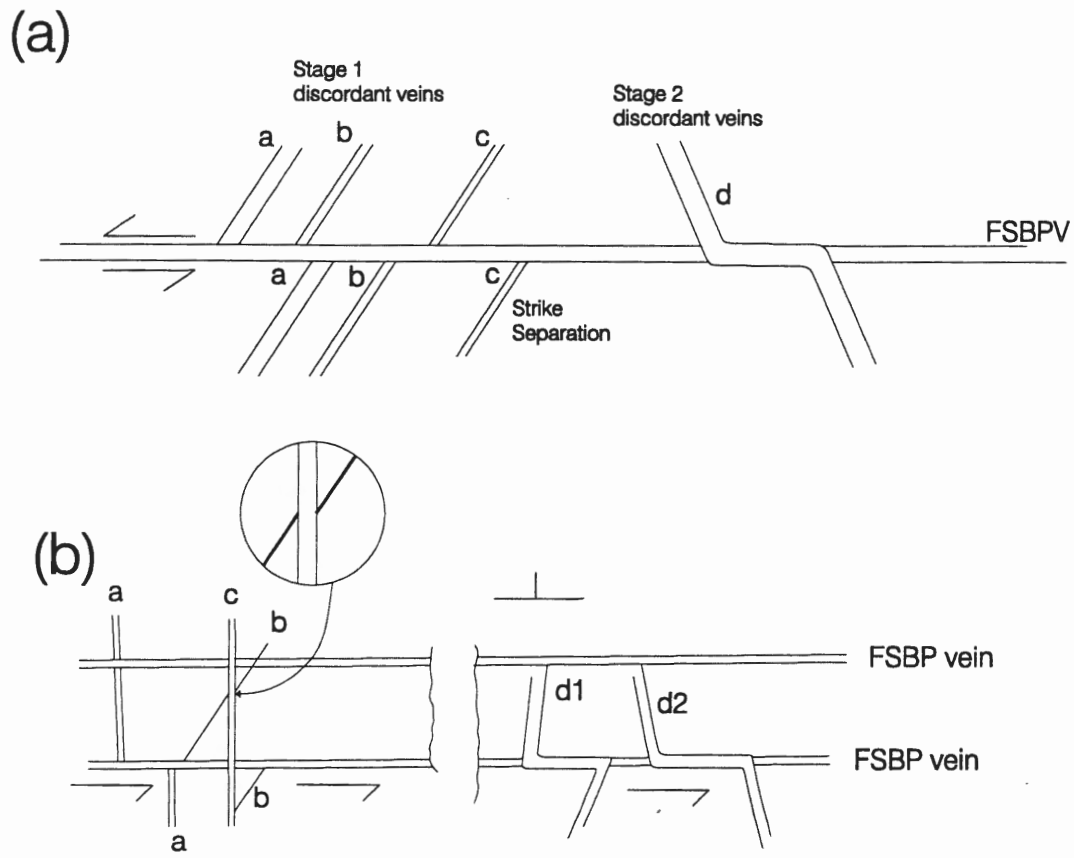

Figure 3.38: Schematic diagram illustrating the relationship between flexural-slip bedding-parallel and discordant quartz veins. Both diagrams represent plan sections (looking down dip) from the south limb of the Ovens Anticline at location RB-1 in Rose Bay (see Fig 3.17).
(a) Three discordant veins to the left (a-c) are offset (sinistral strike separation) along a movement horizon. The flexural-slip vein along the movement horizon cuts the offset veins and is interpreted to postdate offset discordant veins a-c. Discordant vein d shows a similar strike separation as veins a-c, however, is continuous along the movement horizon and truncates the flexural-slip vein. This suggests emplacement of vein d postdates offset of the fractures occupied by vein d.
(b) Discordant veins a and b are offset along a movement horizon and cut by a flexural-slip vein. Discordant vein c cuts the flexural-slip vein and discordant vein b. The latter is illustrated by the offset of vein b resulting from the dilation caused by emplacement of vein c (inset). Discordant veins d1 and d2 are similar to vein d in (a) and truncate the flexural-slip vein. Implied sequence is: emplacement of discordant veins a and b, flexural-slip resulting in offset of veins a and b, emplacement of veins c and d.

log of the north limb of the Ovens Anticline in the Cunard Cove Section illustrates their abundance, indicating an average spacing 0.81 metres (Fig. 3.5). A similar spacing of flexural-slip veins occurs on the south limb in Zone A, Rose Bay (Fig. 3.18, in pocket at back). Flexural-slip veins are rare within the thrust sheets of Zone B in Rose Bay. However, similar veins and slickenfibres occur along the thrust horizons (Figs. 3.18 in pocket at back, 3.27-29).

Local exposure of the fold hinge in Rose Bay indicates that at least some flexural-slip veins are continuous over the fold hinge, where some are buckled in the immediate hinge zone (Fig. 3.33). The flexural-slip veins shown in Fig 3.33 do not display the classic saddle-reef form. However, they are notably thicker in the hinge than along the limbs and they may constitute thin saddle veins. Saddle reef veins also occur in the cliff section above Cunard Cove in the Ovens Park (Fig. 3.6c). The association of flexural-slip veins and saddle reef veins is expected, as the latter implicitly form in response to flexural-slip folding (Ramsay, 1974).

Gold grains were noted in several flexural-slip veins in both the Cunard Cove and Rose Bay areas. Previous mining efforts were focused on bedding-parallel veins on fold limbs (Faribault, 1934; Fig. 3.2). In most cases the old workings are no longer exposed and therefore the vein type is unknown. However, there are several flexural-slip veins exposed in the entrance to Tuckers Tunnel (Fig. 3.4) in the Cunard Cove section, which was reportedly extended as a result of mining activity. In addition, all bedding-parallel veins exposed on the limbs are of the flexural-slip type, suggesting it was these veins which were evaluated for gold.

3.5.3.3 *Discordant, conjugate veins*

Discordant veins consist of two sets of steep, NW-striking veins which form a systematic conjugate set, the nature of which is apparent on bedding surfaces, where their traces define systematic vein sets (Fig. 3.39). The two vein sets have consistent orientations throughout the area (Fig. 3.40), although the small dihedral angle between vein sets makes distinction on stereoplots difficult if individual vein sets are not identified. However, systematic recording of intersecting vein pairs, assigning each vein to a set relative to the other clearly distinguishes systematic vein sets on stereoplots (i.e., paired veins, Fig. 3.40). Veins are distinguished as west-dipping and steeply-dipping (Figs. 3.39, 3.40). West-dipping veins are positioned clockwise to the steep-dipping veins when viewed from the southeast (Fig. 3.39). Tight clustering of data for each vein set on the stereoplots, which represent data for hundreds of metres of strike length, illustrates the consistent orientation of each vein set throughout the area and supports the distinction of systematic vein sets.

Intersections of conjugate veins generally lack crosscutting relationships, implying synchronous emplacement. However, apparent offset of many west-dipping veins, as seen on the bedding plane (Fig. 3.41a), is consistent with opening of the steep vein set perpendicular to the vein wall, and would suggest the west-dipping veins may be generally earlier. In some instances there is significant overlap of vein sets at their intersections, resulting in thickening of the vein (Fig. 3.41b). The thickness of the overlapped intersection is always equal to the thickness of the two vein sets, reflecting uniform dilation during synchronous emplacement of both vein sets.

Discordant veins are typically massive in character, although laminated textures are

locally developed. These veins are generally planar; however some exhibit minor buckling, with apparently steep fold axes (Fig. 3.42a). In addition, all veins exhibit penetrative fracturing which is perpendicular to vein walls (Fig. 3.42b). This fracturing appears to be continuous with, although commonly refracted from, cleavage within the host. In thin section the veins are seen to be fibrous, with fibre growth nearly perpendicular to the vein walls (Fig. 3.43a), indicating the veins are mainly extensional, consistent with apparent vein opening (Fig. 3.41a). The veins exhibit considerable strain, indicated by subgrain boundaries and undulose extinction (Fig. 3.43a). Locally cleavage in the host extends across the vein boundary and into the vein (Fig. 3.43b), suggesting the fracturing observed in outcrop (i.e., Fig. 3.41b) reflects cleavage development. These observations are important as they demonstrate that these veins suffered fold-related strain, consistent with observations above indicating their emplacement during significant flexural-slip folding. In addition, it implies a component of cleavage development overlapped vein emplacement, and therefore flexural-slip folding.

Visual estimates suggest these veins are probably the most abundant vein type in the area, and they are equally abundant in the Cunard Cove and Rose Bay exposures. Discordant veins cut through the hinge zone (zone A) and the flexural-slip thrusts (Zone B) on the south limb in Rose Bay. The occurrence of *abundant* discordant veins is restricted to the hinge area of the Ovens Anticline (i.e., the veined area, Fig. 3.2), similar to the occurrence of flexural-slip veins. This is consistent with a common origin interpreted for both vein sets. Measurement of discordant vein thickness for a one hundred metre, strike-parallel section at the east end of the Rose Bay Section (location RB-1) are given in Table 3.2, and indicate an average spacing of 0.308 metres. A histogram of vein thickness versus frequency for both

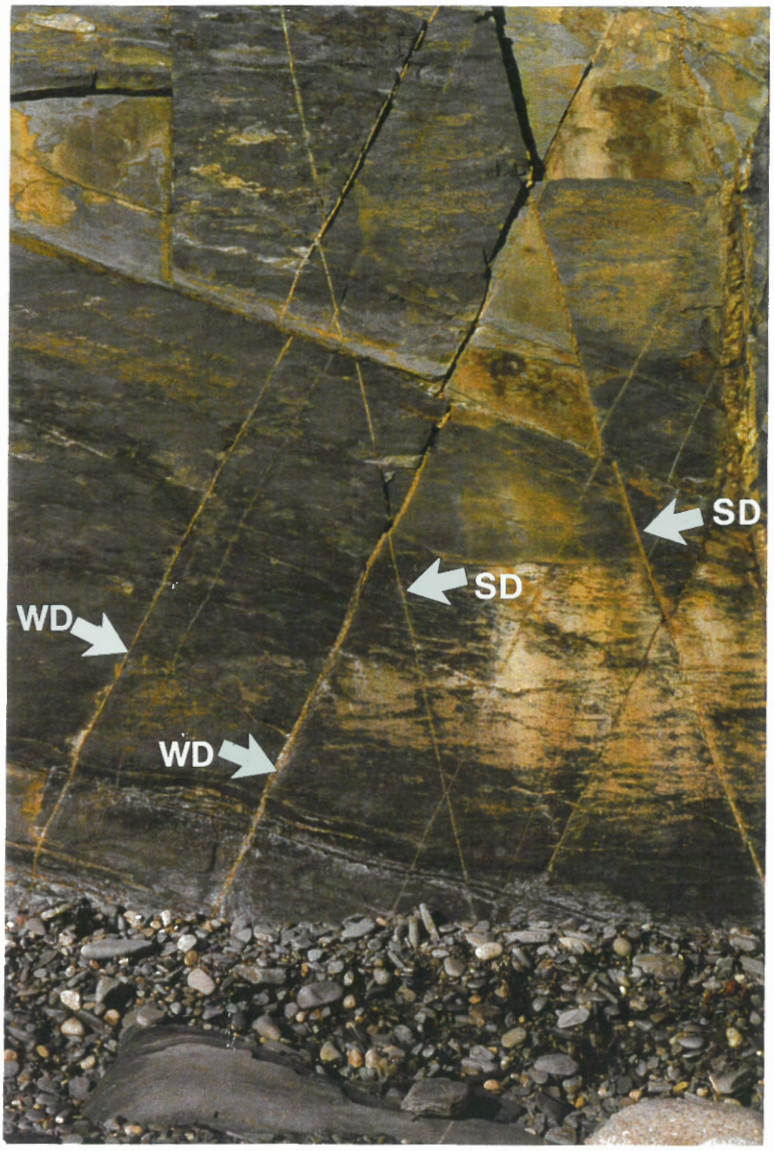

Figure 3.39: Photograph of the trace of conjugate discordant vein sets on a bedding plane of the south limb of the Ovens Anticline, location RB-1 (see Figure 3.17a) Rose Bay. Note consistency in attitude of vein sets. Photograph approximately 2 metres wide and view is looking to the northwest. SD = steep-dipping vein set; WD = west-dipping vein set.

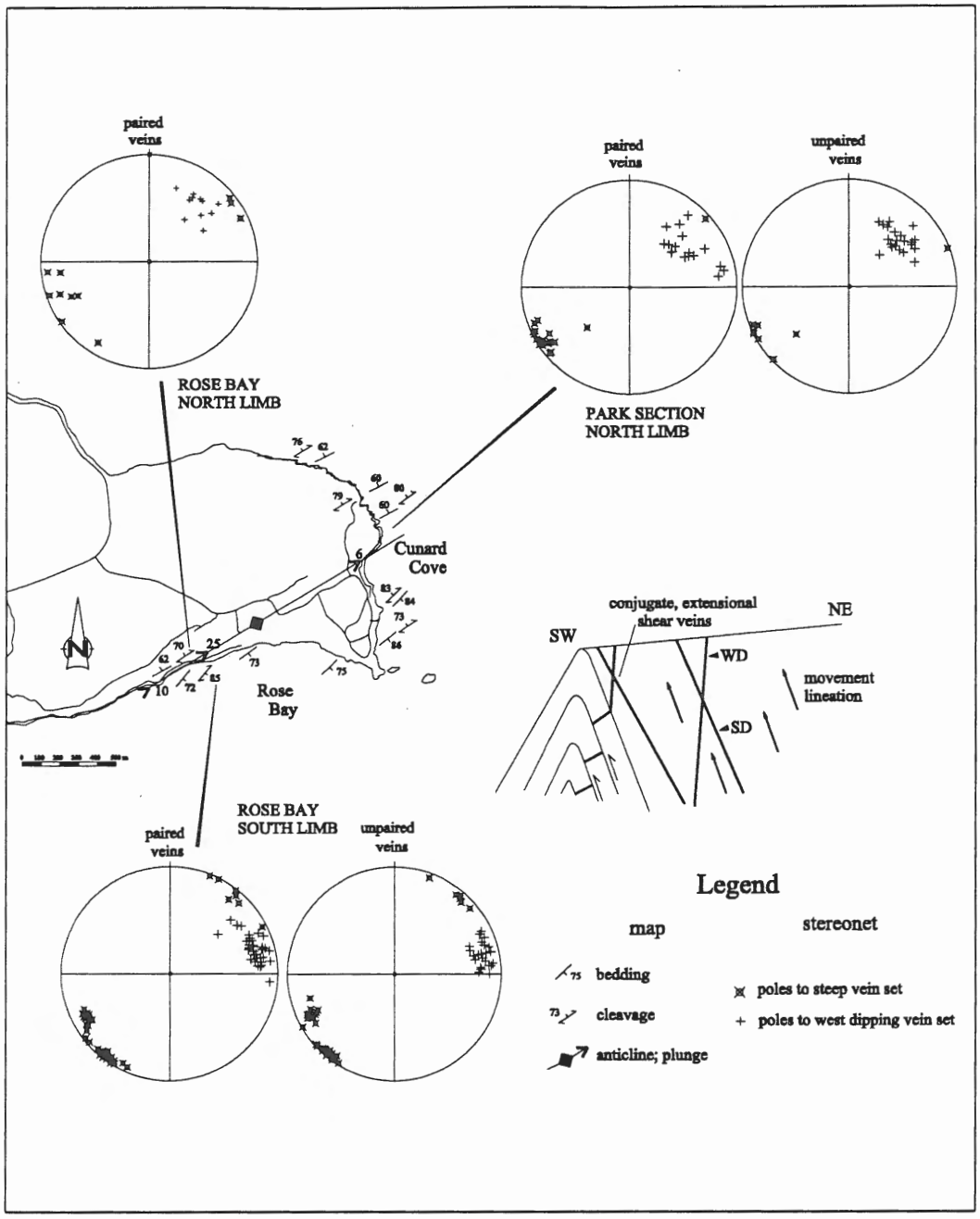

Figure 3.40: Stereoplots of poles to conjugate discordant quartz veins in the Ovens area.

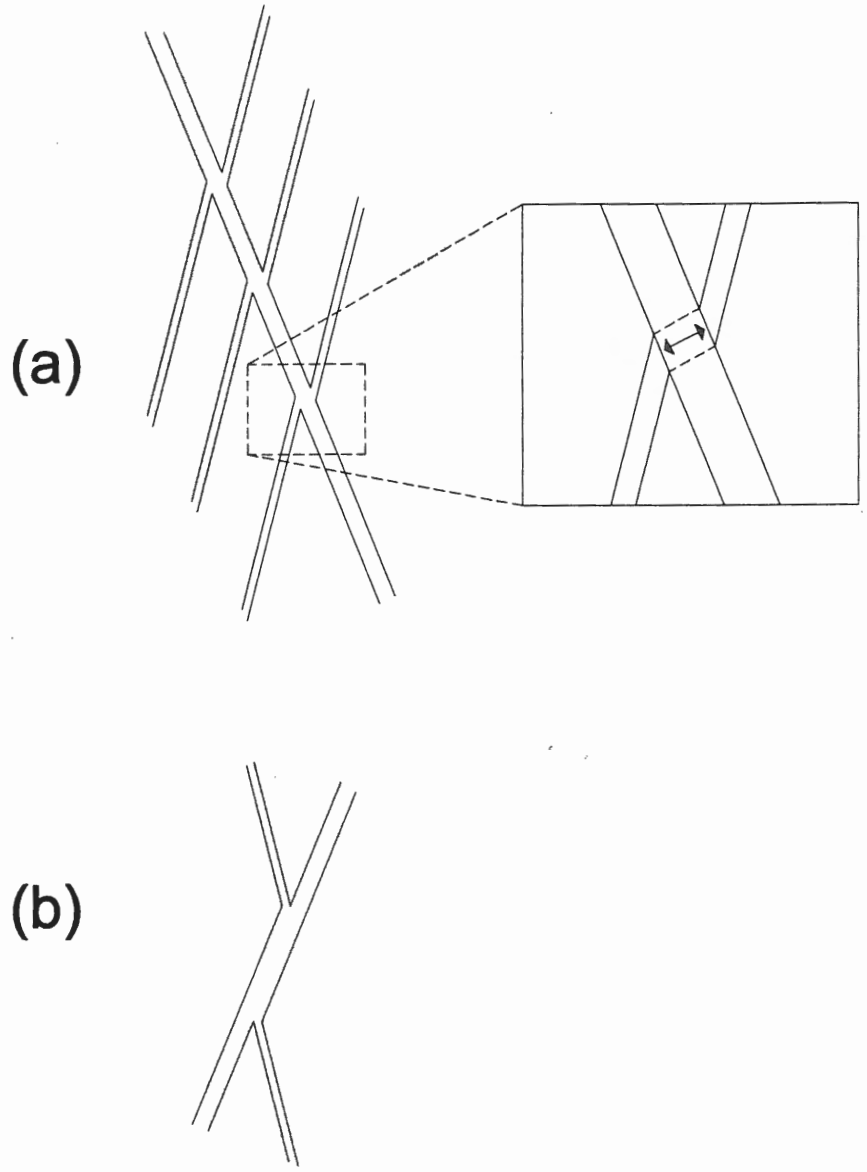

Figure 3.41: Schematic diagram of (a) conjugate vein traces on a bedding plane showing the apparent displacement of the west-dipping vein set across the steep-dipping set as a result of dilation caused by the opening of the latter (inset) and (b) overlapping intersection of conjugate veins showing thickening of overlapped segment is equivalent to the total thickness of both veins.

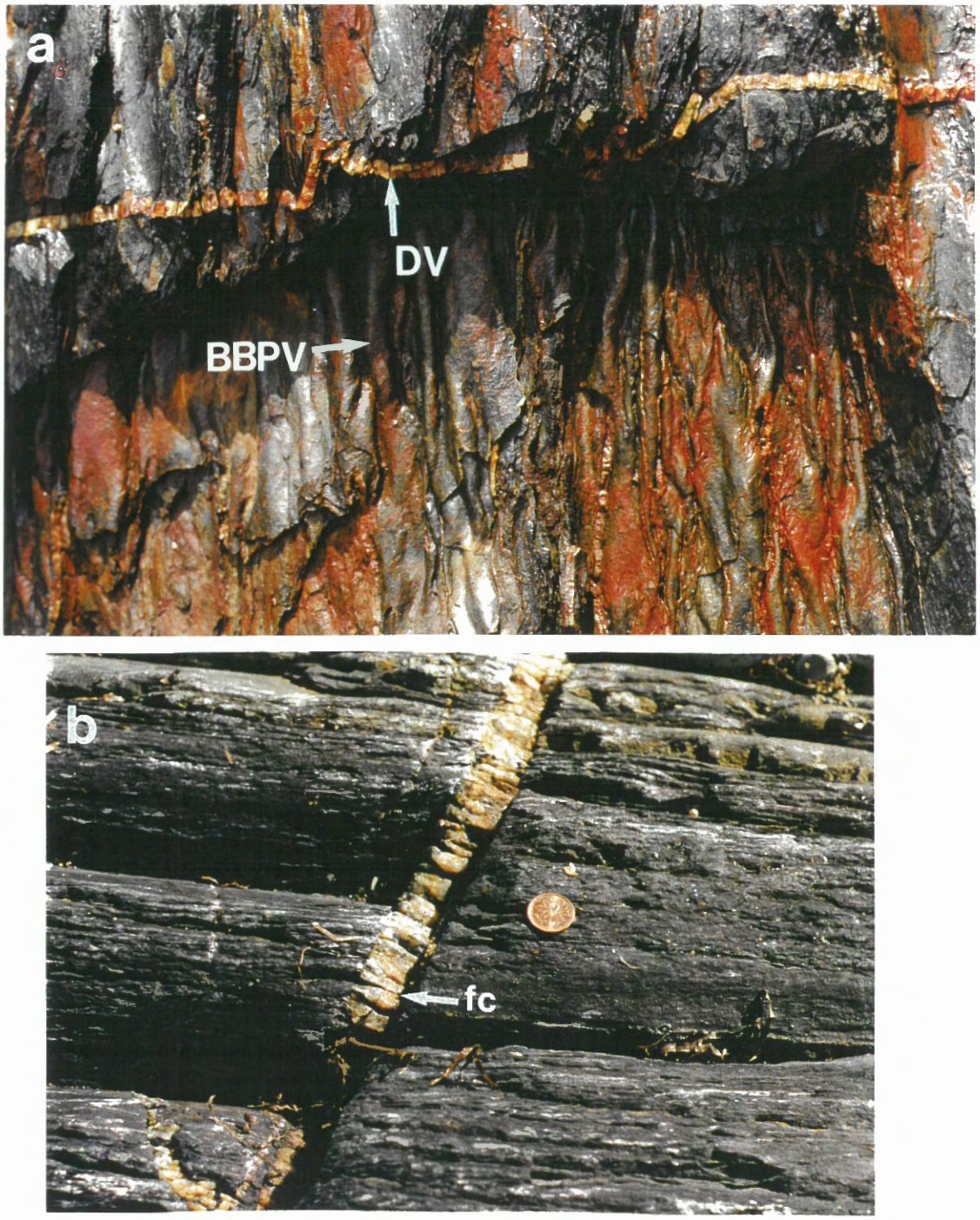

Figure 3.42: (a) Photograph of discordant vein (DV) exhibiting minor buckling, with steep fold hinge, cutting buckled bedding-parallel vein (BBPV)(horizontal hinge) in the hinge of the Ovens Anticline, Cunard Cove (plan view). Buckling of discordant vein is consistent with that in the bedding-parallel vein. Discordant vein 1 cm wide. (b) Photograph of discordant vein exhibiting a penetrative fracture cleavage (fc) roughly perpendicular to the vein walls. Coin is 19mm in diameter.

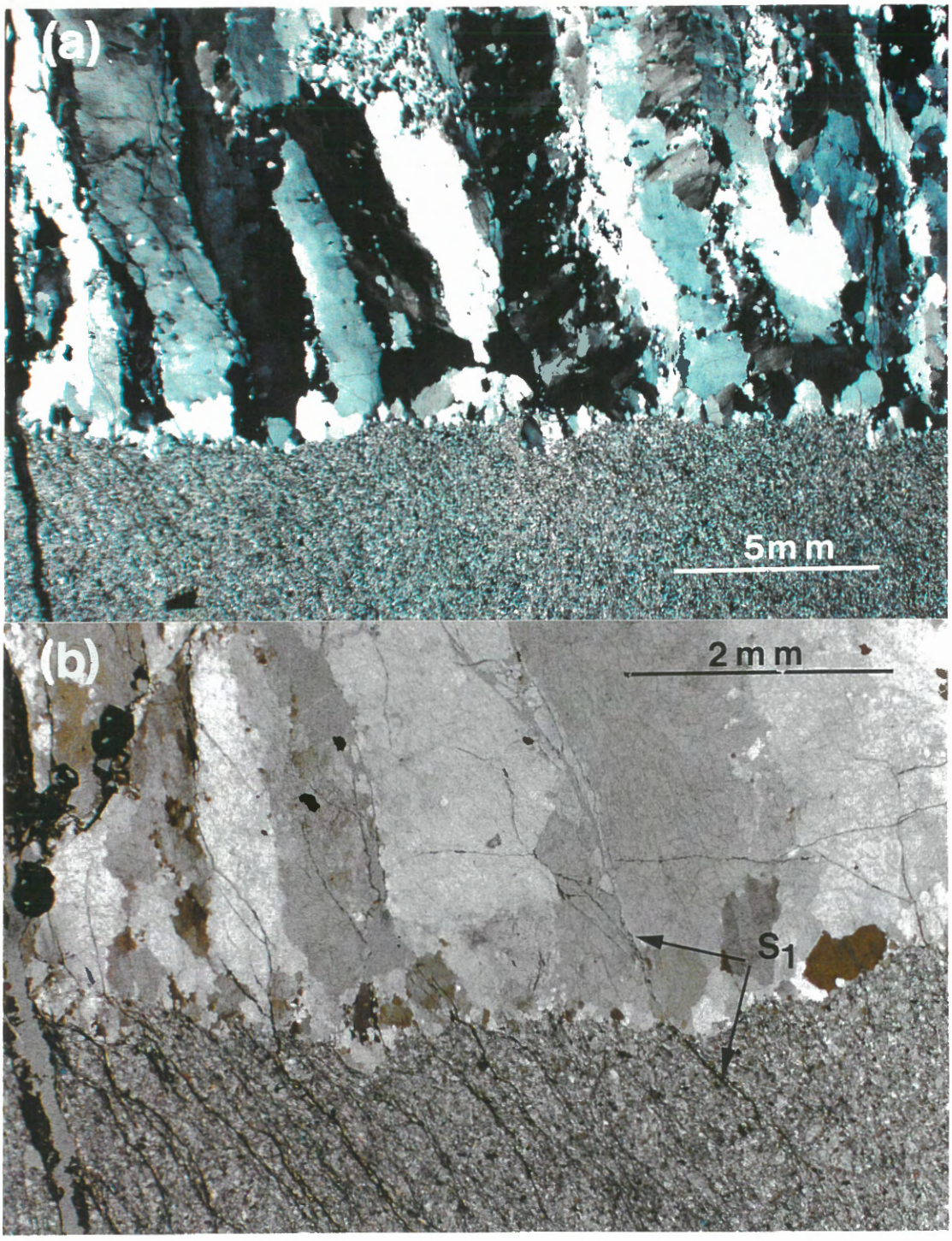

Figure 3.43: Photomicrographs of discordant veins cutting metasandstone layer. (a) Photomicrograph illustrating the fibrous character of veins. Note also subgrains at fibre boundaries and undulose extinction. Crossed polars. (b) Photomicrograph of the lower left part of (a) illustrating continuation of spaced cleavage (S_1) from metasandstone into the vein. Note S_1 in vein is subparallel to fibre boundaries.

(a)

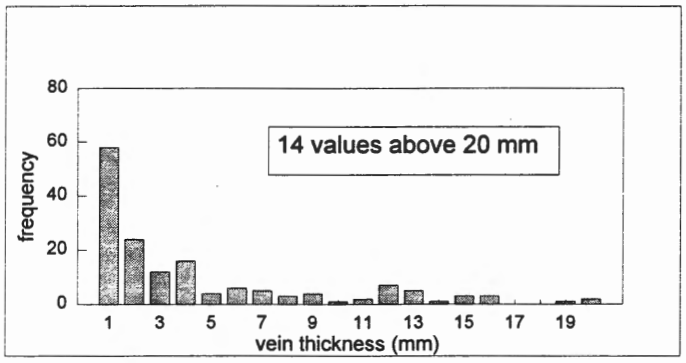

1162.00 sum of vein thickness (mm)
6.80 average vein thickness (mm)
1.00 minimum thickness (mm)
60.00 maximum thickness (mm)
9.49 standard deviation (mm)
3 median thickness (mm)

(b)

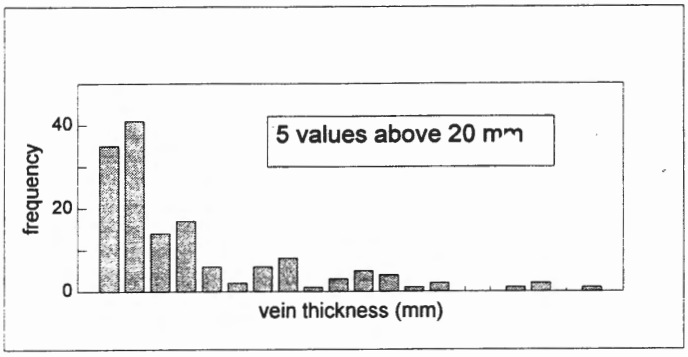

1060.00 sum of vein thickness
7.16 average vein thickness
1.00 minimum thickness
60.00 maximum thickness
9.84 standard deviation
3.00 median thickness (mm)

Figure 3.44: Histograms of vein thickness for (a) steeply-dipping discordant veins and (b) west-dipping discordant veins, for a 100 metre section along location RB-1 (Fig. 3.17), Rose Bay.

	West Veins	Steep Veins	Cumulative
Number of veins	154	171	325
Average spacing	650 mm	585 mm	308 mm
Thickness Range	1-160 mm	1-60 mm	-----
Average Thickness	5.65 mm	6.80 mm	-----
Median thickness	3.0 mm	3.0 mm	-----
Cumulative thickness	870 mm	1162 mm	2032 mm

Table 3.2: *Table of thickness and spacing data for the discordant conjugate vein set for a 100 metre section, Rose Bay Location RB-1 (see Fig. 17a). Measurements taken on bedding surface for all veins intersected at a constant horizontal level. All spacing and thickness values given in millimetres. See Appendix 4 for data.*

vein sets (Fig. 3.44) indicates the majority of veins are thin (median thickness 3 mm), with few veins greater than a centimetre. The cumulative thickness of veins for the measured interval, 2.032 metres, implies ~ 2 % hinge-parallel extension resulting from vein emplacement.

3.5.3.3.1 Relationship to the fold and inferred stress orientations:

The geometry of discordant veins is clearly related to that of the fold. The obtuse bisector of the vein sets is sub-parallel to the fold hinge, and the intersection of the vein sets, calculated from the attitude of intersecting veins, occurs within the ac plane of the fold (Fig. 3.45). Vein intersection data show a considerable range in plunge. However, the clusters for each limb are essentially mutually exclusive, with data from the north limb defining a mirror image of the south limb (Fig. 3.45). The dip of the vein intersections range from normal to bedding (i.e., pole to bedding) to vertical for each limb (Fig. 3.45). The fact that these

relationships are similar on both limbs (i.e., mirror image), and therefore asymmetric within the profile plane, demonstrates these veins do not simply reflect hinge-parallel extension related to regional horizontal stress during folding, but rather they reflect fold-related stress.

Vein intersections are not well exposed in the field and the majority of vein intersection orientations were calculated from the intersection of two planes (veins). There is potential error in deriving intersection orientations in this manner, putting some question on their reliability for determining stress orientation. Minor variations in the orientation of either vein set can result in significant change in the calculated orientation of the intersection of the planes. Such errors could cause a dispersion of the calculated intersections exactly similar to that displayed in the stereoplots (Figs. 3.45 and 3.46). However, several features suggest the data is reliable:

(1) The calculated intersection data are confined to a well defined girdle which is common to both limbs (Fig. 3.45).

(2) Limited measured intersection data coincide with calculated orientations (Fig. 3.46).

(3) The best fit plane through the intersection data bisects the angle between the average planes for the two vein sets (Fig. 3.46).

(4) The intersection of the average planes for the two vein sets occurs in the middle of the field of calculated intersections for individual vein pairs; it also falls nearly in the best fit plane through all intersection data (Fig. 3.46).

The principal stress inferred from intersecting vein geometry, the acute bisector of intersecting vein pairs (Fig. 3.47a), lies within the ac plane, ranging from close to the flexural-slip movement direction lineations (within the bedding plane) to near horizontal (Fig. 3.45).

Displacement of the discordant veins along flexural-slip movement horizons indicates that the orientations of vein intersections and inferred principal maximum stress orientations have been rotated during limb amplification and therefore that the plunge of vein intersections and inferred stress with respect to the fold may not reflect the stress orientation at the time of vein formation. Discordant vein emplacement is synchronous with flexural slip and therefore the amount of rotation of vein intersection is limited to <10° (the amount of limb dip attributed to flexural slip).

Stress orientations inferred from vein bisectors vary from steep to horizontal (Fig. 3.45). Horizontal bisectors are consistent with a roughly horizontal maximum principal stress, similar to that expected for fold development (i.e., perpendicular to the axial plane of the fold). However, a group of intersection data for the south limb and all the data for the north limb are close to the pole to bedding (Fig. 3.45). If these veins resulted from a horizontal stress then they must have formed in the early stages of fold development, at low limb dips. However, evidence supports late a syn-flexural-slip origin for these veins. Another explanation for such vein intersections is that the maximum principal stress is locally within the bedding plane during folding. Such a stress orientation is consistent with flexural slip, where the maximum principal stress is parallel to the movement lineation. Price and Cosgrove (1990) illustrated conjugate shear fractures of this type which they related to flexural slip (Fig. 3.47b, c). This stress orientation requires minimal shear stress along the movement horizon, which could result from high fluid pressure causing separation of movement horizons. This is consistent with the presence of flexural-slip veins along movement horizons, and with the synchronous development of discordant veins and flexural slip.

As mentioned above, the variation in vein intersections, and thus principal stress orientation, for paired discordant veins could reflect minor errors in measuring the attitudes of veins. That this was not a significant problem is suggested by arguments given above. The range of intersections may reflect variation in the orientation in the maximum principal stress during flexural-slip folding. In addition, a possible factor controlling the observed variation in intersections is that is that some veins suffered either flexural flow or homogeneous flattening, which is consistent with the fact that vein intersections are either perpendicular to bedding or steeper.

Gold was noted in several discordant veins, including: (1) A horizontal segment connecting conjugate veins near Tuckers Tunnel (Fig. 3.4). (2) At the intersection of a conjugate vein pair exposed on a bedding surface in Rose Bay, and (3) Within a vein transecting Zone B in Rose Bay (specifically, cutting the "fault propagation fold" in the hanging wall of Thrust 5; i.e., Fig. 3.28). The latter vein is locally extremely rich in gold, as many who have passed through on field trips can attest. It is worthy of note that in each of these instances the location of observed gold does not occur in the vicinity of an intersection with a bedding-parallel vein, as has been documented in many of the Meguma Gold deposits (Malcolm, 1929; Sangster, 1990). Indeed, bedding-parallel veins are uncommon within the thrust sheets of Zone B, where rich discordant veins occur. Coarse scheelite, similar to that observed in flexural-slip veins in Rose Bay, was locally observed within discordant veins in Rose Bay and Cunard Cove.

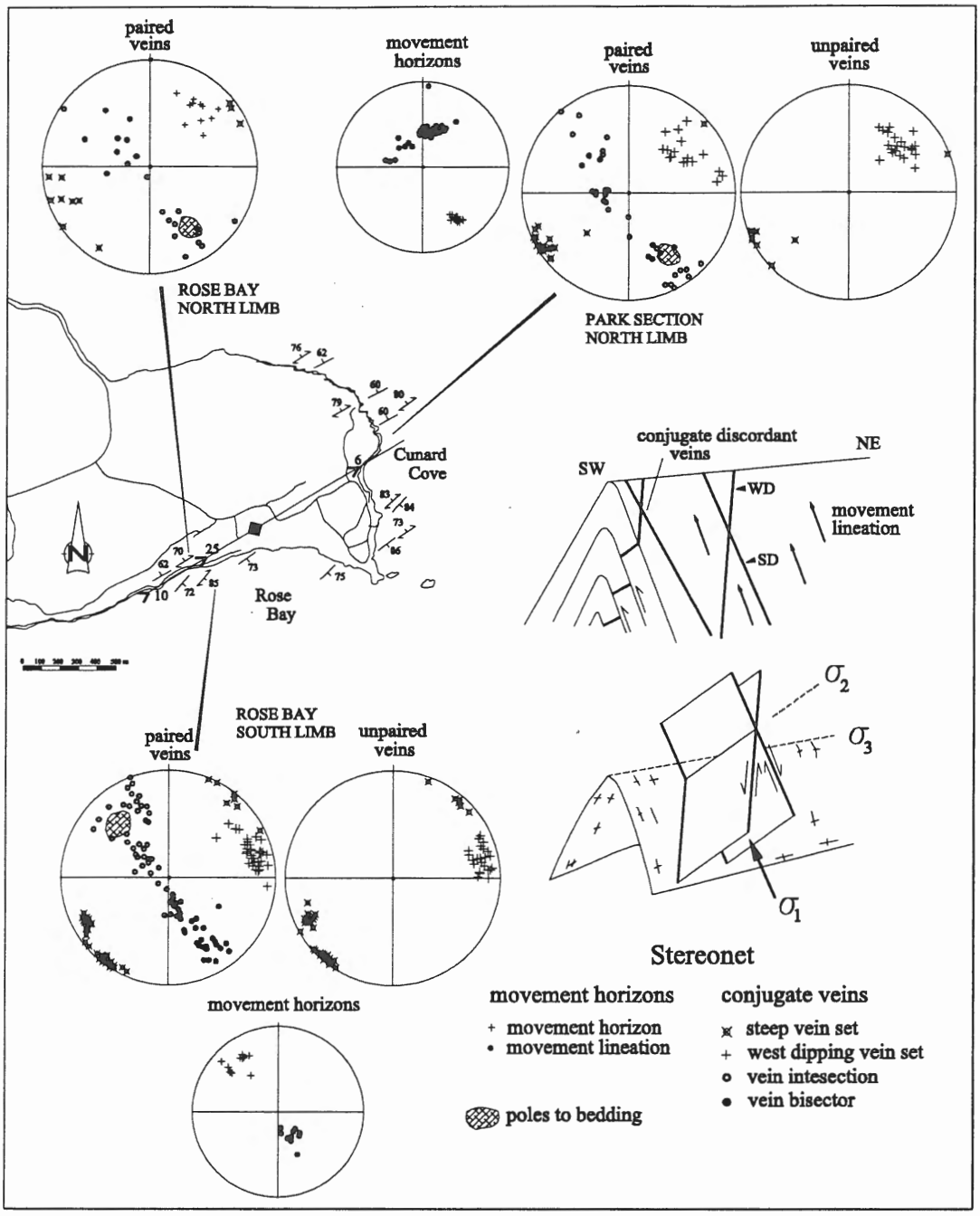

Figure 3.45: Stereoplots of discordant vein orientation data, including calculated vein intersections and acute vein bisectors, and flexural-slip data for the Ovens area.

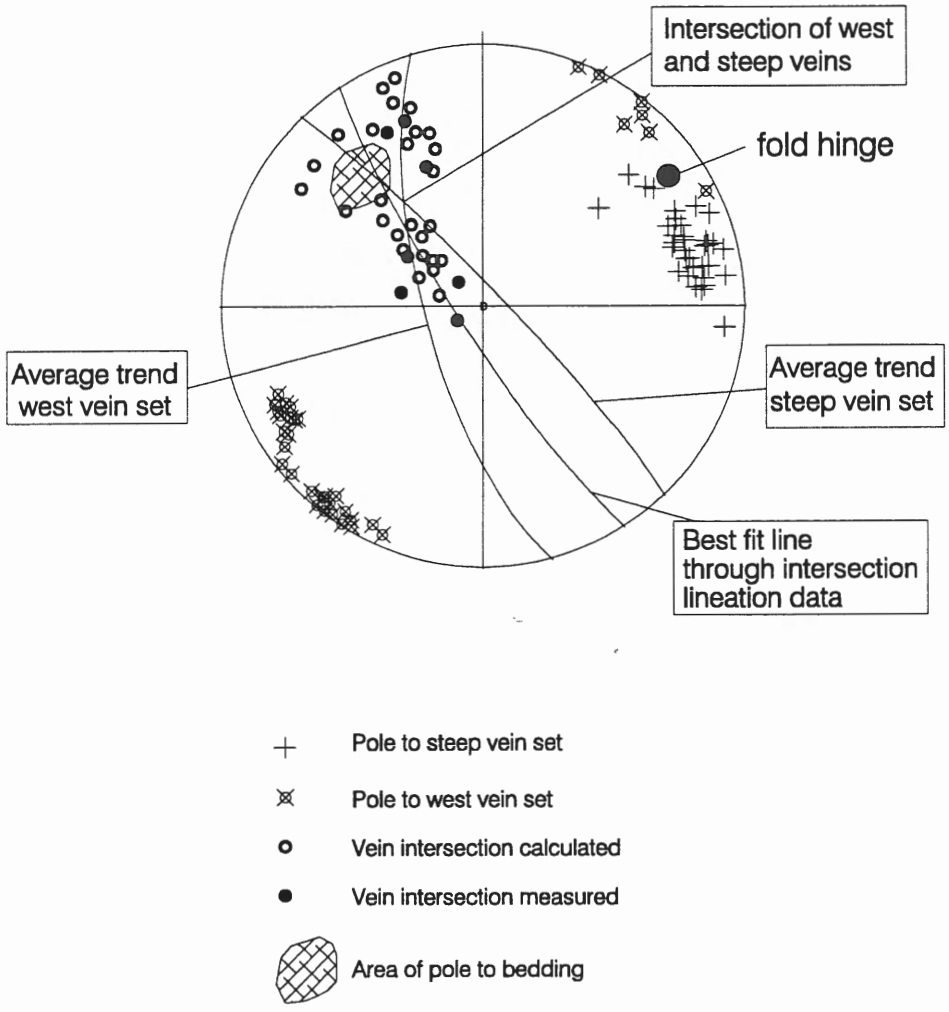

Figure 3.46: Stereoplot of discordant vein data for paired veins from the south limb of the Ovens Anticline, Rose Bay. The intersection of the average trend for each vein set is close to the pole to bedding and the best fit plane through the intersection data for paired veins bisects the two vein sets and is roughly perpendicular to the fold hinge (i.e., represents the ac plane).

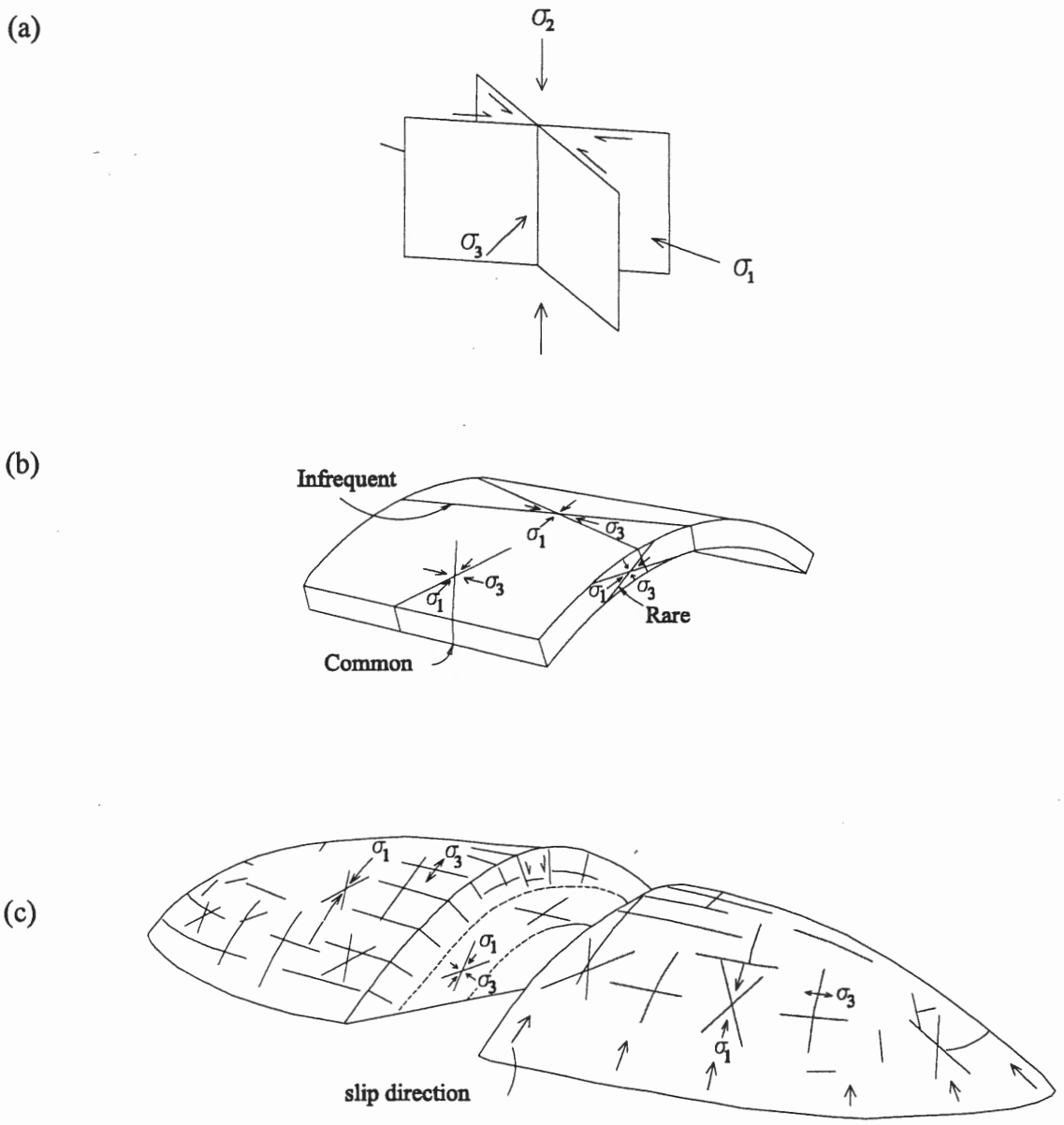

Figure 3.47: Schematic diagrams showing (a) the relationship between conjugate shear fractures and principal stress axes according to the Navier-Colomb theory of failure, (b) the relationship of shear fractures in a folded layer and (c) the relationship of shear fractures around a non-cylindrical fold. Note principal stress orientation for common shear fracture set in b and c parallel the inferred flexural-slip direction. All figures from Price and Cosgrove (1990).

3.6 DISCUSSION OF THE OVENS

3.6.1 Introduction:

Exposure in the Ovens area provides an excellent opportunity to address the structure of regional folds. Evidence of flexural slip in the Ovens area has been well established and the flexural-slip mechanism was clearly important in the late development of the Ovens Anticline. Other structural elements, including cleavage, pressure shadows, thrusts and fractures help to constrain, and allow for discussion of, other aspects of fold development. Localization of systematic vein sets along flexural-slip structures and the recognition of synchronous emplacement of concordant and discordant veins suggests a synfolding origin for the auriferous veins of the Ovens Gold District. Following are discussions of flexural slip, fold development and a model for syn-folding veining for the Ovens Anticline.

3.6.2 Flexural slip

The Ovens Anticline is characterized by classic flexural-slip structures, where, except for en echelon veins, all components of Tanner's flexural-slip model (see Fig. 1.5) have been identified. The basic criteria of relating movement horizons to flexural-slip folding, including movement direction and shear sense, have been established, and flexural slip is consistent with the chevron fold style and the presence of saddle-reef veins and hinge thrusts occurring within the hinge region. Movement horizons are all bedding-parallel, and lateral ramps as described in the Halifax area do not occur. Movement horizons include single movement surfaces as well as flexural-slip duplexes, similar to those described by Tanner (1989; 1992). The identification of movement horizons is paramount in the evaluation of flexural slip and it is

important to point out that their recognition is largely known from the offset of discordant veins, without which many of the simple movement horizons would not have been identified.

The orientation of movement lineations on flexural-slip structures is generally consistent with a flexural-slip origin. A prefolding origin for these lineations is not supported by the brittle character of flexural-slip structures and the systematic change in shear sense across the fold hinge. Movement lineation data from the Cunard Cove section display a large range in trend, and the occurrence of two lineations on some movement horizons suggests a complex movement history, with variation in slip direction through time. Tanner (1989) offered several explanations for variable movement lineation data from flexural-slip structures, including flexural-slip folding of a previously inclined layer, flexural slip during growth of a non-cylindrical fold (Fig. 2.13), pre- or post-folding slip, and development of folds in a transpressive regime. The data from the Cunard Cove section may be best explained as resulting from lateral hinge propagation during non-cylindrical fold development. Lineations developed in the fold termination in the early stages of fold development, which may trend close to the fold axis, are overprinted by later movement lineations which trend perpendicular to the fold hinge (Fig. 3.48; Dubey, 1982). Keppie (1997) suggested non-cylindrical fold growth for the Oldham Anticline, in the central Meguma area, with lateral hinge propagation during fold growth, similar to the model of fold growth presented by Dubey (1982) and Dubey and Cobbold (1977).

Flexural-slip structures are brittle, they deform cleavage (i.e., duplexes), and they offset "late" discordant veins, indicating that flexural slip occurred late in the fold development. Displacement of offset veins indicate flexural slip is responsible for

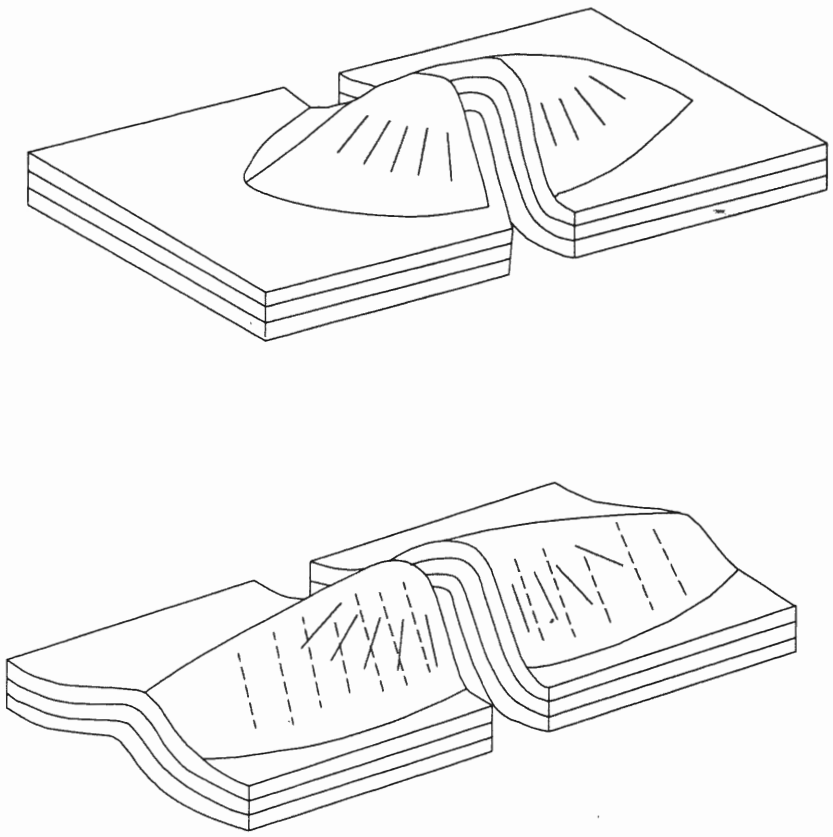

Figure 3.48: Simplified diagram illustrating the directions of interlayer slip during different stages of non-cylindrical flexural slip fold development. Continuous lines represent early slip and dashed lines represent later slip. After Dubey (1982).

approximately 4-8° of limb dip on the north limb of the fold. This amount is considered a minimum as it only records the amount of flexural slip which postdates the offset veins. Earlier flexural slip may be represented by bedding-parallel veins similar in character to those along flexural-slip movement horizons. The late, brittle character of flexural slip suggests that it accounts for the last increments of folding.

Further discussion of the relative age of flexural slip and the relationship of flexural slip and other fold-related strain are discussed in more detail in the following section and in chapter 4. Also, a discussion of movement horizon spacing and slip amount is given in chapter 4. Emplacement of quartz veins was clearly related to flexural slip and further discussion of veining and its role in flexural slip is presented below.

4.6.3 Fold development:

Flexural slip was clearly important in late fold development. Several other structural elements help to constrain a more complete understanding of fold development. Below is a discussion of several features which, in addition to flexural slip, constrain our understanding of fold development. This is followed by a discussion of a possible history of fold development, accounting for all the observed features in the Ovens area.

4.6.3.1 Cleavage pattern in the Hinge Zone

The distinctive, divergent cleavage pattern in fold hinges is consistent with a model in which any layer-parallel shortening, prior to folding, was minor (Ramsay and Huber, 1987). This pattern occurs in the hinge of the regional-scale Ovens Anticline (Fig. 3.6a), around

minor folds of bedding-parallel quartz veins in the hinge of the main fold (Fig. 3.6b), and around folded metasandstone layers and quartz veins within the thrust sheets of Zone B, Rose Bay (Fig. 3.30). The divergent cleavage pattern around the main fold does not support significant pre-Ovens Anticline layer-parallel shortening, but rather suggests mainly syn-folding cleavage development. This pattern within the thrust sheets, where buckling of the veins and thin metasandstone beds occurred at low limb dips, would be consistent with homogeneous layer-parallel shortening of the succession prior to regional folding. However, as discussed below, the observed layer-parallel shortening within the thrust sheets is interpreted to reflect deformation within the flat top of a box fold during folding.

3.6.3.2 Bedding-cleavage relations on the limbs

Bedding-cleavage relations have been interpreted to record flexural-flow deformation of pre-folding cleavage in the Meguma Group, with cleavage refraction between metasandstone and slate reflecting differential shear strain (Henderson et al., 1986). In the example presented by Henderson et al. (1986), the weighted bedding-cleavage angle for a metasandstone-slate sequence accounted for all the predicted shear strain (Fig. 1.7b) and they suggested no flexural-slip occurred. This interpretation suggests bedding-cleavage angles are a measure of angular flexural-flow strain which can be used to understand the folding history. The measured section (C-D) in Cunard Cove, where the amount of flexural slip is known, provides a good opportunity to evaluate the hypothesis of Henderson et al. (1986) that bedding-cleavage angles reflect flexural flow; the combined shear attributed to flexural-flow plus flexural-slip should account for the total shear.

The cumulative amount of flexural flow (ψ_F) indicated from bedding-cleavage angles (β', Fig. 3.49) was calculated for Section C-D, which is characterized by strong cleavage refraction and uniform bedding and cleavage attitudes. Cleavage in the slate intervals is roughly axial planar, well developed and uniform in dip throughout the measured section (e.g., Figs. 3.2 and 3.7). Spaced cleavage in the metasandstone is generally not distinguishable (e.g., Figure 3.8b); however angles are always large where noted. An average β' value of 72° for slate (based on bedding and cleavage measurements throughout the section) and 0° for metasandstone (conservative estimate) was used to determine the weighted obtuse bedding-cleavage angle (β'_W) value for the section, which consists of 23% metasandstone and 77% slate (Fig. 3.5). The results indicate a ψ_F (β'_W) value of 67° (Figure 3.49; Appendix 5).

If shear strain is related to limb dip (60°), and the increment of shear strain attributed to flexural-slip (8.8°) accounts for the last increment of folding, then a flexural-flow strain, or obtuse bedding-cleavage angle (β'_W), of 51.2° would be expected. This leaves a discrepancy of 15.8° with respect to the observed β'_W of 67°. However, if shear strain is related to interlimb angle (~40°), the total shear strain of ~70° is almost exactly accounted for by the observed β'_W of 67° and the related increment of angular shear strain related to flexural slip of 3.8°. This match in observed and expected shear strain is consistent with flexural shear strain for the Ovens Anticline being a function of the interlimb angle.

When considered relative to the interlimb angle, the observed bedding-cleavage relations are consistent with the interpretation of Henderson et al. (1986); that they reflect rotation of an early-formed cleavage by flexural flow. However, a synfolding origin for

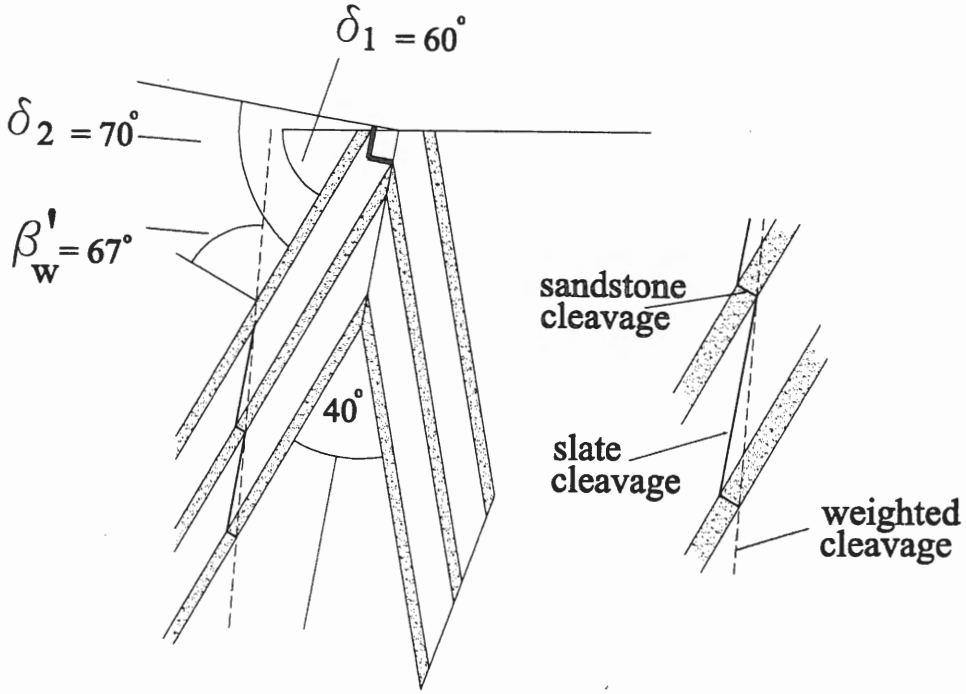

Figure 3.49: Schematic diagram showing the weighted bedding-cleavage angle, β'_w, for a slate-metasandstone sequence. The value of β'_w for the Cunard Cove section is 67° (see Appendix 5). Limb dip relative to the horizontal for the section (δ_1) is 60°, whereas the limb dip relative to the interlimb angle (δ_2), of approximately 40°, is 70°. β' is the obtuse angle between bedding and cleavage.

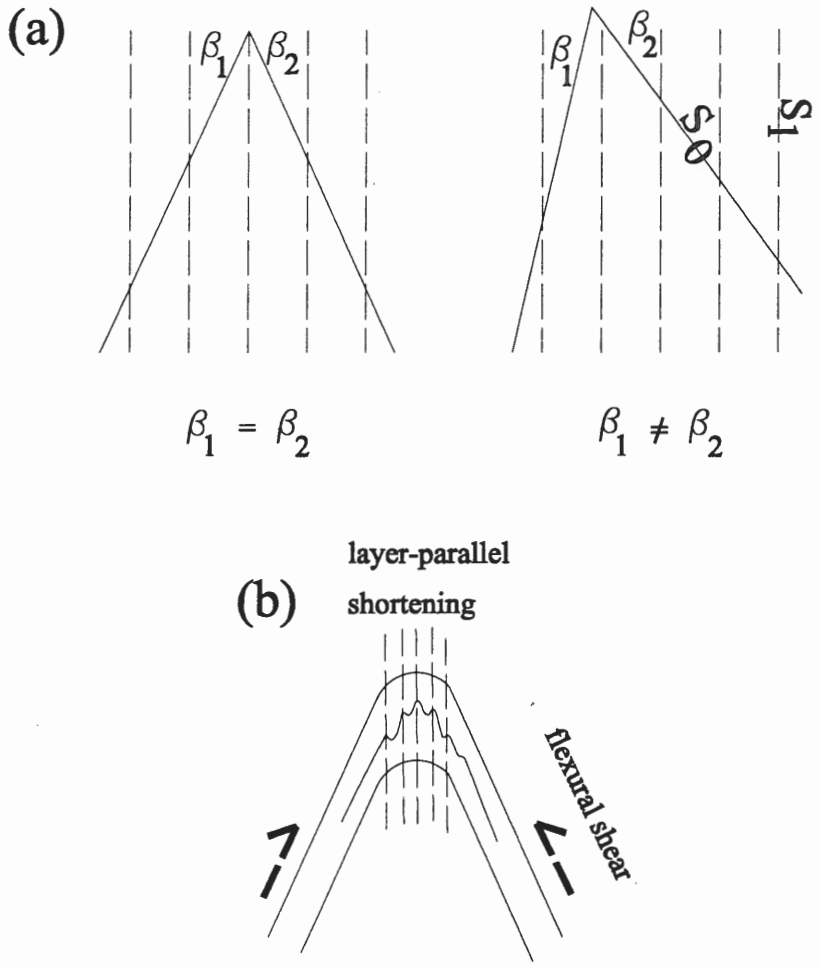

Figure 3.50: (a) Schematic diagram illustrating bedding-cleavage relation resulting from rotation of cleavage by flexural flow for an upright (left) and inclined (right) chevron fold. The bedding-cleavage angle (β) is a function of limb dip and thus equal on both limbs of the upright fold and unequal on the limbs of the inclined fold. S_1 = cleavage, S_0 = bedding.
(b) Schematic diagram showing synchronous flexural-shear on fold limbs and layer-parallel shortening in the hinge zone.

cleavage is suggested by the cleavage pattern in the fold hinge (above) and also the restriction of minor folds to the hinges of regional folds (discussed below). Bedding-cleavage relations, therefore, may not entirely reflect a flexural-flow strain history. Indeed, as discussed by Treagus (1988), there is little difference between the orientation of cleavage sheared during flexural flow and the X axis of the strain ellipsoid for significant shear strain (limb dip), and the difference is very small for large limbs dips such as at the Ovens. Bedding-cleavage relations, therefore, are not a test for the model of Henderson et al. (1986) of prefolding cleavage-development followed by flexural-flow.

3.6.3.3 Pressure shadows

Quartz±muscovite pressure shadows occur on arsenopyrite crystals both within the hinge zone (Fig. 3.22) and on the planar limbs (Fig. 3.25), and the stretching direction is consistent with vertical extension within the cleavage plane during folding. Strain on the limbs is consistent with flexural-flow strain, as suggested by Henderson et al. (1986), although this does not account for the significant stretching observed in the hinge zone. In studies of cleavage development and folding, Henderson et al. (1986) and Wright and Henderson (1992) stated there was no evidence of extension related to cleavage development in the hinge of the folds they studied. In addition, as indicated above, the fibres in the pressure shadows are face controlled and the suture lines are indistinct to poorly developed, and therefore it is difficult to resolve whether they reflect coaxial or non-coaxial deformation. They clearly do not provide evidence of significant non-coaxial deformation, as would occur during flexural-shear. On the other hand, coaxial deformation during fibre growth would support the hypothesis that

bedding-cleavage angles reflect synfolding cleavage development.

Of particular significance here is the age of the strain exhibited by the pressure shadows. The ca 376 Ma $^{40}Ar/^{39}Ar$ age for a muscovite separate, interpreted to represent coarse muscovite occurring within the pressure shadows (Hicks et al., in press; see also Fig. 3.25d), indicates that considerable fold-related strain significantly postdates regional metamorphism and deformation (cleavage development) throughout the Meguma Group (see chapter 1), and which is recorded by whole rock $^{40}Ar/^{39}Ar$ ages of ca 395-399 Ma in the area.

3.6.3.4 Minor folds

Minor folds in the Ovens area are defined by buckled bedding-parallel quartz veins in the hinge zone of the Ovens Anticline and by buckled thin metasandstone beds and bedding-parallel veins within the thrust sheets in Zone B of the Rose Bay section. Minor folds are notably absent on the limbs of the anticline. Some previous studies have suggested that minor folding, particularly of bedding-parallel veins, in the Meguma Group, including the Ovens area, reflects homogeneous layer-parallel shortening prior to folding (Henderson et al., 1986; Graves and Zentilli, 1982). This is apparently supported by the shortening exhibited within the thrust sheets of Zone B in Rose Bay. In this model, minor folds have a parasitic relationship to the later developed folds as a result of flexural shear on the limbs. However, minor folds around the Ovens Anticline are restricted to the hinge zone, with no buckling of folded layers on the planar limbs, which does not support pre-folding development of minor folds. The possibility that the lack of minor folds on the limbs results from "unfolding" is not supported by flexural folding, where folding would be enhanced. Also, as pointed out by

Williams and Hy (1990), the late introduction of these veins does not support an unfolding history; veining occurred during flexural slip, which accounts for the last increment (<10°) of folding. Another explanation for the observed minor folds in the hinge region is that during folding, whereas fold-related strain on the limbs was accommodated largely by flexural shear, fold-related strain was accommodated in the (fixed) hinge zone largely by homogeneous layer-parallel shortening (Fig. 3.50b). Coexisting buckled and non-buckled bedding-parallel veins in the hinge area (i.e., Fig. 3.36) may reflect sequential vein emplacement during folding, with the buckled veins representing relatively early veins which suffered relatively more layer-parallel shortening than later, unbuckled veins. This also explains the coexistence of buckled bedding-parallel veins and late-formed saddle-reef veins (i.e., Fig. 3.6c).

Minor folds and bedding-cleavage relations within the thrust sheets indicate layer-parallel shortening at low limb dips. Although this is consistent with shortening prior to folding, this is not supported by the lack of minor folds on the limbs of the Ovens Anticline. Indeed, the minor folding and mullion structures exhibited by metasandstone layers in the thrust sheets do not occur even within the hinge zone of the Ovens Anticline, where such strain, if pre-folding, would be enhanced. Flexural shear of pre-folding minor folds on the folds limbs would result in asymmetric, parasitic folds. The conclusion, therefore, is that the shortening exhibited within the thrust sheets has a synfolding origin.

An explanation for synfolding layer-parallel shortening in the thrust sheets is that they represent the flat segments of regional box folds, which characterize the Meguma Terrane (Fig. 1.4), where bedding remained subhorizontal during folding. Indeed, similar minor folds and bedding-cleavage relations indicating layer-parallel shortening occur northeast of the

Ovens, in the Blue Rocks area (Henderson et al. 1992; personal observation), which represents the subhorizontal segment of a regional synclinorium north of the Ovens Anticline (section A-B, Fig. 3.1). A regional-scale flat-topped box-fold occurs to the south of the Ovens Anticline (section C-D, Fig. 3.1) and is the likely source of the thrust sheets.

4.6.3.5 Thrusts:

The above discussion suggests that the thrust sheets of Zone B, Rose Bay, represent flat segments of regional box folds which have been thrust onto the south limb of the Ovens Anticline and that thrusting postdates syn-folding layer-parallel shortening in the flat segments of box folds. The kinematics of thrusting are consistent with flexural slip and thrusts are characterized by similar brittle features as flexural-slip structures (movement horizons, duplexes, quartz veins), suggesting that thrusting overlapped flexural-slip folding. This is supported by the fact that discordant veins, which were emplaced during flexural-slip folding, and are restricted to the hinge area in the Ovens Anticline, transect the thrust section and are displaced across the thrusts. The fact that bedding-cleavage relations within thrust sheets reflect pre-thrusting limb dips implies there was no internal fold/thrust-related strain during thrusting; all strain was localized along the thrusts. These observations are consistent with the hypothesis that flexural-slip folding represents a late component of fold development.

4.6.3.6 Summary:

The above discussion of flexural-slip and other fold-related structures suggests a complex strain history. Without further constraints on the absolute and relative age of the

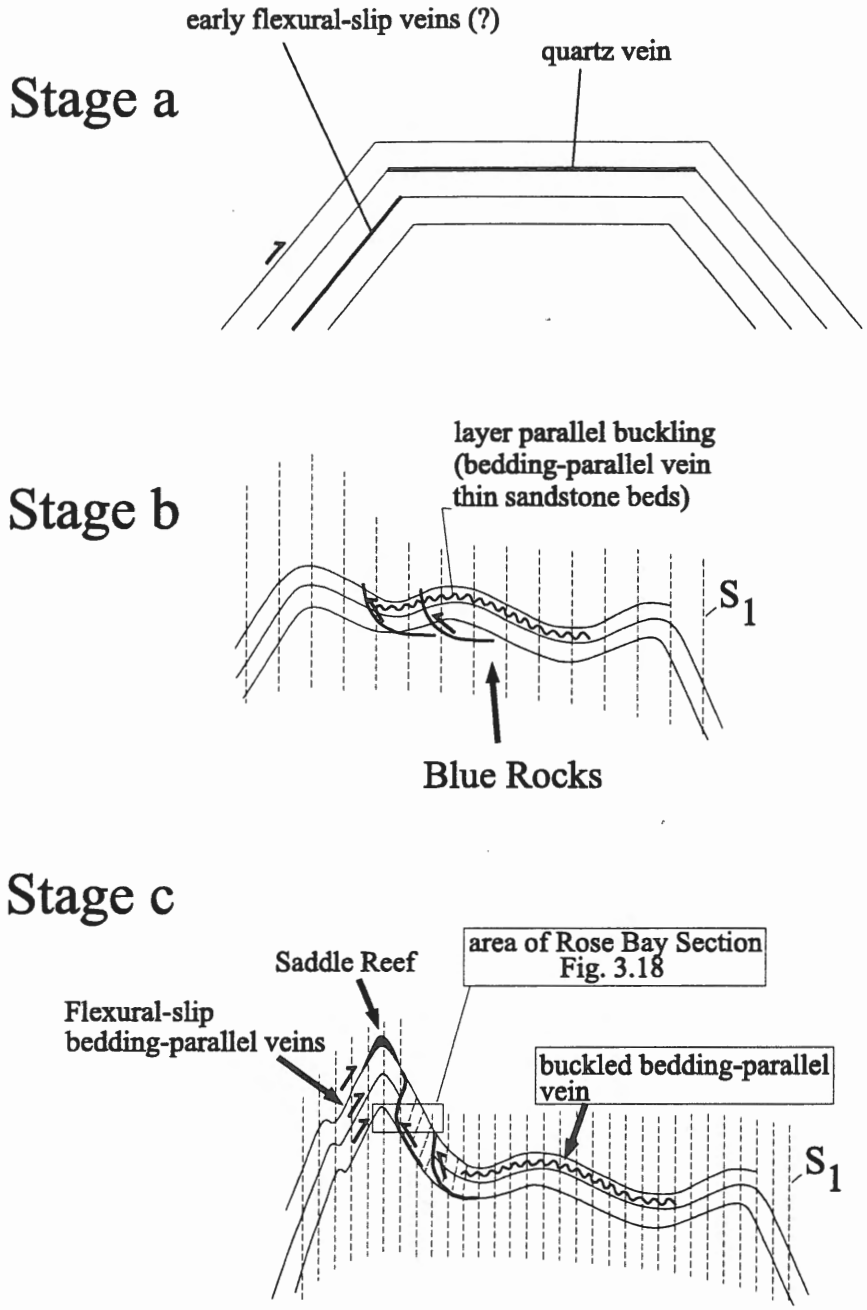

Figure 3.51: Schematic model of fold development constrained by structure in the Ovens area. See text for discussion.

many features discussed it is difficult to understand the complete deformational history of these rocks. However, there are several salient points from the above discussion which must be accommodated, and which therefore constrain a possible sequence of fold development. These include: (1) Flexural-slip was important in late fold development, however accounts for <10° of limb dip; (2) Cleavage pattern in fold hinges implies only minor pre-folding layer-parallel shortening; (3) Minor folds have a synfolding origin, reflecting layer-parallel shortening in the hinge of chevron folds and the flat segments of box folds; (4) Bedding-cleavage relations are consistent with a model of early cleavage formation and flexural-flow; however this is unsupported by synfolding cleavage formation; (4) $^{40}Ar/^{39}Ar$ age data constrain regional metamorphism and early cleavage development to ca. 399-395 Ma. However, they record significant fold-related strain at ca 376 Ma, suggesting episodic deformation; (5) Thrusts represent the flat segment of a box fold emplaced during flexural-slip folding and the preservation of bedding-cleavage relations from low limb dips implies strain was localized along thrusts; (6) Quartz veining accompanied late flexural-slip folding and fluid pressure likely played a significant role in flexural-slip process.

***Folding Model*:**

Fig. 3.51 presents a possible model of fold development for the Ovens based on the above constraints and discussion of this model follows.

Stage a (Fig. 3 .51):

The box-fold and chevron character of regional folds (Fig. 1.4) suggests the earliest stage of folding was represented by the initiation of box folds. This is consistent with the

models of folded multilayered sequences, which follow a box fold to chevron history (chapter 1). Cleavage patterns around fold hinges and the distribution of minor folds imply there was only minor to no layer-parallel shortening (cleavage formation) prior to folding. Bedding-parallel veins may have formed in the flat segments of the box folds, where dilatancy resulted from limb steepening (Fowler and Winsor, 1996). Flexural shear strain on the limbs was likely accommodated by flexural-flow, although some flexural-slip, and veining, may have occurred.

Stage b (Fig. 3.51):

Continued shortening resulted in limb steepening, layer-parallel shortening in the flat hinge of the box fold, which resulted in buckling of thin competent layers and bedding-parallel veins and cleavage development. Cleavage development is interpreted to have been initiated on the limbs as well. This is the major cleavage development stage under regional greenschist metamorphic conditions, the minimum age of which is constrained to ca 395-385 Ma by $^{40}Ar/^{39}Ar$ dating (see chapter 1). Ductile conditions under regional metamorphism probably favoured flexural-flow over flexural slip on the limbs. Thrusting in the flat segments of box folds is conceivable at this time and the thrusting seen in stage c may have been initiated at this time.

Stage c (Fig. 3.51):

Stage c represents the period of flexural-slip folding, with development of the final chevron fold shape observed in the Ovens area. Development of the chevron fold style observed at the Ovens is interpreted to have evolved from the initial box fold, similar to

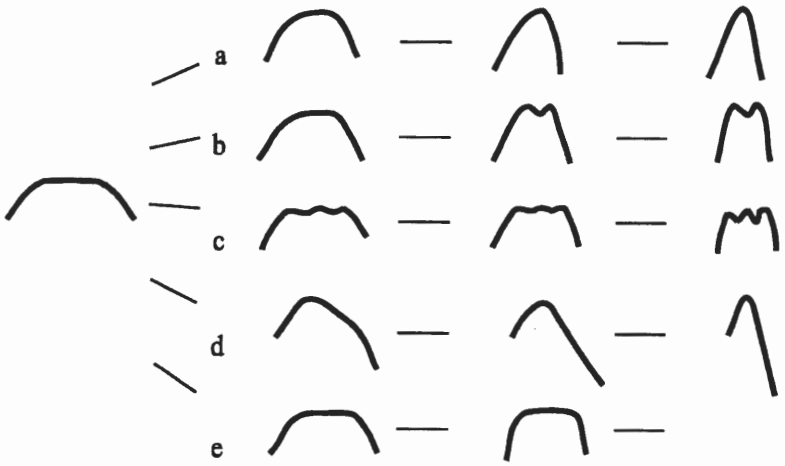

Figure 3.52: Schematic diagram showing possible profile shape changes during boxfold to chevron development. (After Fowler and Winsor, 1996).

examples of chevron development from box folds presented by Fowler and Winsor (1996; Fig. 3.52). The exact history of shape change cannot be known from the study area alone, which includes only a small segment of the resulting chevron, and the geometry of the fold clearly varies along the hinge (compare sections A-B and C-D in Fig. 3.1). The model presented does, however, account for the general fold profile in the area. (i.e., Fig. 3.1).

Flexural slip occurred under brittle (submetamorphic) conditions, implying a probable hiatus in regional deformation between stage b and stage c, during which there was significant uplift and erosion. That cleavage was not forming at this time is indicated by the whole rock $^{40}Ar/^{39}Ar$ age (ca 395 Ma) from within the hinge area (Fig 3.5). However, vertical fold-related extension within the cleavage plane is documented by quartz-muscovite pressure shadows around arsenopyrite porphyroblasts, the age of which is constrained by the age of the muscovite at ca 376 Ma ($^{40}Ar/^{39}Ar$). Similar post-metamorphic ages were indicated in whole rock $^{40}Ar/^{39}Ar$ ages in the area (Muecke and Reynolds, 1978).

Significant shortening and fold-related strain during this late episode of folding is illustrated the by amount of flexural slip and synchronous thrusting recorded. In addition, the distribution of minor folds and late cleavage-parallel strain recorded by pressures shadows reflect syn- (flexural-slip) folding strain. This late strain may include homogeneous flattening during flexural slip. A history of synchronous homogeneous flattening and flexural-slip in formation of chevron folds has been predicted by computer modelling (Fowler and Winsor, 1997).

Although the thrusts are interpreted to have been emplaced during flexural slip, the internal geometry of the thrusts is consistent with an original low limb dip, implying the

thrusts were emplaced late in the flexural-slip history, by which time all the fold-related strain was being partitioned along the thrusts. This would be consistent with the large amount of displacement implied along the thrusts.

A significant number of veins were emplaced during flexural slip and veining likely was important to the flexural-slip process. This is discussed in more detail below.

3.6.4 VEIN EMPLACEMENT AND GOLD MINERALIZATION:

3.6.4.1 Vein emplacement

The above discussion of veins demonstrates that the majority of veins in the Ovens area belong to well defined, systematic, vein sets, including buckled bedding-parallel, flexural-slip bedding-parallel, saddle reef and conjugate discordant veins. Of these, flexural-slip bedding-parallel and conjugate discordant veins account for the majority (~95%) of the veins in the area.

Mutual cross-cutting relationships between flexural-slip bedding-parallel and conjugate discordant veins indicate synchronous emplacement of both vein types. Relationships of flexural-slip and discordant veins with flexural-slip structures associates their emplacement with flexural-slip folding. Saddle reef veins are implicitly related to flexural-slip folding (Ramsay, 1974), which is supported in the Rose Bay area where flexural-slip bedding-parallel veins occurring along movement horizons are laterally continuous with the saddle reef exposed at location RB-6. Saddle reefs, the brittle character of flexural-slip structures, and the degree of deformation of veins, which is consistent with a moderate increment of the folding history, support synfolding vein emplacement late in the folding history.

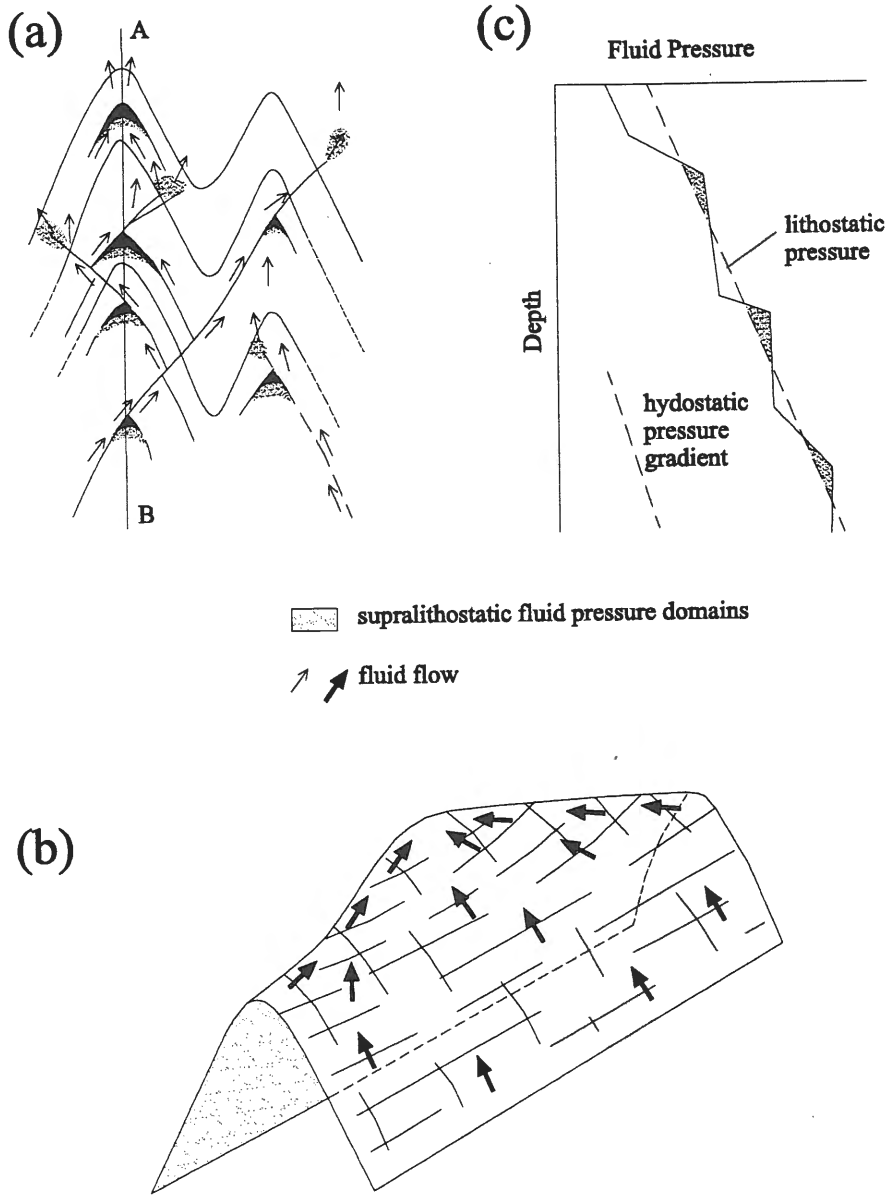

Figure 3.53: (a) Diagram illustrating trapping of fluid in the hinge area of folds. Fluid migrates along bedding-parallel movement horizons during flexural slip and is focused in the hinge, particularly in domes (b). Fluid pressure varies between supra- and sub-lithostatic due to repeated hydro fracturing (c), and results in episodic flexural-slip activity and vein deposition. All Figures after Cox et al., 1991).

Previous studies of the Ovens area proposed an early, pre-folding origin for buckled veins, which were considered to represent the auriferous quartz veins (e.g., Graves and Zentilli, 1982; Henderson et al., 1992). However, as discussed above, buckled veins are here considered to be synfolding, where buckling reflects layer-parallel shortening in the hinge region during folding (i.e., Fig. 3.49). This explains the coexistence of buckled bedding-parallel (early flexural-slip veins) and saddle reef veins (late flexural-slip veins) (i.e., Figs. 3.6c, 3.33). All veins in the Ovens area are here considered to have a synfolding origin.

Abundant concentrations of veins within the hinge area of the Ovens Anticline implies a structural control on their localization, which is consistent with trapping of fluid migrating upward along flexural-slip movement horizons in the hinge zone (e.g., Cox et al. 1991; Fig. 3.53a, b). Fluid trapping would result in cyclic fluid over-pressuring and hydro-fracturing, resulting in episodic high and low fluid pressure (Fig. 3.53c), and may explain synchronous development of bedding-parallel flexural slip and discordant shear veins. This would be consistent with the stick-slip history proposed for flexural-slip. Separation of flexural-slip movement horizons caused by high fluid pressure minimizes shear stress, so that the maximum principal stress lies close to the slip direction. Conjugate discordant shear veins formed at this time will have their intersection (intermediate stress) perpendicular to the movement horizon. Hydro-fracturing and conjugate vein formation would result in release of fluid pressure, thus increasing shear stress on movement horizons, prohibiting slip. High (supralithostatic) fluid pressure determined from fluid inclusions of these veins (Baker, 1996) is interpreted to reflect trapping within the hinge of upward migrating fluid focused along flexural-slip movement horizons. Similar interpretations, relating folding and veining to fluid pressure, have been

proposed by Cox et al. (1991), Cosgrove (1993) and Price and Cosgrove (1990). A genetic relationship between bedding-parallel flexural slip and conjugate discordant veins offers an explanation for the auriferous character of both, as well as the anomalous concentration of both vein sets in the hinge region of the anticline.

3.6.4.2 Gold Mineralization:

The origin of quartz veins is more straightforward than the origin of gold, and this study certainly does not attempt to resolve the genesis of gold. However, given that the gold is undoubtably related to the quartz veins at the Ovens, several constraints can be imposed on the genesis of gold. As stated above, previous studies considered the buckled veins to represent the mineralized veins and distinguished them from other, later vein sets. This is not supported by the results of this study. Buckled veins are here considered part of the synfolding vein array, which include flexural-slip bedding-parallel and discordant veins and, and are restricted to the immediate hinge zone of the fold. Previous mining efforts were concentrated on the north limb of the anticline (Fig. 3.2) where only flexural-slip and discordant veins types occur. In contrast to the idea that one vein set may be responsible for gold mineralization, synchronous emplacement of all vein sets implies a common fluid source for all veins, and therefore similar potential for mineralization. A common fluid for all vein types is supported by the fact that all vein sets are auriferous and other accessory phases, including scheelite and pyrite are common to all vein types. Although only limited sightings of gold were noted, the dominance of flexural-slip and discordant veins suggests these veins are largely responsible for the considerable placer deposits in the near shore areas within and adjacent high concentrations of veins in the hinge area (Fig. 3.2).

CHAPTER 4 DISCUSSION / CONCLUSIONS

4.1 INTRODUCTION:

The previous chapters document the structure, in particular that related to flexural slip, of two areas (Halifax and Ovens) of the Meguma Group. Following is a discussion of the data which will focus on the issues of : (1) the flexural-slip mechanism; (2) fold development in the Meguma Group and; (3) the emplacement of auriferous vein systems in the Meguma Group (Gold Districts).

4.2 FLEXURAL-SLIP MECHANISM:

4.2.1 Introduction:

The flexural-slip process has long been recognized as a folding mechanism and is well understood from a theoretical standpoint. There are, however, few field studies documenting aspects of flexural slip in natural folds. This study indicates that flexural slip was, at least locally, important in fold development in the Meguma Group and provides some fundamental data and observations on the flexural-slip mechanism. The major criteria establishing that structures result from flexural slip, including recognition of movement horizons and determining movement direction and shear sense, have been met. In addition to the basic flexural-slip model (i.e., Fig. 1.5; Tanner, 1989), previously undescribed flexural-slip structures, including lateral ramps and thrusts, have been documented. The first documented account quantifying flexural-slip amount has been presented and veining in the Ovens area has been associated with flexural-slip folding.

The general features related to the flexural-slip mechanism, including movement horizon structures, movement horizon spacing, movement direction, shear sense and slip amount will be discussed here in light of the data from this study. In addition, the age of flexural-slip folding within the Meguma Terrane and how it contributed to regional folding are addressed below in a discussion of fold development.

4.2.2 Flexural-slip structures; a 3-D Flexural-slip model:

In its basic form, flexural slip is a simple process, reflected by bedding-parallel slip perpendicular to the hinge, with displacement of the structurally higher beds toward the hinge (Fig. 1.2). Tanner (1989) presented a model of the flexural-slip mechanism which described various structures developed during flexural slip (Fig. 1.5), and the general aspects of flexural slip have been confirmed by several studies (see chapter 1). In addition to bedding-parallel flexural-slip structures previously documented, this study has recognized lateral ramps, conjugate movement horizons, thrusts and conjugate discordant veins which form a linked system of movement horizons and related structures resulting from flexural slip. This study has also recognized that movement horizons are discontinuous along strike and down dip. The discontinuity of movement horizons and the introduction of non-bedding-parallel movement horizons (lateral ramps, conjugate veins) is not appreciated in simple profile models and therefore a 3-dimensional model (Fig. 4.1) may be more useful.

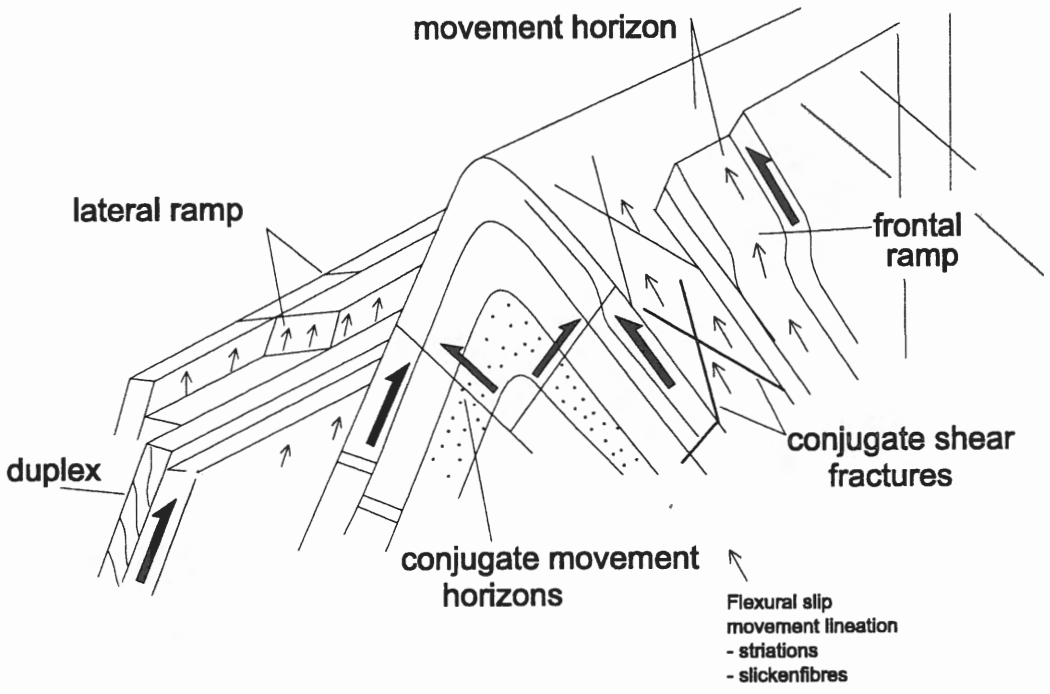

Figure 4.1: Schematic diagram showing the character of structures developed during flexural slip folding in the Meguma Group.

4.2.3 Identification of movement horizon and spacing:

As pointed out in chapter 1, a fundamental limitation on the study of the flexural-slip process is the identification of movement horizons, a concern which clearly extends to the evaluation of movement horizon spacing. Identification of movement horizons is determined by evidence of movement such as striations and slickenfibres and by displacement of planar features (e.g., veins, clastic dykes) which are discordant to the movement horizons. In addition, Tanner (1989) and Fowler and Winsor (1997) consider laminated bedding-parallel veins to represent movement horizons, although others authors interpret a prefolding origin for these same veins (e.g., Fitches et al., 1990; Jessell et al., 1994).

In the railway section, the identification of movement horizons was restricted to striated bedding-parallel surfaces. Many poorly exposed bedding-parallel fractures may indeed represent additional movement horizons. In addition, numerous movement horizons are discontinuous, making evaluation of representative spacing difficult. At the Ovens, bedding-parallel horizons were identified by offset discordant quartz veins and many unidentified, pre-discordant vein, movement horizons may be represented by bedding-parallel veins across which no offset is evident.

Although problems of movement horizon identification plague the evaluation of spacing, data from several studies show similar spacing (Table 4.1; most spacing data falls within the range of 0.5-2.5 metres), suggesting there are general controls governing the development and spacing of movement horizons. Factors which might influence movement horizon spacing include limb dip and lithology, and these are discussed with respect to spacing data presented in this study.

Location / Source	mean spacing (Metres)	Standard Deviation (Metres)	Number
Section A (Halifax)	2.49	2.81	14
Section B (Halifax)	1.97	1.9	36
Section C (Halifax)	1.67	1.12	13
Section D (Halifax)	1.39	1.98	20
Section E (Halifax)	1.19	1.29	32
Section H (Halifax)	4.27	3.76	8
Section C-D (Ovens)	1.09	0.93	63
Chapple and Spang (1974)	0.15 - 0.30		
Borradaile (1977)	0.50 - 0.70		
Kölbel (1949)	0.50 - 0.70		
Tanner (1989)	0.21 - 1.21		
Cloos and Martin (1932)	0.20 - 2.00		
Kenny (1936)	0.80 - 13.00		
Fowler and Winsor (1997)	3.50 - 11.70		
Johnson and Page (1976)	30.00 - 43.00		
Markley and Wojtal (1996)	0. 84	0.57	42
Markley and Wojtal (1996)	0.70	0.40	55

Table 4.1: Table of movement horizon spacing data for the measured intervals in the Halifax area (Sections A-H), the Ovens and several published accounts. (All values given in metres) The majority of the average spacing values, including all except Section H from this study, fall within the .5-2.5 metre range.

4.2.3.1 *Movement horizon spacing:*

General Statement:

Ramsay (1974) suggested that the amount of flexural shear strain is a function of the limb dip (Fig. 1.3a), a relationship which was confirmed experimentally for flexural-slip folds by Behzadi and Dubey (1980) (Fig. 1.3c). Ramsay (1974) also suggested that in flexural folding of layered successions flexural-shear strain is localized within the incompetent layers, and this was supported by finite-element models (Hudleston et al., 1996). Given that strain is focused within the incompetent layers, the thinner the incompetent layer the higher the strain, and strain rate. Localization of flexural-slip strain within incompetent layers is confirmed in studies of natural folds, where movement horizons invariably occur within incompetent horizons, although a relationship to thickness of the incompetent layer is not always evident (e.g., Tanner, 1989; Fowler and Winsor, 1997).

Increasing flexural-slip strain during progressive folding can be accommodated by increased movement along movement horizons or formation of an increasing number of movement horizons. As discussed by Fowler and Winsor (1997), simplistic models of flexural slip assume simultaneous slip on uniformly spaced movement horizons (e.g., experimental buckling of multilayered models where slip is promoted between layers). Tanner (1989), however, documented decreasing movement horizon spacing with increasing limb dip (decreasing interlimb angle), suggesting that this resulted from formation of new movement horizons, between those previously developed, during progressive folding, in order to accommodate increasing shear strain. This was supported by Fowler and Winsor (1997) who documented no relationship between vein thickness (which they correlate with slip amount)

in natural folds or the amount of slip (determined in computer models) and the distance to neighbouring movement horizons. They interpreted this to demonstrate progressive formation of new movement horizons throughout the folding history.

Tanner suggested a relationship between movement horizon spacing and lithology, where the spacing is wider in sequences with thick competent units, within which movement horizons cannot develop. He suggested the lack of newly formed movement horizons in such sequences is accommodated by increased slip on movement horizons This is supported in his study by increased thickness of laminated slickenfibres veins. Fowler and Winsor (1997) found similar results to Tanner for in folds in Australia, where they documented movement horizons within incompetent layers, and where there is a general relationship between vein thickness and spacing.

The studies of Tanner (1989) and Fowler and Winsor (1997) demonstrate a relationship of movement horizon spacing consistent with increasing shear strain which is focused within incompetent layers during folding. However, as noted by Tanner (1989) a quantitative evaluation of movement horizon spacing with respect to limb dip and lithology is hindered by a lack of documented studies which have quantified the amount of flexural slip or evaluated the contribution of flexural flow to flexural-shear strain.

This study

A graph of mean movement horizon spacing against limb dip for each measured interval in the railway section and the measured section in Cunard Cove is shown in Fig.4.2a. At first appraisal this graph does not seem to indicate any straightforward relationships. However, if lithology is considered, a relationship is apparent. Sections A-E, from the slate-

metasandstone lower unit of the railway section and the Ovens (Cunard Cove) section, show a good correlation between spacing and limb dip, with spacing decreasing with increasing limb dip. Sections F and H are from the slate-dominated upper unit along the railway section and, although there are only two points, they show a similar relationship between spacing and limb dip. Indeed, the slope defined for both lithologic groups is similar, with the slate dominated upper unit having larger movement horizon spacing than the slate-metasandstone lower unit for equivalent limb dip. These data suggests movement horizon spacing is controlled by both limb dip and lithology.

Movement horizon spacing in the Halifax area suggests a relationship between spacing and lithology opposite to that suggested by Tanner (1989), with the wider spacing occurring in the slate-dominated upper unit rather than the slate-metasandstone lower unit; for comparable limb dips (Fig. 4.2a). The wider spacing of movement horizons within the slate-dominated upper unit may reflect greater amounts of slip on individual movement horizons, although this clearly does not reflect the presence of thick competent layers as suggested by Tanner (1989). Another interpretation for the variation of spacing between lithologic units may be related to *strain rate* within the incompetent layer, which may influence whether shear strain is accommodated by flexural-flow or flexural-slip. During folding, there will be a higher *rate* of shear strain within the thin slate intervals in the slate-metasandstone lower unit compared with the thick slate intervals in the slate-dominated upper unit. The higher strain rates within the thin slate intervals are more likely to result in flexural slip whereas lower strain rates within the thick slate intervals are more likely to be accommodated by flexural flow. Similar interpretations regarding movement horizon spacing and lithology were

(a)

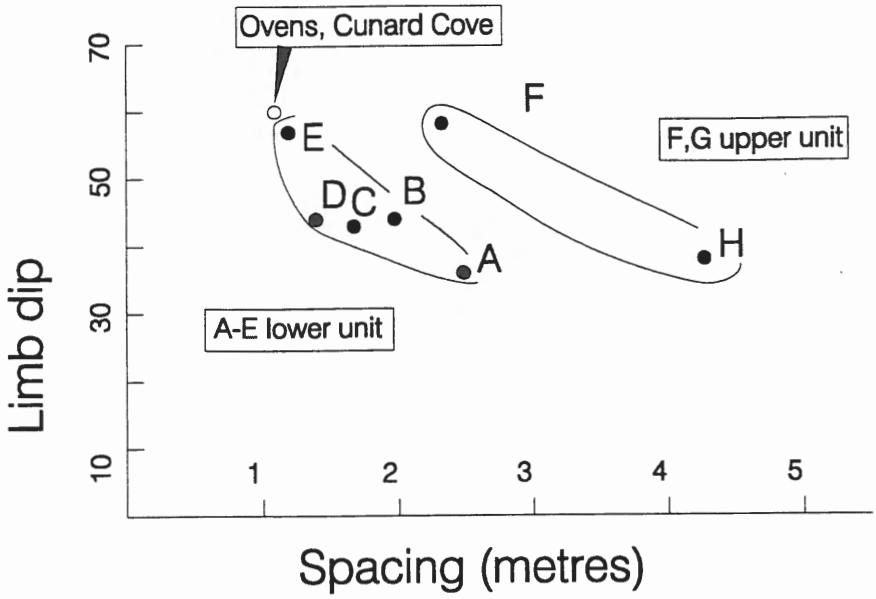

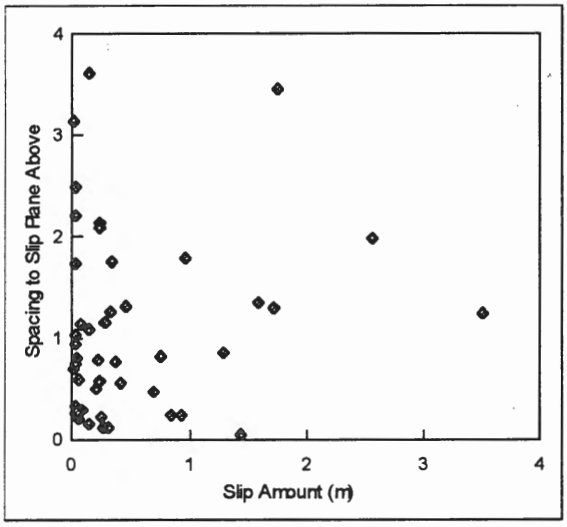

(b)

Figure 4.2: (a) Graph of movement horizon spacing against limb dip for the measured intervals of the Halifax study area (see Fig 2.4, in pocket at back) and the Ovens area (see Fig. 3.5). (b) Graph of slip amount (corrected value) against distance to the movement horizon above for the two intervals in Cunard Cove where slip amount was determined (see Fig. 3.15).

presented by Fowler and Winsor (1997).

A combination of spacing data and slip amount for the Cunard Cove area (Section C-D) allows for a test of the relationship between movement horizon spacing and slip amount proposed by Fowler and Winsor (1997), which was based on the assumption that vein thickness correlated with slip amount. A plot of slip amount against distance to the slip plane above shows no correlation and a dominance of movement horizons with a small slip amount (Fig. 4.2b), similar to the data presented by Fowler and Winsor (1997). These results, therefore, support the conclusion of Fowler and Winsor (1997) of progressive movement horizon development, with the small slip on most horizons reflecting the changing thickness of interval between slip horizons.

Table 3.1 indicates that the mean slip amount along flexural-slip duplexes in Section C-D, Cunard Cove, is approximately six times the average slip amount for simple movement horizons, and it was suggested above that flexural-slip duplexes develop from simple movement horizons. The increased displacement on duplexes implies they formed early and were active for much of the flexural-slip history. Flexural-slip shear strain is uniform for the two intervals of the Cunard Cove section where slip amount was determined, and flexural-slip duplexes are regularly spaced through the section (Fig. 3.15). This suggests regular spacing of early formed movement horizons (duplexes) with progressive development of existing movement horizons and continuous formation of new movement horizons during folding. Such a history of flexural-slip development accounts for the uniform flexural-slip strain recorded at the scale of the intervals measured and the random relationship of slip amount between neighbouring movement horizons. These observations are similar to those in the

Halifax area (railway section), where continuous movement horizons are regularly spaced and separate minor discontinuous movement horizons.

As noted above, Tanner (1989) and Fowler and Winsor (1997) suggest a relationship between slip amount and vein thickness. The largest displacements in the Ovens area, however, occur along duplex structures where slickenfibre sheets and laminated veins are thin and, as described above, flexural-slip veins tend to pinch and swell. In the Halifax area, although slickenfibres are common, laminated veins are uncommon along movement horizons. Vein thickness, therefore, is not considered a reliable estimate of displacement in the areas studied. A relationship between vein thickness and displacement is reasonable if veins develop by a process of accumulated slickenfibre growth. However veins are commonly composite and may form by various mechanisms. In general, vein thickness is presumably a function of the amount of fluid introduced, and of mechanisms for trapping fluids and precipitating minerals from fluids.

Movement horizons in both the Halifax and Ovens areas are restricted to slate intervals and, although not quantified, most occur near the contacts between metasandstone and slate layers (Figs. 2.4, in pocket at back, and 3.5). Location within slate intervals is consistent with partitioning of strain within this lithology. Occurrence of movement horizons near lithologic boundaries was also noted by Tanner (1989) and Fowler and Winsor (1997), which the latter authors suggest reflects competence contrast at lithologic boundaries.

The results of movement horizon spacing of this study are generally consistent with other studies and suggest the following:

(1) Flexural slip is largely partitioned into the incompetent layers and is controlled by limb dip

and thickness of incompetent layers.

(2) Incremental flexural-slip folding is accommodated by the continued development of new movement horizons between earlier formed movement horizons, resulting in a population of movement horizons dominated by low slip amounts.

(3) Large slip amounts occur on regularly spaced movement horizons and result in the formation of continuous movement horizons and flexural-slip duplexes.

4.2.4 Movement Direction:

In the simplest case, flexural slip occurs perpendicular to the fold hinge (Fig. 1.2). Several studies of flexural slip in natural folds have shown there is significant variation in movement direction. However, the average (net) movement direction is close to the perpendicular to the fold hinge and therefore consistent with the flexural-slip mechanism (eg., Tanner, 1989; Markley and Wojtal, 1996; Fowler and Winsor, 1997; Price and Cosgrove, 1990). These observations are similar to the results of this study, where there is considerable variation in trend, although the average orientation is related to the fold geometry.

Variation in movement lineation trend in this study and others is recognized on single movement horizons and between movement horizons. An example of variation from different locations on a single movement horizons is shown in Fig. 2.12. Significant variation has also been noted at a single location of a movement horizon (e.g., see Fig. 15.23, Price and Cosgrove, 1990). Variation in movement lineations has also been noted between different movement surfaces contained within bedding-parallel (flexural-slip) quartz veins, associated with many of the Meguma Gold Districts (Mike Corey, personal communication; Henderson

and Henderson, 1986; Paul Smith, personal communication; and personal observation by the author). The cause of the variation in slip orientation observed is not well understood, although it may reflect irregularity in the movement surface, as suggested in the Halifax area (see above). Price and Cosgrove (1990) suggested that variation in the movement lineation reflects episodic slip, resulting from migration of fluids responsible for movement, with a change in stress orientation from one slip event to the next. Also, the discontinuous nature of movement horizons observed could result in variation in slip orientation, as well as amount, along the movement surface.

The net trend of lineations for all the movement horizon types observed (i.e., bedding-parallel, lateral ramps, frontal ramps, conjugate shears, thrusts, duplexes) is similar for any area and location within the fold, and consistent with a flexural-slip origin. The net movement lineation is not exactly perpendicular to the fold hinge in either the Halifax or Ovens study areas. However, it is related to the fold geometry (dip azimuth) in the Halifax area and in both areas the average trend makes an acute angle with the trend of the fold hinge. As noted above, this likely reflects hinge propagation during non-cylindrical flexural-slip fold growth (e.g., Fig. 3.48).

4.3 FOLD DEVELOPMENT:

4.3.1 Introduction:

A model was presented above for development of the Ovens Anticline which included formation of box folds and chevrons. A complex fold-related strain history is recorded, including synfolding cleavage formation accompanying flexural flow and flexural slip on the limbs and layer-parallel shortening in the angular hinges of chevrons and flat tops of box folds. Folding spanned a long interval, overlapping regional metamorphic (ductile) and submetamorphic (brittle) conditions, and may be episodic in nature. The following discussion will address the application of the Ovens model to the Meguma Group in general.

4.3.2 Box Fold development:

As noted above, cross-sections of the Meguma Group are characterized by distinctive box-folds and chevrons (Fig. 1.4). Although there is undoubtably some error in the many sections published by E.R. Faribault, the general character implied by these sections is considered to be representative of the fold style and has been confirmed in recent studies (e.g., Horne et al., 1998). Stratigraphy is generally conformable and does not suggest regional-scale thrusts accompanied folding. This is supported by the lack of vergence shown by axial planes. The fold profile is similar to profiles of other areas characterized by box folds and chevrons and also consistent with computer and experimental studies of buckled multilayered sequences (e.g. Fig 1.1; see chapter 1) .

Box folds and chevrons are characterized by straight limbs and angular hinges, where fold development is dominated by flexural folding. This is consistent with the results of this

study and those of Henderson et al. (1986) and therefore it is reasonable to assume that flexural folding is important throughout the Meguma Terrane.

4.3.3 Minor folds and cleavage development:

The discussion of cleavage in the Ovens area proposes a syn-folding origin for cleavage development based on cleavage patterns around fold hinges and the distribution of minor folds across the fold. These features will be discussed with respect to folds in general within the Meguma Terrane.

Minor folds:

It was argued that minor folds at the Ovens have a synfolding origin on the basis that they are restricted to fold hinges, where layer-parallel shortening accompanied limb steepening during folding (i.e., Fig. 3.50b). A similar explanation was proposed by Williams and Hy (1990) who suggested that folding of bedding-parallel veins in the hinge region and not on the limbs reflects the fact that " the veins would be in a vein-parallel shortening orientation in the regional fold hinges throughout the folding history". This proposal is also consistent with results from the Goldenville Formation presented by Fueten (1984), who illustrated more intense cleavage-related strain in the hinge zone compared to the fold limbs for the Ruth Falls Syncline.

Documentation of minor folds throughout the Meguma Terrane is mainly limited to buckled bedding-parallel veins and there is little consensus on the distribution of minor folds with respect to regional folds. Henderson et al. (1986; 1987; 1988), Henderson and Henderson (1986) and Graves and Zentilli (1982) suggest minor folds exhibited by these veins

are parasitic to the main fold, extending down the fold limbs, reflecting a prefolding origin for the minor folds. In contrast, Williams and Hy (1990) state that bedding-parallel veins are "generally much more strongly and more periodically folded in regional fold hinges than in regional fold limbs". This observation is supported by Paul Smith (personal communication) who indicated that minor folding of bedding-parallel veins is more common in the hinge than on the limbs of major folds. The most exhaustive evaluation of the distribution of minor folds exhibited by bedding-parallel veins is that presented in Faribault (1913) and Malcolm (1929), where extensive studies by E.R. Faribault were based on observations of fold structures in many gold districts, to which subsequent workers have had limited access. These reports clearly indicate a relationship between the fold hinge and minor folding, stating that "corrugations or crenulations, usually occur at or near the apex of the anticline and sometimes the syncline" and that " the nearer the veins lie to the anticlinal axis the more pronounced the corrugations become". Localization of minor folds within the hinge zone of regional folds is supported by illustrations of these folds in previous reports, which are clearly from fold hinges (e.g., see Fig. 1 in Henderson et al., 1988; Fig. 4 in Henderson et al., 1986; Figs. 4, 5 in Graves and Zentilli, 1982; the many illustrations in Malcolm, 1929 which have been reproduced by several subsequent authors). This fact seems to have been recognized even by Henderson et al. (1986), as they illustrate that minor folds are restricted to the hinge area of regional folds in a schematic profile section of a fold (i.e., Fig 1.7).

The above examples are largely from local fold hinges. In the Ovens area it was noted that evidence of layer-parallel shortening also occurs in the broad, flat segments of box folds now locally occurring within thrusts in Rose Bay, although absent on the steep limbs. It is

worth noting that the study of Henderson et al. (1986), which infers layer-parallel strain to be of pre-folding origin, was conducted mainly from the flat segments of such folds (i.e., Blue Rocks), where it is difficult to distinguish syn- or post-folding layer-parallel shortening. The general lack of similar layer-parallel-shortening on steep limbs, however, supports a syn-folding origin for minor folds.

Bedding-cleavage relations:

As discussed above, Henderson et al. (1986) proposed a history of cleavage formation and folding involving early, pre-folding, cleavage development with flexural flow accounting for all flexural-shear strain (Fig.1.7b). This model is similar to the results of finite-element modelling by Hudleston et al. (1996) where flexural flow in a mulitlayerd sequence is accomplished by excess shear in the incompetent layers. It was shown above that bedding-cleavage relations at the Ovens are consistent with a flexural-flow model when limb dip is considered with respect to the interlimb angle. However, as shown by Treagus (1988), there is little difference between the X direction of finite strain and the direction of sheared early-formed cleavage, and this discrepancy decreases with increasing strain. Therefore, bedding-cleavage relations cannot be used as a test for flexural flow. Indeed, a synfolding origin for cleavage, indicated by cleavage pattern in fold hinges and the distribution of minor folds, is not consistent with the flexural flow model of Henderson et al. (1986).

Similar bedding-cleavage angles on both limbs at the Ovens are not consistent with a simple flexural-flow model (i.e., Fig 3.50a). It is possible that the fold formed as an upright fold and was later tilted. However, similar bedding-cleavage relations have been documented

for other inclined folds in the Meguma Group, including the Lawrentown Anticline (Fig. 2.2) and the Waverley Anticline (Horne et al., 1998), and similar relations have been documented for inclined folds in Australia (see Fig. 2 of Yang and Gray, 1994; Fig 5 of Boulter ,1979), which in some instances verge in opposite directions. The Meguma Group is characterized by pairs of opposite verging folds (Fig. 1.4) and no examples of asymmetric cleavage fans have been documented. It is worth noting, therefore, that the study of Henderson et al. (1986) addressed only upright folds and their conclusion that bedding-cleavage relations versus limb dip reflect flexural-flow strain would not explain the more general asymmetric fold pattern in the Meguma Group. The above discussion is consistent with an hypothesis where bedding-cleavage relations reflect syn-folding cleavage development, with cleavage planes oriented parallel to the axial plane of the fold.

4.3.4 Flexural slip and flexural flow:

Evidence of flexural slip has been locally documented throughout the eastern Meguma Terrane (Smith, 1976; O'Brien, 1983; Keppie, 1976; Faribault, 1899; 1913; Douglas, 1948). The majority of these studies addressed Meguma Gold districts, interpreted here to reflect veining during late flexural-slip folding (see below), with flexural slip occurring within slate layers in the metasandstone-dominated Goldenville Formation. Faribault (1899) describes layer-parallel slip due to flexural-slip folding as brittle in character, defined by "striations and slickensides ... and crushed black slate between the walls", consistent with observations at the Ovens. Similar observation have been made by the author at several Meguma Gold Districts (Renfrew, Oldham, Tangier) and regionally throughout the central part of the Meguma

Terrane. Although documentation is only qualitative, it seems clear that late, brittle, flexural-slip folding was widespread throughout the Meguma Terrane.

Although I have questioned the general hypothesis of Henderson et al. (1986) that cleavage development predates folding and that and that bedding-cleavage angles reflect rotation of cleavage by flexural flow, flexural flow was clearly important. In particular, en echelon veins demonstrate that flexural-flow locally accounts for much of the folding (Henderson et al., 1986).

4.3.5 Timing of folding:

A two stage deformational history is proposed at the Ovens, including: (1) Early folding and cleavage development during regional metamorphism, recorded by $^{40}Ar/^{39}Ar$ whole rock ages of ca 395-399 Ma, interpreted to reflect cleavage-related mica growth during metamorphism, and; (2) Late fold reactivation reflected by flexural-slip folding and associated cleavage-parallel strain, which is constrained by $^{40}Ar/^{39}Ar$ dating of muscovite from pressure shadows around arsenopyrite at 376 Ma. These age data are significant as they demonstrate that folding spans a long period and also that the $^{40}Ar/^{39}Ar$ age of early cleavage has not been affected by significant, late, fold-related strain, which is recorded only by new mineral growth. A similar observation was made in the Yarmouth area, where significant Carboniferous age shear-related strain recorded by $^{40}Ar/^{39}Ar$ ages for muscovite in strain shadows is only partially evident in some whole rock $^{40}Ar/^{39}Ar$ spectra where complete recrystallization of fold-related cleavage due to shear-related strain was suspected (Culshaw and Reynolds, 1997).

Evidence that flexural slip reflects late fold reactivation is also demonstrated in the Halifax area, where porphyroblasts related to the ca. 370 Ma South Mountain Batholith are deformed by flexural-slip structures (Figs. 2.8 and 2.15a). Significant cleavage-parallel strain associated with late flexural-slip folding is supported by strain shadows around prophyroblasts which are consistent with fold-related strain (Fig. 2.15a), and may reflect syn-folding homogeneous flattening.

Regionally, the age of cleavage formation is constrained to the interval ca. 410-385 Ma throughout the Meguma Terrane by whole rock and mineral $^{40}Ar/^{39}Ar$ ages (e.g., Keppie and Dallymer, 1987; Muecke et al., 1988; Hicks et al., in press; Kontak et al., 1998). That the age of regional metamorphism is close to the cooling ages reflected by the $^{40}Ar/^{39}Ar$ data is indicated by the fact that deformation affects only slightly older rock units (Torbrook Formation). As stated above, the range in $^{40}Ar/^{39}Ar$ ages constraining regional metamorphism have been interpreted to possibly reflect diachronous deformation across the Meguma Terrane (Keppie and Dallmeyer, 1987; Kontak et al., 1998).

Aside from the evidence from this study, there is no direct evidence indicating that late flexural slip observed throughout the Meguma Terrane represents regional fold reactivation at ca 370 Ma. Indirect evidence is, however, provided from a study of the age of regional metamorphism and veining within Meguma Gold Districts, where a similar episodic history of folding as shown at the Ovens is suggested. Studies of Kontak et al. (1990; 1993; 1998) have demonstrated that $^{40}Ar/^{39}Ar$ ages for vein minerals (mica and amphibole) constrain the age of veining to ca 373-375 Ma, whereas regional metamorphic ages for the same deposits are constrained to ca. 382-387 Ma by whole rock $^{40}Ar/^{39}Ar$ dating of wall rock adjacent the

veins. The emplacement of quartz veins in Meguma Gold Districts is considered to reflect late flexural-slip folding as at the Ovens (see below), and therefore these age data support a similar and synchronous folding history to that proposed at the Ovens. Kontak et al. (1998) propose that the lack of thermal overprinting of regional metamorphic ages by the hydrothermal veins, which formed from fluids at 400-450°C (Graves, 1976; Kontak et al. 1988; Kontak and Smith 1989; 1993), higher than that required for Ar diffusion, indicate significant thermal disequilibrium between vein fluids and wall rock. This is consistent with the change from ductile conditions during regional metamorphism to brittle conditions recorded by flexural slip, and supports a possible hiatus between early deformation and late fold tightening, during which uplift and erosion depressed the brittle-ductile boundary below the current level of exposure of these deposits. However, if the $^{40}Ar/^{39}Ar$ age data constraining regional metamorphism reflect diachronous deformation, then the late flexural slip documented herein may simply reflect the latest period of continuous Middle- to Late-Devonian deformation.

Late Devonian fold tightening is, in general, consistent with regional transpression recorded throughout the Devonian to Permian history of the Meguma Terrane (see Chapter 1). Specifically, a late Devonian event is coincident with intrusion of significant amounts of granite throughout the Meguma Terrane and emplacement (tectonic?) of the Liscomb Complex. Regional strain within the South Mountain Batholith reflects syntectonic emplacement under regional northwest-directed compression (Horne et al., 1992, Benn et al., 1997) coincident with the age of fold reactivation indicated here. The regional character of this syntectonic magmatic event and emplacement of the Liscomb Complex implies a

significant, deep crustal tectonic event at that time. The nature of this event is not well understood, mainly due to the lack of exposure of basement rocks, and different hypothesis have been proposed, including: obduction of the Meguma Terrane over the Avalon Terrane with thermal rebound following depression of the lithosphere (Keppie and Dallymer, 1987); subduction of the Avalon under the Meguma Terrane resulting in under- and intra-plating of subduction-generated mafic magma which caused production of granitic magma (Clarke et al., 1993) and; delamination of the lower lithosphere (Keppie and Dallmeyer, 1995). Regardless of the style of tectonism, a regional tectonic-magmatic event at ca 370 Ma provides an explanation for widespread regional fold reactivation discussed herein.

4.3.6 Summary:

The above discussion indicates that the features used to constrain the model of folding presented for the Ovens are common throughout the Meguma Terrane, suggesting a complex history of folding and related strain. These observations imply that the finite strain within the Meguma folds reflect contributions from flexural flow, flexural slip, tangential longitudinal strain (and inverse tangential longitudinal strain) and layer-parallel shortening, with the contribution of each likely varying throughout the fold profile. Similar interpretations for development of chevrons in layered, low grade metasedimentary sequences in Australia have been presented by Boulter (1979) and Yang and Gray (1994). Unravelling the deformational sequence related to folding is difficult without precise strain and age data throughout the folds. However, several generalities regarding fold development can be made from the above discussion, which support a general model similar to the one presented above for the Ovens

area.

(1) Folding reflects the formation of regional-scale box folds, consistent with the high degree of anisotropy induced by the character of stratigraphic layering. Fold evolution followed a sequence of box fold to chevron development and folding of the flat segments of box folds.

(2) Cleavage has a syn-folding origin and formed during regional metamorphism constrained to the period of ca.410-385 Ma.

(3) Fold-related strain on the limbs was dominated by flexural shear. Flexural flow is evidenced by sequential development of en echelon veins and was likely important in the early fold growth during regional metamorphism. Significant late flexural slip is at least locally important and represents a period of post-metamorphism fold growth.

(4) Flexural slip was accompanied by significant cleavage modification, indicted by cleavage-parallel strain.

(5) Fold-related strain in fold hinges is represented by layer-parallel shortening resulting in buckling of stratigraphy and bedding-parallel veins. In addition, local strain patterns reflect tangential longitudinal strain in metasandstone and inverse tangential longitudinal strain in slate.

(6) Fluid flow during flexural-slip folding is evident by slickenfibres and local quartz veins along flexural-slip movement horizons and related discordant fractures, and fluid pressure was likely important in the flexural-slip process.

4.4 GOLD DEPOSITS:

4.4.1 Introduction:

As discussed in the introduction, there is no consensus on a model for the formation of the quartz-gold veins which define the numerous Meguma Gold Districts, with various models ranging from pre-folding to late-folding. Convincing evidence presented above favours a flexural-slip (saddle-reef) model for emplacement of the auriferous veins at the Ovens. In light of the fact that the Ovens provides the only extensive exposure of a Meguma Gold deposit available to workers over the past half century, and the fact that the Ovens deposit shares many common features with most other deposits, an evaluation of the flexural-slip model as a general model for Meguma Gold deposits is discussed. Discussion will focus on explaining several well established, or apparent, key elements which are common to many deposits which must be accounted for in interpreting the origin these deposits.

4.4.2 Distribution of deposits:

It has long been recognized that the majority of Meguma gold deposits are localized in anticlinal hinges, in particular the culmination of non-cylindrical folds (domes; Fig. 4.3; Faribault, 1899). In plan view, veins define elliptical patterns outlining domes. In cross section, the deposits illustrate a clear relationship between the location of auriferous veins and fold geometry. Veins occur primarily in two structural environments of folds: (1) symmetrically arranged over steep chevrons and; (2) asymmetrically arranged on box-type folds, where veins are concentrated on steep limbs (Fig. 4.4; also see the many cross sections

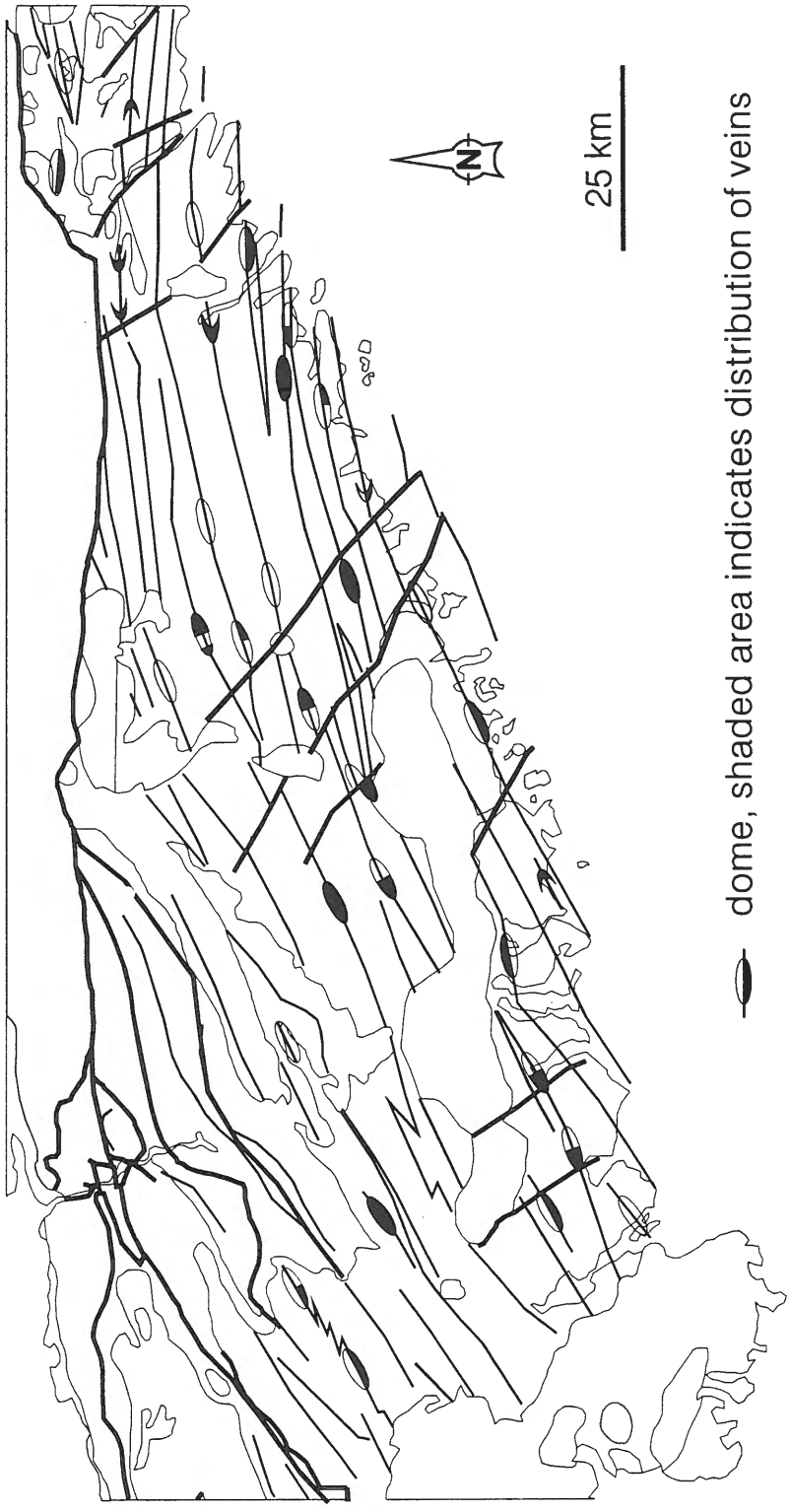

Fig. 4.3: Simplified map of the eastern part of the Meguma Terrane showing the correlation of Gold Districts with domes. (After Fletcher and Faribault, 1911).

Figure 4.4: Cross sections of regional folds within the Meguma Terrane showing the distribution of auriferous quartz veins (thick lines), which are concentrated on steep fold limbs. (a) and (c) after Faribault (1909) and (b) after Faribault (1908b).

of various "Gold Districts" maps by E.R. Faribault). The location of auriferous veins in the plan and section maps is known only from historical mine plans published mainly by E.R. Faribault. The distribution of veins presented by Faribault is supported by some recent authors, who suggest that, generally, bedding-parallel veins are concentrated within fold hinges and thin down-dip where they eventually terminate (e.g., Keppie, 1976; Mawer, 1987; Williams and Hy, 1990). Others, however, suggest that bedding-parallel veins do not thin out down dip and presumably extend through synclines (e.g.; Fig 1.7; Henderson et al., 1986; Henderson et al., 1988). Given that no significant exposure of these deposits has been presented since the historical maps produced by Faribault, it seems reasonable that the distribution of veins should be addressed from these records. The distribution of veins on Faribault's maps is supported by the fact that their recognition was based principally on their discovery for economic exploitation, which imposes no scientific bias.

The similarity of vein distribution within the fold structure of most Meguma Gold deposits implies a control on distribution related to fold development, and an explanation for these observations is central to a general model for these deposits. Proponents of bedding-parallel vein formation prior to folding have suggested the distribution of veins within domes reflects the mechanical influence of quartz veins on fold development (Graves and Zentilli, 1982; Henderson et al., 1990). Although the presence of prefolding veins may influence the location of instabilities leading to folding, it would be extremely fortuitous that the distribution of prefolding vein arrays would so regularly occur as to result in the regular distribution of folds.

A more plausible explanation for the distribution of deposits within domes and the

occurrence of veins on steep fold limbs is that localization of veins was influenced by existing fold structures, consistent with the flexural-slip model presented for the Ovens. The occurrence of veins within domal structures is clearly consistent with a flexural-slip model, reflecting migration of fluid along flexural-slip structures and concentration in the structural trap formed by the fold hinge (i.e., Fig. 3.53). A similar interpretation was advanced by Faribault (1899) and Mawer (1987). The occurrence of veins on steep limbs is also consistent with vein emplacement along flexural-slip movement horizons, which develop in response to high layer-parallel shear strain, especially at high limb dips (Fig. 1.3b). Thus, within tight chevrons, which have two steep limbs, veins occur symmetrically about the fold on both limbs, whereas on box folds, veins are restricted to steep limbs and are largely absent on the flat, median segments. A simplified diagram showing the general distribution of quartz veins on steep fold limbs is shown in Fig. 4.5. This diagram implies stacking of veins, similar to the proposal of Faribault (1899). If veins had a pre-folding origin they would be expected to occur on the flat segments of these box folds in equal proportion to the limbs. The consistent distribution of veins on steep limb implies veining postdates any significant hinge migration related to fold development, supporting late vein emplacement.

4.4.3 Host of veins:

It is well established that bedding-parallel quartz veins in Meguma gold deposits are localized within slate intervals of slate-metasandstone sequences (Faribault, 1899; Malcolm, 1929; Graves, 1976; Graves and Zentilli, 1982; Henderson and Henderson, 1986;

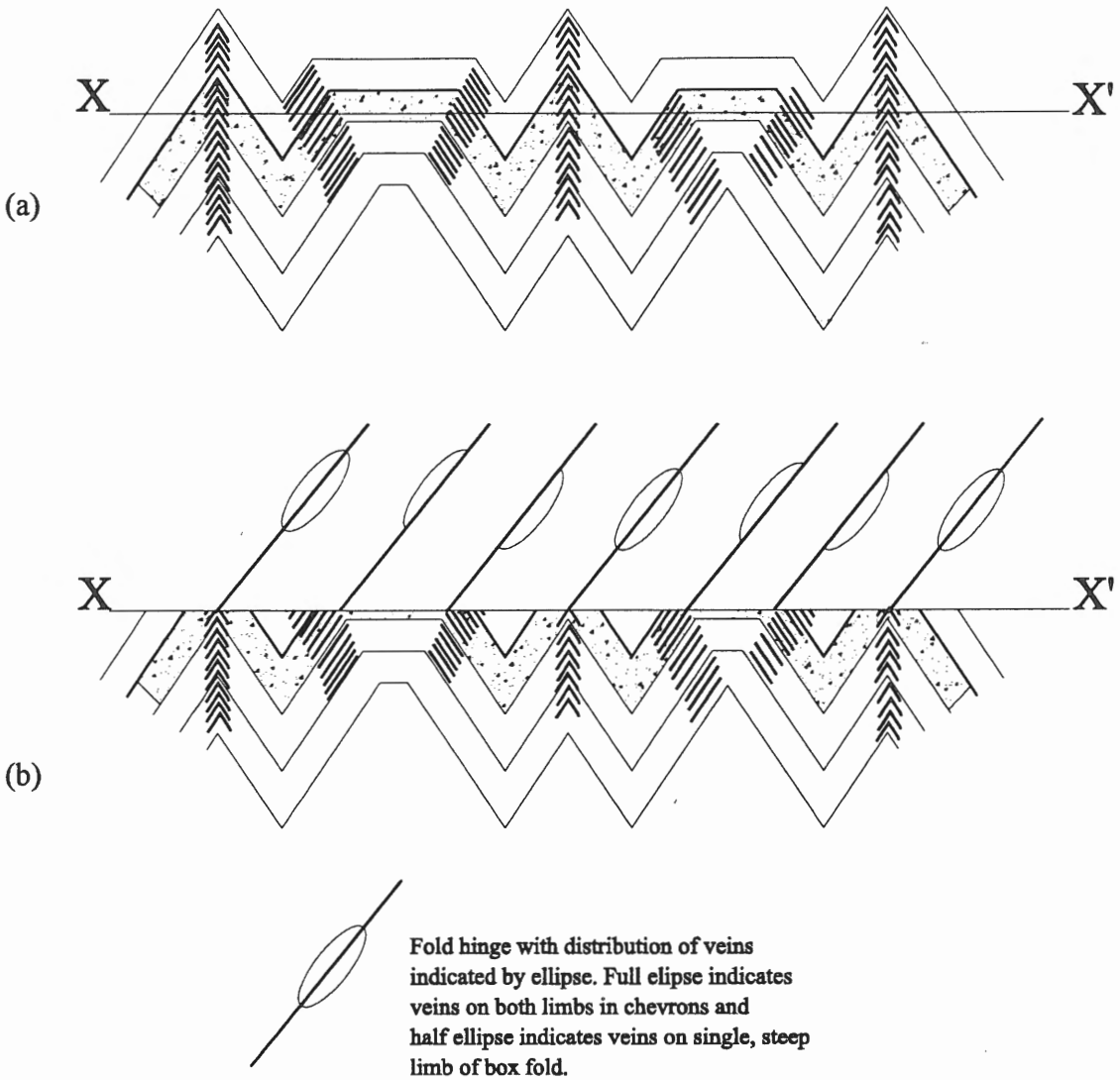

Figure 4.5: (a) Diagram of idealized chevrons and box folds showing the distribution of veins emplaced within flexural-slip structures reflecting high shear strain on steep limbs. (b) Diagram illustrating the distribution of auriferous veins at erosional level X-X'. The vein distribution is similar to that in many gold districts (Fig. 4.3), where vein arrays occur on steep limbs.

Sangster, 1990). Henderson and Henderson (1986) state bedding-parallel veins typically occur "at or near the top of ... Bouma cycle" and also "between thick amalgamated metawacke beds", Sangster (1990) states these veins occur " within or immediately below the upper margins of incompetent, impermeable argillite horizons...", Graves and Zentilli (1982) state that veins occur "within or at either margin of a slate bed", and Faribault (1899) states "quartz veins follow layers of slate, especially when the slate is intercalated between thick beds of hard quartzite". Similar observations have been made in the deposits of the Victoria gold fields in Australia (e.g., Windh, 1995; Cox et al., 1995; Fowler and Windsor, 1997).

As discussed above, flexural shear strain is localized within the incompetent (slate) layers and therefore the occurrence of bedding-parallel veins within slate intervals is entirely consistent with a flexural-slip origin. Higher strains will occur where incompetent layers are thin, resulting in a greater tendency for movement horizons to develop, which may explain the general occurrence of Gold Districts within the Goldenville Formation (Fig. 1.4). As noted above, Fowler and Winsor (1997) attributed the common occurrence of flexural-slip veins at facies boundaries to the high "competence contrast at these boundaries, favouring shear failure".

4.4.4 Movement horizons and lineations:

Evidence of movement along bedding-parallel veins and within slate intervals hosting veins is common within the Meguma Gold deposits (Faribault, 1899; 1913; Douglas, 1934; Henderson and Henderson, 1986; personal observations at Renfrew, Oldham, Tangier) and has been discussed above. Faribault (1899) and Douglas (1948), in particular, emphasized the

importance of movement horizons formed during folding (flexural slip) to the emplacement of bedding-parallel veins, supporting a general flexural-slip model for these deposits.

4.4.5 Relationship of veins to deformation and the age of veins:

The interpretation of bedding-parallel veins as pre-dating folding is based primarily on the structural character of buckled veins and arguments related to the relationship of veins to deformation. Critical observations presented include the intense folded character of some bedding-parallel veins (Henderson et al. 1986; 1987; 1988) and strain shadows around arsenopyrite (Graves and Zentilli, 1982), which is commonly associated with veins. In these studies it is assumed that cleavage-related strain accompanying vein folding and pressure shadow development predates regional folding and therefore the veins and arsenopyrite, which predate this strain, predate regional folding. However, as discussed above, the evidence presented for the Ovens area supports synfolding cleavage development with folding of veins reflecting layer-parallel shortening in the hinge region during folding, and a similar interpretation was presented by Williams and Hy (1990) for deposits in the eastern part of the Meguma Terrane. The strain around arsenopyrite, such as that illustrated by Graves and Zentilli (1982), has been shown at the Ovens to be related to late (ca. 376 Ma), post-metamorphic cleavage-parallel strain, which may reflect homogeneous flattening accompanying flexural-slip. The observations at the Ovens, therefore, support a synfolding origin for strain previously considered to have a prefolding, metamorphic origin.

A late origin for veining is supported by inclusions of cleaved slate within veins (Ovens herein; Mawer, 1987). As discussed above in the section on fold development, a late,

post metamorphic age for veins in several Gold Districts is supported by their association with brittle structures and by $^{40}Ar/^{39}Ar$ dating.

4.4.6 Discordant veins:

Investigations at the Ovens demonstrate a temporal, and probable genetic, relationship between bedding-parallel and discordant veins, with both vein sets associated with flexural-slip folding. Discordant veins are an important component of other Meguma gold deposits (Faribault, 1899; Sangster, 1990; Williams and Hy, 1990) and they are often mineralized (Brookfield, Forest Hills, Caribou; Lake Catcha etc.; see Malcolm, 1929). Discordant veins have been referred to as fissure, ac and angulars and these veins typically illustrate only minor strain (Henderson, 1983; Williams and Hy, 1990). Discordant veins, in particular "ac" veins, have been referred to as "regional" in character, forming late in the folding history, with no relationship to the veins of the gold districts (Sangster, 1990; Williams and Hy, 1990). These observations were presented with the interpretation that the discordant veins are largely unrelated to earlier formed (prefolding) "auriferous" bedding-parallel veins. However, it is clear that the distribution of discordant veins at the Ovens is coincident with bedding-parallel veins, consistent with the mutual cross-cutting relationships, and development of discordant shear fractures is interpreted to be kinematically and temporally related to flexural slip.

Regional mapping in the central Meguma area also illustrates a spatial relation of discordant veins to the hinge area of the Waverley Anticline (Horne et al., 1998), consistent with a common origin for discordant and bedding-parallel veins emplaced during folding. Indeed, most deposits represent *concentrations* of both discordant and bedding-parallel veins

(e.g., Williams and Hy, 1990) supporting a common origin for both vein types, and consistent with a synfolding origin for vein *arrays* which define Meguma Gold Districts.

4.4.7 "Saddle Reefs"

Several proponents of a prefolding origin for bedding-parallel veins point out that these veins are typically uniform in thickness and that there are few true "saddle-reef veins" which support a late, flexural-slip origin. The term saddle reef sensu-stricto refers to veins infilling dilatant zones in the hinge of chevron folds. The dilatancy reflects volume change during folding and generally occurs within the incompetent layers. The amount of dilatancy created is a function of limb dip and thickness/length ratio of competent layers and increases markedly with progressive folding (Ramsay, 1974; Ramsay and Huber, 1987). In the Meguma Group the thickness to length ratio is typically very small (much less than 0.02) and does not favour the formation of significant saddle reefs. Additionally, dilatancy in fold hinges can also be accommodated by flow of incompetent material into the hinge region or hinge collapse (Ramsay, 1974), restricting formation of saddle reefs. This is represented in the Meguma Group by thickening of the slate layers in the hinge region.

There are several saddle reef veins known within the Meguma Group (Ovens, Duffrin, Upper Seal Harbour) which reflect late flexural-slip folding. At the Ovens only a few saddle reefs are developed and down-limb extensions, "leg reefs", occupy flexural-slip movement horizons, where they exhibit features of flexural-slip veins. This illustrates a relationship between flexural-slip and saddle reef veins. The abundant flexural-slip veins without associated saddle reefs at the Ovens clearly illustrate that the absence of true saddle reef veins

in the Meguma Gold Districts does not preclude a late flexural-slip origin for veins, and that the lack of saddle reefs may simply reflect the stratigraphic character and large wavelength of folds in the Meguma Group. Also, as indicated above, many veins are restricted to the steep limbs of asymmetric box folds, where saddle reefs would not be expected.

4.4.8 Summary:

A flexural-slip (saddle reef) model explains the key features common to the majority of Meguma gold deposits and is consistent with abundant evidence for late vein emplacement. Therefore a flexural-slip model, similar to the one proposed to explain the vein array at the Ovens, provides a good general model for the origin of Meguma Gold Districts. Many of the features which support a pre-folding origin for bedding-parallel veins (i.e., minor folding, cleavage) have been shown to have a syn-folding origin at the Ovens, and observations throughout the Meguma Group suggest this is generally the case. A syn-folding, flexural-slip model for Meguma Gold deposits is not a new idea, and variations of the basic model have been proposed by Faribault (1899, 1913), Malcolm (1929), Douglas (1948) Keppie (1976) and Mawer (1987).

As stated by Mawer (1987), a flexural-slip (saddle reef) model results in a predictable distribution of veins (i.e., Fig. 3.5) and thus provides a useful guide for the exploration and discovery of new deposits or for better predicting the distribution of veins within known deposits.

4.5 CONCLUSIONS:

The results of this study have been discussed with respect to their implications to the flexural-slip mechanism, fold development in the Meguma Terrane and the formation of gold deposits within the Meguma Terrane. Following is a summary of the conclusions with respect to each of these issues.

4.5.1 Flexural-slip mechanism:

Flexural slip was important in fold development in the Halifax and Ovens area. Flexural slip occurred primarily on bedding-parallel movement horizons, including flexural-slip duplexes, and also thrusts, lateral ramps and conjugate movement horizons, with all structures forming a linked system of movement horizons accommodating flexural-slip strain. In addition, conjugate discordant (extensional shear) fractures locally formed in response to flexural-slip related stress. All flexural-slip structures are kinematically consistent with the flexural-slip mechanism. Movement orientations suggest flexural slip during progressive non-cylindrical fold development. The complex system of movement horizons requires a three dimensional model.

Movement horizons occur exclusively within incompetent slate layers, consistent with other studies. This reflects partitioning of flexural-shear strain into the slate (incompetent) layers of slate-metasandstone (incompetent-competent) sequences. Average movement horizon spacing data ranges from approximately 1- 4 metres, consistent with published accounts, and is inversely related to limb dip. Spacing is wider in slate-dominated units compared with slate-metasandstone units. Determination of slip amount in this study (the first such study) indicates flexural slip accounts for significant and uniform shear strain in the

Ovens Anticline. Assuming flexural-slip accounts for the last increment of folding, fold tightening of ~4°-8° of the 60° of limb dip is indicated. The slip amount and spacing data indicate that increasing flexural-slip shear strain during incremental folding is accommodated by increased slip on early formed movement horizons and development of new movement horizons between existing movement horizons, resulting in movement horizons dominated by low slip amounts. This sequence of movement horizon development accommodates a relatively uniform distribution of flexural-slip strain throughout the sequence during fold growth.

Flexural slip is a brittle, post-metamorphic deformation, and likely represents late fold growth, with flexural flow important in the early stages of fold growth. Flexural-slip folding occurs contemporaneously with other fold mechanisms (e.g. flexural-flow; tangential longitudinal strain) as well as cleavage-parallel strain, with flexural-slip activity at interlimb angles of up to 40° (Ovens). This supports the conclusions of Fowler and Winsor (1997) of synchronous flexural-slip and homogeneous flattening up to limb dips of 70°.

Ubiquitous slickenfibres in the Halifax area and concentrations of veins along flexural-slip structures in the Ovens reflect fluid flow during flexural slip and fluid pressure was probably important to the flexural-slip process. Flexural-slip related veins at the Ovens area are auriferous.

4.5.2 Fold Development in the Meguma Terrane:

Cross sections of the Meguma Terrane (Fig. 1.4) are characterized by chevron and box-fold geometry, supporting a box-fold to chevron fold history typical of highly anisotropic

successions. Flexural folding was an important folding mechanism on fold limbs, including (early?) flexural flow and (late?) flexural slip. The finite strain pattern, including bedding-cleavage relations, flexural-slip displacement, minor folding and pressure shadows, indicates a complex history of folding involving flexural flow, flexural slip, tangential longitudinal strain, inverse tangential longitudinal strain and layer-parallel shortening.

Age constraints on metamorphic cleavage (ca 410-385 Ma) and flexural-slip related strain (ca. 376 Ma) imply a long duration of fold growth. Fold growth may have been episodic, with late flexural slip reflecting fold reactivation in response to a regional tectonic event which is also responsible for generation of granite magma and lamprophyre dykes, and emplacement of the lower crustal rocks of the Liscomb Complex.

4.5.3 Meguma Gold Deposits:

A flexural-slip (saddle-reef) model is proposed for the auriferous vein array at the Ovens. This model accounts for the character, distribution and relationship between buckled bedding-parallel veins, flexural-slip bedding-parallel veins and conjugate discordant veins, in a related episode of veining during late folding, and therefore explains the concentration of several vein types within the hinge of the Ovens Anticline.

The Ovens vein array shares many common features of Meguma Gold Districts as presented in historical records and discussed in the literature, suggesting that a flexural-slip model provides a good, testable working model for Meguma Gold Districts.

4.6 RECOMMENDED FURTHER WORK

As outlined in the discussion, this study addresses the issues of the flexural-slip mechanism, fold development in the Meguma Group and the origin of Meguma gold deposits. These issues are of both universal and local interest and generally include some well debated issues such as the relationship of cleavage to folding and the origin of bedding-parallel quartz veins. I hope the data and interpretations presented provide at least more insight than confusion. The test of this will only come with time and further study.

The flexural-slip mechanism is well understood, particularly from the recent work of Tanner (1989) and Fowler and Winsor (1997). An outstanding problem has been finding areas where slip amount can be determined thus allowing for a quantitative evaluation of factors controlling flexural slip. The work presented here for the Ovens area is a start, however more areas need to be evaluated in order to quantitatively address parameters such as limb dip and lithology on the flexural-slip mechanism.

The model of fold development for the Meguma Group is based largely on interpretations at the Ovens. Evaluation of strain elsewhere in the Meguma Group, in particular bedding-cleavage relations, flexural flow, cleavage-parallel strain and the distribution of layer-parallel shortening, is required to evaluate whether the conclusions presented here are applicable to the Meguma Group in general. A study of bedding-cleavage relations across a box fold consisting of opposite verging folds is required to test whether bedding-cleavage relations reflect a simple history of flexural flow or a more complex history as suggested here. The long folding history proposed here is based on the sequence and style

of deformation and $^{40}Ar/^{39}Ar$ dates. Key to this is the recognition of new, post-metamorphic mineral growth. Recognition and age dating of metamorphic and post-metamorphic strain will help better evaluate the nature and duration of regional folding in the Meguma Terrane.

A flexural-slip model has been proposed for the auriferous vein array at the Ovens and it is suggested that a flexural-slip model can account for many general characteristics of Meguma Gold deposits. Detailed studies at other deposits are required to evaluate this proposal.

APPENDIX 1

BEDDING-PARALLEL MOVEMENT HORIZON SPACING

RAILWAY SECTION AND THE OVENS

Table A1-1: Table of bedding-parallel movement horizon spacing for measured intervals in the railway section, Halifax, (see Fig. 2.4 in pocket at back) and the Ovens area (see Fig. 3.5 for Cunard Cove section and Fig. 3.18, in pocket at back, for the Rose Bay section), including statistical data for all intervals and frequency data and histograms for 0.2 metre class intervals for some measured intervals.

SECTION A, RAILWAY SECTION

Spacing
2.69
1.94
7.04
3.97
9.98
0.31
1.47
0.15
1.32
0.76
1.19
0.73
0.79

N = 13
2.49 Average spacing
2.81 Standard Deviation
1.32 Median spacing

SECTION B, RAILWAY SECTION

Spacing
1.29
0.2
0.89
0.86
0.16
1.48
0.13
0.3
0.16
1.57
0.43
1.46
3.07
1.2

N = 36
1.97 Average spacing
1.90 Standard Deviation
1.30 Median spacing

Interval (m)	Frequency
0.2	7
0.4	3
0.6	1
0.8	0
1	3
1.2	2

frequency data for 0.2 m class interval of movement horizon spacing

6.2	1.4	4
1.96	1.6	3
4.68	1.8	0
2.14	2	1
0.36	2.2	1
1.3	2.4	0
4.15	2.6	0
0.22	2.8	0
6.58	3	1
0.08	3.2	1
0.12	<3.2	9
1.29		
4.16		
2.98		
0.12		
0.92		
1.33		
3.61		
5.04		
5.85		
3.55		
1.2		

SECTION C, RAILWAY SECTION

Spacing

3.54
1.71
0.2
0.93
0.26
1.7
3.87
2.13
2.17
1.25
0.5
1.75

N = 12

1.67	Average spacing
1.12	Standard Deviation
1.71	Median spacing

SECTION D, RAILWAY SECTION
SPACING

0.33
4.3
0.02
0.48
0.47
0.25
8.4
1
0.95
0.15
0.55
0.99
1.36
0.88
0.82
0.7
0.42
0.91
0.38
4.39

N = 20
1.39 Average spacing
1.98 Standard Deviation
0.76 Median spacing

SECTION E, RAILWAY SECTION
Spacing

0.54
0.1
0.51
0.4
1.5
0.66
5.26
0.27
0.88
0.15
2.01
0.42

N = 13
2.49 Average spacing
2.81 Standard Deviation
1.32 Median spacing

Interval (m)	Frequency
0.2	4
0.4	6
0.6	5
0.8	3
1	1
1.2	1

frequency data for 0.2 m class interval for movement horizon spacing

1.55	1.4	2
2.31	1.6	2
2.8	1.8	1
4.37	2	0
0.29	2.2	1
3.88	2.4	1
1.22	2.6	0
1.38	2.8	1
0.24	3	0
0.73	3.2	0
0.52	<3.2	3
0.07		
1.8		
0.16		
0.32		
0.36		
1.03		
0.72		
0.55		

SECTION F, RAILWAY SECTION

Spacing

5.38
0.6
0.35
0.15
4.37
2.33
10.05
1.15
0.9
1.23
0.52
0.43

N = 12
2.29 Average spacing
2.83 Standard Deviation
1.03 Median spacing

SECTION G, RAILWAY SECTION

Spacing

0.4
1
5.6
10.15
8.65
3.8
0.3

N = 7
4.27 Average spacing
3.73 Standard Deviation
3.8 Median spacing

SECTION C-D, CUNARD COVE

Spacing

0.55
0.49
0.94
0.21
1.14
1.7
0.26
0.29
0.34
2.13
0.26
0.78
0.06
0.81
0.68
0.15
0.58
0.95
0.78
1.16
0.22
1.34
0.12
0.24
0.25
1.78
0.5
0.15

N = 60
1.09 Average spacing
0.92 Standard Deviation
0.78 Median spacing

Interval (m)	Frequency
0.2	6
0.4	12
0.6	5
0.8	9
1	3
1.2	5
1.4	4
1.6	0
1.8	4
2	2
2.2	4
2.4	0
2.6	1
2.8	0
3	0
3.2	2
>3.2	3

frequency data for 0.2m class interval for movement horizon spacing

0.18
1.14
2.12
3.13
3.28
0.28
0.65
1.78
3.6
2.6
0.59
1.75
2.06
0.66
1.09
0.28
0.13
0.77
2.09
3.45
3.13
1.38
0.73
1.13
1.92
1.3
0.65
0.38
1.22
0.77
0.23
1.98

SECTION C-D (MH + FSV)

Spacing

1.75
0.23
0.14
0.09
0.77
1.22
0.31
0.07
0.65
1.28
0.02
1.09
0.69
0.1
0.04
1.13
0.2
0.09
0.03
0.41
1.03
0.35
0.94
0.01
0.04
0.03
2.59
0.74
0.29
0.17
0.87
0.03
0.03
0.97
1.88
1.57
0.07
0.05
1.97
0.11

N = 130
0.52 Average spacing
0.69 Standard Deviation
0.24 Median spacing

Interval (m)	Frequency
0.2	63
0.4	20
0.6	10
0.8	7
1	6
1.2	6
1.4	4
1.6	2
1.8	4
2	3
2.2	1
2.4	0
2.6	2
2.8	0
3	0
3.2	2

frequency data for 0.2m class interval for movement horizon spacing

0.31
0.04
0.05
0.26
0.13
0.28
0.09
0.34
2.06
0.1
0.08
0.02
0.41
0.1
1.04
0.59
0.4
0.02
0.03
2.41
0.14
3.08
0.06
0.27
0.05
0.14
1.78
0.65
0.28
1.4
1.75
0.05
0.08
1.09
0.48
1.32
0.24
1.99
0.12
0.01
0.04
1.1
0.03

0.15
0.07
0.09
0.5
1.78
0.25
0.24
0.12
0.35
0.57
0.11
0.09
0.05
0.03
0.07
0.07
0.04
0.18
0.33
0.83
0.78
0.95
0.58
0.2
0.05
0.11
0.02
0.55
0.33
0.48
0.06
0.44
0.02
0.03
0.29
0.26
0.05
0.18
0.8
0.32
0.09
3.81
0.04

1.43
0.97
0.05

ROSE BAY SECTION

Spacing
1.1
0.35
0.5
0.6
0.1
0.22
0.75
1.93
0.57
1.6
0.58
0.2
0.2
0.5
0.17
0.3
0.08
0.1
0.23
0.25
0.13
0.17
0.63
0.09
0.3
0.07
0.13
0.21
0.37
0.34
0.16
0.5
1.15
0.25
0.1

N = 49
0.46 Average spacing
0.51 Standard Deviation
0.30 Median spacing

Interval (m)	Frequency	
0.2	18	
0.4	12	
0.6	11	frequency data for
0.8	3	0.2m class interval for
1	0	movement horizon
1.2	2	spacing
1.4	0	
1.6	1	
1.8	0	
2	1	
2.2	0	
2.4	0	
2.6	0	
2.8	0	
3	1	
3.2	0	

0.2
0.4
2.9
0.1
0.2
0.6
0.45
0.45
0.55
0.35
0.55
0.15
0.08
0.62

APPENDIX 2

DETERMINATION OF SLIP AMOUNT ON MOVEMENT HORIZONS

SECTION C-D, CUNARD COVE

APPENDIX 2

This appendix explains the method used to calculate the displacement amount along flexural-slip movement horizons determined by offset discordant quartz veins in the Cunard Cove section and the flexural-slip shear strain and angular flexural-slip shear strain indicated by this displacement

Displacement

The method used to determine the displacement is illustrated in Fig. A2.1a. This method requires knowledge of the the rake of the movement lineation (Rs) and the intersection of the offset vein (Ri) on the movement horizon, and the strike separation of the offset vein (Y). This information was either measured in the field or calculated using other measured data for two intervals of measured section C-D in Cunard Cove and all the measured and calculated data are given in Table A2-1.

Rs was calculated from the trend, relative to the movement horizon, and plunge of the movement lineation on the movement horizon (Bs and Sd respectively, Fig. A2-1b). Ri was calculated similarly, using the plunge and trend of the intersection of the offset vein on the movement horizon (Bi and Li-d respectively, Fig. A2-1b). The trend and plunge of the movement lineation (Ss Sd) was measured in the field, whereas the trend and plunge of the intersection of the offset vein on the movement horizon (Li-s and Li-d) was calculated using equal angle stereonet projection of two intersection planes.

The amount of displacement of offset veins has been determined for the total slip amount (Xt) determined for each movement horizon and the corrected slip amount (Xc), which reflects the projection of the total slip in the profile plane of the fold (Table A2-1, Fig. 3.15). The corrected value is a function of the total slip amount and the cosine of the angle between the trend of the movement lineation and the perpendicular to fold hinge (δ; Fig. A2.2a).

Flexural-slip shear strain and increment of angular shear strain from flexural slip

The slip amount determined is a measure of the flexural-slip shear strain (γ_S), and can be given as a ratio of the slip amount to the thickness of the interval (Fig. A2.2b).

The increment of angular shear strain resulting from flexural slip (ψ_S) is a function of the flexural-slip shear strain, however varies as a function of the initial limb dip. The increment of angular shear strain resulting from flexural slip has been calculated for Section C-D, Cunard Cove, assuming flexural slip represents the last increment of folding (Fig. A2.2c).

Determining the angular flexural-slip shear strain for Section C-D, Cunard Cove, assuming flexural-slip was the last increment of folding, a total angular shear strain (ψ_T) equal to the limb dip (60°), and using a flexural-slip strain value for the average, corrected flexural-slip strain for the two intervals (0.48; from Fig. 3.15).

$\psi_S = \psi_T - \psi_F$

where

$\psi_T = 60°$ (limb dip)

and $\psi_F = \tan^{-1} (\gamma_T - \gamma_S)$ where $\gamma_T = \tan 60° (1.73)$

$= \tan^{-1} (1.25)$ $\gamma_S = 0.48$

$= 51.34°$

thus

$\psi_S = 60° - 51.34° = 8.66°$

If the total shear strain is determined relative to the axial plane, then $\psi_T = 90 - 20$ (half interlimb angle of ~40°) = 70°.

$\psi_S = \psi_T - \psi_F$

where

$\psi_T = 70°$ (limb dip)

and $\psi_F = \tan^{-1} (\gamma_T - \gamma_S)$ where $\gamma_T = \tan 70° (2.75)$

$= \tan^{-1} (2.27)$ $\gamma_S = 0.48$

$= 66.23°$

thus

$\psi_S = 70° - 66.23° = 3.77°$

(a)

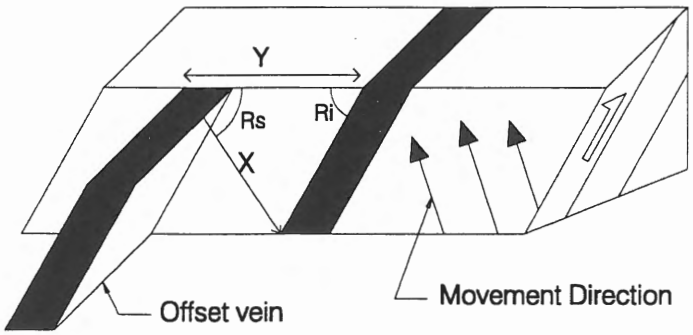

$$X = \frac{Y \sin Ri}{\cos(Rs-(90-Ri))}$$

(b)

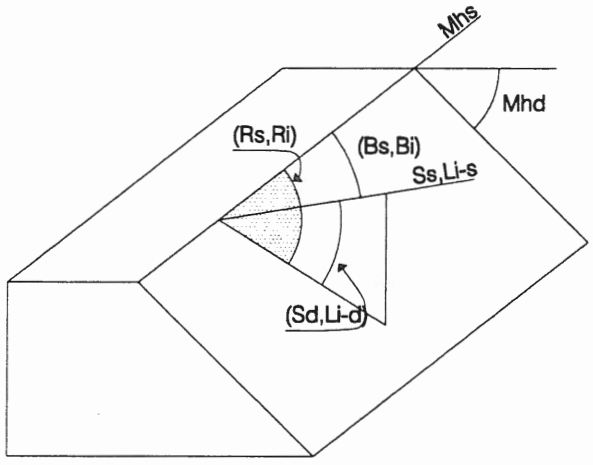

$\cos Rs = \cos Bs \cos Sd$

$Rs = (\cos Bs \cos Sd)\ \cos^{-1}$

$\cos Ri = \cos Bi \cos Li\text{-}d$

$Ri = (\cos Bi \cos Li\text{-}d)\ \cos^{-1}$

Figure A2.1: (a) Schematic diagram showing the method used to determine the displacement along flexural-slip movement horizons. See table A2-1 for explanation of abbreviations. (B) Schematic diagram illustrating the method used to determine the rake of the movement lineation (Rs) and the intersection of offset veins (Ri) on the movement horizon (after Ragan, 1995).See table A2-1 for explanation of abbreviations.

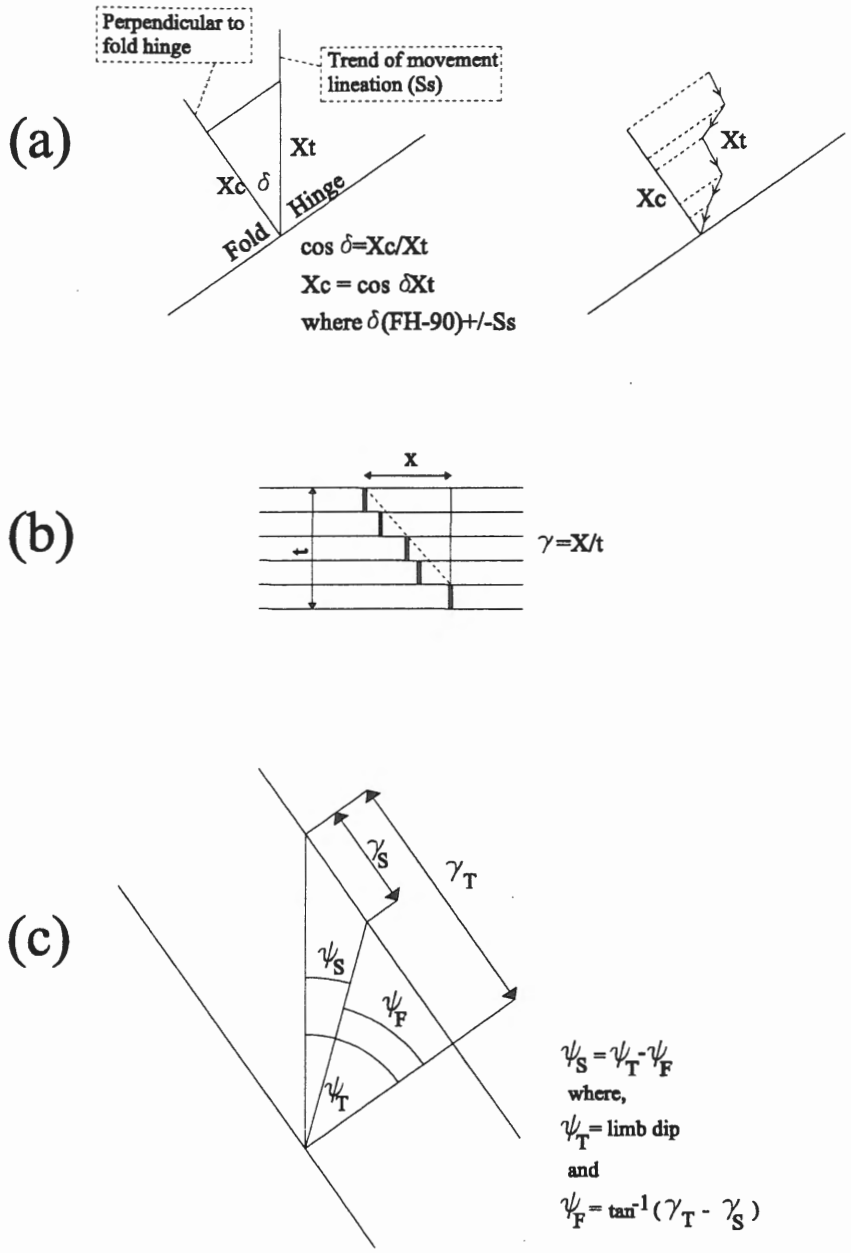

Figure A2.2: (a) Diagrams showing the projection of the slip amount calculated along a movement horizon (Xt) into the profile plane of the fold (Xc) (left) and the calculation of the cumulative total (Xt) and corrected (Xc) slip amounts for the two intervals (right). (b) Schematic diagram showing flexural slip shear strain (γ_S) as a function of slip amount (X) and the thickness of the interval (t). (c) Diagram showing the method of calculating the angular flexural-slip strain (ψ_S) assuming flexural-slip accounts for the last increment of folding. ψ_F = angular flexural-flow strain; ψ_T=total angular shear strain; γ_t = total shear strain; $_S\gamma$ = flexural shear strain.

Table A2-1: Table of data related to calculation of the amount of flexural-slip offset of movement horizons. Explanation of abbreviations on following page.

interval b	MHs	MHd	Ss	Sd	QVs	QVd	Li-s	Li-d	Bi	Bs	Ri	Rs	Y	Xt		Xc
77.52	237	61	30	47	140	50	268	43	31	27	51.18	52.58	2.06	1.65	65.00	0.70
76.96	238	61	26	47	107	63	264	38	26	32	44.91	54.66	1.15	0.85	61.00	0.41
77.48	236	63	25	47	107	66	263	42	27	31	48.54	54.23	1.79	1.38	60	0.69
75.54	236	62	5	52	110	70	268	45	32	51	53.15	67.20	0.04	0.03	40	0.02
75.33	236	60	17	52	110	70	270	44	34	39	53.39	61.42	0.10	0.08	52	0.05
73.19	235	64	10	55	110	55	253	33	18	45	37.10	66.07	0.17	0.11	45	0.07
72.49	236	63	6	50	122	54	263	41	27	50	47.74	65.60	0.01	0.01	41	0.01
72.23	236	63	6	50	122	54	263	41	27	50	47.74	65.60	0.10	0.07	41	0.06
71.94	236	63	6	50	120	59	265	44	29	50	51.01	65.60	0.15	0.12	41	0.09
71.60	236	62	15	52	117	58	264	41	28	41	48.21	62.31	0.05	0.04	50	0.02
69.47	238	61	25	52	120	56	266	40	28	33	47.44	58.91	0.63	0.47	60	0.24
69.21	236	62	20	55	142	54	270	47	34	36	55.57	62.35	0.04	0.03	55	0.02
68.43	236	62	15	60	127	55	266	43	30	41	50.70	67.83	0.45	0.35	50	0.22
68.37	236	62	0	50	127	55	266	43	30	56	50.70	68.93	2.25	1.74	35	1.43
67.56	235	64	284	63	138	52	265	46	30	132	53.02	107.68	0.05	0.06	41	0.04
66.73	237	64	330	64	143	50	266	45	29	86	51.80	88.25	0.88	0.75	5	0.75
66.15	236	64	320	64	138	52	266	45	30	96	52.24	92.63	0.27	0.24	5	0.24
64.42	238	65	15	57	144	47	264	43	26	43	48.90	66.53	0.05	0.04	50	0.02
63.26	236	63	15	52	113	60	262	56	26	38	59.83	60.98	0.51	0.44	50	0.28
63.04	236	64	18	48	108	55	257	36	21	35	40.95	56.76	0.59	0.41	53	0.25
61.70	236	65	4	6	133	46	259	40	23	52	45.16	52.24	2.72	2.04	39.00	1.59
61.58	236	65	4	60	133	46	259	40	23	52	45.16	72.07	0.49	0.35	39.00	0.27
61.34	238	66	354	57	136	48	262	42	24	64	47.24	76.19	1.30	0.96	29.00	0.84
61.09	236	66	8	54	148	54	268	50	32	48	56.97	66.84	1.50	1.27	43.00	0.93
59.31	233	67	10	56	120	47	253	38	20	43	42.23	65.86	2.00	1.36	45.00	0.96
58.81	233	66	332	67	136	53	262	47	29	81	53.38	86.50	0.24	0.21	7.00	0.21
58.66	233	66	7	55	113	65	265	45	32	46	53.15	66.52	0.23	0.18	42.00	0.14
57.34	233	67	7	55	110	60	257	44	24	46	48.92	66.52	0.80	0.60	42.00	0.45
20.18	interval b thickness												total x	15.84	total	11.00
interval a																
38.91	237	61	8	53	142	50	269	6	32	49	32.50	66.74	0.12	0.07	43.00	0.05
37.16	235	60	280	54	128	56	268	43	33	45	52.17	65.44	0.61	0.48	45.00	0.34
34.67	237	62	7	53	127	58	269	45	32	50	53.15	67.24	0.05	0.04	42.00	0.03
34.39	238	61	7	56	140	62	280	50	42	51	61.47	69.40	0.06	0.05	42.00	0.04
34.26	238	60	8	56	126	64	275	46	37	50	56.30	68.93	0.49	0.41	43.00	0.30
33.49	238	63	0	52	130	65	276	50	38	58	59.57	70.96	0.50	0.44	35.00	0.36
31.40	238	62	7	55	150	60	282	52	44	51	63.71	68.84	0.33	0.31	43.00	0.23
27.95	238	62	256	59	160	32	257	32	19	62	36.69	76.01	8.00	4.79	69.00	1.72
24.82	238	62	30	48	158	39	263	38	25	28	44.42	53.79	0.02	0.01	65.00	0.01
21.21	237	62	280	58	132	65	277	51	40	43	61.18	67.20	0.22	0.20	45.00	0.14
19.95	236	62	310	61	145	65	284	55	48	74	67.43	82.32	0.30	0.33	15.00	0.32
19.10	236	62	0	55	122	55	264	41	28	56	48.21	71.29	2.10	1.57	35.00	1.28
18.02	237	62	355	58	335	85	344	61	107	62	98.15	75.59	0.09	0.16	30.00	0.14
16.05	238	65	10	58	160	42	262	41	24	48	46.41	69.23	5.00	3.62	45.00	2.56
14.75	240	61	30	46	140	55	274	46	34	30	54.84	53.02	4.90	4.05	65.00	1.71
13.72	242	60	13	53	150	78	310	58	68	49	78.55	66.74	0.03	0.03	48.00	0.02
12.48	240	60	20	52	140	55	275	45	35	40	54.60	61.86	7.50	6.11	55.00	3.51
11.73	238	55	357	55	135	80	302	52	64	61	74.34	73.85	0.02	0.02	32.00	0.02
9.52	240	54	320	54	140	69	295	48	55	80	67.43	84.14	0.03	0.03	5.00	0.03
29.39	interval a thickness												total x	22.75	total x	12.82

See following page for explanation of abbreviations.

Explanation of abbreviations for Fig. A2.1 and Table A2-1

Location	relative stratigraphic position in metres; (measured)
Mhs	strike of movement horizon; (measured)
Mhd	dip of movement horizon; (measured)
Ss	trend (azimuth) of movement lineation (measured)
Sd	plunge of movement lineation; (measured)
QVs	strike of offset vein; (measured)
QVd	dip of offset vein; (measured)
Li-s	trend of intersection lineation between movement horizon and the offset vein; calculated as intersection of planes using stereonet projections (SpheriStat)
Li-d	plunge of intersection lineation between movement horizon and the offset vein; calculated as intersection of planes using stereonet projections (SpheriStat)
Bi	acute angle between Li-s and Mhs; calculated
Bs	acute angle between Ss and Mhs; calculated
Ri	pitch of intersection of the offset vein on the movement horizon; calculated where cos Ri=cosBi cosLi-d (from Ragan, 1985, p. 51)
Rs	pitch of Ss on the movement horizon; calculated, where cosR=cosSs cosSd (from Ragan, 1985, p. 51).
Y	horizontal strike separation of offset vein (measured).
Xt	actual displacement of offset vein (calculated, see Fig. A2-1a)
δ	angle between Ss and the perpendicular to the fold hinge in the B-C plane of the fold. (calculated).
Xc	value of X projected into the ac plane
γt	total flexural-slip shear strain
γc	corrected flexural-slip shear strain

APPENDIX 3

DUPLEX THICKNESS AND SLIP AMOUNT

SECTION C-D, CUNARD COVE

Table A3-1: Table of displacement amounts for (simple) movement horizons and flexural-slip duplexes for two intervals of Section C-D, Cunard Cove. (See Fig. 3.15 and Table A2-1).

movement horizons	flexural-slip duplexes	
1.65	1.38	
0.85	0.47	
0.03	0.04	
0.08	2.04	
0.11	0.96	
0.01	1.36	
0.07	0.48	
0.12	4.79	
0.04	0.33	
0.03	1.57	
0.35	3.62	
1.74	4.05	
0.06	6.11	
0.75		
0.24		
0.44		
0.41		
0.35		
1.27		
0.21		
0.18		
0.6		
0.0		
0.0		
0.0		
0.4		
0.4		
0.3		
0.0		
0.2		
0.1		
0.03		
0.02		
0.03		
11.36	27.2	sum of offset (metres)
0.17	1.38	median offset (metres)
0.33	2.09	average offset (metres)

APPENDIX 4

DETERMINATION OF THICKNESS AND SPACING OF DISCORDANT VEINS

LOCATION RB-1, ROSE BAY

Table 4.1: Table of vein thickness for steep dipping and west dipping veins for a 100 metre strike-parallel section in Rose Bay (location RB-1, Fig. 3.17).

steep veins	west veins	thickness	frequency	
2	1			
1	6	thickness	frequency	
5	18	1	58	
7	1	2	24	
9	2	3	12	
1	3	4	16	
1	3	5	4	
1	1	6	6	frequency data for
28	1	7	5	1 mm class intervals
1	1	8	3	for vein thickness
1	2	9	4	for steep-dipping veins
4	2	10	1	
1	20	11	2	
1	13	12	7	
1	17	13	5	
1	1	14	1	
1	4	15	3	
1	1	16	3	
4	1	17	0	
13	2	18	0	
2	8	19	1	
15	2	20	2	
1	3	>20	14	
1	1			
1	1			
3	2			
9	1			
1	4			
6	1			
3	1			
8	2			
3	3			
1	2			
1	2			
1	1			
14	1			
1	5			
1	3			
1	4			
9	2			

STATISTICAL DATA FOR VEIN THICKNESS OF STEEP-DIPPING VEIN SET	
1162.00	sum of vein thickness (mm)
6.80	average vein thickness (mm)
1.00	minimum thickness (mm)
60.00	maximum thickness (mm)
9.49	standard deviation (mm)
3	median thickness (mm)

10	5
3	2
3	2
12	2
12	2
28	2
4	2
16	2
30	2
2	12
4	8
1	4
5	2
1	1
2	14
1	1
1	24
7	1
2	2
6	7
2	7
11	160
12	3
1	1
1	3
2	2
1	7
1	10
2	2
1	4
13	10
2	3
2	1
4	11
33	5
12	7
4	2
8	1
6	12
1	9
31	30
21	1
16	8

STATISTICAL DATA FOR VEIN THICKNESS OF WEST DIPPING VEIN SET

1060.00	sum of vein thickness
7.16	average vein thickness
1.00	minimum thickness
60.00	maximum thickness
9.84	standard deviation
3.00	median thickness (mm)

thickness	frequency (west veins)
1	35
2	41
3	14
4	17
5	6
6	2
7	6
8	8
9	1
10	3
11	5
12	4
13	1
14	2
15	0
16	0
17	1
18	2
19	0
20	1
<20	5

frequency data for 1mm class intervals for vein thickness of west-dipping vein set

1	11
1	26
4	3
1	4
5	2
2	1
4	1
13	2
12	1
2	2
6	3
1	1
4	7
2	2
2	3
4	5
13	4
9	2
3	4
12	14
1	2
1	8
3	4
7	4
1	4
52	4
15	4
5	2
1	1
1	2
60	3
19	2
3	3
1	12
2	7
20	2
2	2
16	5
1	8
1	8
1	1
13	2
2	1

11	1
4	2
1	1
1	25
4	4
3	2
26	11
2	4
3	5
46	8
2	1
15	2
12	18
1	4
1	2
4	3
3	2
4	4
1	11
27	2
2	8
4	1
24	1
6	12
2	1
28	11
1	
7	
2	
2	
3	
1	
4	
6	
8	
1	
1	
7	
24	
1	
1	
2	
1	

20
1

APPENDIX 5

DETERMINATION OF WEIGHTED BEDDING-CLEAVAGE ANGLE FOR SECTION C-D, CUNARD COVE

APPENDIX 5

Following is the method applied to determine the weighted bedding-cleavage angle (β'_w) (Fig. A5.1a,b) for the measured section in Cunard Cove.

β' can be related as a tangent function of the section thickness (t) and the amount of displacement of cleavage from the bedding normal across the section (γ), where $\tan \beta' = \gamma/t$ (Eq. 1) (Fig. A5.1a). The weighted bedding-cleavage angle (β'_w) for the section can be determined using the cumulative γ and t values for the metasandstone and slate intervals (Fig. A5.1b).

The cumulative value of t for metasandstone and slate intervals was determined from the stratigraphic log (Fig. 3.5) and, for convenience the value of t is given here as a percentage, with the total value of t for the section = 1; Metasandstone comprises 22.88 % of the measured section and thus t for the cumulative metasandstone (t_{SD}) is 0.2288. Conversely, t for slate in the section (t_{ST}) is 0.7712.

The value of γ for the metasandstone - slate section can be calculated by arranging eq.1
$\tan\beta' = \gamma/t$
$\tan\beta'\ (t) = \gamma$

For the measured section the value of γ for the weighted, or combined slate and metasandstone, (γw) is the sum of γ for the slate and metasandstone.

$\gamma w = (\tan \beta'_{SD}\ (t_{SD})) + (\tan \beta'_{SL}\ (t_{SL}))$; where
β'_{SD} = the bedding-cleavage angle in the metasandstone, here given a value of 90°,
t_{SD} = the cumulative thickness of metasandstone, given as a percentage (0.2288);
β'_{SL} = the bedding-cleavage angle for the slate interval, 72°
t_{SL} = the thickness of the slate interval, given as a percentage (0.7712).

$\gamma_W = (\tan 0\ (.2218)) + (\tan 72\ (.7712))$
$= (0) + (2.374)$
$= 2.374$

The weighted bedding-cleavage angle (β'_w)for the section is ...

$\tan \beta'_W = \gamma_w/t_w$
(for $t_W = 1$)
$\tan \beta'_W = \gamma_w$
$\beta'_W = \gamma_w\ (\tan^{-1})$
(for $\gamma_w = 2.374$)
$\beta'_W =$ **67.15°**

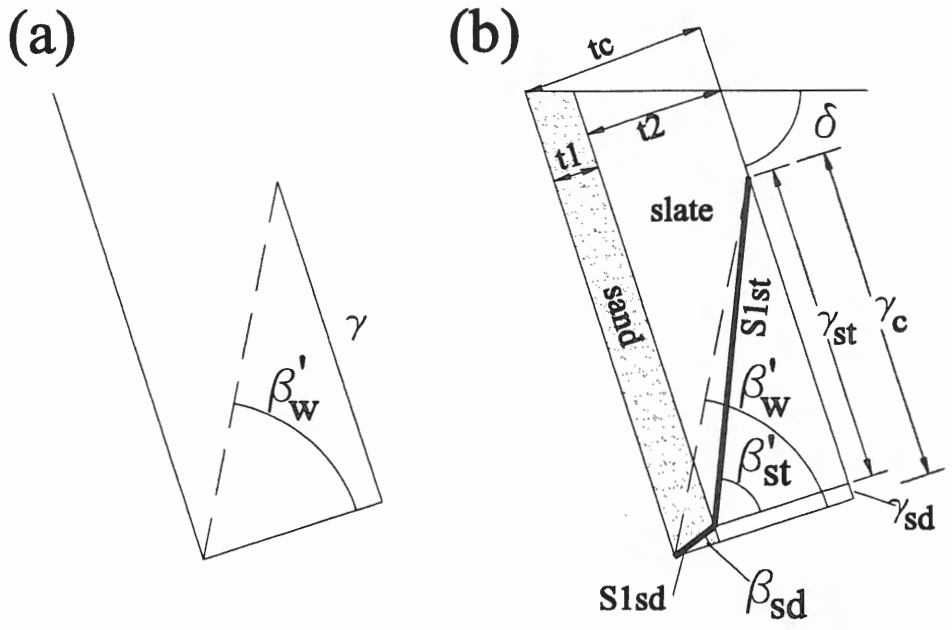

$\tan\beta'_w = \gamma c/tc$
where tc= 1
$\tan\beta'_w = \gamma c$
$\beta'_w = \gamma c(\mathrm{Tan}^{-1})$

where $\gamma c = \gamma sd + \gamma st$
and
$\gamma sd = \tan\ t1\beta'_{sd}$
and
$\gamma st = \tan\ t2\ \beta'_{st}$

Figure A5.1: (a) Schematic diagram showing the geometric relationship between bedding-cleavage angle (β') and shear strain (γ). (b) Schematic diagram showing the geometric elements used to determine the weighted bedding-cleavage angle (βw) for a sandstone-slate pair. S1 = cleavage; δ = bedding dip; β'sd = bedding-cleavage angle in metasandstone; β'st = bedding-cleavage angle in slate; γsd = shear strain in metasandstone; γst = shear strain in slate; γc = combined shear strain; tc = combined thickness.

REFERENCES:

Baker, D.E.L. 1996. Fluid inclusions and microstructure of flexural-slip bedding-concordant veins within the Ovens Anticline, Lunenburg, Nova Scotia. Unpublished B.Sc. thesis, Dalhousie University, Halifax Nova Scotia, 74 p.

Behzadi, H. and Dubey, A.K. 1980. Variation of interlayer slip in space and time during flexural folding. Journal of Structural Geology, 2, p. 453-457.

Benn, K., Horne, R.J., Kontak, D.J., Pignotta, G. and Evans, N.G. 1997. Syn-Acadian emplacement model for the South Mountain Batholith, Meguma Terrane, Nova Scotia: Magnetic fabric and structural analyses. Geological Society of America Bulletin, 109, p. 1279-1293.

Biot, M.A. 1965. Mechanic of incremental deformation. Wiley, New York, N.Y. 505p.

Boehner, R.C. 1991. Seismic interpretation: potential overthrust geology and mineral deposits in the Kennetcook Basin, Nova Scotia; In Mines and Mineral Branch, Report of Activities 1990, ed. D.R. MacDonald. Nova Scotia Department of Mines and Energy Report 91-1, p. 37-47.

Borradaile, G.J. 1977. On cleavage and strain: results of a study in West Germany using tectonically deformed sand dykes. Journal of the Geological Society of London, 133, p. 146-164.

Boulter, C.A. 1989. Four dimensional analysis of geological maps; Techniques of Interpretation. John Wiley and Sons.

Boulter, C.A. 1979. On the production of two inclined cleavages during a single folding event; Stirling Range, S.W. Australia. Journal of Structural Geology, 1, p. 207-219.

Bouyx, E., Blaise, J., Brice, D. Gourvennec, R., Lardeux, H. And LeMenn, J. 1992. Implications paléogéephiques des affinités nord-gondwaniennes et rhénanes des faunes dévoniennes de la zone de Meguma (Appalaches septentrionales). Comptes Rendus de l'Académie des Sciences de Paris, 315, p. 337-343.

Chapple, W.M. and Spang, J.H. 1974. Significance of layer-parallel slip during folding of layered sedimentary rocks. Geological Society of America Bulletin, 85, p. 1523-1534.

Clarke, D.B., MacDonald, M.A., Reynolds, P.H. and Longstaffe, F.J 1993. Leucogranites from the eastern part of the South Mountain Batholith. Journal of Petrology, 34, p. 653-679.

Clarke, D.B., Chatterjee, A.K. and Giles, P.S. 1993. Petrochemistry, tectonic history, and Sr-Nd systematics of the Liscomb Complex, Meguma Lithotectonic Zone, Nova Scotia. Canadian Journal of Earth Sciences, 30, p. 449-464.

Clarke, D.B. and Chatterjee, A.K. 1988. Physical and chemical processes in the South Mountain Batholith. In recent advances in the geology of granite-related mineral deposits, eds. R.P. Taylor and D.F. Strong. Canadian Institute of Mining and Metallurgy, Special Volume 39, p. 223-233.

Cloos, H. and Martin, H. 1932. Der gang einer Falte. Fortschritte Geologie und Palaeontologie Berlin, 11, p. 74.

Cobbold, P.R., Cosgrove, J.W. and Summers, J.M. 1971. Development of internal structures in deformed anisotropic rocks. Tectonophysics, 12, p. 23-53.

Cosgrove, J.W. 1993. The interplay between fluids, folds and thrusts during deformation of a sedimentary succession. Journal of Structural Geology, v. 15, p. 491-500.

Cosgrove, J.W. 1995. The interplay between fluids, folds and thrusts during deformation of a sedimentary succession: Reply. Journal of Structural Geology, v. 17, p. 1479-1480.

Cox, S.F., Sun, S.S.,Etheridge, M.A., Wall and V.J., Potter, T.F. 1995. Structural and geochemical controls on the development of turbidite-hosted gold quartz vein deposits, Wattle Gully Mine, central Victoria, Australia. Economic Geology, 90, p. 1722-1746.

Cox, S.F., Wall, V.J., Etheridge, M.A. and Potter, T.F. 1991. Deformational and metamorphic processes in the formation of mesothermal vein-hosted gold deposits - examples from the Lachlan Fold Belt in central Victoria, Australia. Ore Geology Reviews, 6, p. 391-423.

Crosby, D.G. 1962. Wolfville map area, Kings and Hants Counties, Nova Scotia. Geological Survey of Canada

Culshaw, N. And Liesa, M. 1997. Alleghanian reactivation of the Acadian fold belt, Meguma Zone, southwest Nova Scotia: Canadian Journal of Earth Sciences, 34, p. 833-847.

Culshaw, N. and Reynolds, P. 1997. 40Ar/39Ar age of shear zones in the southwest Meguma Zone between Yarmouth and Meteghan, Nova Scotia. Canadian Journal of Earth Sciences, 34, p. 848-853.

Cummings, L.M. 1985. Halifax Slate graptolite locality, Nova Scotia. In Current Research, Paret A, Geological Survey of Canada, Paper 85-1A, p. 215-221.

de Sitter, L.U. 1958. Boudins and parasitic folds in relation to cleavage and folding. Geologie en Mijnbouw, v. 20, p.272-286.

Dallmeyer, R.D. and Keppie, J.D. 1987. Polyphase Late Paleozoic tectonthermal evolution of the southwestern Meguma Terrane, Nova Scotia: evidence from 40Ar/39Ar mineral ages. Canadian Journal of Earth Sciences, 24, p. 1242-1254.

D'Orsay, A.M. 1981. Depositional analysis of the Upper Meguma (Halifax Formation) at the Ovens Park, Luenburg Ciunty, Nova Scotia. Unpublished B.Sc. thesis, Dalhousie University, Halifax, Nova Scotia.

Douglas, G.V. 1948. Structure of the gold veins of Nova Scotia. In Structural Geology of Canadian Ore Deposits, 1, Canadian Institute of Mining and Metallurgy Jubilee Volume. p. 919-926.

Dubey, A.K. 1982. Development of interlayer slip in non-cylindrical flexural slip folds. Geoscience Journal, v3, no. 2, p. 103-108.

Dubey, A.K. and Cobbold, P.R. 1977. Noncylindrical flexural-slip folding in nature and experiment. Tectonophysics, 38, p. 223-239.

Durney, D.W. and Ramsay, J.G. Incremental strains measured by syntectonic crystal growth. In Gravity and Tectonics, eds De Jong, K.A. and Scholten, R.. Wiley, New York, p. 67-96.

Eberz, G.W., Clarke, D.B., Chatterjee, A.K., and Giles, P.S. 1991. Chemical and isotopic composition of the lower crust beneath the Meguma Lithotectonic Zone, Nova Scotia: evidence from granulite facies xenoliths. Contributions to Mineralogy and Petrology, 109, p. 69-88.

Eisbacher, G.H. 1969. Displacement and stress field along part of the Cobequid Fault, Nova Scotia. Canadian Journal of Earth Sciences, 6, p. 1095-1104.

Erslev, E.A. and Ward, D.J. 1994. Non-volatile element and volume flux in coalesced slaty cleavage. Journal of Structural Geology, v. 16, o. 4, p. 531-553.

Faribault, E.R. 1899. On the gold measures of Nova Scotia and deep mining. The Canadian Mining Review, 18, no.3, p. 78-82.

Faribault, E.R. 1908a. City of Halifax, Canada Department of Mines, Geological Survey Branch, Map 68, scale 1:63,360.

Faribault, E.R. 1908b. Elmsdale Sheet. Canada Department of Mines, Geological Survey Branch, Map 1005, scale 1:63,360.

Faribault, E.R. 1909. Waverley Sheet. Canada Department of Mines, Geological Survey Branch, Map 1025, scale 1:63,360.

Faribault, E.R. 1913. The gold deposits of Nova Scotia. The Canadian Mining Journal, 34, no. 22, p. 108-109 and no. 24, p. 780-781.

Faribault, E.R. 1929. Bridgewater Sheet. Canada Department of Mines, Map no. 89. Scale 1:63 360.

Faribault, E.R. 1934. Ovens Gold District, Lunenburg County, Nova Scotia. Nova Scotia Department of Natural Resources Open File Map 34-005, scale 1:3000.

Fitches, W.R., Cave, R, Craig, J and Maltman, A.J. 1990. The flexural-slip mechanism: Discussion. Journal of Structural Geology, 12, p. 1081-1087.

Fletcher, H. and Faribault, E.R. 1911. Southeast Nova Scotia. Canada Department of Mines, Geological Survey, Map 53A, scale 1:250,000.

Fowler, T.J. 1996. Flexural-slip generated bedding-parallel veins from central Victoria, Australia. Journal of Structural geology, 18, p. 1399-1415.

Fowler, T.J. and Winsor, C.N. 1996. Evolution of chevron folds by profile shape changes: comparison between multilayer deformation experiments and folds of the Bendigo-Castlemaine goldfields, Australia. Tectonophysics, 258, p. 125-150.

Fowler, T.J. and Winsor, C.N. 1997. Characteristics and occurrence of bedding-parallel slip surfaces and laminated veins in chevron folds in the Bendigo-Castlemine goldfields: implications for flexural-slip folding. Journal of Structural Geology, 19, p. 799-815.

Fueten, F. 1984. Spaced cleavage formation in the metagreywackes of the Goldenville Formation, Meguma Group, Nova Scotia. Unpublished M.Sc. thesis, McMaster University, Hamilton, Ontario, Canada.

Fyson, W.K. 1966. Structures in the Lower Paleozoic Meguma Group, Nova Scotia. Geological Society of America Bulletin, 77, p. 931-944.

Gibbons, W., Doig, R., Gordon, T., Murphy, B., Reynolds, P. And White, J.C. 1996. Mylonite to megabreccia: tracking fault events within a transcurrent terrane boundary in Nova Scotia, Canada. Geology, 24, p. 411-414.

Graves, M.C. 1976. The formation of gold-bearing quartz veins in Nova Scotia: Hydraulic fracturing under conditions of greeenschist regional metamorphism during early stages of deformation. Unpublished M.Sc. thesis, Dalhousie University, Halifax, Nova Scotia, Canada.

Graves, M.C. and Zentilli, M. 1982. A review of the geology of gold in Nova Scotia: In Geology of Canadian Gold Deposits, ed R.W. Hodder and K.W. Petruk. Canadian Institute of Mining and Metallurgy, Special Volume 24, p. 233-242.

Hall, L.R. 1981. Geology of the Lahave River area, Lunenburg County, Nova Scotia. Unpublished M.Sc. Thesis, Acadia University, Wolfville, Nova Scotia, Canada.

Haynes, S.J. 1986. Geology and geochemistry of turbidite-hosted gold deposits, greenschist facies, eastern Nova Scotia. In Turbidite-hosted gold deposits. Ed. By J.D. Keppie, R.W. Boyle and S.J. Haynes. Geological Association of Canada, Special Paper 32, p. 161-178.

Harper, C.L. 1988. On the nature of time in the cosmological perspective. Unpublished Ph.D. thesis, Oxford University.

Haysom, S.J., Horne, R.J. and Pe-Piper, G. 1997. The opaque mineralogy of metasedimentary rocks of the Meguma Group, Beaverbank - Rawdon area, Nova Scotia. Atlantic Geology, 33, p. 105-120.

Henderson, J.R. 1983. Analysis of structure as a factor controlling gold mineralization in Nova Scotia. In Mines and Minerals Branch Report of Activities, 1992, ed. K.A. Mills. Nova Scotia Department of Mines and Energy, Report 83-1, p. 265-282.

Henderson, J.R. and Henderson, M.N. 1987. Meguma Gold Deposits; nested saddle reefs or early hydraulic extension veins. In Mines and Mineral Branch Report of Activities 1987, Part A, eds. J.L. Bates and D.R. MacDonald. Nova Scotia Department of Mines and Energy Report 87-5, p. 213-215.

Henderson, J.R. and Henderson, M.N. 1986. Constraints on the origin of gold in the Meguma Zone, Ecum Secum area, Nova Scotia. Maritime Sediments and Atlantic Geology, 22, p. 1-13.

Henderson, J.R. and Henderson, M.N. 1990. Crack-seal texture in bedding-parallel, gold-bearing columnar-quartz veins: evidence of fossil water sills. In Mineral Deposits of Nova Scotia, Volume 1, ed A.L. Sangster. Geological Survey of Canada, Paper 90-8, p. 163-168.

Henderson, J.R. and Henderson, M.N. and Wright, T.O. 1990. Water-sill hypothesis for the origin of certain veins in the Meguma Group, Nova Scotia, Canada. Geology, 18, p. 654-657.

Henderson, J.R., Wright, T.O. and Henderson, M.N. 1986. A history of cleavage and folding: and example from the Goldenville Formation, Nova Scotia. Geological Society of America, 97, p. 1354-1366.

Henderson, J.R., Wright, T. O. and Henderson, M.N. 1988. Mechanics of formation of gold-bearing quartz veins, Nova Scotia. In Mines and Minerals Branch Report of Activities 1988, Part A, eds. D.R. MacDonald and Y. Brown. Nova Scotia Department of Mines and Energy Report 88-3, p. 221-223.

Henderson, J., Wright, T. and Henderson, M.N., 1992. Strain history of the Meguma Group, Lunenburg and Ecum Secum areas, Nova Scotia. Geological Association of Canada, Mineralogical Association of Canada Joint Annual Meeting, Wolfville, Nova Scotia; Field Excursion C-11: Guidebook.

Hicks, R. 1996. Low grade metamorphism in the Meguma Group, southern Nova Scotia. Unpublished M.Sc. thesis, Dalhousie University, Halifax, Nova Scotia, Canada, 352 p.

Hicks, R., Jamieson, R.A. and Reynolds, P.H. in press. Detrital and metamorphic 40Ar/39Ar ages from muscovite and whole-rock samples, Meguma Supergroup, southern Nova Scotia. Canadian Journal of Earth Sciences.

Horne, R.J. 1995. Update on bedrock mapping of the Rawdon Syncline. In Minerals and Energy Branch Report of Activities 1994; Nova Scotia Department of Natural Resources, Minerals and Energy Branch Report 95-1, p. 57-61.

Horne, R.J. 1996. Preliminary stratigraphy and structure of the Meguma Group in the Central Meguma project area. In Minerals and Energy Branch, Twentieth Annual Review of Activities. Nova Scotia Department of Natural Resources, Mineral and Energy Branch Information Series 23, p. 15-17.

Horne, R.J., Baker, D., Feetham, M. and MacDonald L. 1997(b). Preliminary geology of the Waverley-Halifax Airport area, central Meguma Project area: with some insights on the timing of deformation and veining in the Meguma Group. In Minerals and Energy Branch, Report of Activities, 1996, eds. D.R. MacDonald and K.A. Mills. Nova Scotia Department of Natural Resources, Report 97-1, p. 55-72.

Horne, R.J., MacDonald, L.A., Bhatnagar, P. And Ténière, P. 1998. Preliminary bedrock geology of the Lucasville-Lake Major area, central Meguma Mapping Project, central Nova Scotia. In Minerals and Energy Branch, Report of Activities, 1997, eds. D.R. MacDonald and K.A. Mills. Nova Scotia Department of Natural Resources, Report 1998-1, p. 15-25.

Horne, R.J. MacDonald, M.A., Corey, M. and Ham, L. 1992. Structure and emplacement of the South Mountain Batholith. Atlantic Geology, 28, p. 29-50.

Horne, R., Boehner, King, S. and Harvey, P. 1997(a). Geological and geophysical interpretation of the Rawdon Fault, Rawdon area, Nova Scotia: implications for Carboniferous age tectonics and basin development. In Program with Abstracts, Geological Association of Canada Annual Meeting, Ottawa 1997.

Hudleston, P.J., Treagus, S. and Lan, L. 1996. Flexural flow folding: Does it occur in nature? Geology, 24, p. 203-206.

Jessell, M., Willman, C.E and Gray, D.R. 1995. Bedding parallel veins and their relationship to folding. Journal of Structural Geology, 16, p. 753-767.

Johnson, A.M. and Page, B.M. 1976. A theory of concentric, kink, and sinusoidal folding and of monoclinal flexuring of compressible, elastic multilayers. VII: Development of folds within Huasna Syncline, San Luis Obispo County, California. Tectonophysics, 33, p. 97-143.

Keppie, F. 1996. Noncylindrical single phase folding: An example; the Oldham Anticline, Meguma Terrane, Nova Scotia. Unpublished B.Sc. thesis, St. Xavier University, Antigonish, Nova Scotia.

Keppie, J.D. 1983. Geological history of the Isaacs Harbour area, parts of 11F/3 and 11F/4, Guysborough County, Nova Scotia. In Mines and Minerals Branch Report of Activities, 1992, ed. K.A. Mills. Nova Scotia Department of Mines and Energy, Report 83-1, p. 109-143.

Keppie, J.D. 1976. Structural model for the saddle reef and associated gold veins in the Meguma Group, Nova Scotia. Canadian Institute of Mining and Metallurgy Bulletin,

Keppie, J.D. 1979. Geological Map of Nova Scotia. Nova Scotia Department of Natural Resources, Halifax, Nova Scotia, scale 1:500 000.

Keppie, J.D. 1993. Synthesis of Palaeozoic deformational events and terrane accretion in the Canadian Appalachians. Geol Rundsch, 82, p. 381-431.

Keppie, J.D. and Dallmeyer 1987. Dating transcurrent terrane accretion: an example from the Meguma and Avalon composite terranes in the northern Appalachians. Tectonics, 6, p. 831-847.

Keppie, J.D. and Dallmeyer, R.D. 1995. Late Paleozoic collision, delamination, shot-lived magmatism, and rapid denudation in the Meguma Terrane (Nova Scotia, Canada): constraints from 40Ar/39Ar isotopic data. Canadian Journal of Earth Sciences, v. 32, p. 644-659.

Keppie, J.D. and Muecke, G.K. 1979. Metamorphic map of Nova Scotia. Nova Scotia Department of Natural Resources, Halifax, Nova Scotia, scale 1:1 000 000.

Kenny, J.P.L. 1936. Gold Stairs Mine, Greenborough. Records of the Geological Survey of Victoria, Australia, 5 (II), p. 222-223.

Köbel, H. 1949. über verformung von Kluften bei der Schichtenfaltung am Beispiel des Salzgitterer Sattels. Geologische Rundschau, 31, p. 188-197.

Kontak, J.D., Cormier, R.F. 1991. Geochronological evidence for multiple tectono-thermal overprinting events in the East Kemptville muscovite-topaz leucogranite, Yarmouth County, Nova Scotia, Canada. Canadian Journal of Earth Sciences, 28, p. 209-224.

Kontak, D.J., Horne, R.J., Sandeman, H., Archibauld, D. and Lee, J.K.W. 1998. 40Ar/39Ar dating of ribbon-textured veins and wall-rock material from Meguma lode gold deposits, Nova Scotia: implications for timing and duration of vein formation in slate-belt hosted vein gold deposits. Canadian Journal of Earth Sciences, 35, p. 746-761.

Kontak, D.J., MacDonald, D. And Smith, P.K. 1988. Fluid inclusion study of the Beaver Dam gold deposit, Meguma Terrane, Nova Scotia. In Mines and Minerals Branch Report of Activities 1988, Part A, ed. D.R. MacDonald. Nova Scotia Department of Mines and Energy, Report 88-3, p. 63-70.

Kontak, D.J. and Reynolds, P.H. 1994. 40Ar/39Ar dating of metamorphic and igneous rocks from the Liscomb Complex, Meguma Terrane, southern Nova Scotia, Canada. Canadian Journal of Earth Sciences, 32, p. 1643-1653.

Kontak, D.J. and Smith, P.K. 1989. Preliminary results of a fluid inclusion study of the Stockwork Zone vein mineralization, Caribou deposit, Nova Scotia. In Mines and Minerals Branch Report of Activities 1989, Part A, ed. D.R. MacDonald. Nova Scotia Department of Mines and Energy, Report 89-3, p. 65-70.

Kontak, D.J., Smith, P.K., Kerrich, R. and Williams, P.F. 1990. Integrated model for Meguma Group lode gold deposits, Nova Scotia, Canada. Geology, 18, p. 238-242.

Kontak, D.J., Smith, P.K., Reynolds, P. and Taylor, K. 1990. Geological and 40Ar/39Ar constraints on the timing of quartz vein formation in the Meguma Group lode-gold deposits, Nova Scotia. Atlantic Geology, 26, p. 201-277.

Kontak, D.J., Smith, P.K., Reynolds, P. and Taylor, K. 1993. Geology and 40Ar/39Ar geochronology of the Beaver Dam gold deposit, Meguma Terrane, Nova Scotia, Canada: evidence for a 370 Ma age of mineralization. Economic Geology, 88, p. 139-170.

Krogh, T.E. and Keppie, J.D. 1990. Age of detrital zircon and titanite in the Meguma Group, southern Nova Scotia, Canada: Clues to the origin of the Meguma Terrane. Tectonophysics, 177, p. 397-323.

Latham, J.P. 1985. A numerical investigation and geological discussion of the relationship between folding, kinking and faulting. Journal of Structural Geology. 7, p. 237-249.

Malcolm, W. 1929. Gold Fields of Nova Scotia. Geological Survey of Canada, Memoir 385, 253 p.

Markley, M and Wojtal, S. 1996. Mesoscopic structure, strain, and volume loss in folded cover strata, Valley and Ridge Province, Maryland. American Journal of Science, 296, pp. 23-57.

Mawer, C.K. 1987. Mechanics of formation of gold-bearing quartz veins, Nova Scotia, Canada. Tectonophysics, 135, p. 99-119.

Mawer, C.K. and White, J.C. 1987. Sense of displacement on the Cobequid-Chedabucto fault system, Nova Scotia, Canada. Canadian Journal of Earth Sciences, v. 24, p. 217-223.

Messervey, J.P. 1930. Ovens Gold District. In Province of Nova Scotia, Department of Public Works and Mines. Annual Report on the Mines, 1928, Part 2. P. 123-129.

Muecke, G.K., Elias, P. and Reynolds, P.H. 1988. Hercynian/Alleghanian overprinting of an Acadian Terrane: 40Ar/39Ar studies in the Meguma Zone, Nova Scotia. Chemical Geology, 73, p. 153-167.

Nicholson, R. 1995. The interplay between fluids, folds and thrusts during deformation of a sedimentary succession: Discussion. Journal of Structural Geology, v. 17, p. 1473-1477.

O'Brien, B.H. 1983. The structure of the Meguma Group between Gegogan Harbour and Country Harbour, Guysborough County. In Mines and Minerals Branch, Report of Activities, 1992, ed. K.A. Mills. Nova Scotia Department of Mines and Energy Report 83-1, p. 145-181.

O'Brien, B.H. 1988. A study of the Meguma Terrane in Lunenburg County, Nova Scotia. Geological Survey of Canada Open File Report 1823, 80 p.

Pickerill, R.K. and Keppie, J.D. 1981. Observations on the ichnology of the Meguma Group (?Cambrian-Ordovician) of Nova Scotia. Maritime Sediments and Atlantic Geology, 17, p. 130-138.

Poole, W.H. 1971. Graptolites, copper and potassium-argon in Goldenville Formation, Nova Scotia. Geological Survey of Canada, Paper 71-1A, p. 9-11.

Pratt, B.R. and Waldron J.W.F. 1991. A Middle Cambrian trilobite faunule from the Meguma Group of Nova Scotia. Canadian Journal of Earth Sciences, 28, 1843-1853.

Price, N.J. and Cosgrove, J.W. 1990. Analysis of Geological Structures. Cambridge University Press, Cambridge.

Pryer, L.L. 1984. Strain measurements from deformed quartz grains in metagreywackes of the Goldenville Formation, Meguma Group, Nova Scotia. Unpublished B.Sc. thesis, McMaster University, Hamilton, Ontario, Canada.

Raeside, R.P. and Mahoney, K.M. 1996. The contact aureole of the South Mountain Batholith, southern Nova Scotia. Geological Association of Canada - Mineralogical Association of Canada, Program with Abstracts, 21, A77.

Ramsay, J.G. 1967. Folding and Fracturing of Rocks, McGraw-Hill, New York.

Ramsay, J.G. 1974. Development of chevron folds. Geological Society of America Bulletin, v. 85, p. 1741-1754.

Ramsay, J.G. and Huber, M.I. 1983. The techniques of Modern Structural geology, Volume 1: Strain Analysis. Academic Press, London.

Ramsay, J.G. and Huber, M.I. 1987. The techniques of Modern Structural geology, Volume 2: Folding and Fracturing. Academic Press, London.

Reynolds, P.H. and Muecke, G.K. 1978. Age studies on slate, applicability of the 40Ar/39Ar stepwise outgassing method. Earth and Planetary Science Letters, 40, p. 111-118.

Ryan R,J., Fox, D., Horne R.J., Corey, M.C. and Smith, P.K 1996. Preliminary stratigraphy of the Meguma Group in central Nova Scotia. In Mines and Minerals Branch Report of Activities, 1995, eds D.R. MacDonald and K.A. Mills. Nova Scotia Department of Natural Resources, Report 96-1, p. 27-34.

Sangster, A.L. 1990. Metallogeny of the Meguma Terrane, Nova Scotia. In Mineral Deposits of Nova Scotia, Volume 1, ed A.L. Sangster. Geological Survey of Canada, Paper 90-8, p. 115-162.

Schenk, P.E. 1991. Events and sea-level changes on Gondwana's margin: The Meguma Zone (Cambrian to Devonian) of Nova Scotia. Geological Society of America Bulletin, 103, p. 512-521.

Schenk, P.E. 1995. Meguma Zone. In Geology of the Appalachian-Caledonian Orgen in Canada and Greenland, ed H. Williams. Geological Survey of Canada, Geology of Canada, No. 6, p. 261-277..

Smith, P.K. 1976. The structural geology of the south-eastern part of the Kentville area (21H/2E), Nova Scotia. Unpublished M.Sc. Thesis, Acadia University, Wolfville, Nova Scotia. Canada, 76 p.

Smith, P.K. and Kontak, D.J. 1988. Meguma gold studies II: Vein morphology, classification and information, a new interpretation of "crack seal" quartz veins. In Mines and Minerals Branch Report of Activities 1987, Part B, eds. D.R. MacDonald and Y. Brown. Nova Scotia Department of Mines and Energy, Report 88-1, p. 61-76.

Smitheringale, W.C. 1960. Geology of the Nictaux - Torbrook map area, Annapolis and Kings Counties, Nova Scotia. Geological Survey of Canada, Paper 60-13.

Tanner, P.W.J. 1989. The flexural-slip mechanism. Journal of Structural Geology 11, no. 6, pp. 635-655.

Tanner, P.W.J. 1990. The flexural-slip mechanism: Reply. Journal of Structural Geology, 12, p. 1081-1087.

Tanner, P.W.J. 1992. Morphology and geometry of duplexes formed during flexural-slip folding. Journal of Structural Geology 14, no. 10, pp. 1173-1192.

Treagus, S.H. 1988: A history of cleavage and folding: An example from the Goldenville Formation, Nova Scotia: Discussion and Reply. Geological Society of America Bulletin, v. 100, p. 152-154.

Tucker, R.D., Bradley, D.C., Ver Straeten, C.A., Harris, A.G., Ebert, J.R. and McCutcheon, S.R. 1998. New U-Pb zircon ages and the duration and division of Devonian time. Earth and Planetary Sciences Letters, 158, p. 175-186.

Waldron, J.W.F. 1992. The Goldenville-Halifax transition, Mahone Bay, Nova Scotia: relative sea-level rise in the Meguma source terrane. Canadian Journal of Science, 29, p. 1091-1105.

Windh, J. 1995. Saddle reef and related gold mineralization, Hill End Gold Field, Australia: Evolution of an auriferous vein system during progressive deformation. Economic Geology, 90, p. 1764-1775.

Williams, P.F. and Hy, C. 1990. Origin and deformational and metamorphic history of gold-bearing quartz veins on the Eastern Shore of Nova Scotia. In Mineral Deposits of Nova Scotia, Volume 1, ed A.L. Sangster. Geological Survey of Canada, Paper 90-8, p. 169-194.

Woodman, J.E. 1904. Nomenclature of the gold-bearing metamorphic series of Nova Scotia. American Geologist, 33, p. 364-370.

Wright, T.O. and Henderson, J.R. 1992. Volume loss during cleavage formation in the Meguma Group, Nova Scotia, Canada. Journal of Structural Geology, v.4, no. 3, p. 281-290.

Yang, X. and Gray, D.R. 1994. Strain, cleavage and microstructure variations in sandstones: implications for stiff layer behaviour in chevron folding.

Yoe, G. M. and Ruixiang, G. 1986. Late Carboniferous dextral movement on the Cobequid-Hollow fault system, Nova Scotia: evidence and implications. In Current Research, Part A. Geological Survey of Canada, Paper 86-1, p. 399-410.

Young, J.O. 1961. History of the Ovens, A story of the 1861 gold rush.

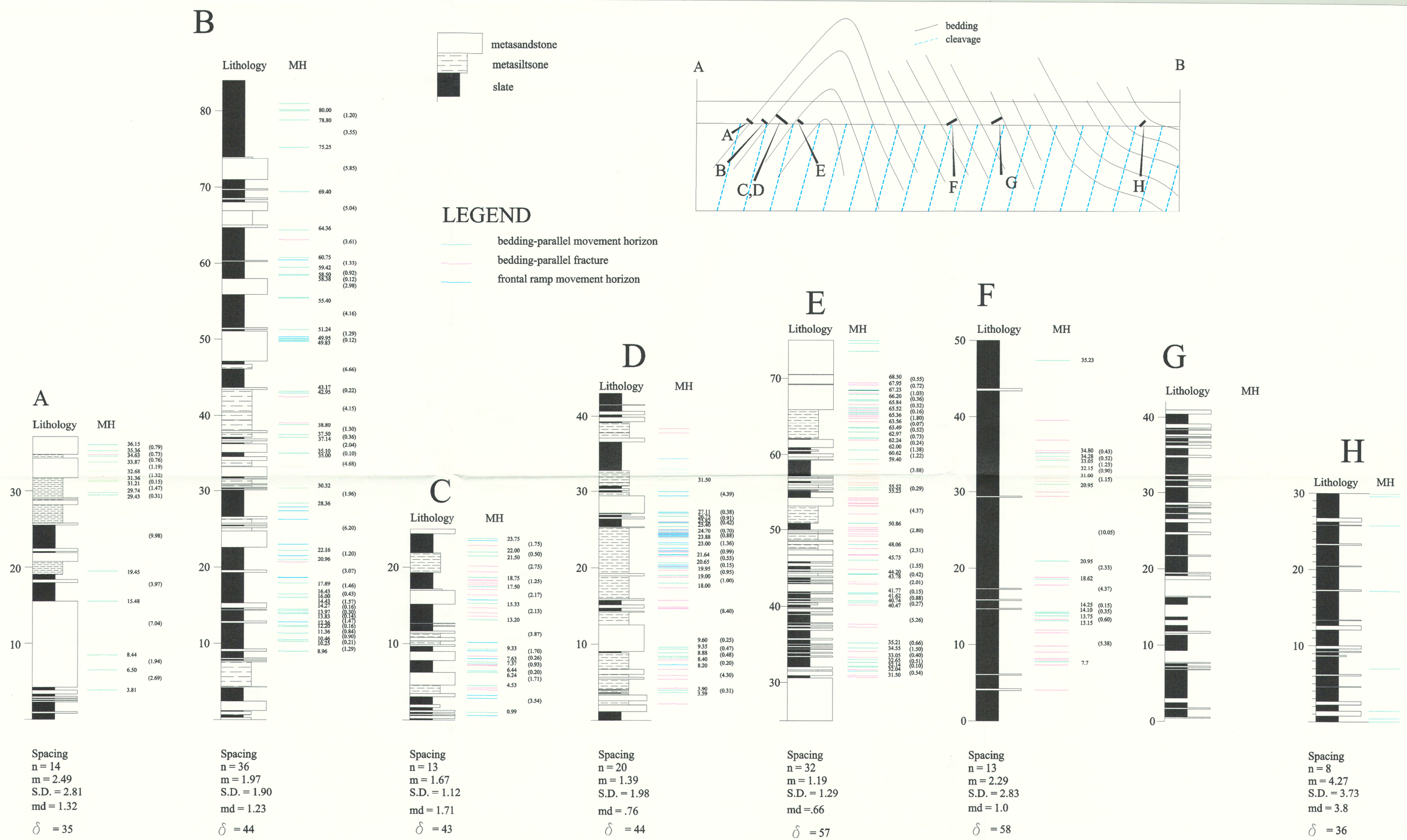

Figure 2.4: Detailed stratigraphic - structural logs for several intervals of the railway tracks study area showing the location of bedding-parallel movement horizons, bedding-parallel fractures which may represent movement horizons and strike-parallel, discordant "frontal ramp" movement horizons. Location of bedding-parallel movement horizons indicated beside symbol and distance between movement horizons indicated in brackets. Spacing data at the bottom of each log is for bedding-parallel movement horizons; n = number of bedding-parallel movement horizons, m = mean spacing, md = median spacing, S.D. = standard deviation, δ = limb dip. Location of log intervals indicated on cross-section.

b Lateral Ramp

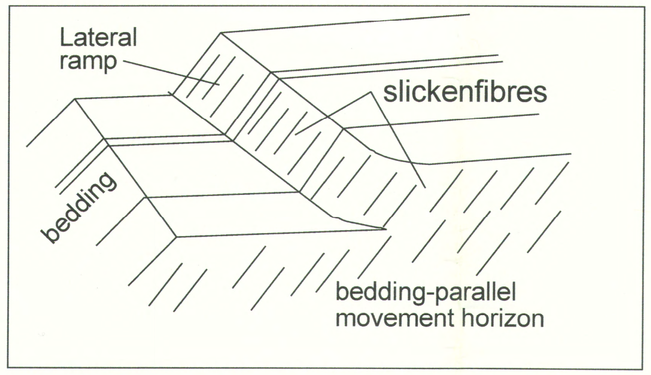

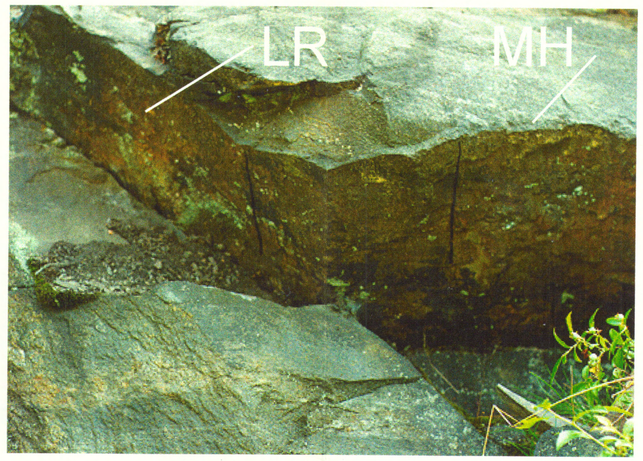

c Frontal Ramp - Duplex

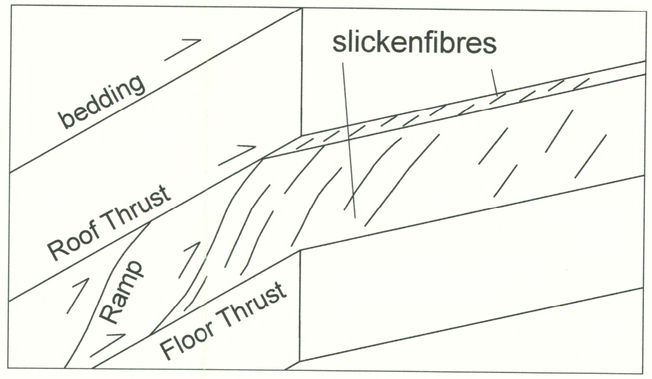

a

LR=Lateral ramp movement horizons
MH= bedding parallel movement horizons

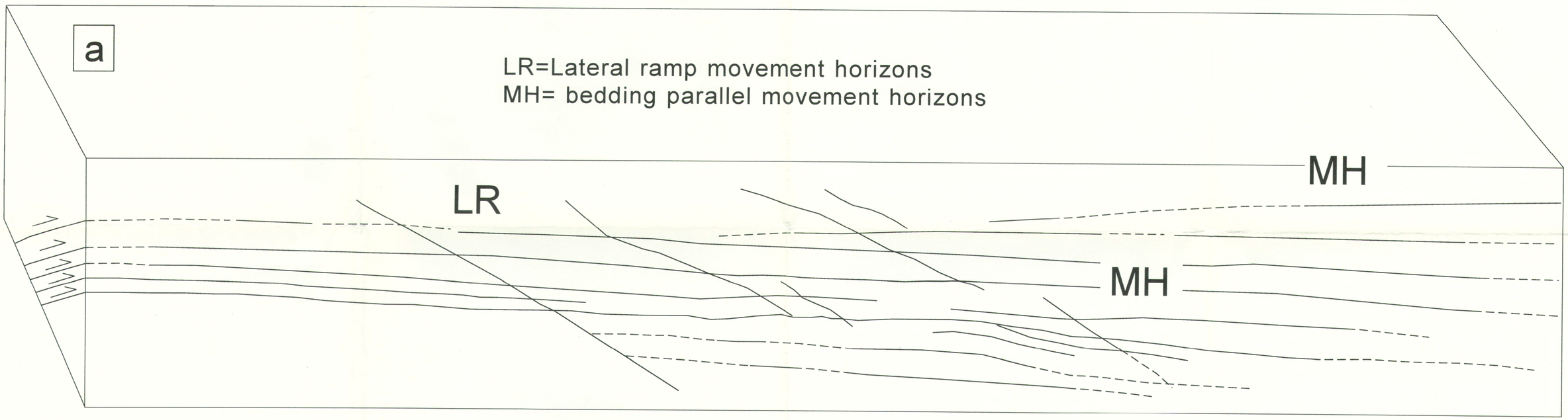

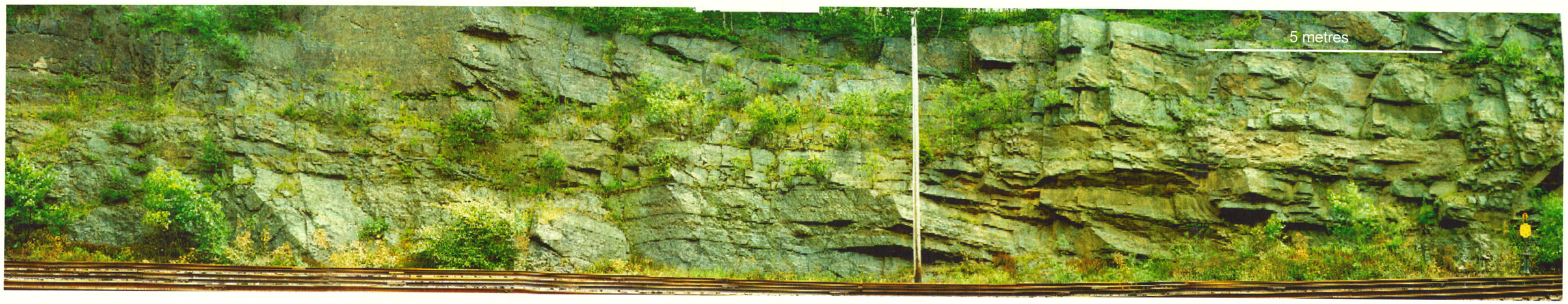

Figure 2.10 (a) Photograph and sketch of a strike-parallel section at the east end of the railway tracks study area showing the location, continuity and density of bedding-parallel movement horizons and lateral ramp movement horizons - view looking southeast (b) Diagram and photograph illustrating the relationship between bedding-parallel movement horizons and lateral ramp movement horizons. Note movement lineations are parallel on both movement horizons and also parallel the intersection of the two movement horizons (c) Diagram illustrating the relationship between bedding-parallel movement horizons and frontal ramp movement horizons.

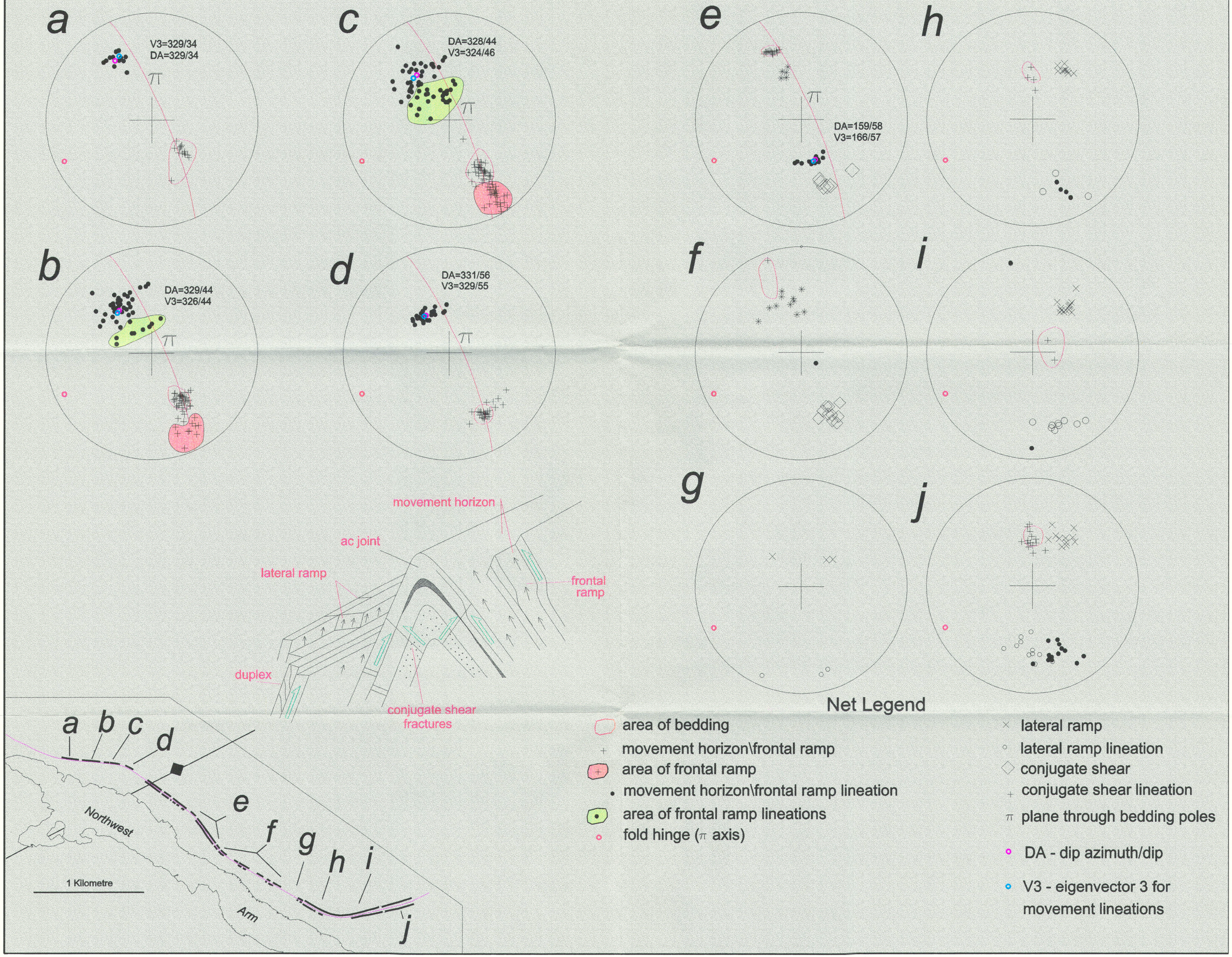

Figure 2.11: Stereonet plots of flexural-slip and fold data for several intervals of the railway tracks study area. Locations of intervals indicated on inset map.

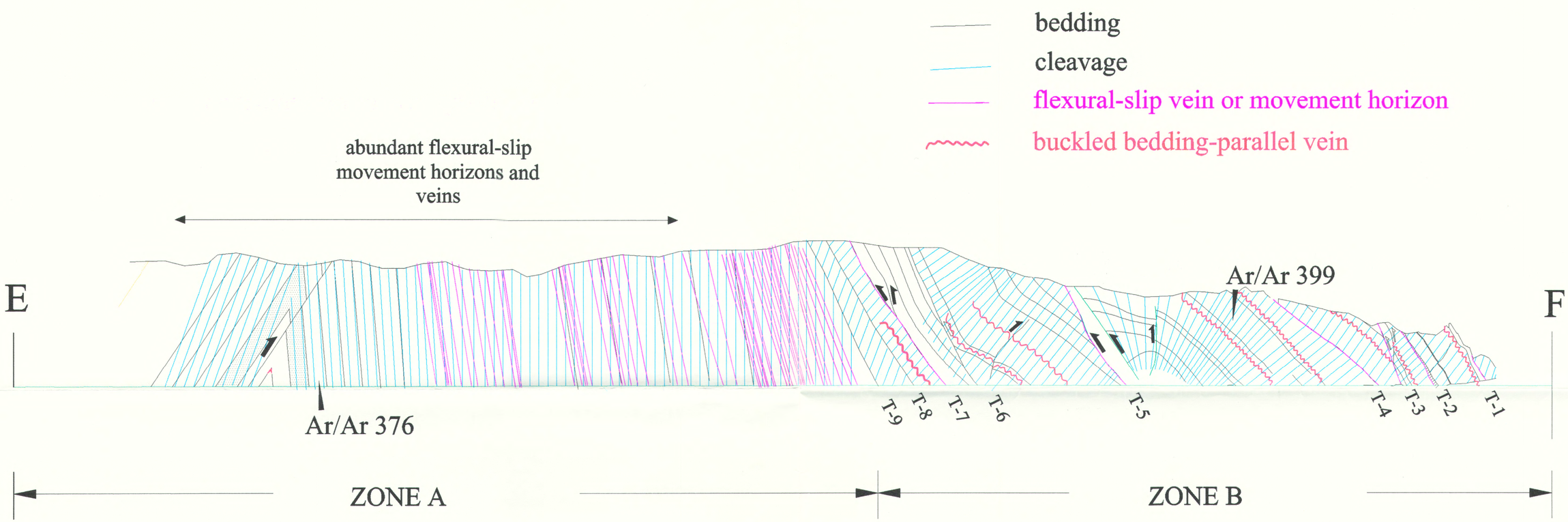

Rose Bay section (E-F), looking northeast

Figure 3.18: Cross section of the Ovens Anticline in the Rose Bay area showing the contrasting structural character of Zones A and B. A more detailed cross section is found in a pocket in the back. See Figure 3.17a for location of section line.